ANALYSIS OF STEEL FRAME STRUCTURES IN FIRE

BY

SHA'ARI ABU

THESIS SUBMITTED TO THE UNIVERSITY OF SHEFFIELD

FOR THE DEGREE OF DOCTOR OF PHILOSOPHY

DEPARTMENT OF CIVIL AND STRUCTURAL ENGINEERING

FEBRUARY 1991

TO MY BELOVED WIFE AND DAUGHTERS

ACKNOWLEDGEMENTS

The author would like to express his sincere gratitude to Dr. R. J. Plank and Dr. I. W. Burgess for their supervision, advice, patient discussion and ecouragement during the period of this study.

Finally the author wishes to thank Professor T. H. Hanna the Head of the Department of Civil and Structural Engineering, and the members of the staff for their co-operation.

TABLE OF CONTENTS

CHAPTER TWO : LITERATURE REVIEW

CHAPTER THREE : GEOMETRIC AND MATERIAL NON-LINEARITIES IN MATRIX STIFFNESS ANALYSIS.

LIST OF FIGURES

LIST OF TABLES

SUMMARY

The main aim of the present research is to develop a method of analysis for structural frames exposed to fire including the effects of material and geometric non-linearities. A matrix stiffness method based on a secant stiffness approach is used providing a full temperature deformation history. The approach has previously been used for the analysis of continuous beams and is extended in the present work to include axial forces. These not only affect the longitudinal displacement, but also reduce the member stiffness and create secondary moments due to the p-delta effect.

The influence of material unloading on the moment-axial force-curvature relationship is studied by examining a cross-section subjected to different combinations of bending moment and axial force at both ambient temperature and in fire.

A computer program, based on the method is used to conduct a limited parametric study. This includes the influence of slenderness ratio, the magnitude of axial load and moment, the size of cross-section and grade of steel. Both uniform and non-uniform temperature profiles are considered for isolated beams, columns and simple portal frame. The important of the p-delta effect is also investigated.

LIST OF SYMBOLS

A	Area of cross-section.
A_i	Area of i'th strip.
$A_{s\,i}$	Axial secant stiffness coefficient.
b	Width of cross-section.
$(EI)_{eff}$	Effective flexural stiffness coefficient.
$(EA)_{eff}$	Effective axial stiffness coefficient.
E_{20}	Young's Modulus at 20°C.
E_T	Young's Modulus at temperature T°C.
$f(\varepsilon)$	Stress as a function of strain.
H_p	Heated parameter.
I	Second moment of area of cross-section.
k	Curvature.
k_{th}	Free thermal curvature.
k_t	Total curvature in the presence of moment, axial force and temperature.
L	Span of structural member.
M	Bending moment.
M_i	Bending moment of i'th element.
M_{int}	Internal moment.
M_p	Moment carrying capacity at ambient temperature in the absence of axial force.
M_{pc}	Moment carrying capacity in the presence of axial force.

$M_{p\,t}$ Moment carrying capacity and elevated temperature.

P Axial force.

P_i Internal axial force of i'th strip.

P_{int} Internal axial force.

P_y Squash load

$S_{s\,i}$ Flexural secant stiffness coefficient.

s Number of cross-sectional strips.

t Time.

T Temperature.

Y_i Distance from the centroid of the cross-section to the centre of the strip.

Vector and matrices.

$[K]$ Assemblage of stiffness matrix.

$\{D\}$ Vector of displacement.

$\{d\}_m$ End displacements of an element.

$\{p\}$ Load vector

$\{K\}_m$ Element stiffness matrix.

$\{p\}_{f\,m}$ Fixed end moments and forces in the element axis.

$[T]_m$ Element transformation matrix.

Greek symbols.

α_T Coefficient of thermal expansion.

ε Strain.

ε_i Strain of i'th strip.

ε_{y20}	Yield strain at 20°C.
ε_o	Centroidal axial strain.
ε_{oa}	Resultant centroidal axial strain.
ε_c	Creep strain.
ε_T	Thermal strain.
σ	Stress.
σ_i	Stress of i'th strip.
σ_{y20}	Yield stress at elevated temperature.
Θ	Angle of rotation.

CHAPTER ONE

INTRODUCTION

1.1 INTRODUCTION.

In many countries steel has become the first choice of architects and structural engineers for the framework of multi-storey buildings. The material and the construction methods associated with it have proved the most cost effective and reliable in many different situations [1] due to advantages over other systems such as speed of erection, high strength/weight ratio, reliability and durability. However, although steel is very strong under normal conditions, this strength reduces dramatically when it is exposed to the high temperatures experienced in a building fire [2],[3]. Building designers must therefore include appropriate measures to minimise these effects, including suitable means of alarm and escape, and insulation of the steel elements to ensure structural stability. In the latter case it has been reported that the cost of such fire protection has accounted for about 30% of the total cost of various forms of building construction [4],[5],[6]. Because of this, the subject of fire in steel framed buildings has in recent years received considerable attention in terms of research throughout the world. The aim has been to develop

a better understanding of the complexity of fire behaviour and its effect on steel structures, as well as developing more cost-effective methods for fire protection.

The subject of fire and its effect on steel building frames is complex. For convenience research in this subject can be classified into four categories [7],[8]:

1. General principles relating to fire and its spread in buildings.

2. Properties of steel exposed to fire.

3. Fire resistance tests on structural elements.

4. Methods of calculating the behaviour of protected and unprotected steel structural elements and frame structures in fire.

At present, the basic problems of prediction of hot gas temperature in an enclosure and the resulting steel temperatures, as stated in the first and second categories, are still not solved conclusively, but are being studied by a number of investigators in different parts of the world [11]. A considerable amount of work has been carried out on the third category, since in most countries fire safety design is based on standard fire resistance tests [1]. Contributions in the fourth category are relatively few in

number [7]. Thus the main aim of the present research is to establish a method of calculating the structural response of steel building frames in fire. The objective is to determine the deformation histories of steel frame structures in fire, as well as to obtain the critical temperatures and times of these structures.

1.2 FIRE STATISTICS AND FIRE LOSSES.

One notable fire which destroyed a very large area was The Great Fire of London in 1666 [9]. Two square miles of the city were ruined and 1300 houses were destroyed. Other fires which have caused a considerable loss of life are shown in Table 1.1 [9].

In Great Britain it has been estimated that fire losses for 1987 were over £450 million [2]. Table 1.2 and Figure 1.1 show the annual total for estimated fire losses for England, Wales and Scotland for 1975 - 1987 [2]. From Table 1.2 and Figure 1.1, even though the statistics are confined to Great Britain only, it is clear that fires can have a disastrous effect on both life and property. Safety measures should be taken to reduce or eliminate the risk of personal injury or death due to fire and to reduce the total loss of building, plant and goods. Fire safety policies will be discussed in the following section.

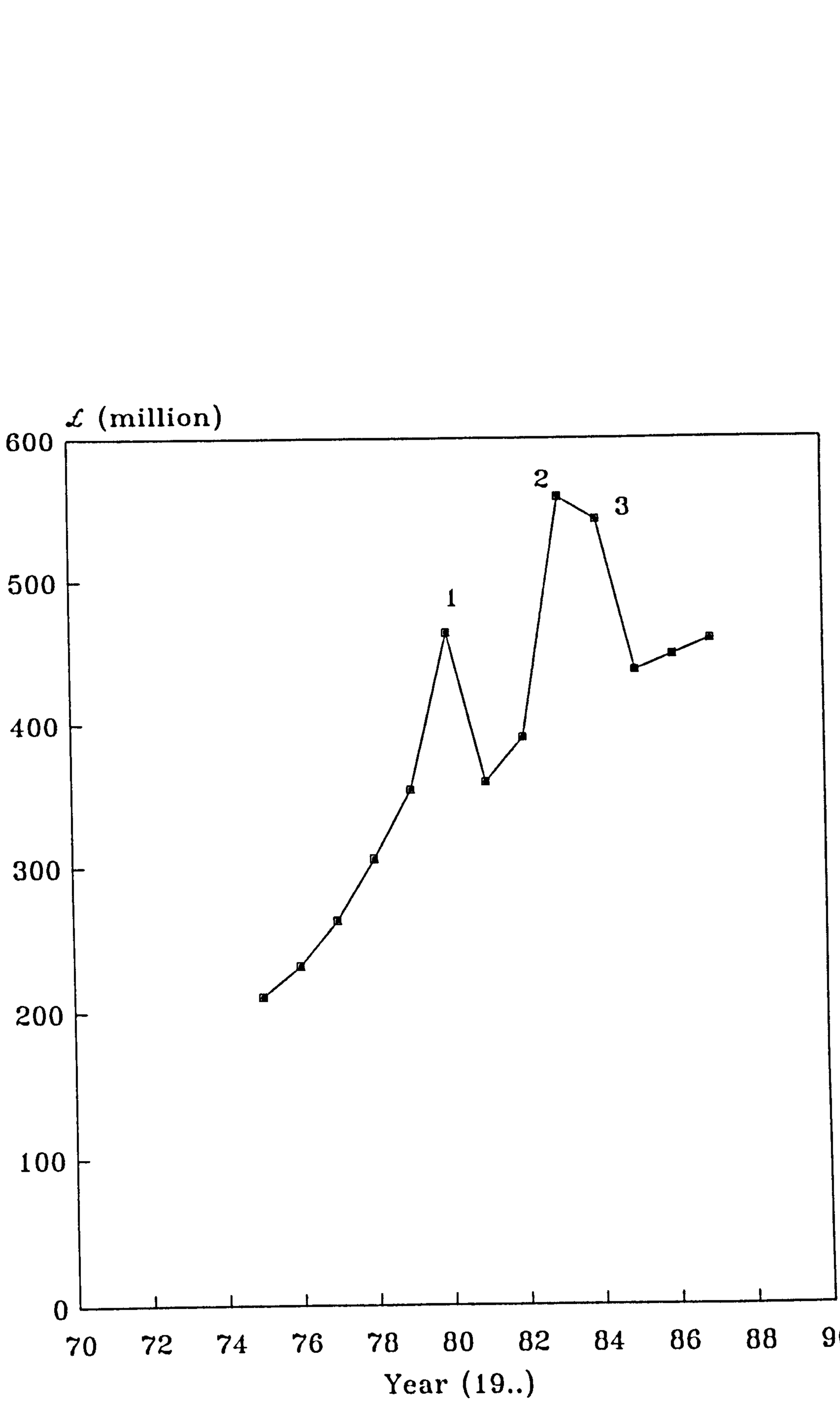

Figure 1.1: Annual total of fire losses for England, Wales and Scotland (1975–87)

Year	Place	Country	Lives Loss
1970	Dance Hall, Saint Laurent du pont	France	142
1971	Hotel, Seoul	Korea	163
1972	Night Club, Osaka	Japan	118
1973	Department Store	Japan	103
1974	Jeolma Office Building	Brazil	179
1975	Discotheque, La Louvieres	Belgium	15
1976	Hotel	Algeria	36
1977	Night Club, Kentucky	USA	164
1977	Jail, Colombia, Tennessee	USA	42
1978	Hotel, Boras	Sweden	20
1979	Bank, Warsaw	Poland	49
1980	Drinking Club, London	UK	37
1980	MGM, Grand Hotel, Las Vegas	USA	85
1981	Stardust Disco, Dublin	Ireland	48
1982	Hotel, Tokyo	Japan	32
1983	Cinema, Turin	Italy	40
1983	Disco, Madrid	Spain	80
1985	Football stands, Bradford	U.K	56
1986	Old People's Home, Beauvais	France	24

Table 1.1: Notable fires which have caused large loss of life.

Year	£ Million
1975	210.50
1976	231.58
1977	263.16
1978	305.26
1979	352.63
1980	463.16 (1)
1981	357.90
1982	389.47
1983	557.89 (2)
1984	542.11 (3)
1985	436.84
1986	447.37
1987	457.89

Table 1.2: Annual total for fire losses for England, Wales and Scotland for 1975-1987.

(1). Including British Aerospace, Weybridge (£72.5 million) and Alexandra Palace (£31 million).

(2). Including Army Ordnance Depot, Donnington (£165 million).

(3). Including two London warehouse totalling over £81 million.

1.3 FIRE SAFETY POLICIES.

The common historical reference point for fire safety policies is The Great Fire of London which lasted for 3 days. King Charles II issued a royal proclamation which required walls of new constructions to be made of brick or stone and streets to be widened. Surveyors were appointed to draft regulations on the construction of new buildings [9]. In principle the aims of fire safety policies cover many aspects including means of escape, preventing rapid growth of fire, preventing external fire spread and ensuring structural stability. These are described briefly as follows:

(a) Providing adequate means for escape.

Analysis of fire casualties over a 10-year period has shown that annually between 800 and 900 people lose their lives and 8000 people are injured [9]. Because of this the main aim of fire safety policies is to ensure rapid evacuation of all occupants to a safe place. These escape routes should be available from all parts of the building and should remain safe and effective for the duration for which they are needed. In addition they must be clearly visible to all users, and be suitably located and of sufficient size to meet the needs of all occupants.

(b) Preventing rapid growth of fire.

The main aim is to ensure that the chance of fire occurring in a building is minimised. If a fire does occur its rate of growth and spread should be controlled to permit evacuation.

(c) Preventing fire spread (i.e containment).

The main aim is to ensure that under fully developed fire conditions the building and its structure will not suffer collapse or become unstable. The fire will be contained within boundaries in order to prevent further damage to adjacent compartments or buildings.

(d) Preventing external fire spread.

The main aim is to ensure that the possibility of a conflagration due to external fire exposure is reduced and fire spread from one building to another is prevented. Such measures which can be used include extinguishing systems, facilities for fighting fires and walls up to roof level.

Based on the above policies more secure and safe buildings can be achieved.

1.4 RATE AND DEVELOPMENT OF FIRE IN A COMPARTMENT.

In this section the behaviour of fire in a compartment is discussed. If a fire is left unattended, it will progress through three distinct stages, namely a growth period, a steady combustion period and a decay period. A curve representing the corresponding temperature development is shown in Figure 1.2. This shows that fire generally commences with a slow increase in temperature (growth period), followed by a rapid rise in temperature until a peak is reached (steady combustion period) and ending in a relatively slow decrease in temperature (decay period). The detailed features of each period are discussed below:

(a) Growth period.

The temperatures during this period are generally low, seldom exceeding 250°C [10]. Its duration depends on the nature of the combustible materials involved and the environmental factors such as fire load and air supply. The duration of this period is extremely important because the chance of escape is relatively high and the temperature is very low. Also evacuation of important properties and the most effective operation of fire brigades are best achieved during this period.

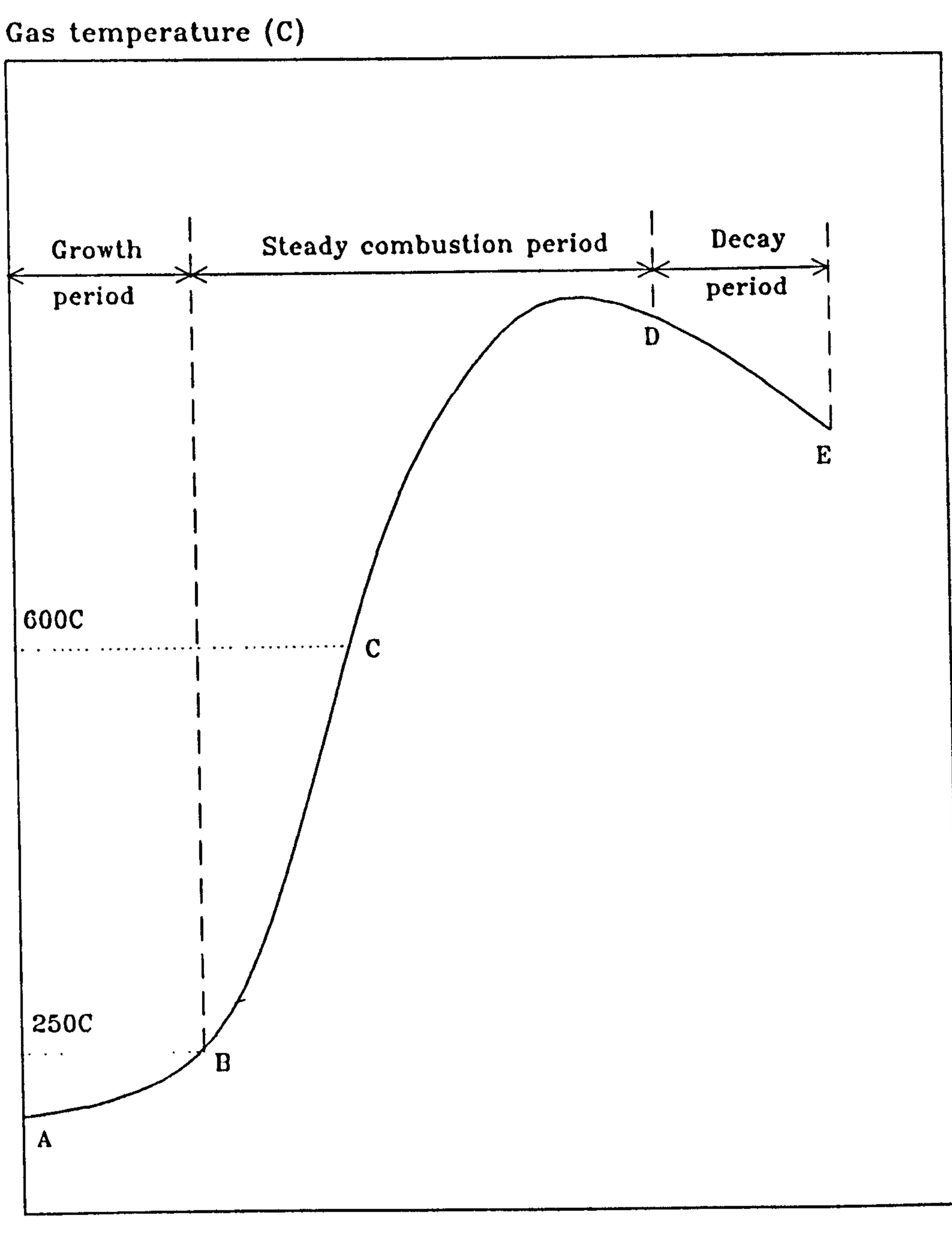

Figure 1.2: Typical temperature development in a natural fire.

(b) Steady combustion period.

The period commences at point B in Figure 1.2. The burning material begins to generate flammable vapours causing the spread of fire to accelerate very rapidly. The temperature continues to rise, but much more rapidly, and when it exceeds 600°C [10] there is a spontaneous combustion of all organic materials in the compartment. This phenomenon is referred to as `flashover' and is characterised by sharply rising temperature. During this period flaming can be observed throughout the compartment volume. The temperature continues to rise but at a decreasing rate until a balance is reached between the heat produced in the enclosure and the heat losses to walls and surroundings.

(c) Decay period.

The duration of the decay period depends upon the total amount of combustible materials and the rates at which they can decompose. After most of the material has been burnt, and assuming that fire has not been controlled, the fire reduces in intensity and the temperature reduces progressively to ambient temperature. Malhotra [10] has stated that " a well-designed building can withstand the complete burnout of the contents without suffering collapse or permitting the fire to escape from the protected areas".

The second and third periods of fire development in a

compartment can lead to structural instability or collapse because the structural steel elements are at very high temperatures, and consequently the strength of the material is greatly reduced. These periods should therefore be of primary interest to structural engineers [5].

1.5 STANDARD TIME-TEMPERATURE CURVE.

The behaviour of fire in a compartment is a very complex matter. This is due to the fact that the fire severity depends not only on the fire load density but also on other factors such as ventilation, burning rate, fire duration and the thermal construction of the enclosure [12],[13]. Such variations cannot be realistically represented in comparing fire characteristics of different systems, and a standard time-temperature curve has therefore been adopted internationally to represent the fire behaviour in a compartment.

The equation of the standard fire curve relating gas temperature in a compartment to time was proposed by Inberg [5],[12]. It is defined in British Standard 476:Part 8 [13] and ISO 834 [1],[12] and takes the form:

$$T - T_o = 345\log_{10}(8t + 1) \quad \text{.....(1.1)}$$

where T = gas atmosphere temperature (°C)

T_o = ambient temperature (°C)

t = time (min)

In BS 476: Parts 20 and 30 [14] standard fire tests are required to operate according to the standard time-temperature relationship shown in Equation 1.2.

$$T - 20 = 345\log_{10}(8t + 1) \quad \ldots\ldots\ldots\ldots(1.2)$$

The equation is shown graphically in Figure 1.3.

However it is important to recognise that this does not represent the time-temperature relationship observed in real fires, in which temperatures may rise more rapidly and reach higher values than in the standard time-temperature curve. Figure 1.4 shows a comparison between BS 476: Part 8 and the results of natural fire tests [1],[12]. This shows the early growth of temperature may be greater than the standard curve, but unlike the standard curve the temperature peaks and then begins to fall. However the standard time-temperature curve does provide a basis for comparison. It can be related to natural fire behaviour using a time-equivalence concept as proposed, for instance, by Law as reported in [17]. The relationship relates the fire severity, fire load and ventilation as shown below:

$$t_f = C(L/\sqrt{A_w A_T \sqrt{H}}) \quad \ldots\ldots\ldots\ldots(1.3)$$

where t_f = fire severity expressed as duration of exposure

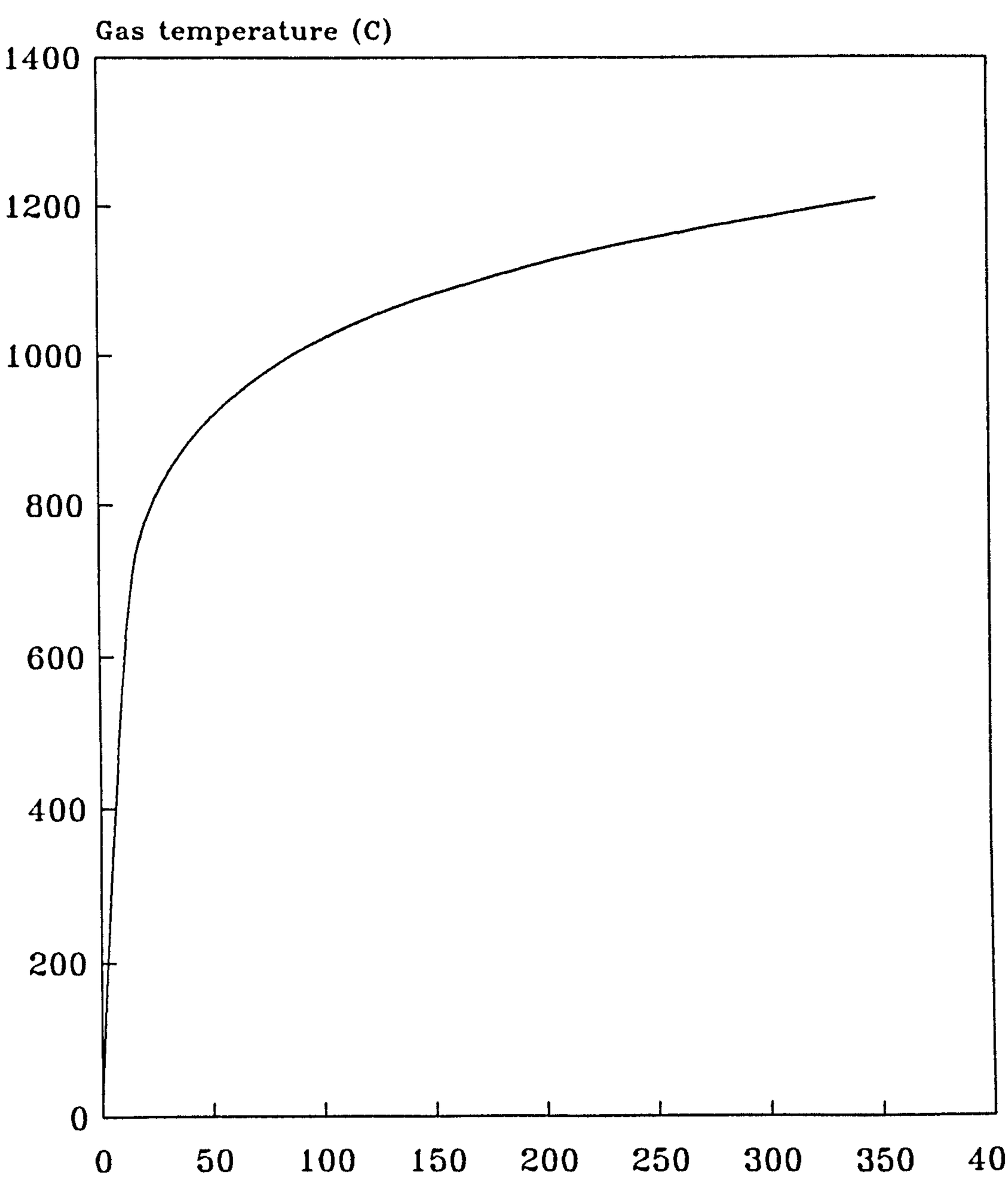

Figure 1.3: Standard fire time–temperature curve

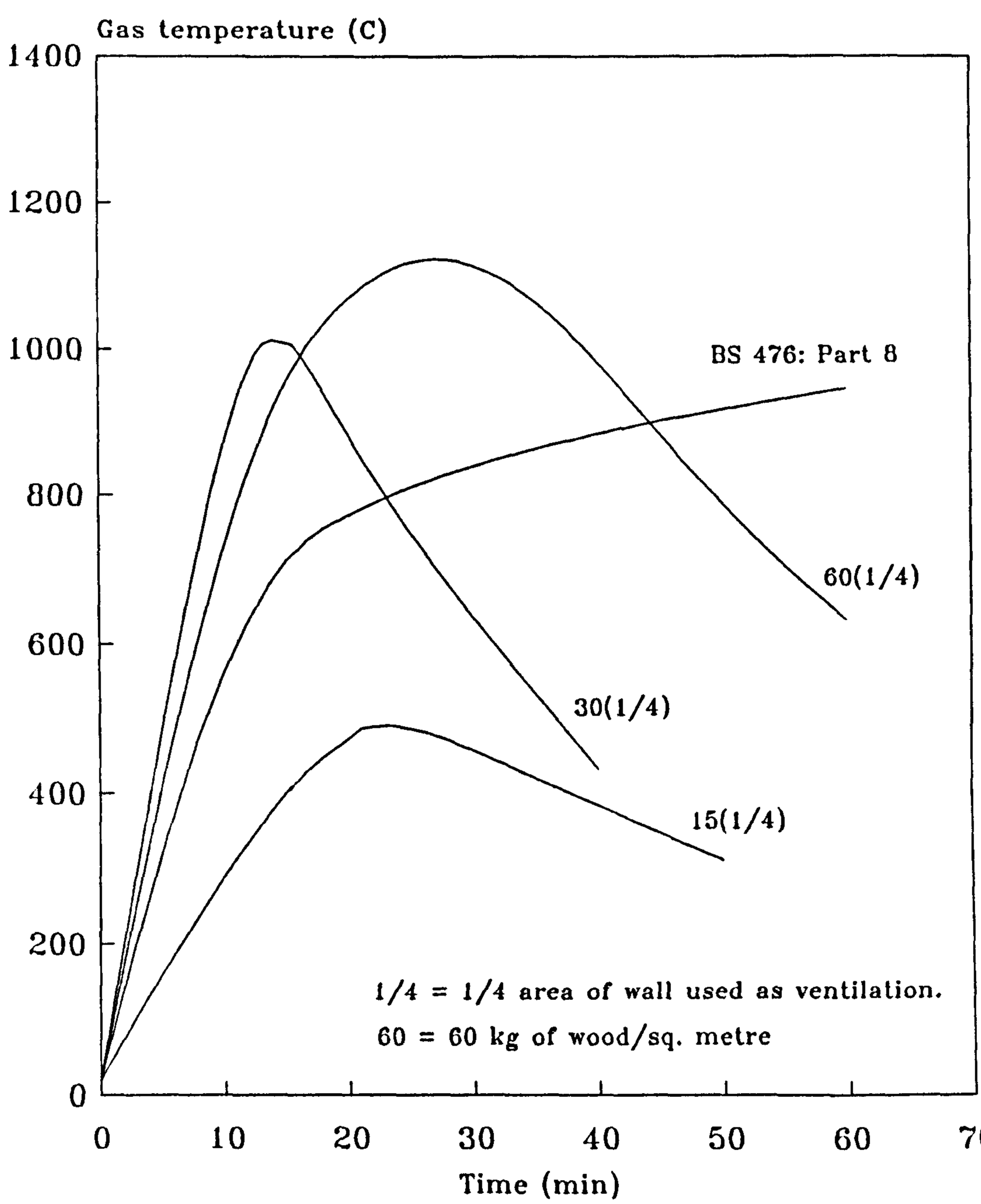

Figure 1.4: Gas temperature for various fire load densities and ventilation systems.

to a standard fire.

L = total fire load.

A_w = area of the opening in the room.

A_t = total bounding surface of the room.

H = height of the opening in the room.

C = a coefficient.

1.6 STANDARD FIRE RESISTANCE TESTS.

Building regulations define the required survival periods for structural steel elements which correspond to their performance as measured in the standard fire resistance test. Fire resistance is defined in BS 4422 : Part 1 [9] as the ability of an element of building construction to withstand the effects of fire for a specified period of time without the loss of its fire-separating or load-bearing functions. Internationally, the generally accepted method for design of load-bearing structural elements under fire action is still based on the standard fire resistance test as shown in Figure 1.5 [15]. In the UK the fire resistance of an element is determined in accordance with BS 476: Part 8, now replaced by BS 476: Parts 20 to 23 [9],[13] which specify the laboratory procedure and test criteria. This test is based on the procedure first issued in 1932 following work by the British Fire Prevention Committee and standardization by ASTM [9],[12].

The lengths of column and beam specimens for the test are

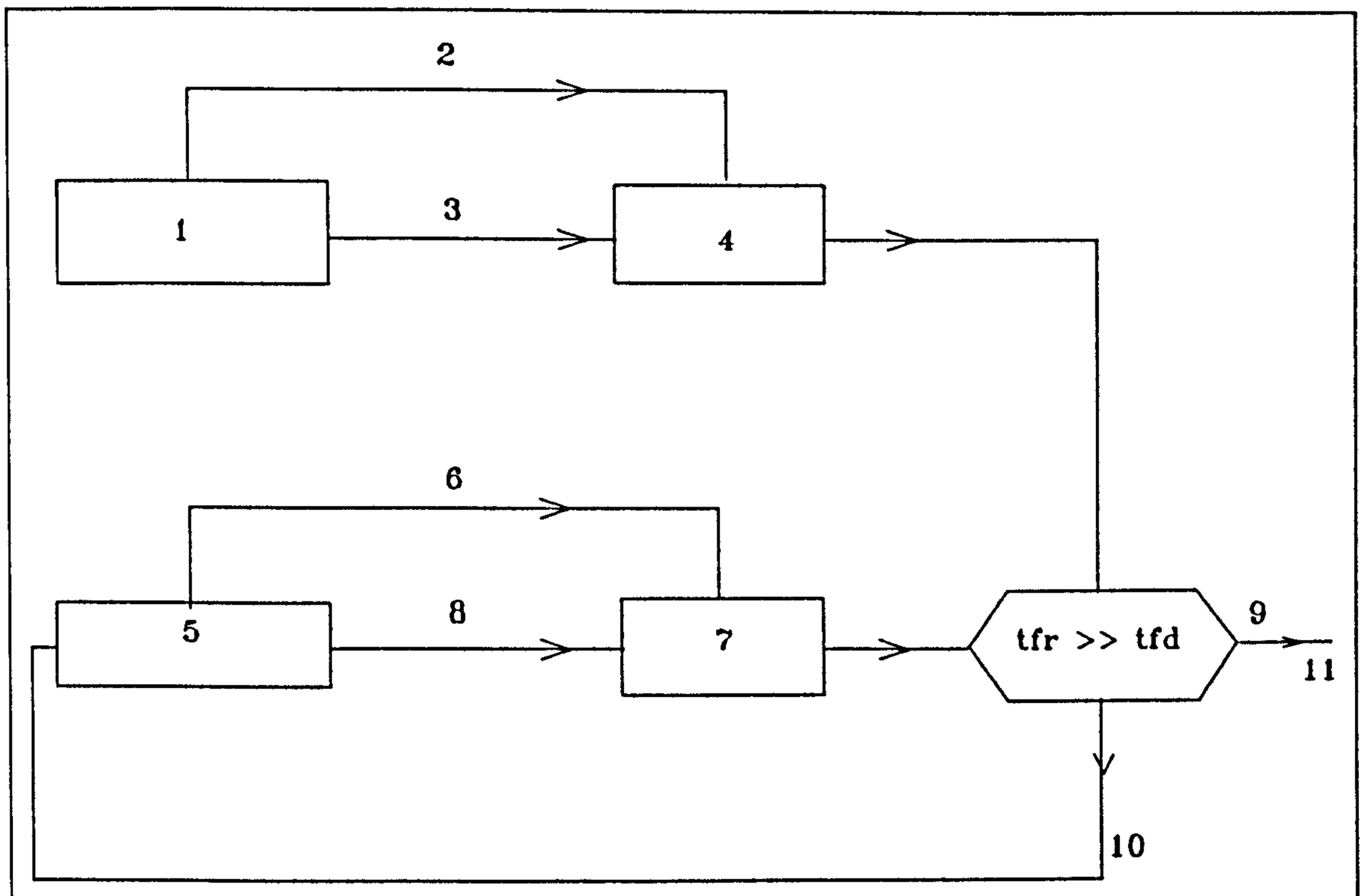

1. Structural application.
2. Requirement by public agencies.
3. Building code.
4. Required fire duration tfd.
5. Structural element.
6. Complience by designers.
7. Fire resistance tfr.
8. Standard fire resistance test.
9. Yes.
10. No.
11. End.

Figure 1.5: Standard fire resistance test in relation to fire safety design [15].

typically 3m and 4m respectively. The period of fire resistance of the element is obtained when it reaches a defined failure condition. In the case of beams this has been when the central deflection reaches 1/30 of the span [13]. However this criterion has now been superseded by an amendment of BS 4822:1985 reflecting the suggestion of Robertson and Ryan [16]. This allows a maximum deflection of 1/20 of span, provided the rate of deflection R does not exceed the following limiting value:

$$R = L^2 / (900d) \text{ mm/min}$$

where L = span of the test element (mm).

d = distance from the top of the cross-section to the bottom of the design tension zone (mm).

1.7 THE FIRE ENGINEERING APPROACH.

While the building regulation system has proved effective in that structural collapse in fire is extremely rare alternative methods, generally described as Fire Engineering, based on a more rational and analytical approach, are being developed. The motivating influences in the development of Fire Engineering are as follows [1],[15]:

(a) The information needed to design structures rationally for fire safety cannot be provided solely by the results of

standardised tests, because the behaviour of structures in fire is extremely complex and testing facilities are both limited in size and are expensive.

(b) On several occasions claims have been pressed for the abandonment of the present classification systems shown in Figure 1.5 and the standardised fire resistance test, which both present serious deficiencies [15].

(c) Analytical methods for predicting thermal and structural response are becoming increasingly sophisticated. The use of computers allows such an approach.

The Fire Engineering approach can be divided into three steps [1]:

1. Determination of a time-temperature curve of the atmosphere in a fire.

2. Prediction of steel temperatures, taking account of any fire protection which is provided.

3. Determination of the structural performance.

The above mentioned categories will be discussed in the following section.

1.7.1 The time-temperature curve in a compartment.

As mentioned in Section 1.4 the gas temperature in a fire is influenced by factors such as the fire load, ventilation and the thermal properties of the surrounding area [1],[2],[10].

The fire load in a compartment is established by listing the masses of its contents and the materials used in the construction. Conversion factors are then used to relate their calorific value to wood. The total fire load is then obtained by summing all the individual calorific values. The floor area is measured and the fire load in terms of kg of wood/m^2 is established. As the fire load is increased the potential for fire severity is increased [1].

Gas temperatures in fire are often controlled by the air supply. A well ventilated fire will produced a shorter and hotter time-temperature curve compared with a restricted ventilation system [2]. The importance of fire load and ventilation on the rate of development in a compartment was demonstrated by studies carried out by the Fire Research Station [1]. Magnusson, Pettersen and Thor [18] have developed a mathematical model to represent the time-temperature curves in a compartment by considering the balance between the heat produced and that removed from the compartment. It should be noted that using these techniques the time-temperature curve used models the actual behaviour of a fire (that is the growth period, fully

developed period and decay period). This is not the case in the standard time-temperature curve.

1.7.2 Steel temperatures attained in fire.

The prediction of steel temperatures in fire is very important, since the strengths of the structural steel elements depend on their temperatures. The temperature and heating rate of a steel structure is influenced by several factors [1],[2] such as:

(a) Steel size and shape represented by the H_p/A factor, where H_p is the exposed perimeter of steel exposed in fire and A is the cross-sectional area of the member. The temperature of a member with low H_p/A ratio will rise at a slower rate than one with higher H_p/A.

(b) Location, thickness and nature of any protection applied. The location of a steel member will affect the amount of heat transferred to it by radiation and convection. In reference [1] the position of the steel member is taken into account by using an emissivity variable which has values in the range 0.3 to 0.7. This effect is shown in Figure 1.6 in relation to the location of structural steel columns. In Figures 1.6(a) and 1.6(b) the emissivity variable has values 0.3 and 0.7 respectively.

The thickness and nature of any fire protection material

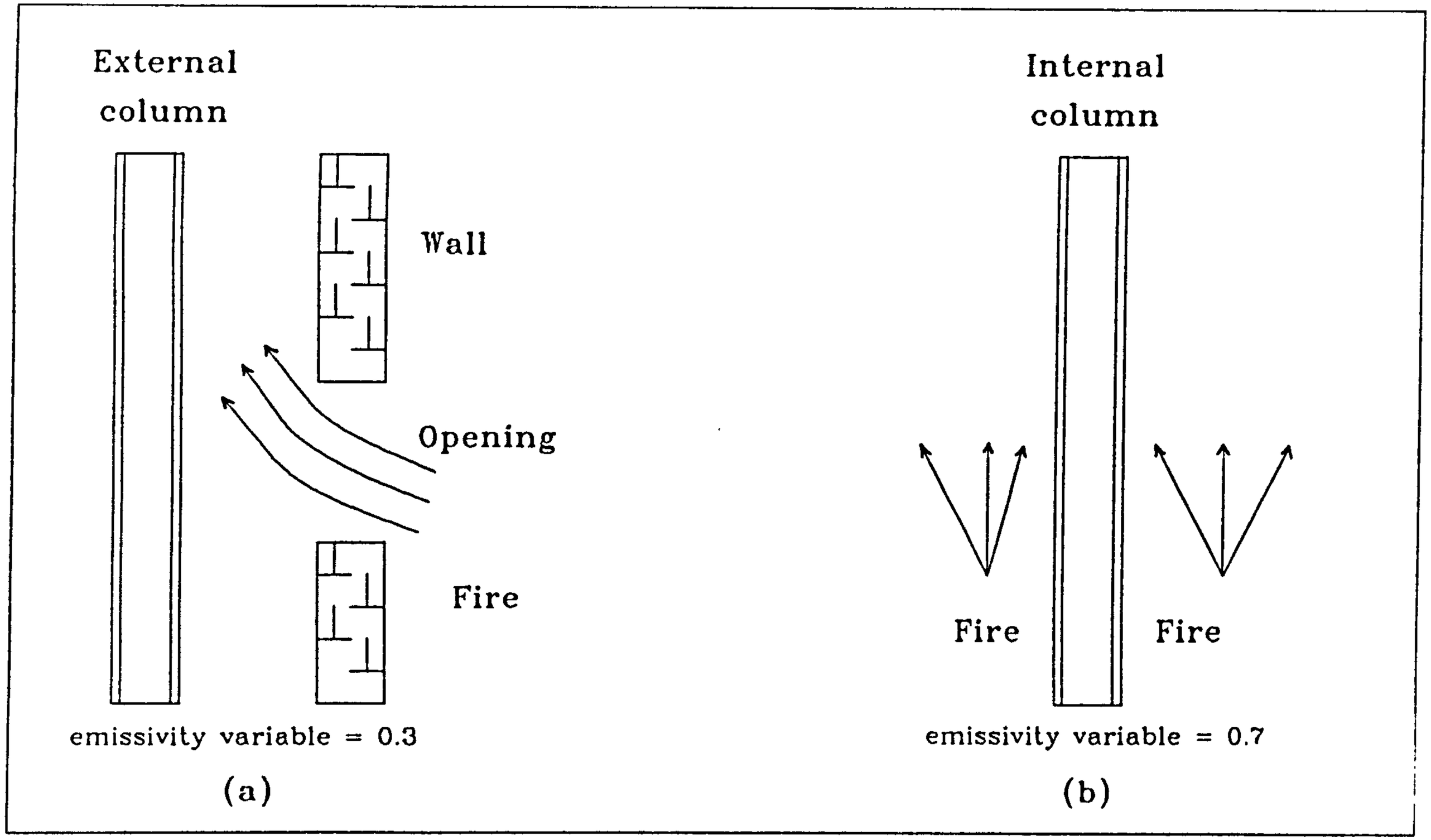

Figure 1.6: Emissivity values related to different column locations.

will affect the steel temperature [19]. For example, a member which has 100 mm thickness of fire protection material will be heated at a much slower rate than a member with 10 mm thickness of the same material.

Different forms of construction can also give widely differing steel temperatures in fire, as shown in Figure 1.7. The figure shows that a concrete slab or concrete blocks placed between the flanges of the cross-section of beams and columns will act both as a heat sink and as shielding, resulting in a non-uniform temperature profile across the section [5],[20].

The prediction of steel temperatures in fire has been studied by several authors [19],[22]. Such techniques have been used in computer programs such as FIRES-T3 [22].

1.7.3 Structural response of steel structures in fire.

This area covers the structural behaviour of steel-framed structures when exposed to fire conditions and is the main concern of the present research. Structural analysis for fire conditions is very complicated since the behaviour of steel in fire is influenced by the effect of increasing temperature in different ways. The principal effects are stated below:

1. Degradation of stress-strain curves with increasing

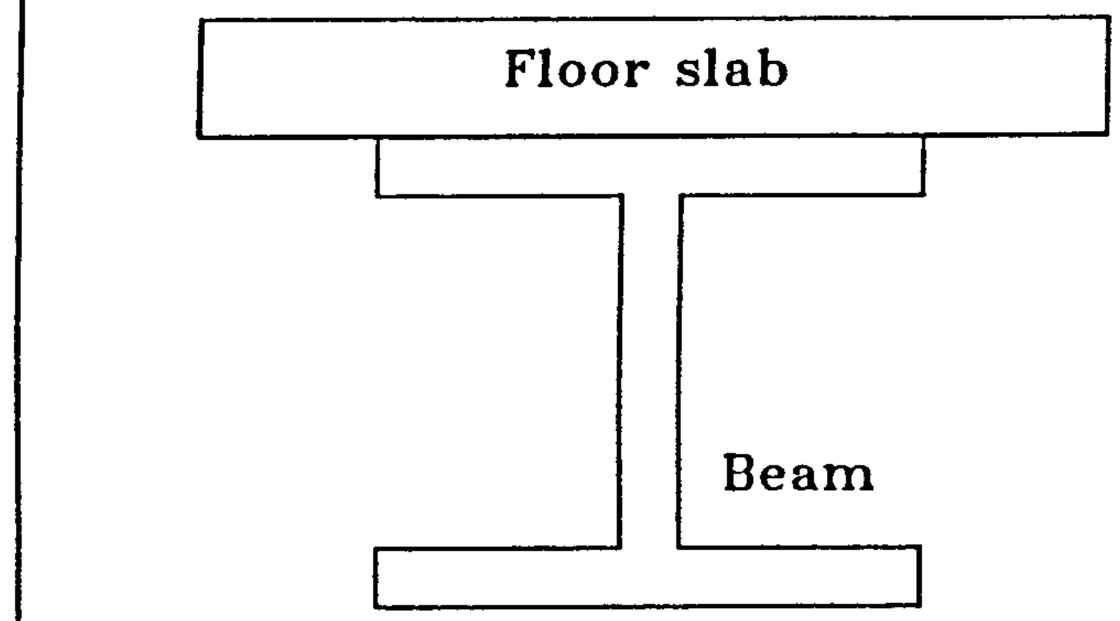

(a) Conventional floor construction

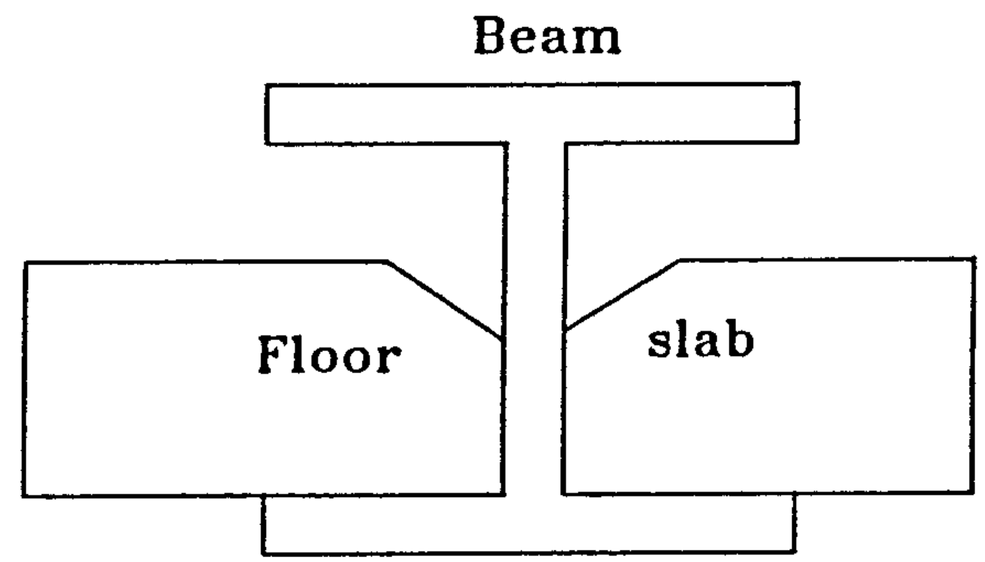

(b) Slim-floor construction

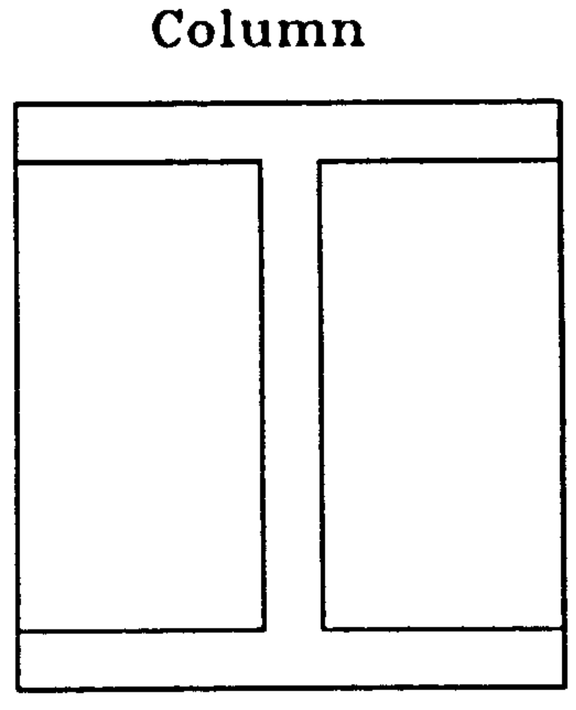

(c)

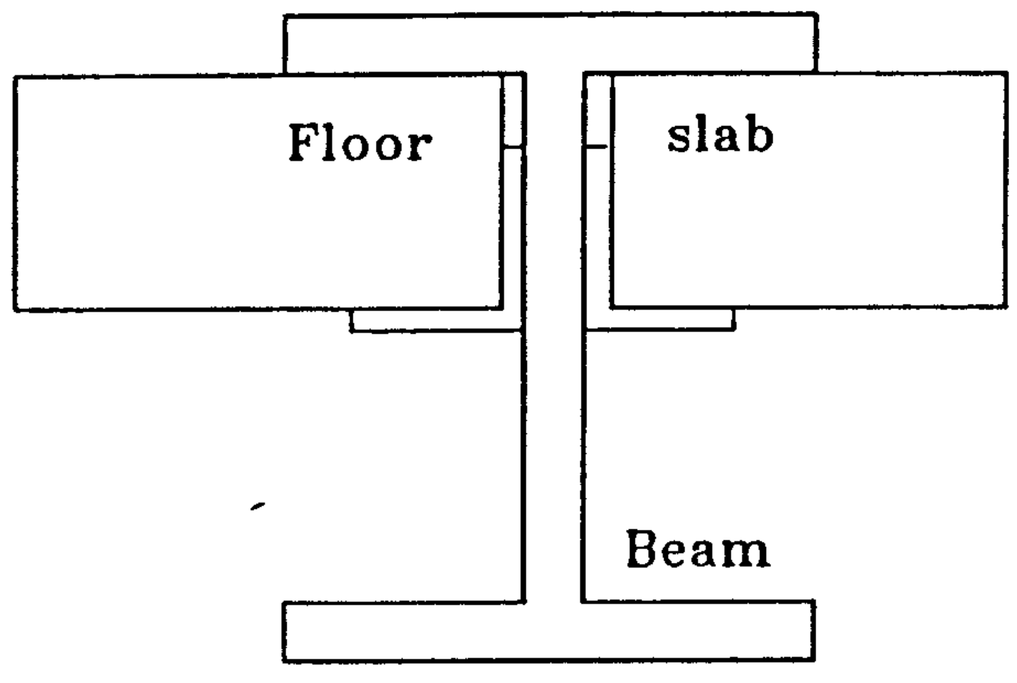

(d) Shelf angle floor construction.

Figure 1.7: Different forms of construction of beams and columns.

temperature.

2. Variation of steel temperature within the section and along the span of the member.

3. Expansion of a confined or restrained member which may result in significant axial forces or in additional bending being applied to the member.

1.8 SCOPE OF THE PRESENT RESEARCH.

The main aim of this research is to develop an analytical tool which can analyse the behaviour of steel frame structures in fire. The method will be used to investigate the effects of material and geometric non-linearities at ambient temperature and also in fire. The material non-linearities are due to the non-linear stress-strain curves and also to the reduction of stiffness due to the presence of axial force within the steel element. Geometric non-linearities arise due to the effect of bowing affecting the longitudinal expansion, and also the effect of axial force which creates extra bending moments in the element.

The matrix stiffness method was chosen as a basis for the analysis because of its practicality and suitability for computer analysis.

In Chapter 2 the literature on the effect of increasing

temperature on the behaviour of steel structures in fire is reviewed. A review of several methods which have been adopted for the analysis of frame structures in fire is presented. The derivation of moment-axial force-curvature relationships at ambient temperature is also reviewed.

In Chapter 3 a practical approach for the analysis of plane frame structures at ambient temperature is developed. The analysis includes the effects of material and geometric non-linearities. The approach is based on the secant stiffness concept rather than the more usual tangent stiffness treatment. A validation of the theory is also presented.

In Chapter 4 an investigation is carried out to highlight the effect of material unloading on the moment-axial force-curvature relationship at ambient temperature and in fire.

In Chapter 5 the method which was discussed in Chapter 3 is extended to analyse the behaviour of frame structures in fire. It illustrates how the effect of increasing temperatures on the frame structure can be included in the method of analysis described in Chapter 3. Such effects include variation of stress-strain curves due to changes in temperature profile, thermal expansion, restraint conditions and also the effect of non-uniform temperature profiles.

In Chapter 6 a validation and calibration of the accuracy of the present method is presented. A series of comparisons

are made with some of the reported results from tests, and also from theoretical studies.

In Chapter 7 a parametric study is conducted in order to achieve a better understanding of the factors that may influence the behaviour of frame structures in fire. The studies are conducted on a single member and a simple portal frame in fire.

Lastly, in Chapter 8 general conclusions are drawn and suggestions for future work are presented.

CHAPTER TWO

LITERATURE REVIEW

2.1 INTRODUCTION.

In this chapter the analysis of frame structures at ambient temperature is reviewed briefly, leading to a more detailed study of research work related to the behaviour of building frames in fire. The derivation of moment-axial force-curvature relationships in determining the flexural and axial stiffness coefficients at ambient temperature is also reviewed. A review of certain factors that influence the behaviour of steel frame structures in fire, including material softening and variation of steel temperature within the cross-section or span of the member, is also discussed in this chapter.

2.2 THE ANALYSIS OF FRAME STRUCTURES AT AMBIENT TEMPERATURE.

The deformation of a frame structure under applied loads depends on a number of factors including the mechanical properties of the material used, as represented by its stress-strain curve. In early methods of frame analysis the

material was assumed to behave in a linear elastic manner following Hooke's Law, ignoring the non-linear parts of the stress-strain curve. Based on this behaviour, in the middle of this century Maney, Cross, Southwell and Kani developed the slope-deflection, moment distribution, relaxation and shear distribution methods respectively [23]. These methods became very popular in engineering offices because of their simplicity and adaptability to hand calculation.

With the development of powerful computer equipment, the so-called matrix stiffness method was developed [23]. In this method, the structure is represented by an assembly of beams and columns connected at nodes, and the analysis requires the solution of a large number of simultaneous equations. The form of each beam or column is assumed to be prismatic. This method offers advantages in cases where the structural analysis cannot be carried out by hand calculation or when the structure is very complex.

However, if the applied load is irregular or the structural elements are nonprismatic the structure can no longer be represented so simply. This led to the development of the finite element method in the early 1960s [25] with plate as well as bar elements. It should be noted that the matrix stiffness method is essentially one form of finite element method. The finite element method has proved to be a very powerful tool but usually needs computers which are quite powerful in terms of speed and storage to accommodate the

software and data. Large amounts of data need to be prepared prior to performing the analysis. Such limitations need to be considered when a practical method of analysis is to be developed. For implementation on personal computers the matrix stiffness method offers a more practical and suitable basis for the analysis of frame structures because it requires much less data to be prepared prior to performing the analysis than does the finite element method.

The matrix method has been applied successfully to a wide range of linear structural problems [23]. It has also been extended to include problems with material and geometric non-linearities. The non-linear effects are very important, especially when determining the maximum loads of frame structures in which some parts undergo elasto-plastic conditions which consequently affect the deflected shape of the structure. The subject of material non-linearities includes the nonlinear stress-strain curve of steel and also the reduction of member stiffness due to the presence of axial force [26],[27]. On the other hand geometric non-linearties include the effects of joint displacement, axial shortening due to bending and the presence of the "p-delta" effect [26],[27],[28].

A technique which is widely used to cater for these non-linear effects is the incremental solution procedure which was developed in the early 1960s [24],[26],[28]. The load is increased in small increments and local linear analysis

is carried out based on the tangent stiffnesses at the corresponding points of the stress-strain curve. A geometric stiffness matrix is also included in the element stiffness matrix in order to cater for the effect of geometric non-linearity [30]. The approach requires an iterative local correction of the calculated deformations at any load increment. This local correction is cumulative and the results from any iteration depend on the results of the previous iteration. At any load increment the results will be kept as initial values when the next load increment is to be analysed. The process is repeated until the corresponding external load is achieved as shown in Figure 2.1. The accuracy of this analysis can be improved by reducing the size of load increments and/or implementing a Newton-Raphson method, but this can be time consuming. The method provides a full load-deformation history, and for each load increment the solution is obtained directly using conventional matrix stiffness analysis.

An alternative method which can provide a more direct solution is the secant stiffness approach [35],[36],[37]. From Figure 2.1, a more direct solution can be achieved by introducing an appropriate linear relationship between the axial load and the corresponding deflection as shown in line OA. The approach offers more accurate results than the incremental approach because the secant stiffness relates the load to the actual deformation. Instead of stepping along the load-deflection curve to achieve a final solution

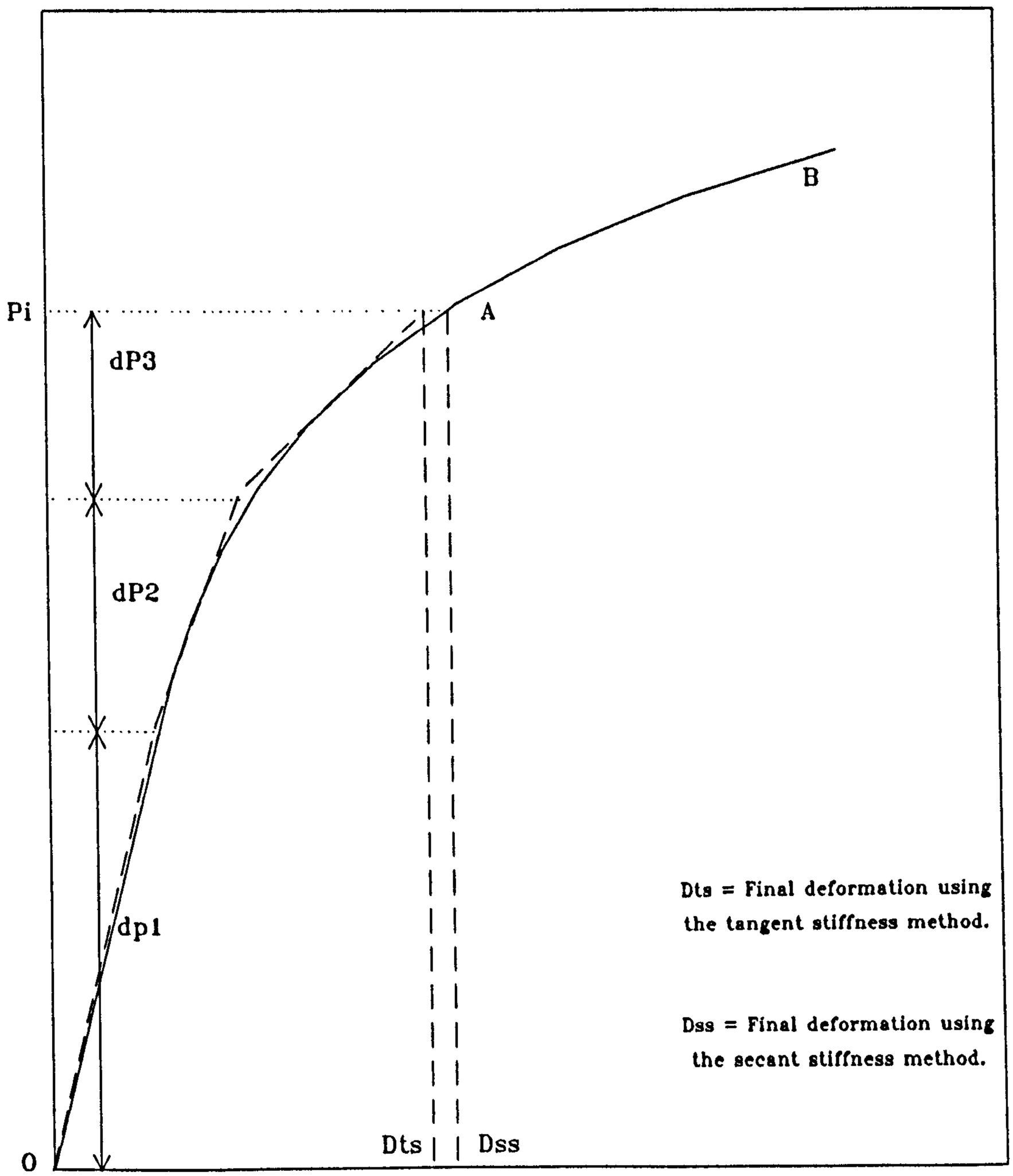

Figure 2.1: Illustration of the principle of the tangent stiffness method and the secant stiffness method.

during the structural analysis, the secant stiffness can relate the load directly to the corresponding non-linear deformation. This approach offers an advantage for frame analysis, especially when the stress-strain characteristic of the material is in the form of a continuous curve, which consequently reduces the local errors during the structural analysis [35],[37].

Ramberg and Osgood [31] and Phillips [32] in 1943 and 1956 respectively introduced analytical expressions for a non-linear stress-strain curve with a continuous change of slope. Instead of introducing a bi-linear form, a single equation can be established to represent closely the corresponding non-linear stress-strain curve. The expression takes the form:

$$\sigma = E\varepsilon - B\varepsilon^n \qquad (n>1) \qquad \text{.....(2.1)}$$

in which B and n are parameters dependent on the shape of the stress-strain curve to be approximated. Thus the moment- curvature relationship corresponding to Equation 2.1 is:

$$M = EI\phi - BK\phi^n \qquad \text{.....(2.2)}$$

in which, for rectangular sections:

$$K = bh^{n+2} / (n+2)(2^{n+1}) \qquad \text{.....(2.3)}$$

and for wide flange shapes:

$$K = (b_w h_1^{n+2} + b_f (h^{n+2} - h_1^{n+2}))/(n+2)(2^{n+1}) \quad \ldots\ldots(2.4)$$

where b and h = width and depth of cross-sections respectively.

b_f and b_w = flange and web width of I sections.

h_1 = web depth of wide flange section.

The above expression for a stress-strain curve has been used by Chajes [36] in determining the inelastic deflections of beams.

Szuladzinski in 1980 [38] developed a modified form of the Ramberg-Osgood stress-strain formula as shown in Equation 2.5 which was used to analyse the deflected shape of beams with non-linear material characteristics.

$$\varepsilon = \sigma/E + (\sigma/E_n)^n \quad \ldots\ldots(2.5)$$

2.3 THE EFFECT OF MATERIAL UNLOADING ON MOMENT-AXIAL FORCE-CURVATURE RELATIONSHIP AT AMBIENT TEMPERATURE.

In linear elastic or elasto-plastic conditions the moment-axial force-curvature relationship is basic to the structural analysis, and the corresponding curvature will be used to obtain the value of axial and flexural stiffness

coefficients of beam-column elements. The curve can be determined from consideration of equilibrium, equating the internal and calculated axial force and bending moment of the element as shown in Equations 2.6 and 2.7.

$$P_{int} = \int_A \sigma(\varepsilon) dA \quad \ldots\ldots\ldots\ldots\ldots\ldots\ldots\ldots (2.6)$$

and

$$M_{int} = \int_A \sigma(\varepsilon) y dA \quad \ldots\ldots\ldots\ldots\ldots\ldots\ldots\ldots (2.7)$$

where P_{int} = internal force.

M_{int} = internal moment.

In determining these relationships it is very important to recognise that there is a possibility that the order of application of the loads acting on the element is not necessarily coincident. It may be, for example, that the bending moment is applied first to the element, followed by the axial force, or vice versa. In elasto-plastic conditions the stiffness relationships due to these cases will be different, due to the fact that different elastic material unloading will happen from the respective plastic regions.

The influence of different combinations of bending moment

and axial force on the strain and stress distributions of the cross-section is shown in Figure 2.2. The amount of bending moment and axial force for each case as shown in Figures 2.2a to 2.2c is the same except that they are applied in a different order to the element. For instance, Figure 2.2c shows the initial and final stress distributions when bending moment is first applied, taking some zones into the plastic region, followed by the axial force. In this condition the influence of material unloading in the plastic region is shown by the final stress profile. Figure 2.2b shows the initial and final stress distributions of the beam-column element, when axial force is first applied, followed by bending moment. The figures show that, despite having identical bending moment and axial force the two final stress patterns are totally different, consequently affecting the stiffness relationships. This has been considered in the derivation of moment-axial force-curvature relationships by a number of authors.

Among the first to consider the subject of material unloading was Engesser in 1895 [30], when he proposed a method for evaluating the buckling behaviour of columns which was called the Reduced Modulus Theory. Material unloading happens because the load is assumed to remain constant during buckling, and as bending deformation increases material unloading occurs on the convex face of the column.

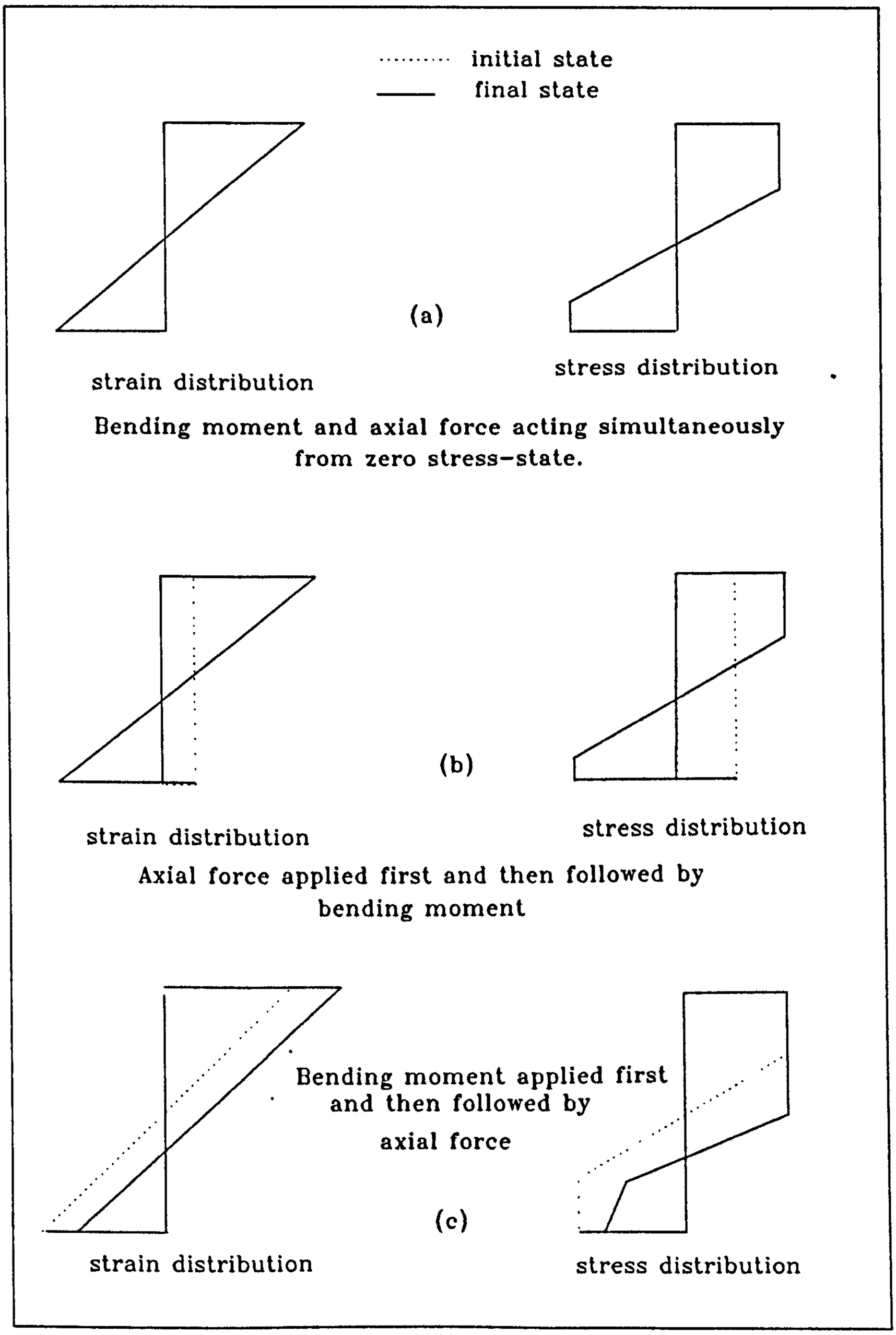

Figure 2.2: Influence of different loading sequence by axial load and bending moment on beam-column element

In 1942, Shanley [41] developed a new theory of inelastic column buckling which proved to be more accurate than the theory that was proposed by Engesser. The axial load is assumed to act at the centroid of the cross-section. The analysis is based on the assumption that the column begins to bend as soon as the tangent modulus buckling load is reached. After reaching the tangent modulus buckling load and if the axial load is progressively increased, bending moment changes simultaneously. As the deformation increases, strain reversal will progressively occur on the convex face of the cross-section of the column. In deriving the moment-axial force-curvature relationship, he assumed that bending moment and axial force are caused simultaneously. To include the effect of material unloading the previous strain distribution of the cross-section was taken as the initial value when the next increment of axial load was applied. He then conducted a test in order to support his theory, in which a few electric strain gauges were placed around the cross-section to measure the strain distribution as the axial load was increased on the pin-ended column. The test results showed that material unloading does occur on the cross-section if the axial load is progressively increased beyond the tangent modulus buckling load.

It should be noted that inelastic column buckling analysis is based on the assumption that the pin-ended column is axially loaded at the centroid of the cross-section

[41],[42]. This idealised problem is, however, of little significance for real structures due to the fact that initial imperfections always exist in real columns. These include eccentricity of axial loads, or subjection of columns to lateral loads or end moments. Thus, to determine the strength or deformed shape of such members, the stiffness relationships should include both the influence of bending moment and axial load acting on the structural elements.

In 1956, Horne [42] derived expressions for the curvature of an initially straight prismatic member of rectangular cross-section subjected to a combination of axial load and bending moment about its principal axis. He assumed that material unloading in the plastic range does not take place, provided that the loads on an initially stress-free structure are increased proportionately from zero, and consequently the degree of unloading appears to be very small. A previous investigation (Baker 1949) indicated that, if the unloading which does occur is neglected, then the predicted collapse loads will be conservative.

In 1957, Driscoll and Beedle [43] conducted tests to demonstrate the reduction of plastic moment due to axial load. The tests were carried out by applying an axial force eccentric to the column. The load was progressively increased and the corresponding curvature was also recorded. It should be noted that in this case, axial force and

bending moment are happening simultaneously due to eccentricity of the axial load. The moment-curvature relationship was shown to be in very good agreement with the theoretical results based on the assumption that material unloading could be ignored.

Timoshenko and Gere [44],[45], Galambos and Ketter [48] also described the derivation of a moment-axial force-curvature relationship based on the assumption that bending moment and axial force are both acting simultaneously and in proportion on an initially stress-free structure. A non-linear stress-strain curve was used and the influence of material unloading was ignored.

In 1965, Lay and Gimsing [46] presented the results of an experimental study of the moment-axial force-curvature relationship. The experimental set-up was similar to that used by Driscoll and Beedle [43] with different test specimens. The moment-curvature relationship was then plotted and compared well with the theoretical results which were again based on the previous assumption (i.e material unloading was ignored). The moment carrying capacity, which ignored the influence of material unloading, was calculated and then compared with the values from the test results carried out by Hendry [40],[47]. In these tests, bending moment was first applied on the specimen and an axial force was subsequently increased until the member was fully plastified. The comparison of the moment carrying

capacities shows very good agreement with the results obtained from the theory which ignored the influence of material unloading.

Nowadays the derivation of a moment-axial force-curvature relationship is based on the method suggested by Baker and reported, for instance, by Horne [42] in which the influence of material unloading was ignored. Chen and Lui in 1975 [53] and Chen and Atsutsa in 1987 [30] developed empirical formulas for the moment-axial force-curvature relationship for rectangular and I-sections in which they ignored the influence of material unloading.

2.4 MECHANICAL PROPERTIES OF STEEL IN FIRE.

2.4.1 Stress-strain relationship.

The relationship between stress and strain for a particular material is normally determined by means of tensile tests in which a specimen, usually in the form of a round bar, is placed in the testing machine and subjected to an increasing tension. The force and elongation of the bar are measured as the load is increased. The corresponding stress (force divided by the cross-sectional area) and strain (elongation divided by the gauge length over which it occurs) enables a complete stress-strain diagram to be plotted for the material. This diagram is assumed to be identical in

tension and compression [11],[55].

The relationship between stress and strain for steel at elevated temperatures has been studied experimentally by several authors such as Witteveen, Twilt and Bijlaard [56], Skinner [57], Jorgenson and Sorenson [58] and Saito [59]. The testing procedures in obtaining a stress-strain relationship can be classified into two types known as isothermal and anisothermal creep tests [57]. Even though the same material is used in each type of test, the stress-strain curves obtained for steel are different. This is because of the influence of creep, which is time dependent and only occurs at high temperature and/or high stress [57],[60],[61]. The experimental procedure for each type of test is as follows:

1. Isothermal creep tests.

This test is carried out in the manner of conventional constant temperature, constant load creep tests [5],[57]. Normally tests are made over the temperature range 350°C to 650°C, due to the fact that creep has no significant influence on the stress-strain curve below 350°C [57]. At a constant temperature and constant load, the strain is measured and plotted against load, and further increase of strain is then recorded continuously against time. A wide range of loads is used during the tests in order to give a wide range of strain rates covering from low to high rates

of deformation.

In reference [56], an isothermal test was carried out on steel using both high and low rates of deformation (200mm/min and 0.5mm/min). It was found that at temperatures below 400°C creep has no significant influence on stress-strain curves. The results also show that at higher temperatures the strain rates due to the creep effect increase considerably. The stress-strain curves measured from low speed tests are presented in Figure 2.3.

2. Anisothermal creep tests.

The specimen is subjected to constant load at increasing temperature [56],[57]. Witteveen, Twilt and Biijlaard [56] have used the corresponding tests, called warm-creep tests, carried out at heating rates between 5°C/min and 50°C/min, and it was noted that the effect of rate of heating is insignificant. The measured stress-strain relationships were then constructed by transforming the temperature-strain curves at constant loading to stress-strain curves at constant temperature. It should be noted that the influence of creep is implicitly included in these stress-strain curves since the tests are carried out in real time. Thus, in the analysis of steel structures in fire, the material properties determined from this test offer an advantage due to the fact that the effect of creep is implicitly included in the stress-strain curves. The

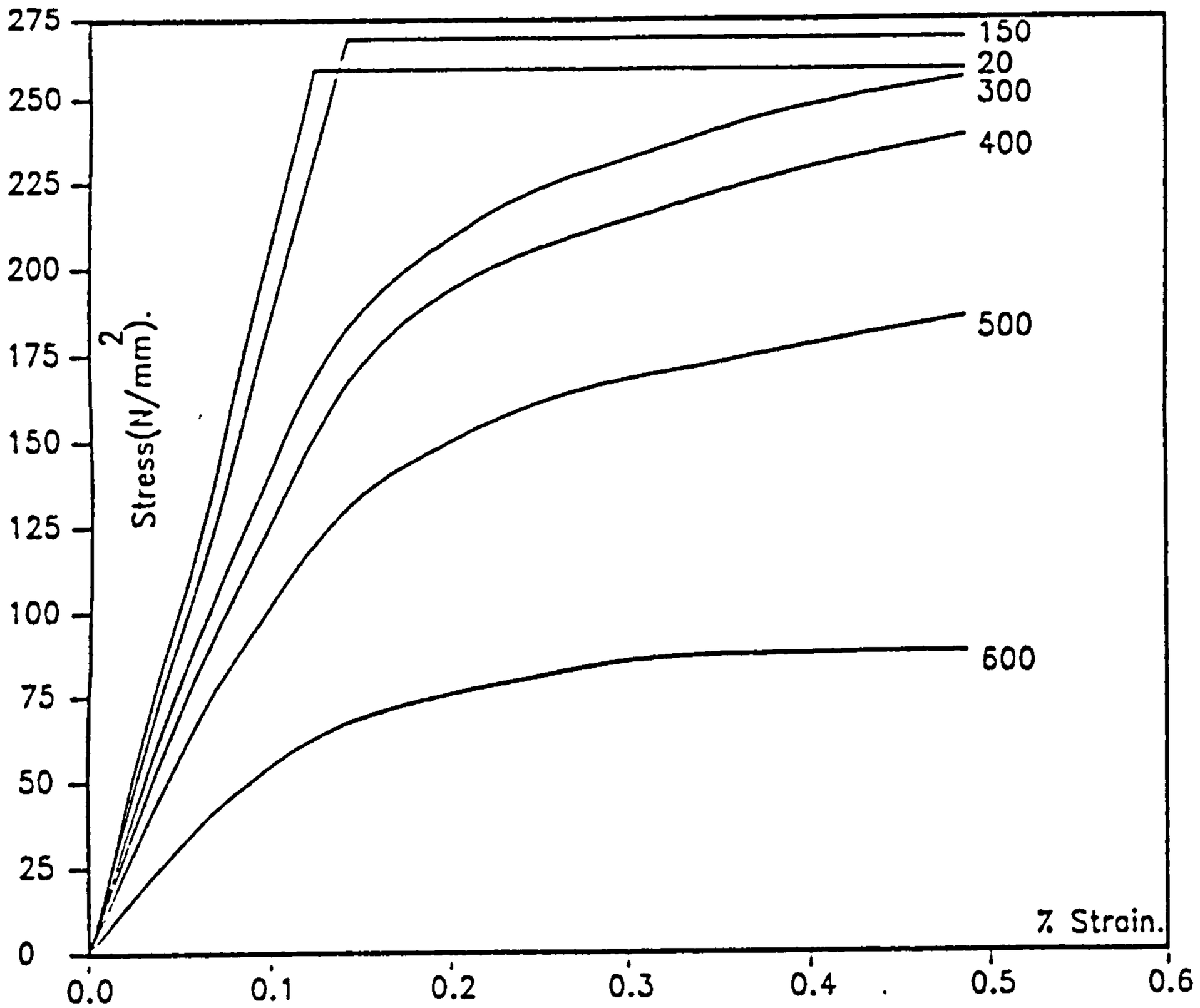

Fig.2.3: Low-speed test.

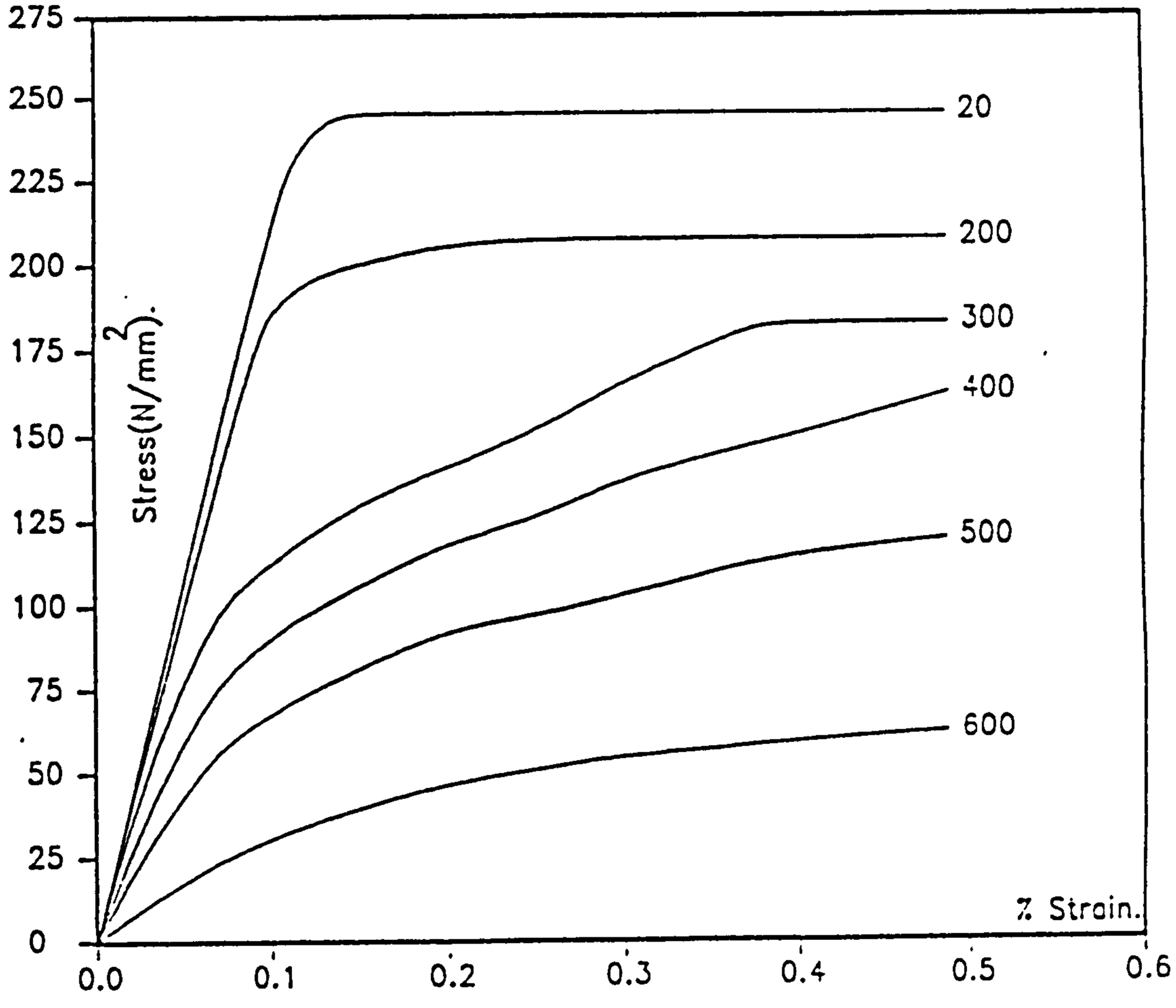

Fig.2.4: Warm-creep test.

Figure 2.3-4: Experimental stress-strain curves of steel at elevated temperature

stress-strain curves obtained from a warm-creep test are shown in Figure 2.4.

More recently, in 1985 Baba and Nagura [7] conducted a study on the effect of material properties on the deformation of steel frames in fire. In this study the authors used both a high- temperature tensile test and a high-temperature creep test to determine the modified stress-strain curves at elevated temperature. The analysis was carried out by using two material models, differing only in their consideration of the effect of creep. The results showed that creep had little effect on the total deformation.

2.4.1.1 Mathematical representation of stress-strain curves.

Normally the stress-strain curves of steel determined from test results are non-linear in form [7],[56]. The idealised form of stress-strain curve is usually expressed as a perfectly elastic-plastic relationship which is characterised by Young's Modulus and yield stress at elevated temperature. The mathematical models for the variation of Young's Modulus and yield stress at elevated temperature postulated by several authors will be discussed in the following section.

Bi-linear stress-strain representations for steel at elevated temperature have also been adopted by some authors

to represent approximately its material properties in fire [11],[63],[64],[65],[66]. The general mathematical form for this approximation is given by:

$$\sigma = E_1 \varepsilon \qquad \varepsilon \leq \varepsilon_1$$

$$\sigma = E_1 \varepsilon_1 + E_2 (\varepsilon - \varepsilon_1) \qquad \varepsilon \geq \varepsilon_1 \qquad \text{.....2.8}$$

where σ is stress, ε is strain, ε_1 is the limiting strain and E_1 and E_2 are the slopes of the straight lines as shown in Figure 2.5. However, to obtain a close representation of the non-linear stress-strain curves, the number of linear steps should adapt to the shape of the curves as shown in Figure 2.6. Cooke [20] introduced multi-linear stress-strain curves of steel in fire.

An alternative method of representing mathematically the stress-strain curves of steel in fire is by a single form of non-linear equation. The approach offers an advantage in describing curves with a continuous change of slope, which eliminates the analytical difficulty of dealing with discontinuous curves which are described by two or more equations [38]. Authors who have introduced such relationships include Nagura and Baba [7], Cheng [68], Burgess, El-Rimawi and Plank [67]. In the latter case a basic form of the Ramberg-Osgood equation was used to represent the family of curves for steel at elevated

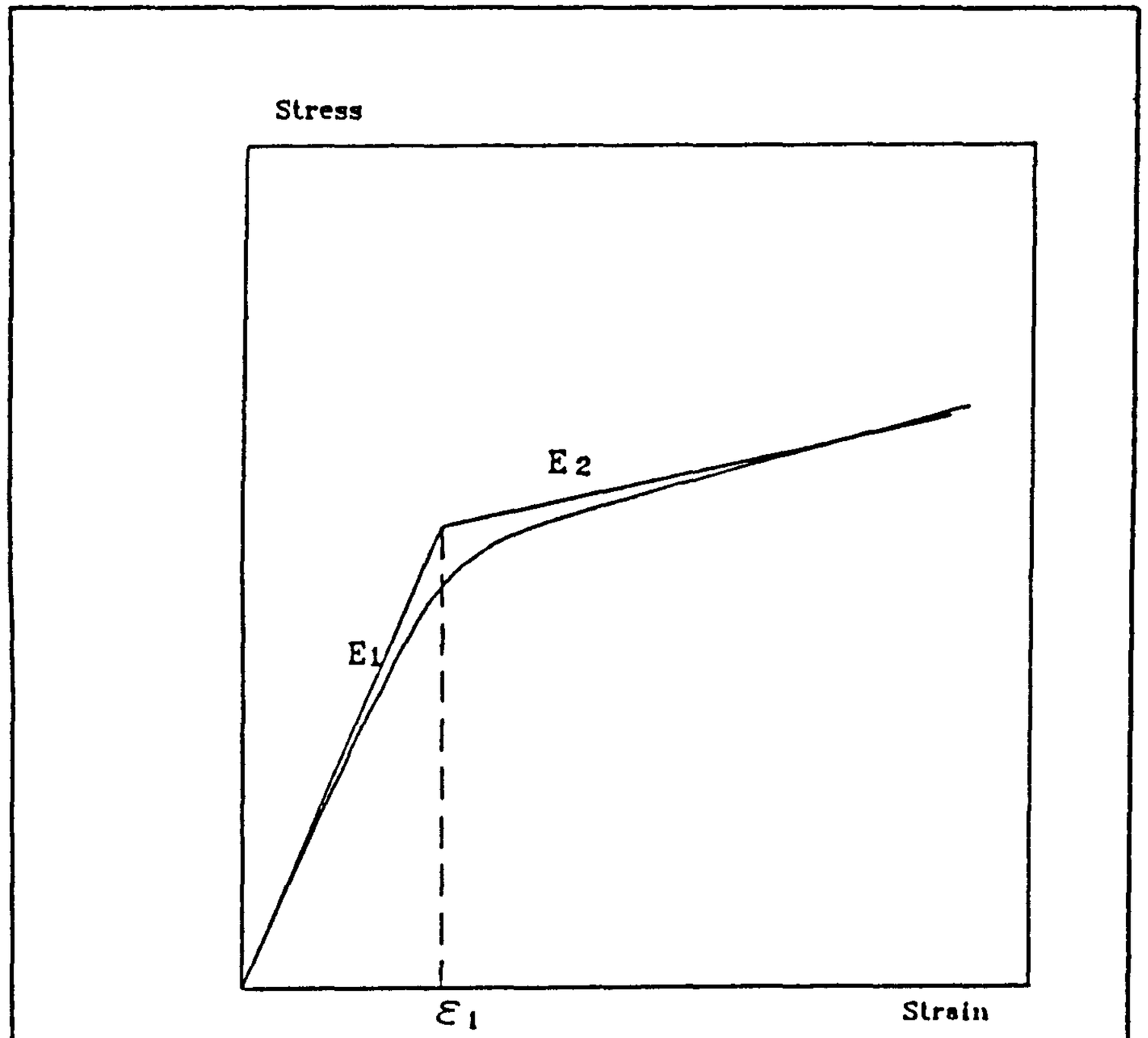

Figure 2.5: Bi-linear representation of stress-strain curve.

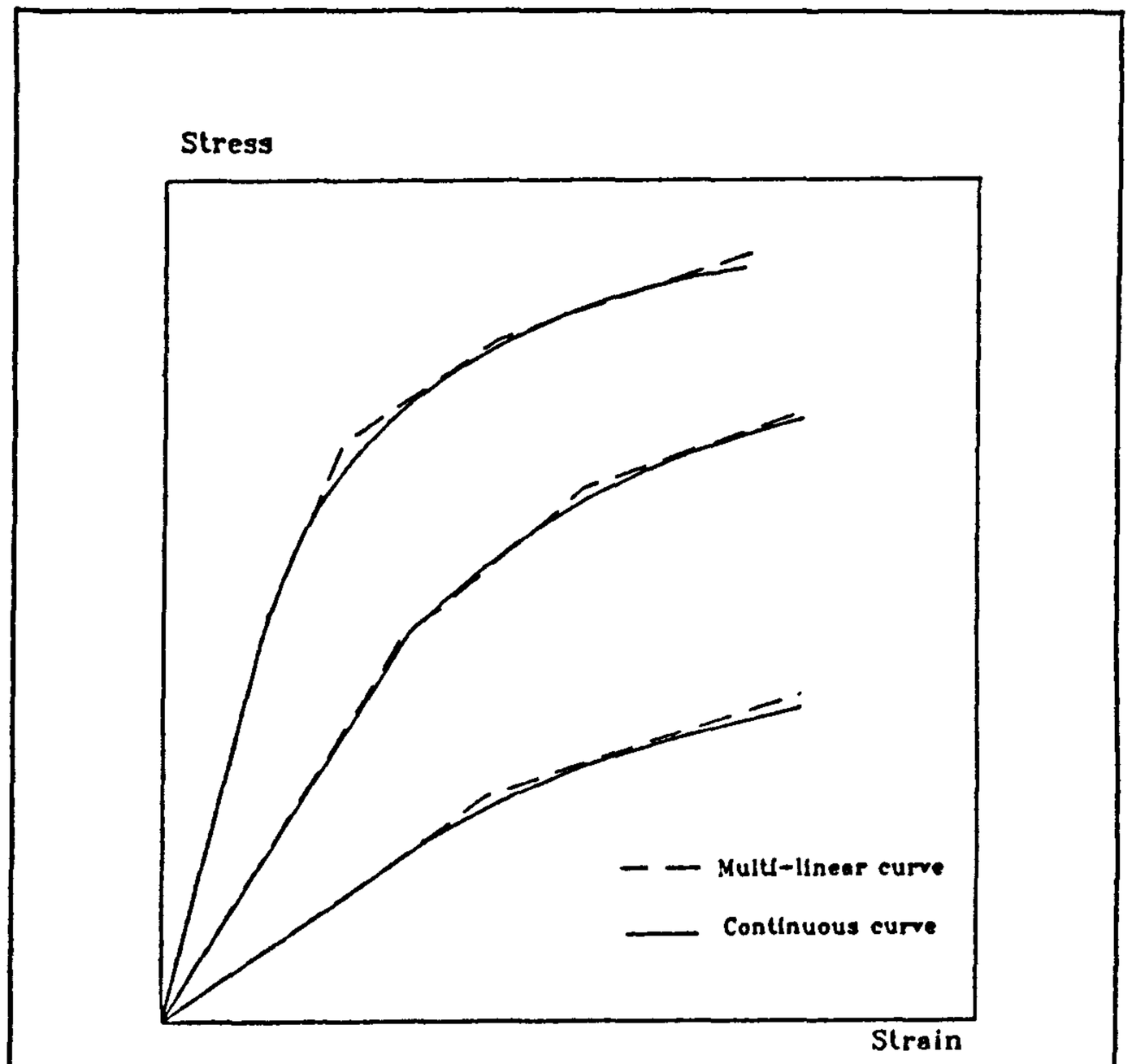

Figure 2.6: Multi-linear representation of non-linear stress-strain curves.

temperature contained in the draft British Standard BS 5950: Part 8 [69], based on results given by Kirby [70]. The weakness of this approach is the difficulty of fitting a family of stress-strain curves with a single equation [38].

2.4.1.2 Young's Modulus.

As was mentioned earlier the simplified form of stress-strain curves of steel at elevated temperature is in perfectly elasto-plastic form characterised by Young's Modulus and yield stress. Mathematical models have been introduced by several authors [60],[71],[73]. From the reported results it is generally agreed that Young's Modulus decreases with increasing temperature. However the precise rate of decrease depends on the exact composition and treatment of the material. As an example it is reported [75] that the Young's Modulus of cold drawn steel is lower than for hot-rolled steel by as much as 20% at 600°C.

Several mathematical models have been suggested to represent the effect of temperature on Young's Modulus [60],[73],[76],[77]. The equations suggested by the ECCS and CTCIM are as follows:

1. ECCS [73].

$$E_t = E_{20} (1 - 17.2\times10^{-12}T^4 + 11.8\times10^{-9}T^3 - 34.5\times10^{7}T^2 + 15.9\times10^{-5}T) \quad \text{.....(2.9)}$$

2. CTCIM [60].

$$E_t = E_{20} \left(1 + T / \left(2000 \ln (T/1100) \right) \right) \quad \ldots\ldots\ldots (2.10)$$

where E_t = Young's Modulus at elevated temperature.

E_{20} = Young's Modulus at ambient temperature (20°C)

T = temperature in °C.

These two equations are plotted in Figure 2.7.

Comparing the ECCS and CTCIM recommendations for Young's Modulus, the curves show a similar relationship up to a temperature of 450°C, after which they no longer coincide. It can be seen that the curve from ECCS is more conservative than CTCIM when the steel temperature is beyond 450°C. It is possible that this is due to different materials or different types of testing procedure.

2.4.1.3 Yield Stress.

For continuously varying stress-strain curves of steel at elevated temperature, there is no sharply defined yield point at which the elastic behaviour ends [5],[67]. However, for practical purposes a yield stress (or proof stress) is defined when the plastic strain reaches a considerable value such as 1%, as was proposed by Skinner [57]. In BS 5950: Part 8 [69], yield stress is defined

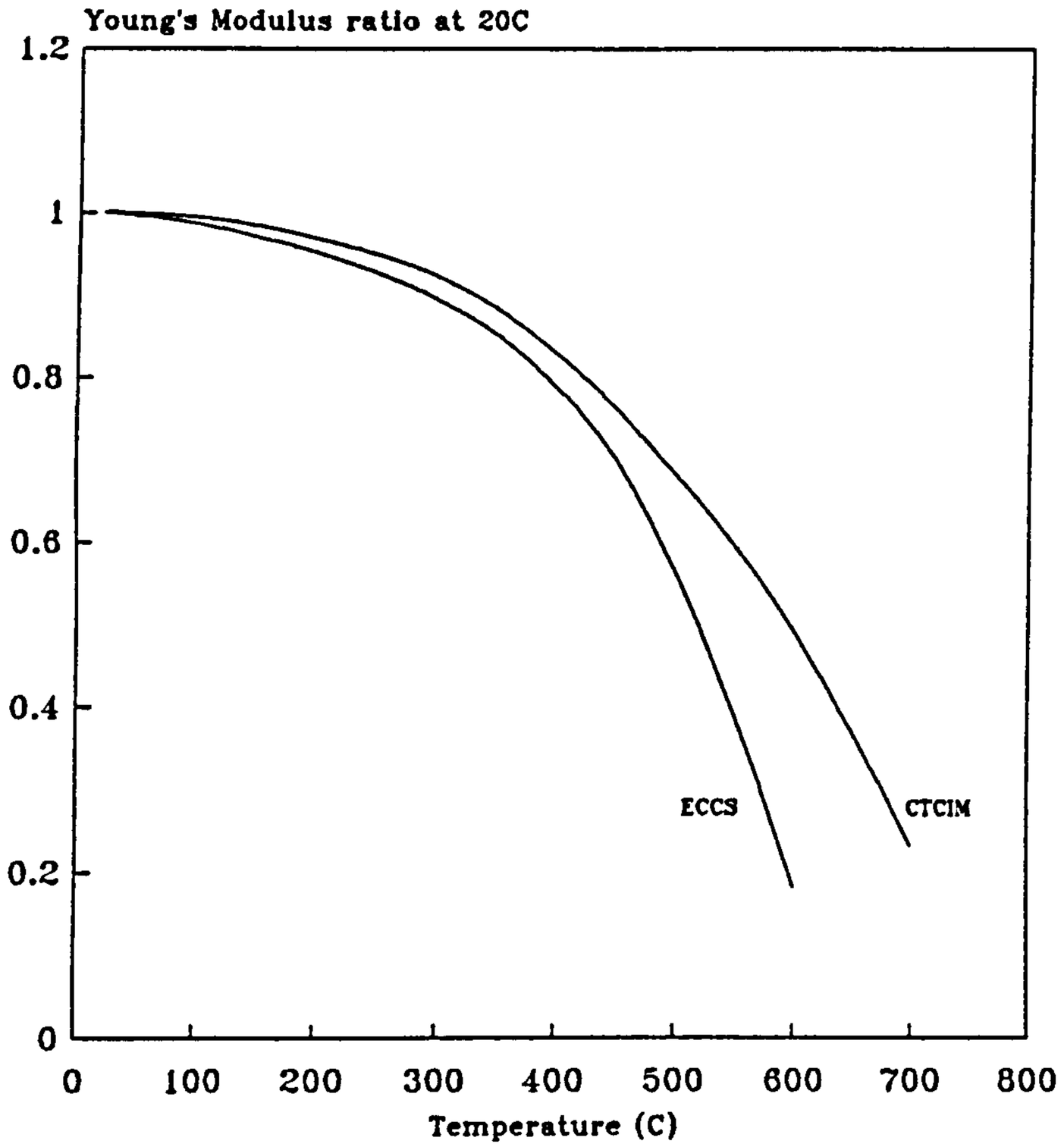

Figure 2.7: Variation of Young's Modulus with temperature.

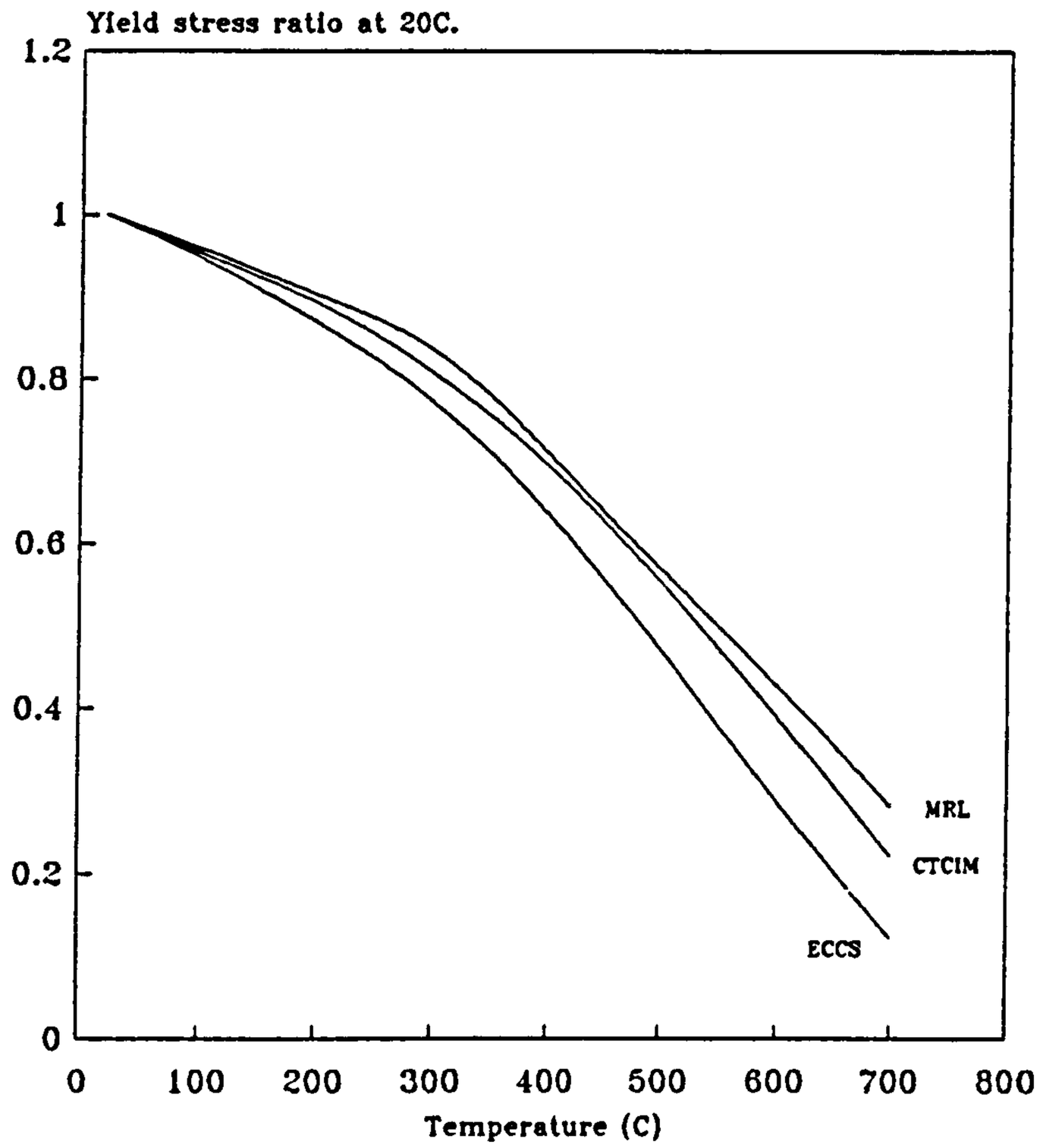

Figure 2.8: Variation of yield stress with temperature.

when the strain at elevated temperature reaches 1.5%.

Mathematical models of the yield stress of steel from ECCS, MRL and CTCIM are shown below:

1. ECCS [73]

$0 \leq T \leq 600°C$

$$\sigma_{yT} = \sigma_{y20}\left(1 + \frac{T}{767\ln(T/1750)}\right) \quad \text{.....(2.11)}$$

$600°C \leq T \leq 1000°C$

$$\sigma_{yT} = \frac{\sigma_{y20}108\ (1 - (T/1000))}{T-440} \quad \text{.....(2.12)}$$

2. CTCIM [60].

$0 \leq T \leq 600°C$

$$\sigma_{yT} = \sigma_{y20}\left(1 + \frac{T}{900\ln(T/1750)}\right) \quad \text{.....(2.13)}$$

$$\underline{600°C \leq T \leq 1000°C}$$

$$\sigma_{yT} = \frac{\sigma_{y20}\ (\ 340 - 0.34T)}{T-240} \quad \text{.....(2.14)}$$

3. MRL [78]

$$\underline{0 \leq T \leq 300°C}$$

$$\sigma_{yT} = \sigma_{y20}\ (\ 1 - (T/2000)) \quad \text{.....(2.15)}$$

$$\underline{300°C \leq T \leq 895°C}$$

$$\sigma_{yT} = \frac{\sigma_{y20}\ (\ 895 - T\ )}{700} \quad \text{.....(2.16)}$$

where σ_{yT} = yield stress at elevated temperature.

σ_{y20} = yield stress at ambient temperature (20°C)

T = temperature in °C

The equations are plotted in Figure 2.8.

It can be seen that the ECCS recommendation is more conservative than either of the others.

2.4.2 Thermal expansion.

The effect of temperature increase on thermal expansion is normally characterised by the coefficient of thermal expansion α_T [57],[73] which is defined as the tangent of the temperature-strain curve at the corresponding temperature. A typical curve of expansion of steel with temperature is shown in Figure 2.9 [5],[20],[79]. The figure shows that thermal expansion increases steadily as temperature increases up to 700°C. Between 700°C and 900°C there is a discontinuity in the expansion due to the phase transformation from Ferrite to Austenite, but at higher temperatures the rate of expansion once again becomes almost constant.

Mathematical models for free thermal expansion that have been suggested by certain authors [11],[73] are as follows:

1. $\varepsilon_T = \alpha T$

where ε_T = thermal strain.

T = temperature difference in °C.

α = coefficient of thermal expansion

= 1.4×10^{-5} °/C [73].

2. $\varepsilon_T = 5.04 \times 10^{-9} T^2 + 1.13 \times 10^{-5} T$ [11].

The equations are plotted in Figure 2.10.

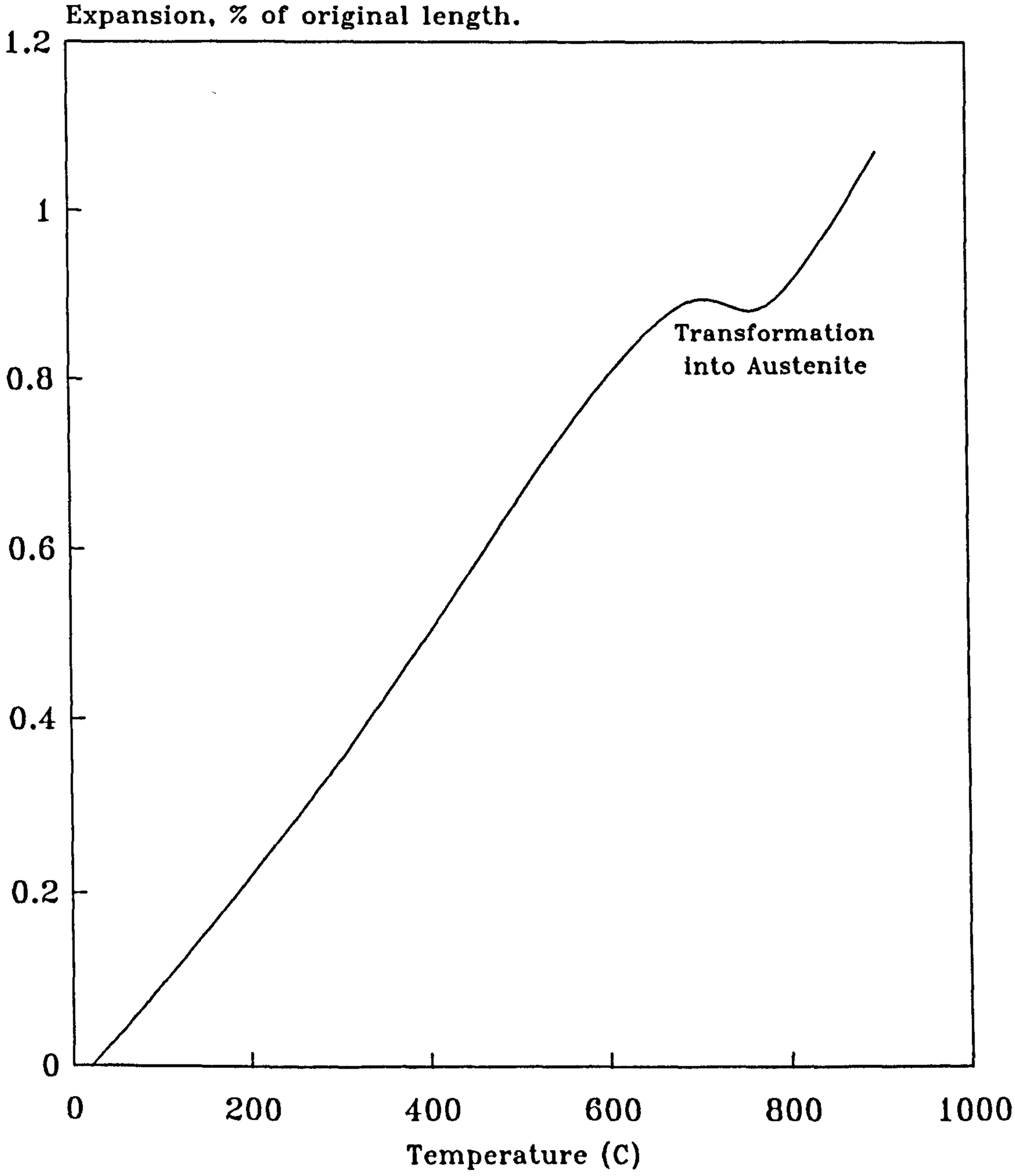

Figure 2.9: Typical curve of expansion of steel with temperature.

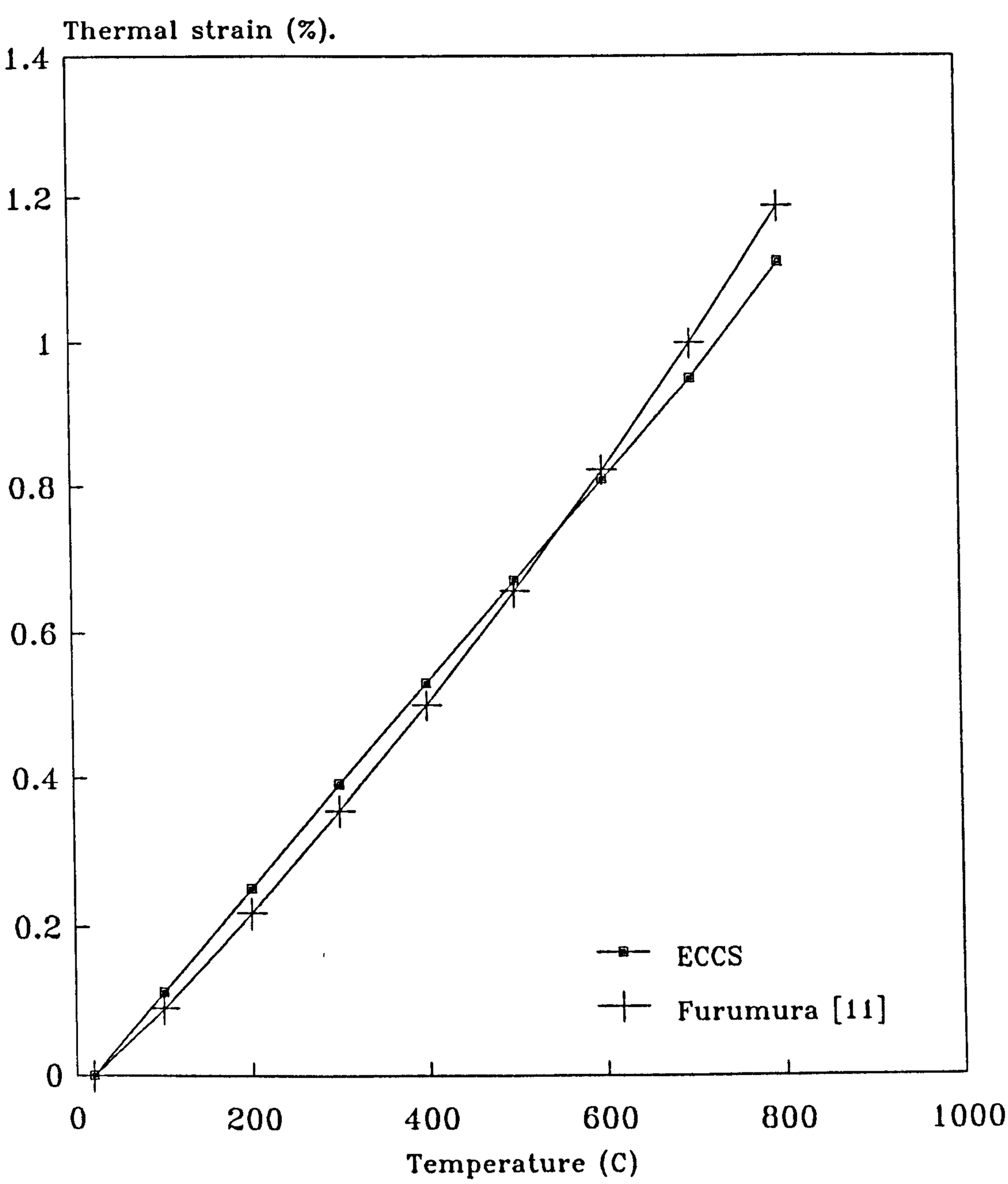

Figure 2.10: Thermal strains from different mathematical models.

2.5 STEEL TEMPERATURE IN FIRE.

The prediction of steel temperature in fire is a very complex matter because of the many variables involved, including the rate of development of the fire and its duration. In the ECCS, CTCIM and MRL recommendations, the simplified heat flow analysis is based on the fundamental heat transfer laws [19],[80], including conduction, convection and radiation [19]. One of the simplifying assumptions commonly made is that the steel temperature is uniform, that is that the thermal conductivity of the steel is infinite [57]. In general a high thermal conductivity will lead to a lower temperature gradient and hence less thermal distortion. This approach generates a very good approximation of the steel temperature in fire if the steel element is heated on all sides, or if it is fully protected by fire protection material. Several mathematical models have been developed based on this principle to determine the protected and unprotected steel temperatures in fire [1],[19],[81].

However, when the steel element is protected by floor slabs or walls or is not heated on all sides the steel temperature profile within the cross-section can become highly non-uniform. The floor slabs or walls can act as heat sinks which consequently decrease the adjacent steel temperatures [20]. The influence of the presence of floor slabs or walls and the direction of fire on the structural steel

elements are shown in Figures 2.11 and 2.12. In this case thermal conductivity is an essential parameter in determining the steel temperatures [57]. A lower value of thermal conductivity will increase the temperature gradient and hence increase the thermal distortion. It is very important to recognise that the variation of steel temperature within the section generates a variation of strength across the member and consequently affects the performance of an element [5],[82]. In addition thermal bowing will occur, consequently increasing the deflected shape of the structure [20]. Excessive thermal bowing alone can sometimes create a limiting deflection [20].

Several authors have been involved in developing methods to determine the steel temperature profiles in fire [22],[83],[84],[85],[86]. Among the computer programs which have been developed are FIRES-T3 [22], TASEF-2 [83] and CEFICOSS [84]. The program FIRES-T3 is a three dimensional finite element heat transfer program. It is suitable for use in evaluating the temperature history of solid composite materials such as fire-protected structural steel and reinforced concrete. The model allows consideration of the non-linear thermal properties of the materials and heat transfer from the fire exposure. The solution technique requires an iterative integration process within each time step throughout the exposure period. The model allows consideration of the following design parameters:

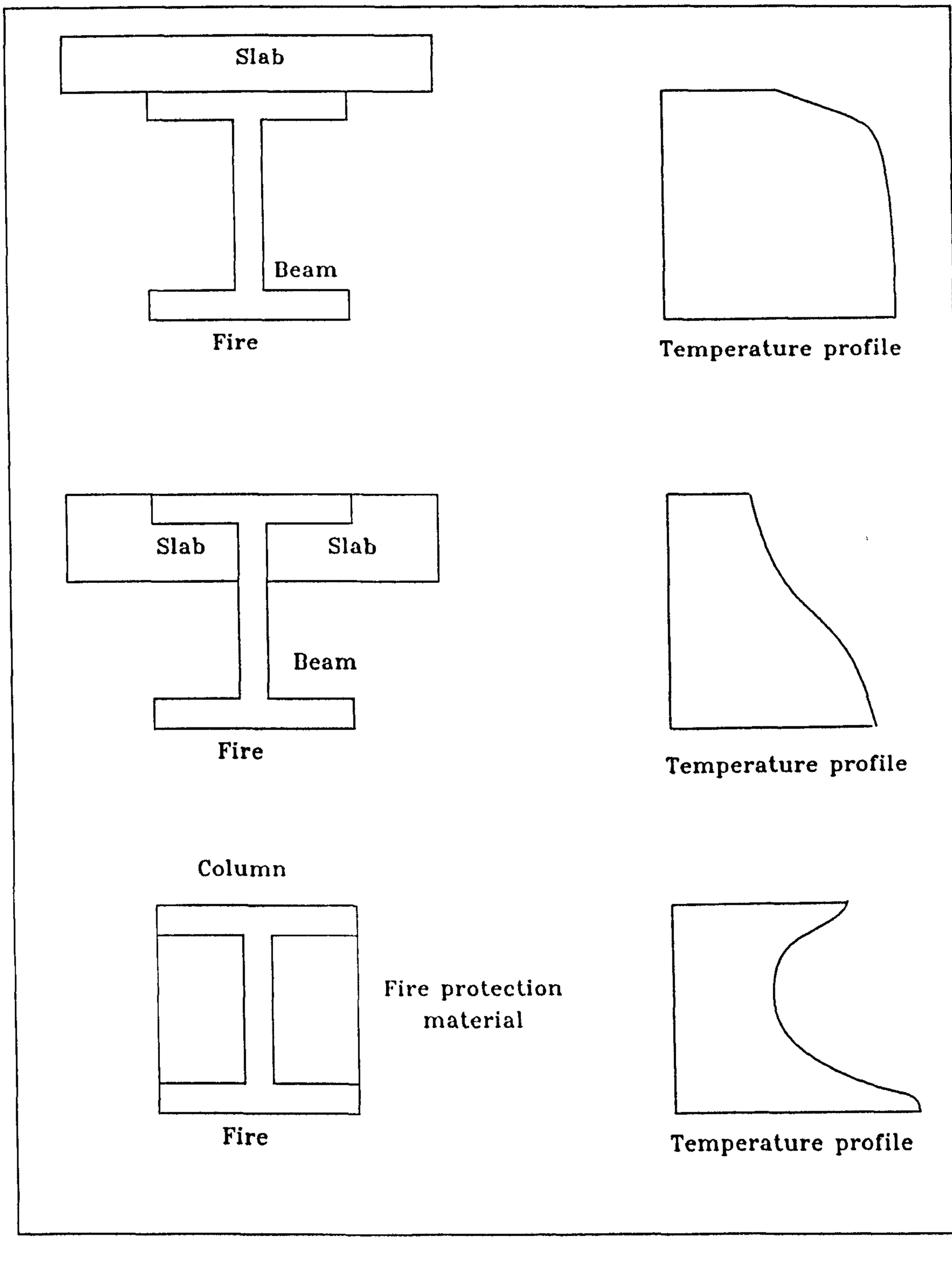

Figure 2.11: Typical variations of steel temperature within the cross-section of different construction forms.

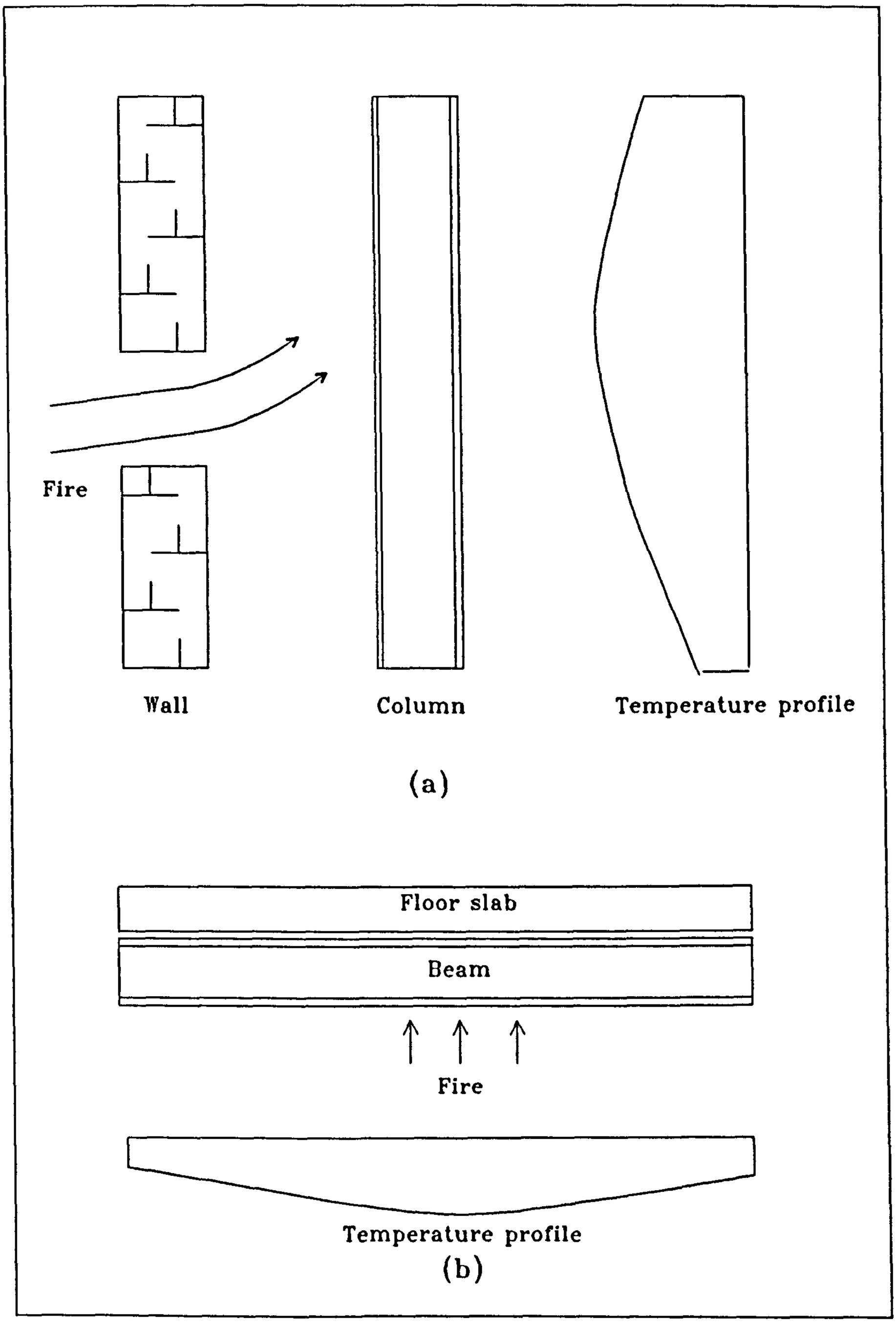

Figure 2.12: Variation of steel temperature along a column and a beam span.

1. Material properties - thermal properties (thermal conductivity and specific heat) and density of materials are considered with respect to their change in value at elevated temperature.

2. Fire environment - the time-temperature history of the fire environment is considered by specifically defining the temperature at each time step during the solution. It can take any form, for example constant temperature, linear change or natural burning.

3. Heat transfer - the heat transfer process due to fire exposure is modelled as convection and radiation across the fire boundary and as conduction through the member. The emissivity of the flame and surface, view factor and surface absorption are considered in calculating radiation effects.

4. Geometry - The shape and size of the structural element can be considered in one, two, or three dimensions.

The program TASEF-2 [83], is a two-dimensional finite element heat transfer program. Structures with voids, where heat exchange occurs by radiation and convection between enclosure surfaces can also be analysed.

The results obtained from the two programs described above are intended to produce thermal data for separate computer programs for evaluating the structural response. However

there are cases in which the structural response can affect the thermal analysis. An example of this is the spalling of concrete or a fire-protective coating [84]. In this case alternate thermal and structural analyses can be carried out. The computer program CEFICOSS [84] implements such a procedure. The thermal analysis is based on a finite difference method, where the values of the temperature at a given time are obtained explicitly at the end of the previous time step.

2.6 METHODS OF ANALYSIS OF FRAME STRUCTURES IN FIRE.

In the early stages of development of analytical methods for steel structures in fire, the analysis evolved around the concept of "critical temperature", which rests on two major assumptions [88],[89],[90]:

1. For protected and unprotected steel elements the steel provides the main strength of the structural unit.

2. Fire resistance is only concerned with the time of collapse of a structural element, not with its deformation history prior to collapse or its possible reusability after a fire.

The above assumptions were only valid for steel with perfectly elastic-plastic stress-strain curves, for which the critical temperature of a structural element is defined

as the average cross-sectional temperature at which the element can no longer support the design loads [88]. However, in the case where the stress-strain curves in fire are non-linear, the maximum strength of the steel cannot be firmly defined due to the fact that no definite yield point exists. Because of this the collapse criterion is based on the concept of limiting deflection [20].

It is suggested that the response of a structural element can be calculated in two steps:

1. Calculation of the thermal response; that is the steel temperature history after the commencement of the fire.

2. Calculation of the deformation history of the element up to the point of collapse or limiting deflection.

In the 1960s methods of analysis for steel structures in fire received the attention of a number of researchers from all over the world [91]. In 1967, Witteveen [3] applied plastic analysis to determine the ultimate carrying capacity of statically determinate and indeterminate beams in fire. For instance, the corresponding yield stress ($\sigma_{y\,T}$) and collapse temperature of a simply supported beam can be determined from the relationship given in Equation 2.17.

$$M_p = \sigma_{y\,T} Z_p \quad \ldots\ldots\ldots\ldots\ldots (2.17)$$

where $M_p = wL^2/8$ (for simply supported beam)

Z_p = plastic modulus of cross-section.

w = uniformly distributed load (kN/m)

In 1972, Marchant [75] reported a method of analysis to analyse the behaviour of steel frame structures in fire. The analysis was based on the concept of a limit state of collapse corresponding to the formation of plastic hinges, reducing the statically indeterminate structure into a mechanism. The analysis included the effect of material softening which is represented by variation of Young's Modulus and yield stress. A linear steel temperature variation within the section and thermal expansion were also included. The change of mechanical properties and thermal expansion in each element at increasing temperature were calculated from the steel temperature. In the analysis the end forces of each element were output for every temperature increment and were then compared with the ultimate moments of resistance. When the ultimate moment at any section in the elements is reached a plastic hinge forms and the location and value of the plastic moment are printed. Any excess moment which appears at the hinge is redistributed to the remainder of the building. A further process of redistribution of load is carried out if the moment of resistance is exceeded at any point.

In 1972 [92], Knight developed a method of evaluating the structural performance of a beam subjected to temperature

increase. The analysis includes the effect of variation of Young's Modulus and yield stress, coefficient of thermal expansion and creep at elevated temperature. The beam analysis was carried out in two parts. The first is the elastic-plastic stage, which is governed by elastic-plastic bending theory and covers the temperature range from 20°C to about 250°C. The second stage is when the steel temperature is beyond 250°C, in which the creep effect is included in the analysis. Curvature conditions are calculated at various positions along the beam, and by integrating twice the deflected shape is found. The design stress level and any restraint to expansion were both reported to have a great bearing on the failure times of steel members.

In 1973, Ossenbrugen, Aggarwal and Culver [93],[94],[95] presented a method of analysing the behaviour of axially loaded steel columns subject to thermal gradients across the cross-section. The stress-strain curves at elevated temperature were assumed to be elastic-perfectly plastic as suggested by Brockenbrough [55]. The method of analysis used by the authors is based on Newmark's numerical integration method. The column is discretised into segments along its length and a moment-axial force-curvature-temperature (m-p-k-T) relationship is developed. By using the numerical integration and the m-p-k-T relationship the deflected shape of the column can be determined. To determine the deflected shape of the column at elevated temperature, the following steps are followed:

1. The magnitude of the initial deflections must be chosen such that the maximum moment does not exceed the ultimate moment.

2. Determine the moment at each node along the length of the column. The moment at each node will be equal to the axial force multiplied by the assumed deflection at the node.

3. The curvature associated with the moment at each node can be determined from the m-p-k-T relationship. Since the curvature is now known, the deflection at each node can again be determined. The process is repeated until the calculated and assumed deflections agree to within an acceptable tolerance.

In 1973, Lie and Stanzak [88],[98] developed a method for calculating critical temperatures of protected steel columns. The stress-strain curves of the material are assumed perfectly-elastic plastic. A uniformly heated steel temperature profile is assumed and the buckling stress is given by:

$$\sigma_{cr} = \Pi^2 E_t / (KL/r)^2 \quad \text{.....(2.18)}$$

where $E_t = E/((1+30(F/F_y)^9)/7)$

E = Young's Modulus at temperature T.

σ = stress.

σ_y = yield stress at temperature T.

σ_{cr} = buckling stress.

K = effective length factor.

L = length of column.

r = radius of gyration.

For low slenderness ratios the calculated values of buckling stress will exceed the yield strength of the steel. In this case the failure stress is considered to be the yield strength of the steel at the temperature under consideration.

In 1975, Cheng and Mak [61] developed a computer program to evaluate the large displacement elasto-plastic thermal creep deformation behaviour of steel frame structures. The method of analysis was based on the finite element displacement method which was then extended to include the instantaneous and creep deformations. In the analysis it was assumed that the total strain ε is a combination of instantaneous and time-dependent components which take the form of:

$$\varepsilon = \varepsilon_e + \varepsilon_p + \varepsilon_c + \varepsilon_T \quad \text{.....(2.19)}$$

where ε_e and ε_p = instantaneous elastic and plastic strain.

ε_c = temperature dependent creep strain.

ε_T = thermal strain.

A classical tangent stiffness method was used to determine

the deformation history. The applied load was assumed to remain constant during the fire and a small time increment, dt, is introduced until the failure criterion is reached.

In 1978, Furumura and Shinohara [11],[100] studied the inelastic behaviour of protected steel columns, beams and frames in fire using an elastic-plastic finite element creep analysis. It was noted that the method is basically the same in principle as reference [61] except that they were using different material properties in respect of free thermal strain, stress-strain curves and creep equations.

In 1976, Lie and Stanzak [17] proposed formulas for determining the critical temperatures of structural steel members such as columns, beams and trusses in fire. The formulas depend on the type of the structural member, the length of fire exposure, the material yield strength and its elastic or creep properties.

In 1979, Kruppa [60] investigated the collapse temperatures of steel structures or components such as beams and columns. He also examined the case of elements which cannot freely expand. The stress-strain curves of steel under temperature increase were considered perfectly elastic-plastic and creep was considered as negligible. Various types of temperature profile within the section were considered to determine the collapse temperatures of the structural steel elements. For statically indeterminate beams the collapse temperature was

obtained from the static theorem of plasticity and solved by linear programming.

In 1981, Contro and Giacomini [71] developed a method for analysing frame structures exposed to fire. The method was based on a combined elasto-plastic and limit analysis known as Restricted Basic Linear Programming. The stress-strain curves at elevated temperature assumed perfectly elastic-plastic behaviour characterised by Young's Modulus and yield stress.

In 1982, Iding and Bresler [66] developed a computer program called FASBUS II specifically designed to analyse the fire endurance of steel framed floor systems. The model utilises the finite element method, in which beam elements and triangular plate bending elements are used to represent the frame and slab respectively. The incremental solution used by the model provides for consideration of changes in temperature, with corresponding changes in material properties, throughout the exposure period. Bi-linear stress-strain curves for steel were assumed for the analysis. Using an iterative process the model determines the displacements necessary to bring the structure to a point of static equilibrium under the loads and heating conditions imposed. In addition a creep model for steel at high temperature was also included.

In 1983, Jain and Rao [102] developed a method of analysis

of steel frames in a fire environment. The analysis was based on the finite element method which adopted incremental and iterative procedures. A linear behaviour characterised by Young's Modulus at elevated temperature was assumed, and the effect of geometric non-linearity (creep and large deformation) was included. It was assumed that the total strain is given by:

$$\varepsilon = \varepsilon_e + \varepsilon_c + \varepsilon_T \quad \text{.....(2.20)}$$

where ε_e, ε_c and ε_T are elastic, creep and thermal strains respectively.

The Newton-Raphson technique was used in order to obtain the final solution for displacement at elevated temperature. An iterative process was carried out in order to meet the convergence criterion of displacement.

In 1985, Baba and Nagura [7] developed a method of analysis which was used to evaluate the effect of time-dependent material properties on the structural behaviour of steel structures in fire. The method is based on the finite element method, and uses the incremental approach and an iterative process to determine a full deformation history. A non-linear stress-strain curve with a continuous change of slope, derived from experimental results in which the material was subjected to high-temperature tensile and creep tests, was included in the analysis. They concluded that:

1. Creep has a small effect on the total deformation.

2. Strain hardening should not be neglected in the fire problem.

In 1986, Proe, Bennetts and Thomas [82], proposed a method of calculating the collapse temperature for structural steel members such as beams, columns and frames. The method is based on plastic analysis which includes the effect of non-uniform temperature variation within the section. A simplified design method was also proposed and a comparison was made with the experimental results such as with reference [103].

In 1988, Dotreppe, Franssen and Schleich [84], developed a finite element program called CEFICOSS for composite and steel structures in fire. The simulation of the structure's behaviour when subjected to fire is performed in two steps. Firstly, the structure is analysed under small increments of load at ambient temperature. At each increment the internal forces and displacements are based on the linearised tangent-stiffness matrix. An iteration process based on the Newton-Raphson method is used in order to achieve static equilibrium. This procedure continues at ambient temperature until the design loads have been reached. These are then kept constant during the next stage. Secondly, a time-step is introduced for which a thermal analysis is performed. The current material properties of the cross-section are then calculated based on

the current temperature profile. Next the out-of-balance forces are calculated. These are applied incrementally to the structure until the level of the design loads is reached again and a Newton-Raphson correction is used in order to achieve convergence in displacements. The process is repeated until equilibrium can no longer be obtained.

In 1988, Burgess, El-Rimawi and Plank [67], developed a method of analysis to investigate the behaviour of continuous beams under fire conditions. The analysis is based on the matrix stiffness formulation which utilises the secant stiffness concept. A beam finite element with four degrees of freedom was used which ignores axial deformations. The analysis incorporates material non-linearities and thermal loading due to temperature variation within the section, but geometric non-linearities were ignored. A modified version of the Ramberg-Osgood equation was established to represent the family of stress-strain curves of steel in fire obtained from the BS 5950: Part 8 1985 draft version [70]. Because of the non-linear nature of the problem the solution is iterative. The iterative solution used resembles the mathematical formulation of the Newton-Raphson Method.

2.7 CONCLUSION.

As was mentioned earlier, the stress-strain relationships of steel at elevated temperatures are normally non-linear with

a continuous change of slope, so that a definite yield point cannot be determined. Because of this, the maximum strength of a structural steel element is normally determined on the basis of limiting deflection, as in BS 476:Part 8: 1972 [13].

From the literature review, it was noted that the finite element method has been widely used to evaluate the deformation history of frame structures in fire. However this method requires very powerful computing equipment in terms of storage and computation speed. For implementation on personal computers, matrix stiffness analysis offers a more practical and suitable method than finite elements in evaluating the deformation history of frame structures in fire. This is because the former method requires much less data prior to performing the analysis, and this is of major concern in the present research. Matrix stiffness analysis is very well established as a tool for linear structural problems and can be extended to include non-linear effects.

With regard to non-linear structural analysis the traditional way of implementing the matrix stiffness method is by an incremental approach. In this approach the applied load is divided into small increments, and at each load increment the unknown displacements are determined by the local matrix stiffness analysis. An iterative process is carried out in order to determine the correct value of displacements for each load increment by using the Newton-

Raphson method. It should be noted that the local error is cumulative due to the fact that the error on each load increment depends on the previous value. Greater accuracy can be achieved by reducing the size of load increment but this is time consuming.

An alternative approach is called the secant stiffness method in which, instead of stepping along the load-deflection curve to achieve the final solution, a more direct solution can be achieved by introducing a linear relationship between the load and the actual displacement. The approach offers advantages compared with the incremental approach for the following reasons [38]:

1. A full load-deformation history is not required.

2. The computing time required for the incremental approach is greater than for the secant stiffness approach.

3. The secant stiffness methods relates the load to the actual deformation which consequently increases the inherent accuracy of the analysis. This is unlike the incremental approach in which the local error is cumulative and the analysis at the current load increment depends on the previous analysis.

The approach has been applied successfully in matrix stiffness analysis with which it has been used to evaluate

the deformation history of continuous beams at ambient temperature and in fire [67]. However, it has been noted that the degrees of freedom per member in this analysis were taken as four, so that axial deformation was ignored. In addition, geometric non-linearities were ignored in the analysis. This approach will be extended in the current work to enable it to incorporate the effect of material and geometric non-linearities.

In the present research the matrix stiffness method which utilises secant stiffness will be used to evaluate the behaviour of steel frame structures in fire. The number of degrees of freedom of each member will be taken as six, in order to include axial deformation. The geometric non-linearities which result from the axial shortening due to bending of the member and the p-delta effect will be included in the analysis. The influence of axial force on the moment-curvature relationship will also be included.

In the present research, an idealised form of multi-linear stress-strain curves of steel at elevated temperature are suggested by the author to represent the test results given by Kirby [70]. The data is presented in Table 2.1. The idealised form of the stress-strain curves is shown in Figure 2.13. The figure represents the stress-strain curves of steel for temperatures 20°C, 100°C, 200°C, 300°C, 400°C, 500°C, 600°C and 700°C. In between these temperatures interpolation is used.

	Temperature (C).								
% Strain.	20	100	200	300	400	500	600	700	800
0.00	0.000	0.000	0.000	0.000	0.000	0.000	0.000	0.000	0.000
0.01	0.072	0.072	0.065	0.061	0.052	0.037	0.022	0.008	0.007
0.02	0.144	0.140	0.130	0.123	0.105	0.075	0.045	0.016	0.015
0.03	0.216	0.212	0.195	0.184	0.157	0.112	0.067	0.024	0.022
0.04	0.288	0.281	0.260	0.245	0.209	0.150	0.089	0.032	0.029
0.05	0.360	0.353	0.325	0.306	0.262	0.187	0.111	0.041	0.037
0.06	0.432	0.421	0.389	0.368	0.314	0.224	0.134	0.049	0.044
0.07	0.503	0.493	0.454	0.429	0.366	0.262	0.156	0.057	0.051
0.08	0.575	0.562	0.519	0.490	0.418	0.299	0.177	0.065	0.058
0.09	0.647	0.634	0.584	0.518	0.458	0.336	0.190	0.073	0.055
0.10	0.719	0.702	0.649	0.535	0.477	0.374	0.201	0.081	0.055
0.12	0.863	0.842	0.779	0.567	0.516	0.401	0.220	0.097	0.056
0.14	1.000	0.918	0.816	0.597	0.547	0.426	0.238	0.105	0.056
0.16	1.000	0.935	0.837	0.623	0.572	0.445	0.252	0.110	0.057
0.18	1.000	0.950	0.853	0.645	0.593	0.465	0.265	0.116	0.058
0.20	1.000	0.960	0.867	0.666	0.613	0.482	0.278	0.122	0.059
0.25	1.000	0.965	0.899	0.711	0.658	0.519	0.303	0.137	0.060
0.30	1.000	0.965	0.917	0.752	0.697	0.550	0.325	0.150	0.062
0.35	1.000	0.965	0.931	0.783	0.729	0.574	0.343	0.161	0.064
0.40	1.000	0.965	0.938	0.812	0.754	0.594	0.358	0.171	0.065
0.50	1.000	0.965	0.946	0.845	0.798	0.622	0.378	0.186	0.068
0.60	1.000	0.965	0.948	0.885	0.829	0.649	0.394	0.194	0.070
0.70	1.000	0.965	0.950	0.905	0.861	0.676	0.407	0.197	0.071
0.80	1.000	0.965	0.952	0.923	0.892	0.695	0.421	0.198	0.073
0.90	1.000	0.965	0.953	0.936	0.913	0.711	0.432	0.200	0.073
1.00	1.000	0.965	0.955	0.946	0.935	0.722	0.438	0.201	0.073

Table 2.1: Elevated temperature stress–strain data for steel BS 4360, Grade 43.

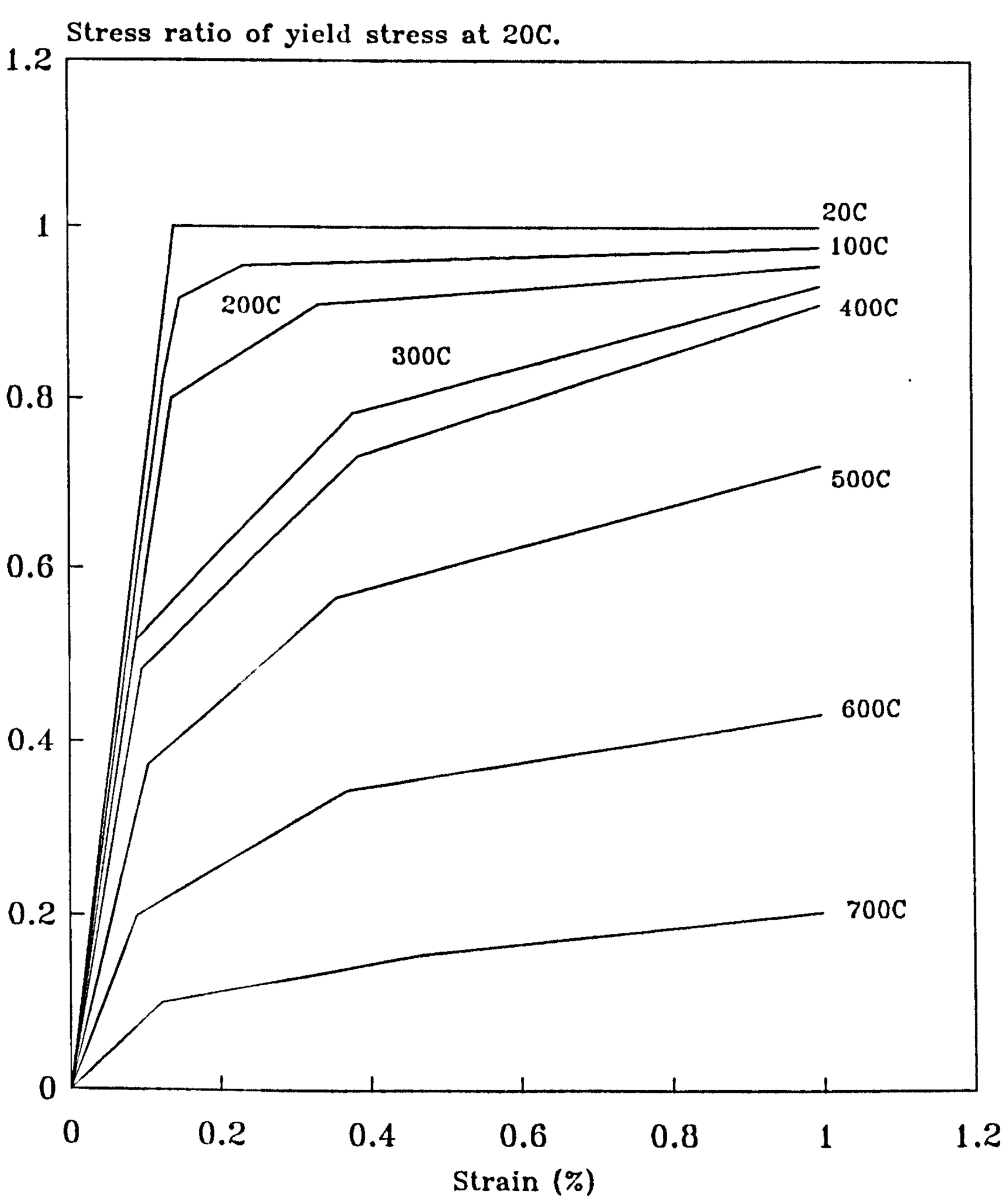

Figure 2.13: Idealised stress–strain curves of steel at elevated temperature.

It should be noted that the stress-strain data of Table 2.1 represents the stress at any temperature as a proportion of the yield stress at 20°C. A value of 205000 N/mm² is assumed for Young's Modulus at 20°C and consequently the corresponding yield stress in Figure 2.13 is equal to 287 N/mm². The curves in Figure 2.13 will be modified in order to cater for any grade of steel which has a different value of yield stress at 20°C. To suit any grade of steel the initial yield strain at elevated temperature is modified to take the form:

$$\varepsilon_{T1} = \sigma_{y20}\,\varepsilon_{t1}/287 \quad \text{.....(2.21)}$$

where ε_{T1} = the yield strain at T°C for the steel grade considered.

ε_{t1} = the yield strain at T°C of figure 2.13.

Figs. 2.14 and 2.15 show a comparison of the proposed multi-linear stress-strain curves of steel of grades 43 and 50 respectively against the results obtained from tests [5],[70]. It can be seen that the curves have shown very good agreement. In case of strains greater than 1%, the slope of stress-strain curves is taken as one tenth of the previous slope at the corresponding temperature level.

The other aspect which is examined in some detail in the present work is the effect of material unloading on the moment-axial force-curvature relationship. A 'beam-column'

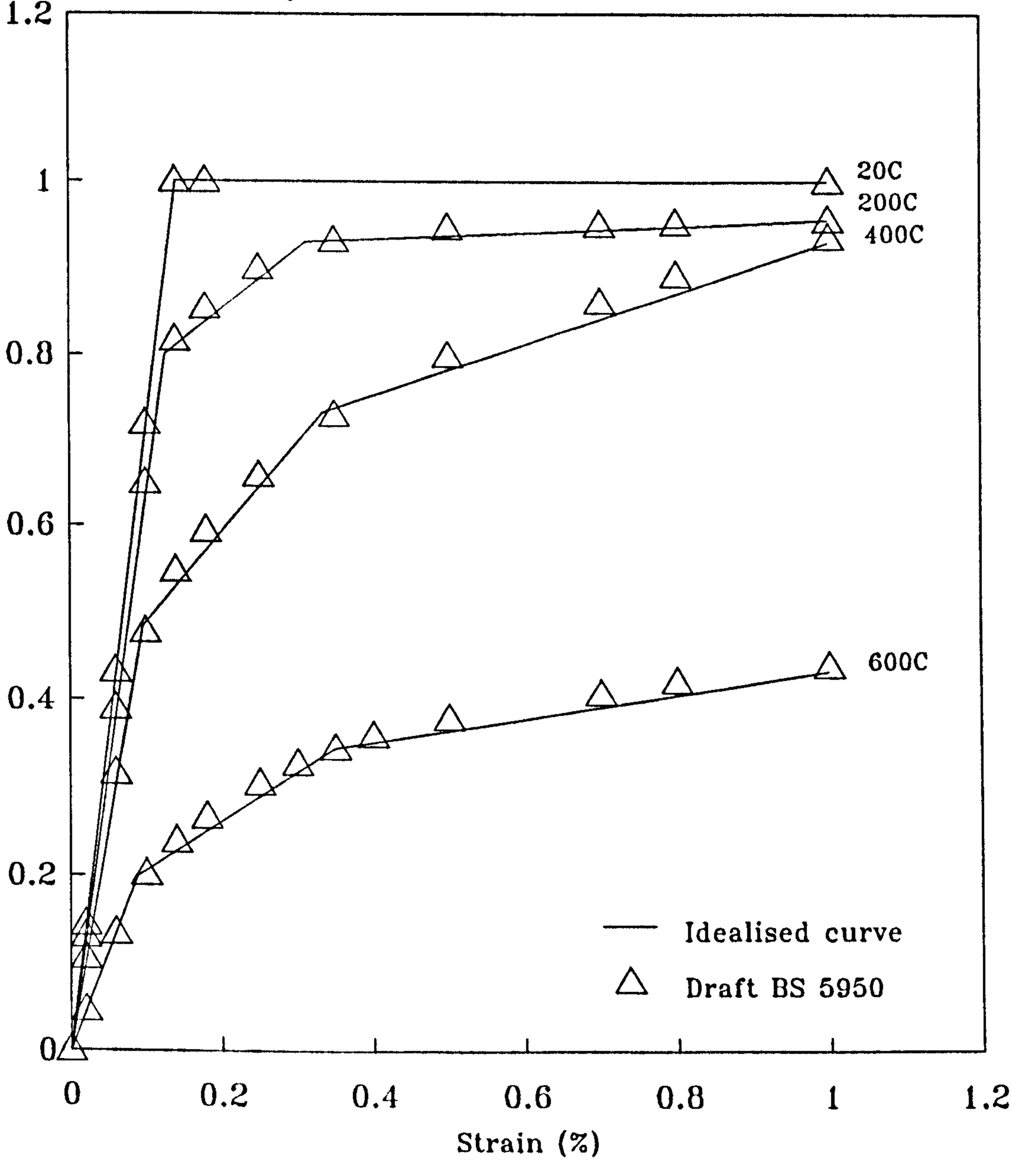

Figure 2.14: Comparison of idealised stress–strain–temperature curves with BS 5950: Part 8 data (draft) for grade 43.

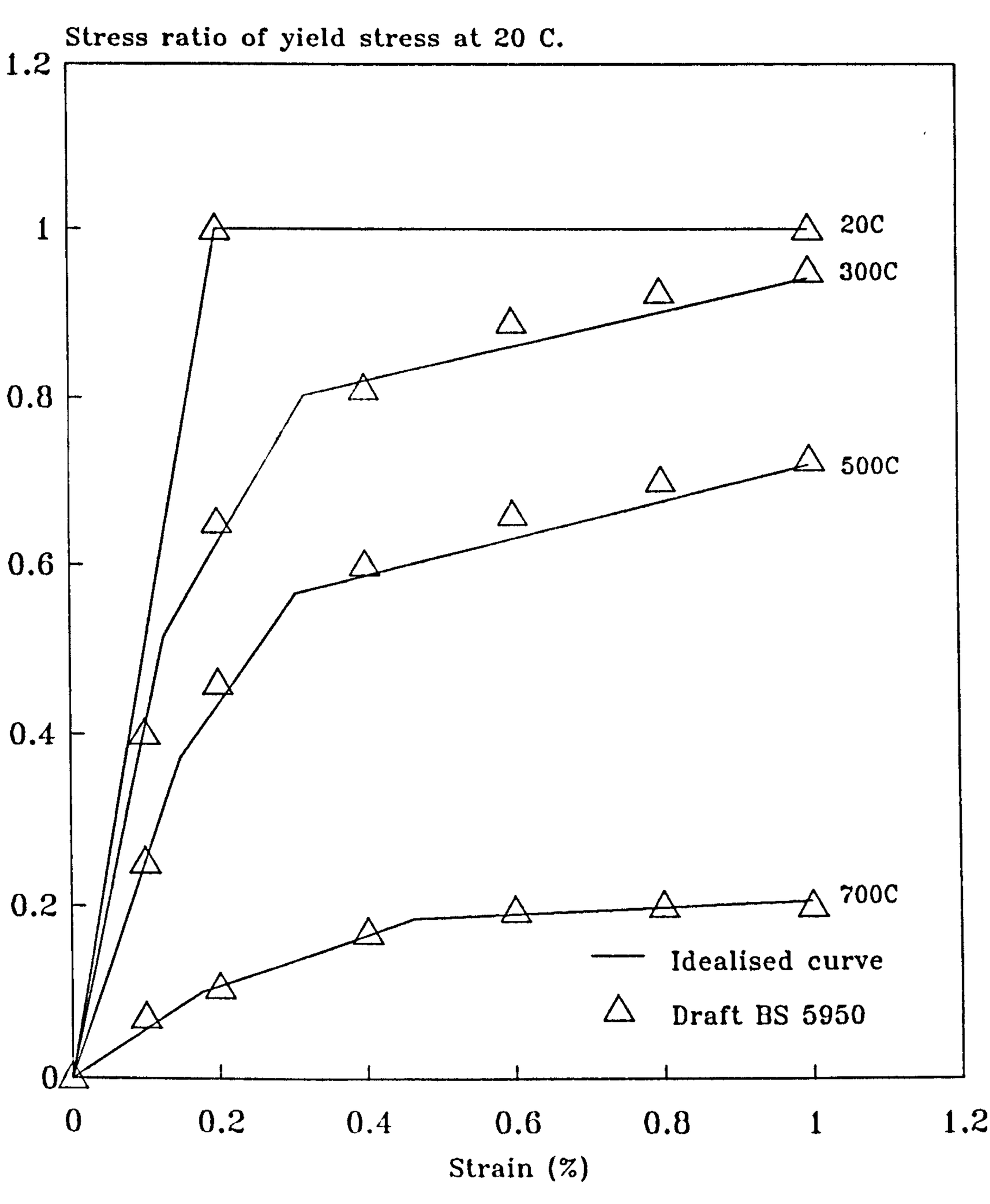

Figure 2.15: Comparison of idealised stress–strain–temperature curves with BS 5950: Part 8 data (draft) for grade 50.

element is defined as an element that is subjected both to bending moment and axial force, but the rates at which these loads are applied to the element are not clearly defined. From the literature review it has been demonstrated that the derivation of moment-axial force-curvature relationship is often based on the assumption that bending moment and axial force are applied simultaneously and in proportion from a zero stress-state. This is not necessarily the case when temperature effects are included and hence this problem will be investigated further.

The effect of material unloading will be extended to the case of fire. This is because, apart from the variation of stress-strain curves in fire, material unloading inevitably happens to an element if it is fully restrained from longitudinal expansion. Suppose the element is subjected to bending moment at ambient temperature and fully restrained against thermal expansion. If heating is then introduced an axial force is induced, and consequently the position of the neutral axis shifts in order to create an equilibrium condition. As a result material unloading inevitably happens.

CHAPTER THREE

GEOMETRIC AND MATERIAL NON-LINEARITIES IN MATRIX STIFFNESS ANALYSIS

3.1 INTRODUCTION.

When loading is applied to a structural frame, the frame can no longer maintain its geometrical shape. The method that is normally used to evaluate the corresponding deformation is the matrix stiffness method. This has been applied successfully to a wide range of linear elastic structural problems [23],[116] in which the flexural and axial stiffness in the element stiffness matrix are characterised by Young's Modulus `E', cross-sectional area `A', and second moment of area of the cross-section `I'. The stress-strain curve of the steel material is assumed to behave in a linear-elastic manner without yielding.

However the behaviour of a frame structure depends, beyond its initial loading range, on non-linear terms governing its material properties and its geometric behaviour. These effects are ignored in linear elastic analysis. Thus, in order to provide an accurate assessment of the behaviour of frame structures over a greater loading range, such non-

linear effects must be included in the formulation. Material non-linearities are caused by the non-linear nature of the stress-strain relationship of steel, and to the reduction of member strength and stiffness due to the presence of axial force. Geometric non-linearities include axial shortening due to bending of the structural members, and secondary bending caused by axial thrusts acting on the deflected shape, known as the "p-delta effect".

As has been mentioned in the previous chapter the traditional method of solution where these non-linear effects are included in the matrix stiffness method is by using a load increment procedure. This requires gradual stepping along the load-deflection curve. An alternative which provides a more direct solution is the secant stiffness approach. This has been developed for flexural analysis (ignoring axial deformation) [36],[38],[67] and has proved to be more economic in terms of computation time. In the present work, the method is extended to include geometric non-linearities as well as axial load effects for the analysis of in-plane behaviour. In this chapter, the development of a general non-linear matrix stiffness method for structural analysis is discussed. The method is developed initially for ambient temperature conditions and is validated by comparison with other theoretical studies. It is then extended in Chapter 5 to enable non-linear analysis of frames in fire.

3.2 MATRIX STIFFNESS ANALYSIS.

In matrix stiffness analysis of frames the structure is typically represented by an assembly of bar elements (or members) interconnected at nodes (or joints). A complete cycle of analysis involves the determination of both the internal forces and displacements at each node. The equilibrium condition of the structure is described by a system of simultaneous algebraic equations in which the nodal displacements are unknown. A brief review of the process of matrix stiffness analysis which is now well documented - see for example reference [116] - is given below:

1. The number of degrees of freedom for every element is defined. In plane frame structures, in which both bending moment and axial force are considered, the number of degrees of freedom is 6 (i.e 3 at each end of the element). These are the rotation `δΘ', and two displacement components at each node, as shown in Figure 3.1. A coordinate system is established to identify the location of nodes and direction of displacements at those nodes.

2. The element forces, corresponding to each of the degrees of freedom, are introduced at the nodes as shown in Figure 3.2. These forces are related to the displacements using an appropriate `elastic' relationship and the condition of equilibrium for each individual element.

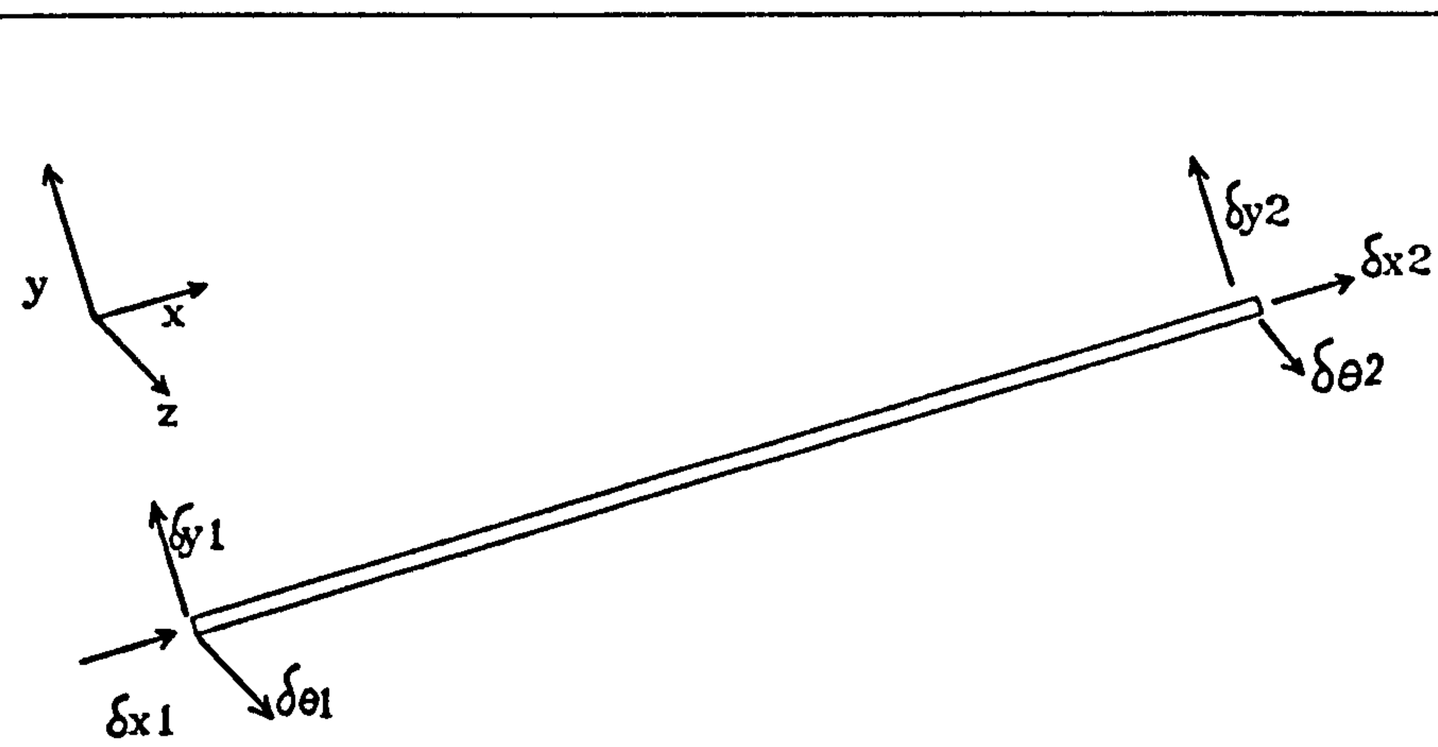

Fig.3.1: Displacements of beam-column element

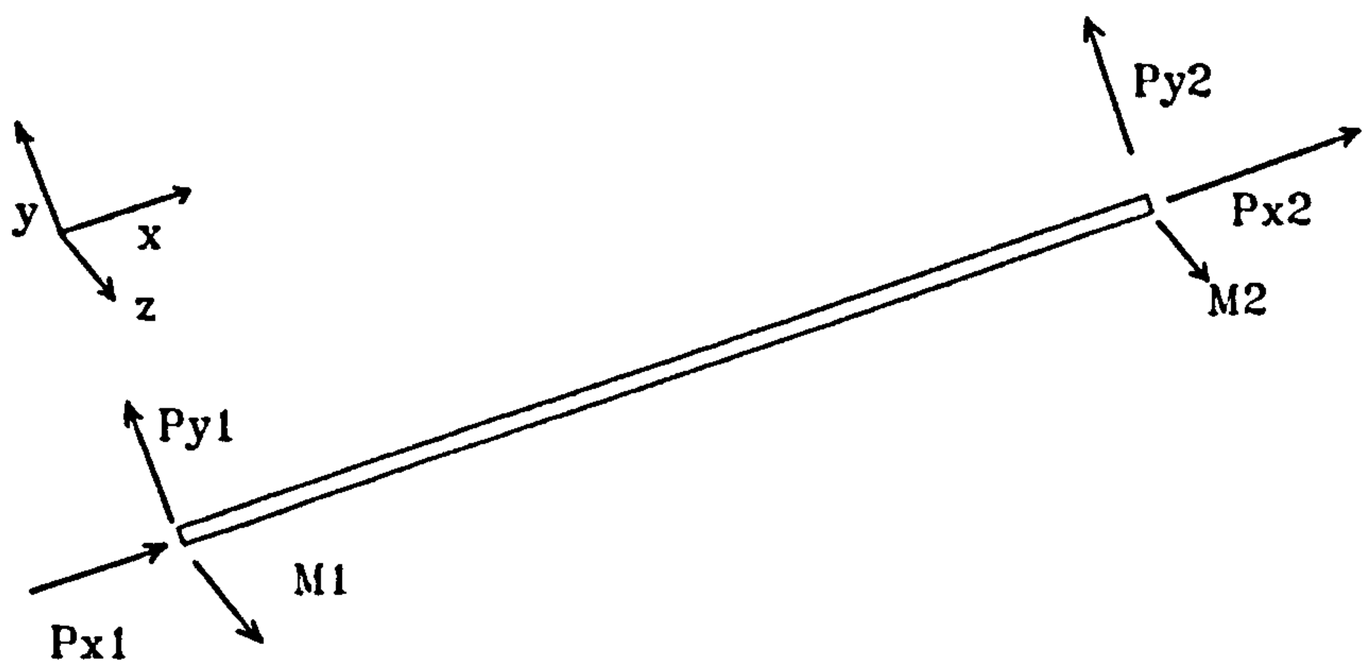

Fig.3.2: Forces of beam-column element

3. A complete analysis involves the determination of both displacements and forces at both ends of each element. The unknown nodal displacements can be determined by solution of simultaneous equations based on the condition of compatibility at each joint. In matrix notation:

$$[K]\{D\} = \{p\} \quad \ldots\ldots\ldots\ldots\ldots\ldots\ldots (3.1)$$

where $[K]$ = the overall stiffness matrix.

$\{D\}$ = vector of displacements.

$\{p\}$ = vector of external loads.

The overall stiffness matrix [K] is obtained from the combination of the individual element stiffness matrices and the procedure is described in [116]. The load vector $\{p\}$ is obtained from a combination of the fixed end forces for every element meeting at a joint.

Having solved for the node displacements, the final stage of the analysis is to determine the forces in each element. To do this the equation takes the form:

$$\{p\}_m = [K]_m [T]_m \{d\}_m + \{p\}_{fm} \quad \ldots\ldots\ldots\ldots (3.2)$$

where $\{p\}_m$ = end forces of each element.

$\{p\}_{fm}$ = fixed end forces of each element which can be calculated from the standard tables [116].

$[K]_m$ = element stiffness matrix.

$[T]_m$ = the condensed element transformation matrix.

$\{d\}_m$ = end displacements of each element in terms of structure, not the element axis.

The method has been applied successfully for linear elastic analysis [23],[116] which is based on the first order linear elastic relationships between member end forces and displacements. However, material and geometric non-linearities can be included by using appropriate force-displacement relationships. In the present work the secant stiffness approach is utilised to cater for the material non-linearity and an iterative procedure is adopted to account for geometric non-linearities.

3.3 ELEMENT STIFFNESS MATRIX.

A beam-column element is an element which is subjected to a combination of axial force and bending moment. In general all members in a frame structure are beam-columns and the corresponding element stiffness matrix will include both effects.

In the present work the formation of the element stiffness matrix is based on small deflection theory, implying the assumption that the curvature of an element is expressed sufficiently accurately by d^2y/dx^2. In addition the flexural and axial stiffness coefficients are assumed constant along the element. The stiffness corresponding to each degree of

freedom is calculated by assuming a corresponding unit displacement while preventing or restraining others as shown in Figure 3.3. In the case of rotation and displacement perpendicular to the element the resulting forces are then calculated using the strain-energy method [116]. In the case of axial displacements the axial force is expressed in terms of the end displacements, neglecting the influence of curvature on end shortening.

The nodal forces and displacements can be written in the form of an element stiffness equation:

$$\{p\}_m = [K]_m \{D\}_m \quad \ldots\ldots\ldots\ldots\ldots\ldots \quad (3.3)$$

where $\{p\}_m$ and $\{D\}_m$ = vector of element force displacement.

$[K]_m$ = element stiffness matrix.

The stiffness matrix $[K]_m$ for a beam-column element is given by Equation 3.4 (shown in Figure 3.4). In linear elastic analysis the axial and flexural stiffness coefficients of a beam-column element, represented in Equation 3.4 by '$(EA)_{eff}$' and '$(EI)_{eff}$' respectively, are equal to 'EA' and 'EI'.

For non-linear materials such as those with multi-linear stress-strain curves described in Chapter 2, the stiffness of the material gradually decreases with load level and

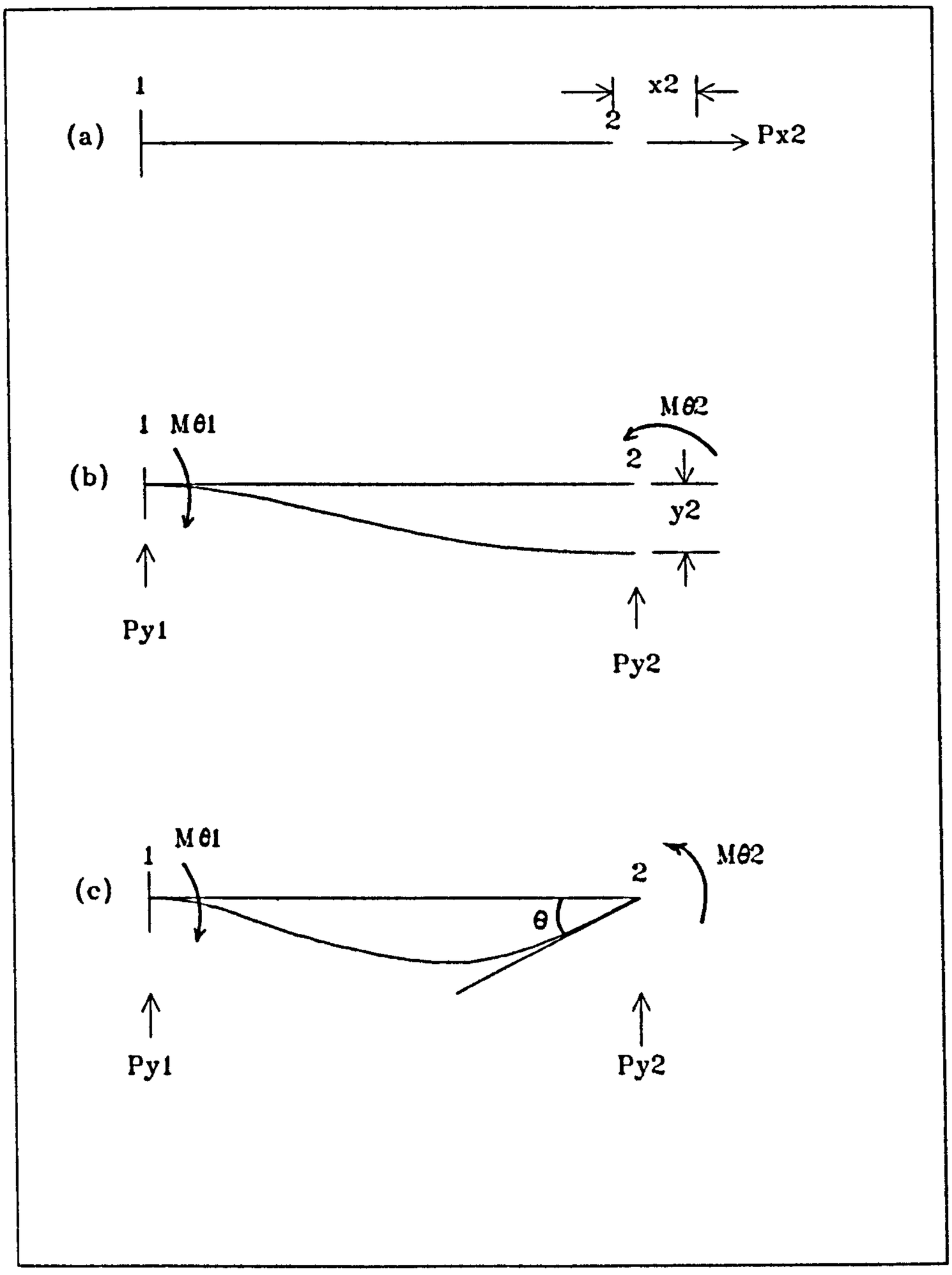

Figure 3.3: Scheme of unit displacements of calculating stiffness components.

$$
[K]m = \left[\begin{array}{ccc:ccc}
(EA)eff/L & 0 & 0 & -(EA)eff/L & 0 & 0 \\
0 & 12(EI)eff/L^3 & 6(EI)eff/L^2 & 0 & -12(EI)eff/L^3 & 6(EI)eff/L^2 \\
0 & 6(EI)eff/L^2 & 4(EI)eff/L & 0 & -6(EI)eff/L^2 & 2(EI)eff/L \\
\hdashline
-(EA)eff/L & 0 & 0 & (EA)eff/L & 0 & 0 \\
0 & -12(EI)eff/L^3 & -6(EI)eff/L^2 & 0 & 12(EI)eff/L^3 & -6(EI)eff/L^2 \\
0 & 6(EI)eff/L^2 & 2(EI)eff/L & 0 & -6(EI)eff/L^2 & 4(EI)eff/L
\end{array}\right]
$$

..... EQ. 3.4

Figure 3.4: Beam–column element stiffness matrix

there is no unique value of Young's Modulus to be used in calculating the stiffness coefficients.

In cases where the material is assumed to be elastic-perfectly plastic, the effective area and second moment of area of a cross-section are typically calculated by ignoring the yielded part of the section [26]. These values are then multiplied by the Young's Modulus E to obtain the effective flexural and axial stiffness coefficients. However, the presence of axial force not only causes axial displacement but also changes the effective stiffness and strength of the section. The combined effect of material non-linearity and axial load can best be obtained from an appropriate moment-axial force-curvature relationship. This procedure is described in the following section.

3.4 DERIVATION OF MOMENT-AXIAL FORCE-CURVATURE RELATIONSHIP.

The curvature k of a beam-column element can be obtained from a consideration of equilibrium, equating the internal and external axial force and bending moment of the element as shown in Equations 2.6 and 2.7.

The relationship between curvature k and the strain distribution across the section can be expressed as:

$$k = (\varepsilon_1 - \varepsilon_2)/h \quad \text{.....(3.5)}$$

where ε_1 = strain at the top of the section.

ε_2 = strain at the bottom of the section.

h = depth of the section.

In determining the curvature k, the cross-section is represented by horizontal strips at uniform strain, as shown in Figure 3.5. If the number of strips is increased, then their depth is decreased, resulting in a more accurate moment-axial force-curvature relationship. Each strip is identified by a subscript i, with i = 1 at the bottom and i = s at the top of the cross-section in which s is the number of strips. Also, from the figure it can be seen that the elongation or contraction of any strip is given by:

$$\varepsilon_i = \varepsilon_o + (k y_i) \quad \text{.....(3.6)}$$

where ε_o = axial strain at the centroid of the section.

y_i = distance from the centre of the i'th strip to the centroid of the section.

The stress σ_i corresponding to the strain in each strip can be calculated from the stress-strain curve for the material. Then the internal axial force dP_i and bending moment dM_i for each strip can be computed as:

$$dP_i = dA_i \sigma_i \quad \text{.....(3.7)}$$

$$dM_i = dP_i y_i \quad \text{.....(3.8)}$$

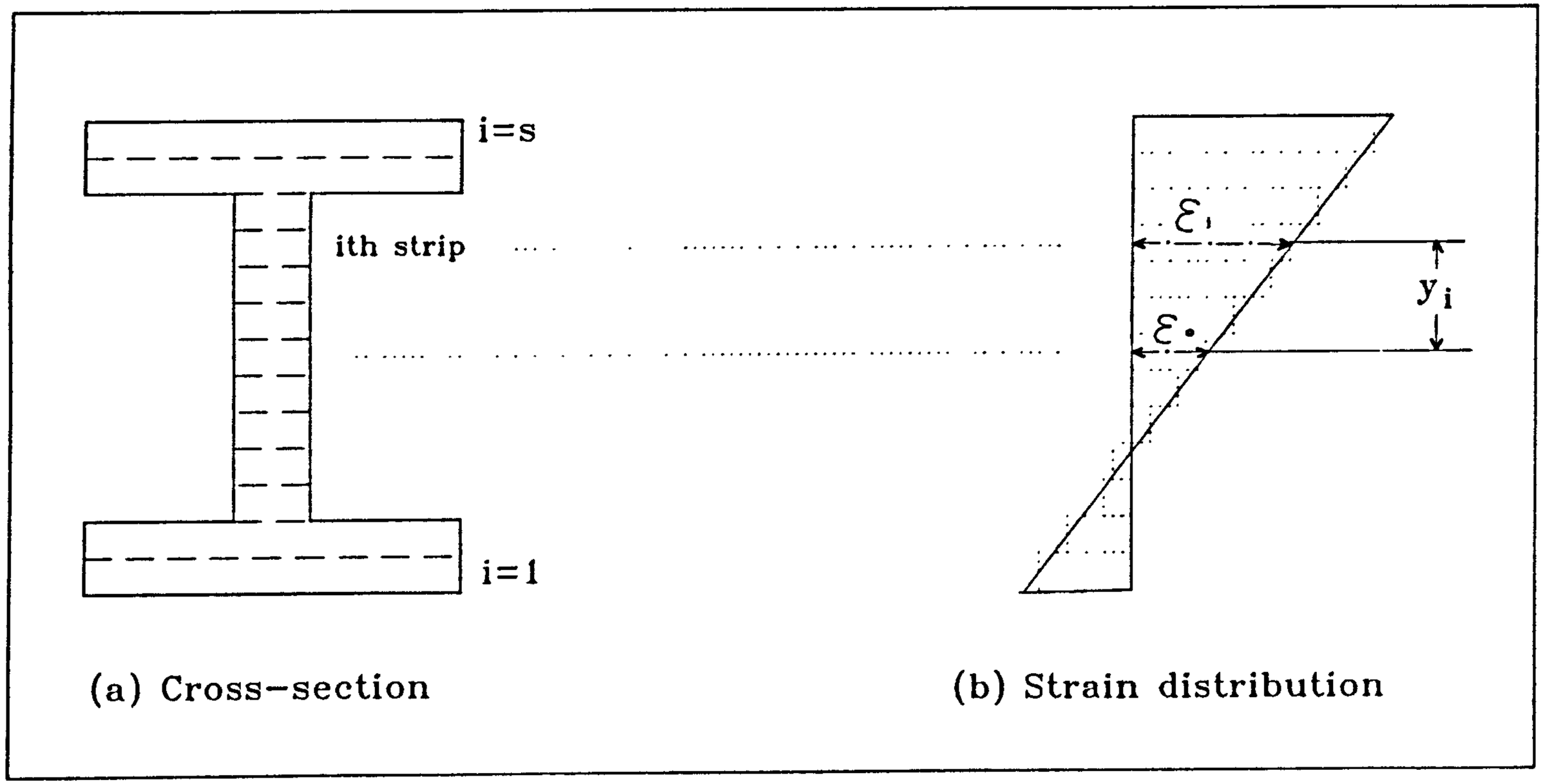

Figure 3.5: Schematic representation for determining the strain in each strip.

where dA_i = area of i'th strip.

The internal axial force and bending moment for the complete cross-section can then be expressed as follows:

$$P_{int} = \sum_{i=1}^{s} dP_i \quad \ldots\ldots\ldots\ldots\ldots\ldots\ldots\ldots (3.9)$$

$$M_{int} = \sum_{i=1}^{s} dP_i y_i \quad \ldots\ldots\ldots\ldots\ldots\ldots\ldots\ldots (3.10)$$

The determination of the moment-axial force-curvature relationship is summarised in the flow chart shown in Figure 3.6. The figure shows the process of iteration which is used to satisfy the equilibrium condition. A curvature k and centroidal axial strain ε_o are assumed and the corresponding stress is calculated for each strip. The internal axial force is then calculated using Equation 3.9, and is checked to see if it balances the external force. If not, a new centroidal axial strain ε_o is assumed and the process repeated until the difference `dN' between the assumed and external axial forces (as shown in Equation 3.11) is sufficiently small. The internal moment is then compared with the external moment; if unbalanced a new curvature k is assumed and the process repeated until the difference `dM' between the assumed and external moments (as shown in Equation 3.12) is also sufficiently small.

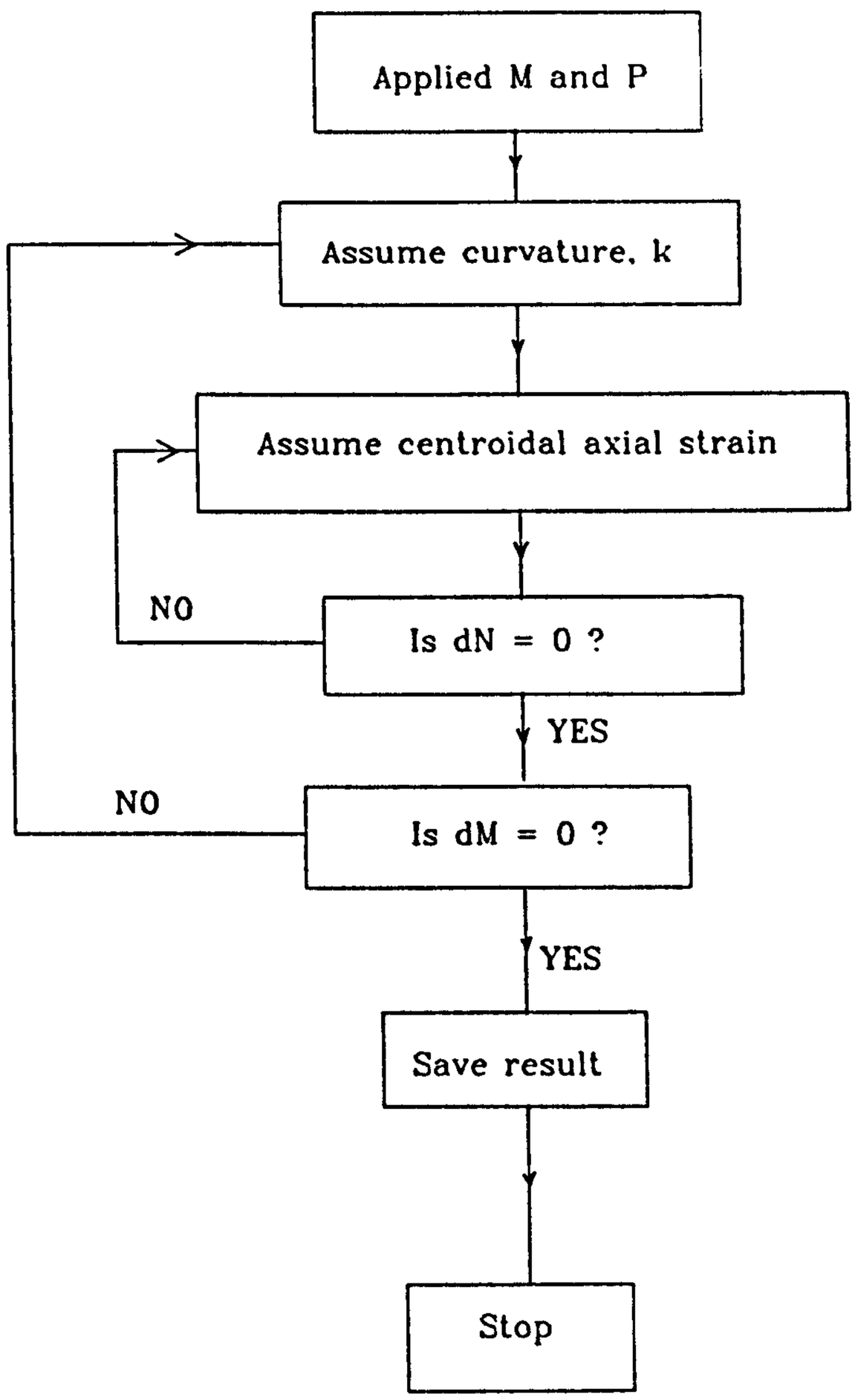

Figure 3.6: Logical sequence of the algorithm for obtaining the moment–axial force–curvature relationship

$$dN = |P_{int} - P| \quad \text{.....(3.11)}$$

$$dM = |M_{int} - M| \quad \text{.....(3.12)}$$

where P = external axial force.

M = external bending moment.

The influence of axial force on the moment-curvature relationship for a rectangular cross-section is expressed in Figure 3.7. The curvature is achieved by initially imposing a constant value of axial force, and then progressively increasing bending moment until a large amount of curvature is achieved. The figure shows that in the absence of axial force, the fully plastic moment is equal to M_p. This reduces to $0.96M_p$ when the axial force is set at $0.2P_y$ and reduces further as the axial force is increased. It is clear that the strength and stiffness of the material is always reduced in the presence of axial force, irrespective of whether this is tensile or compressive.

3.5 THE SECANT STIFFNESS.

Generally the stress-strain curves of steel, particularly at high temperatures, are non-linear with a continuous change of slope. A load increment tangent stiffness method has often been adopted for structural analysis where such material properties are used but this can be time consuming. An alternative approach, providing a more direct solution,

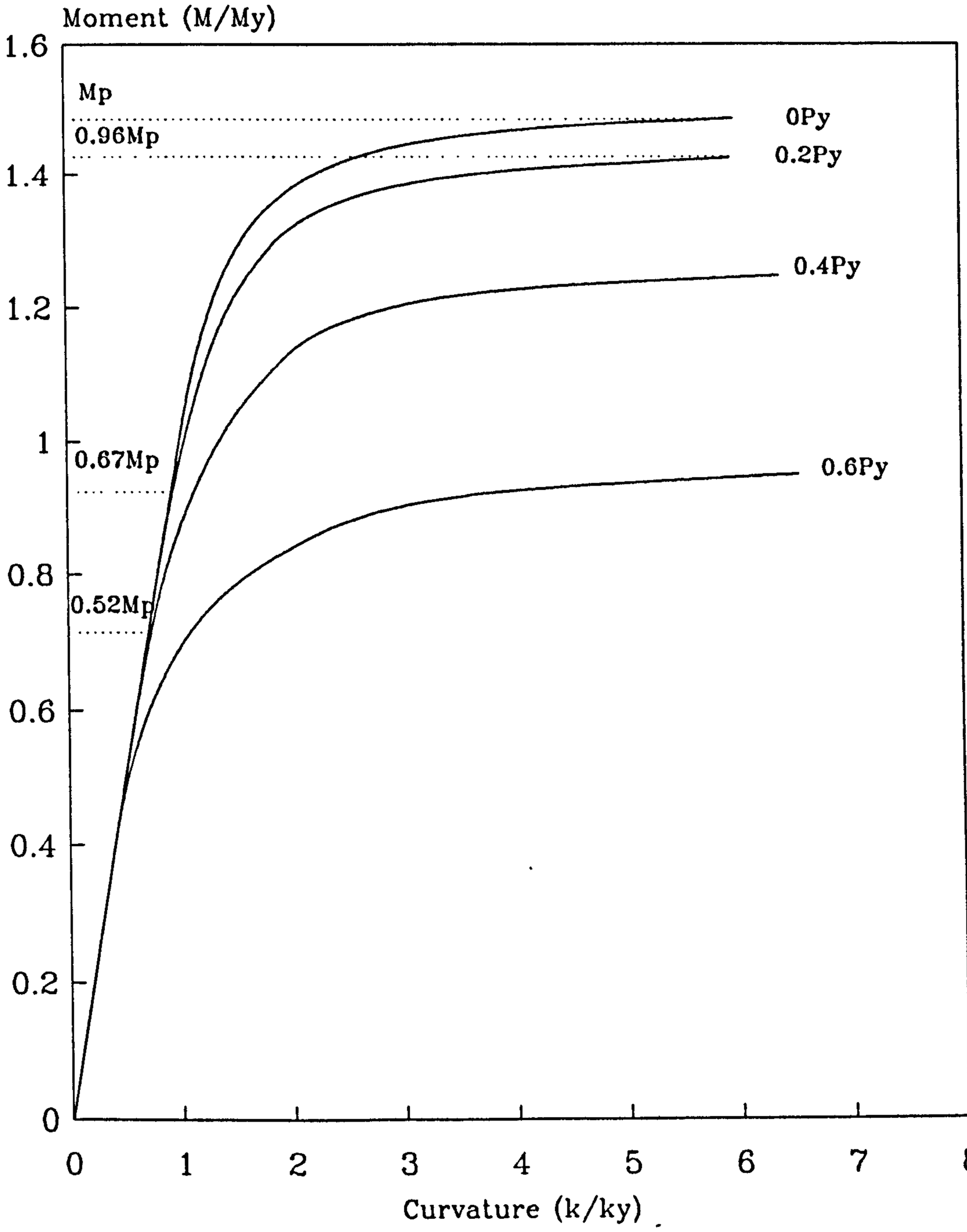

Figure 3.7: The effect of axial force on moment–curvature relationship for a rectangular beam–column element.

is to use the concept of secant stiffness. The basic principle of this can be illustrated by considering the non-linear behaviour of a spring as shown in Figure 3.8. The non-linear curve OA is represented by the functional relationship:

$$F = f(\delta) \quad \text{.....(3.13)}$$

in which F = axial load

δ = deformation.

If a load F_1 is applied to the spring the deformation will be δ_1, so that $F_1 = f(\delta_1)$. This same state of equilibrium could be achieved if the load-deflection curve of the spring were given by the line OA. This can be represented by an equation of the form:

$$F = \frac{f(\delta_1)\delta}{\delta_1} \quad \text{.....(3.14)}$$

or

$$F = S\delta \quad \text{.....(3.15)}$$

where S = secant stiffness of the spring.

It should be noted that the secant stiffness relates the load directly to the actual deformation, which is not the case with the tangent stiffness.

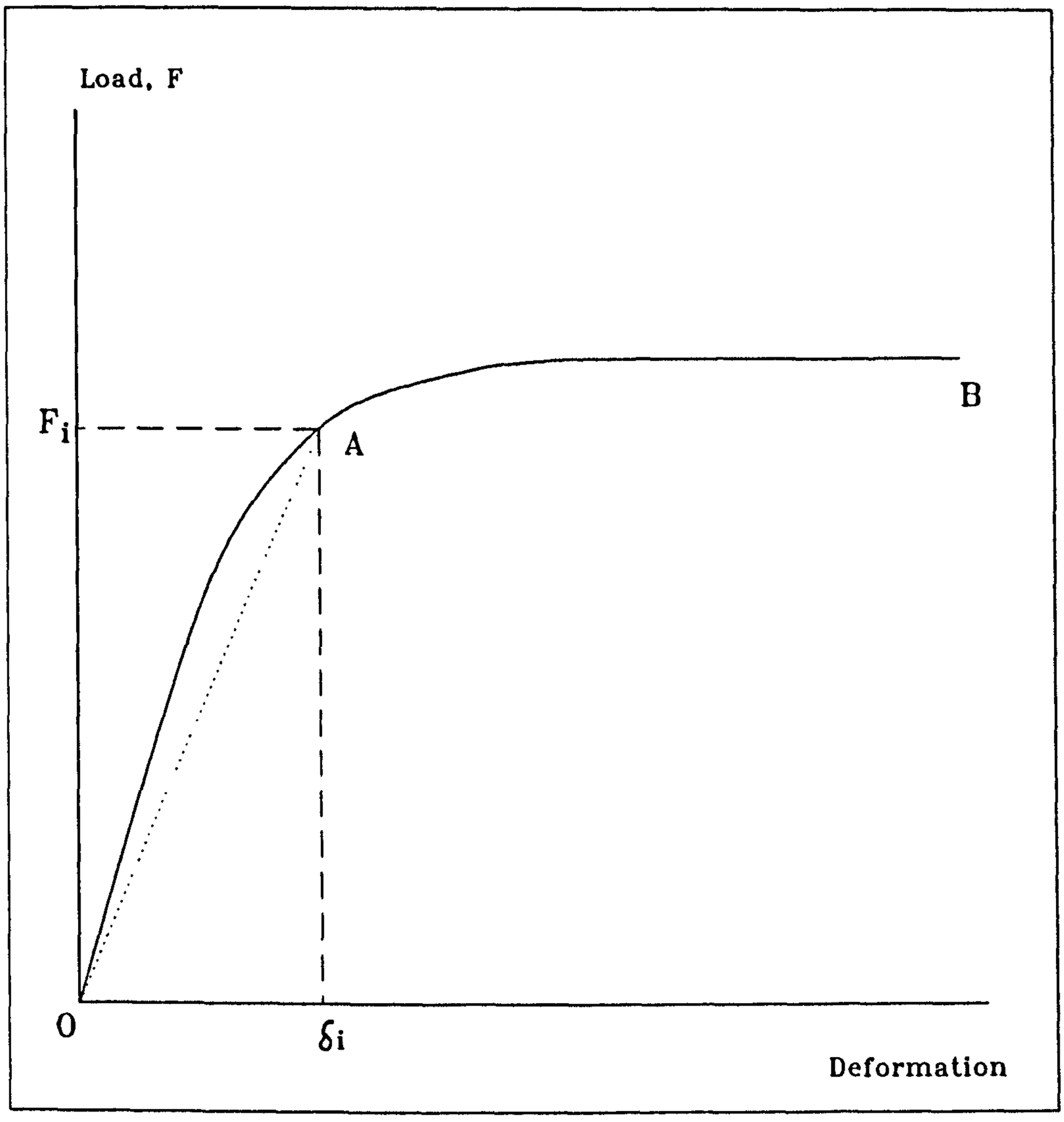

Figure 3.8: Load deformation curve showing the secant stiffness line OA.

The secant stiffness approach can be used in setting up the element stiffness matrix. The formation of the flexural secant stiffness coefficient will be considered first. In linear elastic analysis the basic flexural stiffness is EI; in secant analysis terms the moment-curvature relationship takes the form:

$$S = M/k \quad \text{.....(3.16a)}$$

where M = bending moment.

S = flexural stiffness coefficient.

In this case a linear relationship exists between the moment M and curvature k resulting in a constant flexural stiffness coefficient S. In addition, the curvature is independent of axial load P.

However, for elasto-plastic conditions a non-linear relationship exists between the curvature and moment as shown in Figure 3.9a. In this case the flexural stiffness coefficient is no longer constant. Suppose an element is subjected to a combination of moment M_1 and axial force P_1, and the corresponding curvature is k_1 (Figure 3.9a). The same state can exist by introducing a secant line relating the moment M_1 and the corresponding curvature k_1 as shown in line OA. The relationship takes the form:

$$S_{s\,1} = M_1/k_1 \quad \text{.....(3.16b)}$$

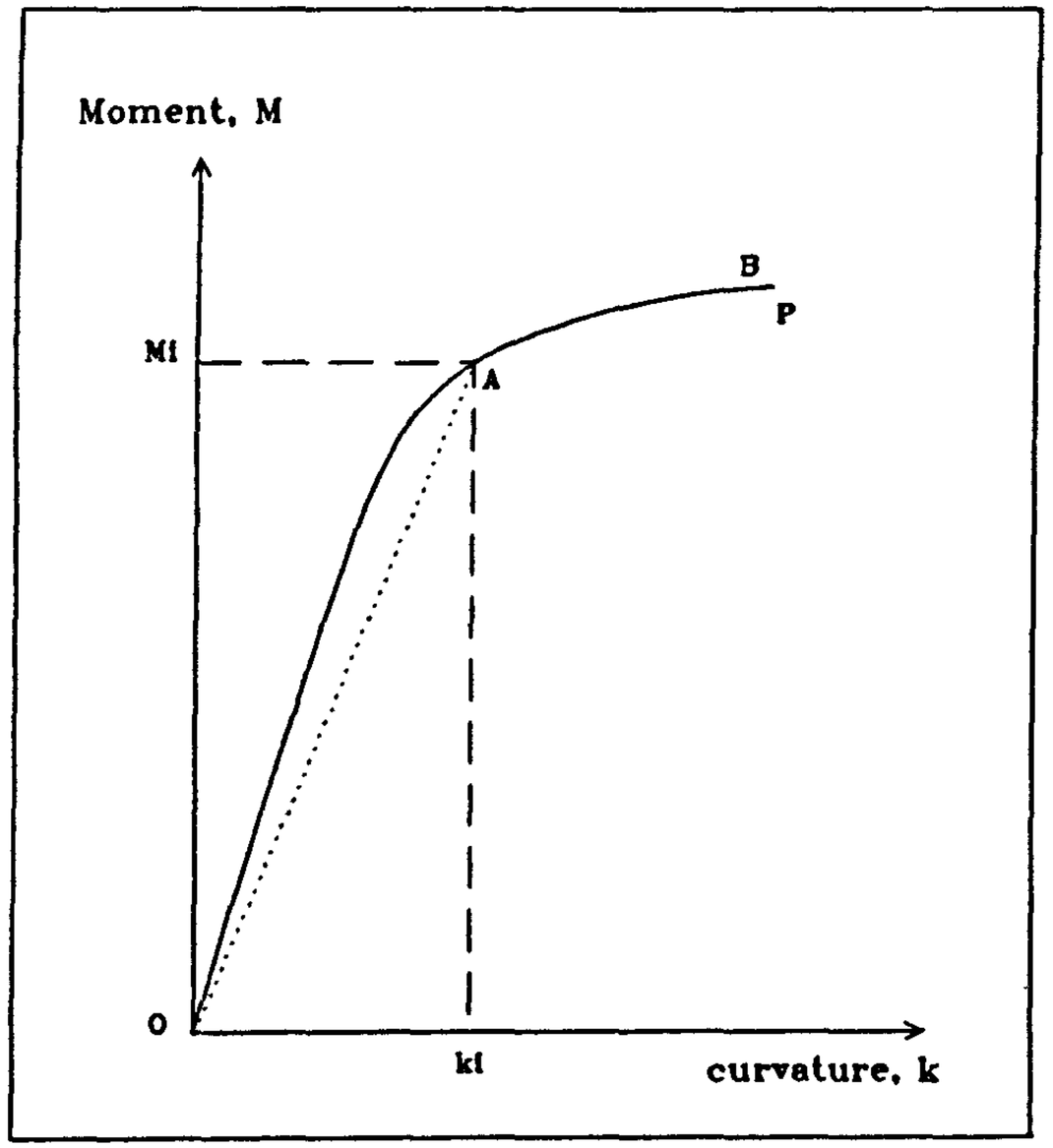

Figure 3.9a: Determination of flexural secant stiffness coefficient.

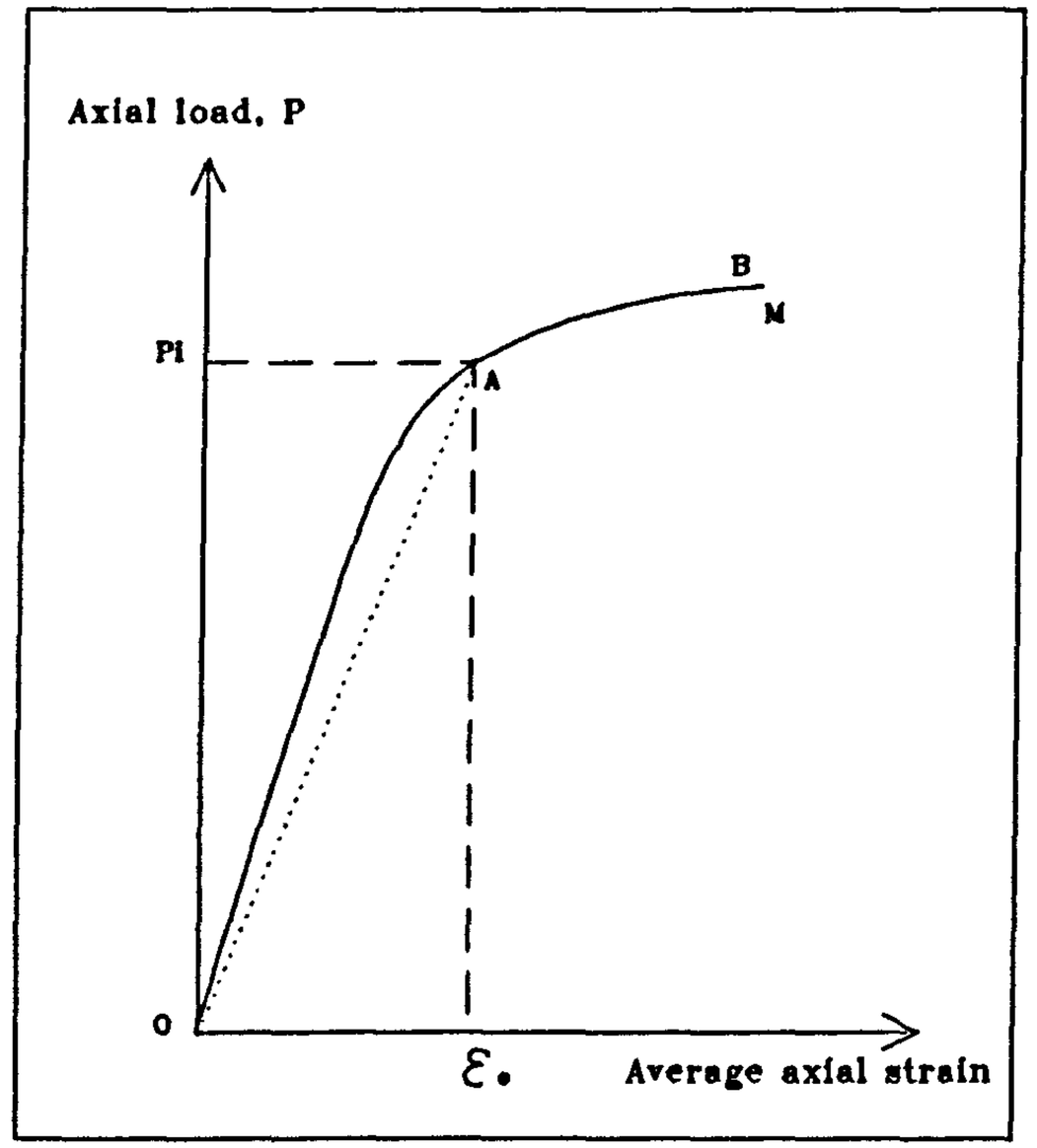

Figure 3.9b: Determination of axial secant stiffness coefficient.

where $S_{s\,i}$ = flexural secant stiffness coefficient.

The concept of the axial stiffness coefficient is similar. In linear elastic analysis the basic axial stiffness is EA. Alternatively it can be determined from:

$$A_L = P/\varepsilon_o \quad \text{.....(3.17a)}$$

where A_L = axial stiffness coefficient.

P = axial force.

ε_o = average axial strain.

In this case a linear relationship exists between the axial force P and average axial strain ε_o. This results in a constant axial stiffness coefficient which is independent of bending moment M.

However for elasto-plastic conditions a non-linear relationship exists between the axial force P and the average axial strain ε_o as shown in Figure 3.9b. As a result the axial stiffness coefficient is no longer constant. Suppose a beam-column element is subjected to a combination of bending moment M_i and axial force P_i, and the corresponding average axial strain is $\varepsilon_{o\,i}$ (Figure 3.9b). The same state can be established by introducing a secant line relating the axial force P_i with the corresponding axial strain $\varepsilon_{o\,i}$ as shown in line OA. The relationship takes the form:

$$A_{s\,i} = P_i / \varepsilon_{o\,i} \quad \ldots\ldots\ldots\ldots\ldots\ldots\ldots (3.17b)$$

where $A_{s\,i}$ = axial secant stiffness coefficient.

Having defined the axial and flexural secant stiffness coefficients in the manner of Equations 3.16b and 3.17b the element stiffness matrix given in Equation 3.4 is then modified with the values of $(EA)_{eff}$ and $(EI)_{eff}$ replaced by $A_{s\,i}$ and $S_{s\,i}$ respectively. These are used in the present analysis, the average axial strain ε_o and curvature k being determined from the derivation of moment-axial force-curvature relationship described in Section 3.4.

3.6 THE EFFECT OF AXIAL SHORTENING DUE TO BENDING ON THE FORMULATION OF THE SECANT STIFFNESS COEFFICIENT.

The approach can be extended to include the influence of the geometric non-linearity which results from axial shortening due to bending. This will affect the axial displacement of a beam-column element, and hence the corresponding secant stiffness coefficient.

Suppose a beam AB is pinned at one end and is free to move longitudinally at the other end as shown in Figure 3.10. When the beam is bent, end B will move horizontally through a small distance d from B to B'. The displacement d is the difference between the initial length L of the beam and the length of the chord AB' of the bent beam.

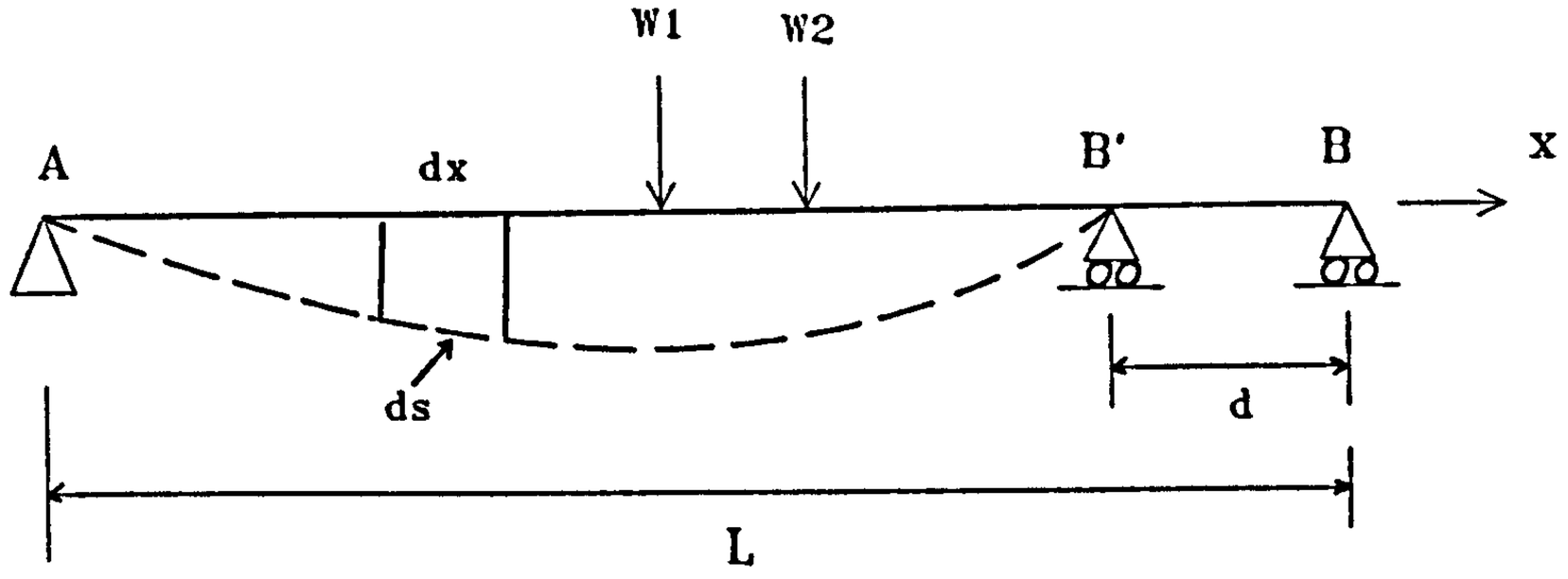

Figure 3.10: Horizontal displacement of the end of the beam due to curvature.

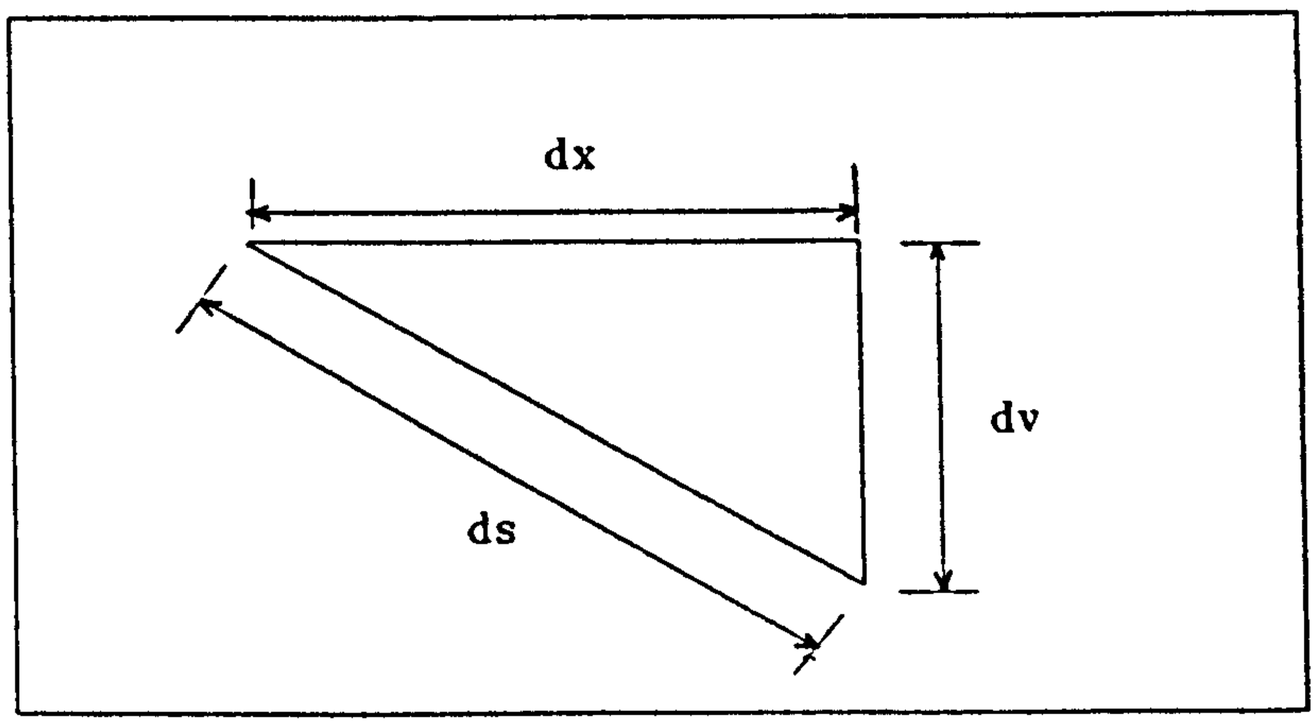

Fig.3.11: Relationship between the chord length, ds, and horizontal projection, dx, of an element.

To find this distance, consider an element of length ds measured along the curved axis of the beam as shown in Figure 3.11. The projection of this element on the x axis has a length dx. The difference between the length ds and its horizontal projection is

$$ds - dx = \sqrt{(dx^2 + dv^2)} - dx$$

$$= dx\ (\sqrt{\ 1 + (\ dv^2/dx^2)}) - dx$$

$$= dx\ (\ 1 + t)^{1/2} - dx \qquad .....(3.18a)$$

where v represents the vertical deflection of the beam. By expanding the term $(1 + t)^{1/2}$ using the binomial theorem, this becomes:

$$(1 + t)^{1/2} = 1 + t/2 - t^2/8 + t^3/16 - .....(3.18b)$$

Provided that t is numerically very small the terms involving t^2, t^3, and higher orders can be ignored. Thus:

$$(1 + t)^{1/2} \approx 1 + t/2 .....(3.19)$$

Hence Equation 3.22 becomes:

$$ds - dx = dx\ [\ 1 + 1/2(dv/dx)^2\ ] - dx$$

$$= 1/2\ (\ dv/dx)^2\ dx .....(3.20)$$

The equivalent axial strain is therefore:

$$\varepsilon_{oa} = (ds - dx)/dx = 1/2\ (dv/dx)^2 \quad \text{.....(3.21)}$$

where ε_{oa} = average effective axial strain due to bending in each element.

dx = length of an element

dv = the difference of the lateral displacements of the two nodes in the element.

The resultant average axial strain in each element is given by:

$$\varepsilon_t = \varepsilon_o - \varepsilon_{oa} \quad \text{.....(3.22)}$$

where ε_t = resultant strain in the element.

ε_o = centroidal axial strain obtained from m-p-k relationship

In the secant stiffness method the axial stiffness shown in Equation 3.17b is modified because of the effect of axial shortening due to bending and becomes:

$$A_{s1} = P/\varepsilon_t \quad \text{.....(3.23)}$$

where P = axial force acting on the element.

A_{s1} = axial secant stiffness.

3.7 ANALYSIS OF FRAME STRUCTURES INCLUDING MATERIAL NON-LINEARITIES AND THE EFFECT OF AXIAL SHORTENING.

The non-linear analysis of frame structures including both material and geometric non-linearities will now be considered. To start with, Equations 3.1 and 3.2 for the matrix stiffness method are modified and become:

$$[K_s]\{D_n\} = \{p\} \quad \ldots\ldots\ldots\ldots\ldots\ldots(3.24)$$

and

$$\{p\}_m = [K_s]_m[T]_m\{d\}_m + \{p\}_{fm} \quad \ldots\ldots\ldots\ldots(3.25)$$

where $[K_s]$ = overall secant stiffness coefficient.

$\{D_n\}$ = non-linear displacement vector.

$\{p\}$ = load vector.

$[T]_m$ = condensed element transformation matrix.

$\{d\}_m$ = end displacements of the element in global terms.

$[K_s]_m$ = element secant stiffness matrix.

In the linear elastic condition, only one cycle of iteration is required to obtain a complete solution for displacements. In the current non-linear structural analysis an iterative process is used to satisfy the conditions of Equations 3.16b, 3.23 and 3.24. The analysis is summarised in Figures 3.14 and 3.12. The process is based on assumed curvature

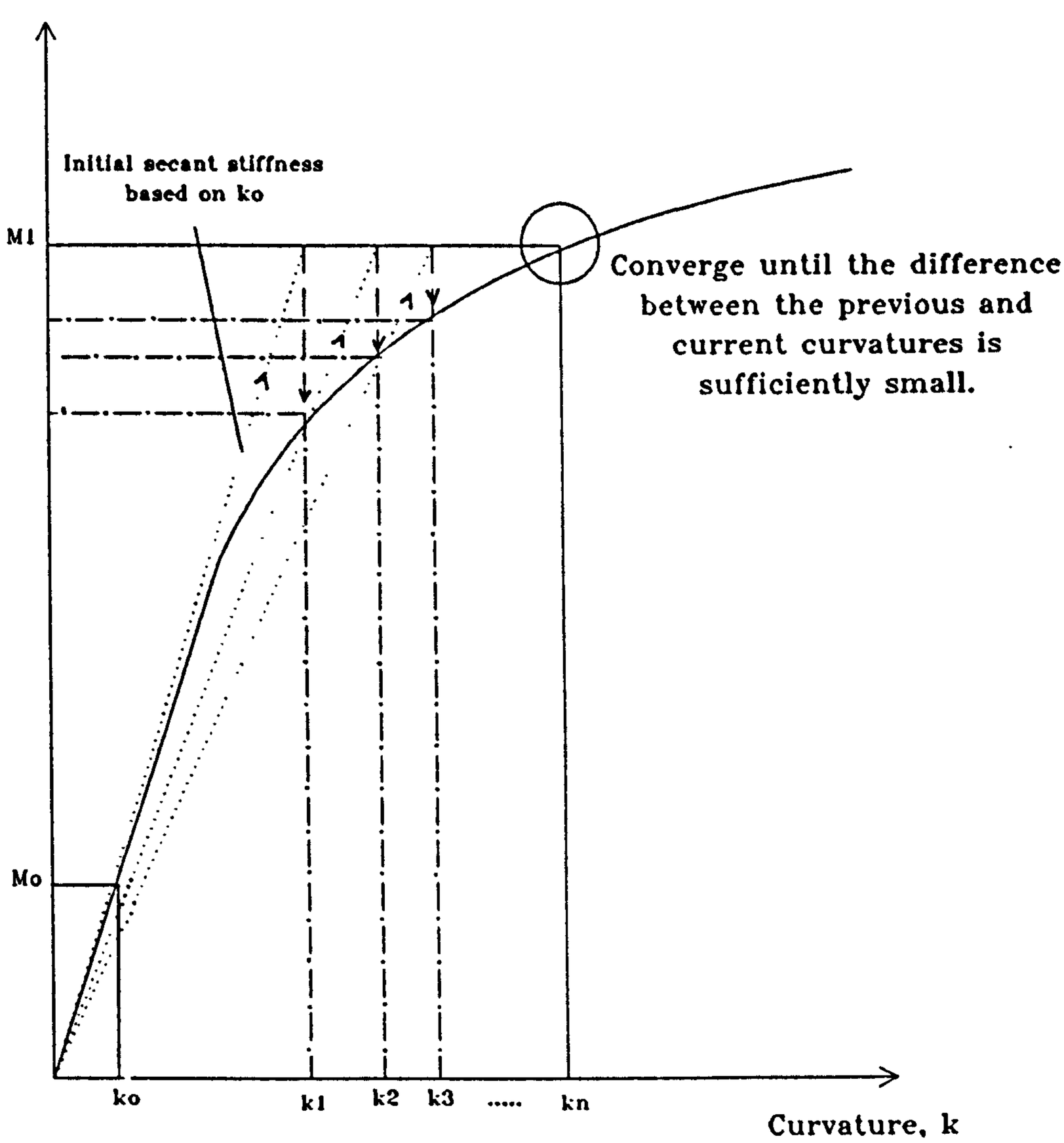

Figure 3.12: Schematic representation of non-linear frame analysis using secant stiffness approach.

and stops when the difference between the current and previous curvatures in each element is sufficiently small.

Initially the analysis is carried out by ignoring axial shortening in the members. A small value of curvature 'k_o' and axial force 'P_o' are assumed for each element. The corresponding moment 'M_o' is obtained from the moment-axial force-curvature relationship and the condition that the internal and external axial force are approximately equal as shown in Figure 3.13. The flexural and axial secant stiffness coefficients can then be calculated using Equations 3.16b and 3.23 respectively based on the corresponding curvature k_o and centroidal axial strain ε_o.

The nodal displacements are calculated from the solution of the simultaneous algebraic equations given in matrix form in Equation 3.24. The element forces can then be calculated from Equation 3.25.

It should be noted that the nodal displacements obtained from Equation 3.24 are in fact denoted in terms of the coordinate axes of the overall structure. These are then converted into the element axes based on Figure 3.1. Thus, the end displacements for each element take the form:

$$\{d_m\} = [T]_m \{d\}_m \quad \ldots\ldots\ldots\ldots\ldots\ldots (3.26)$$

where $\{d_m\}$ = node displacements in terms of element axes.

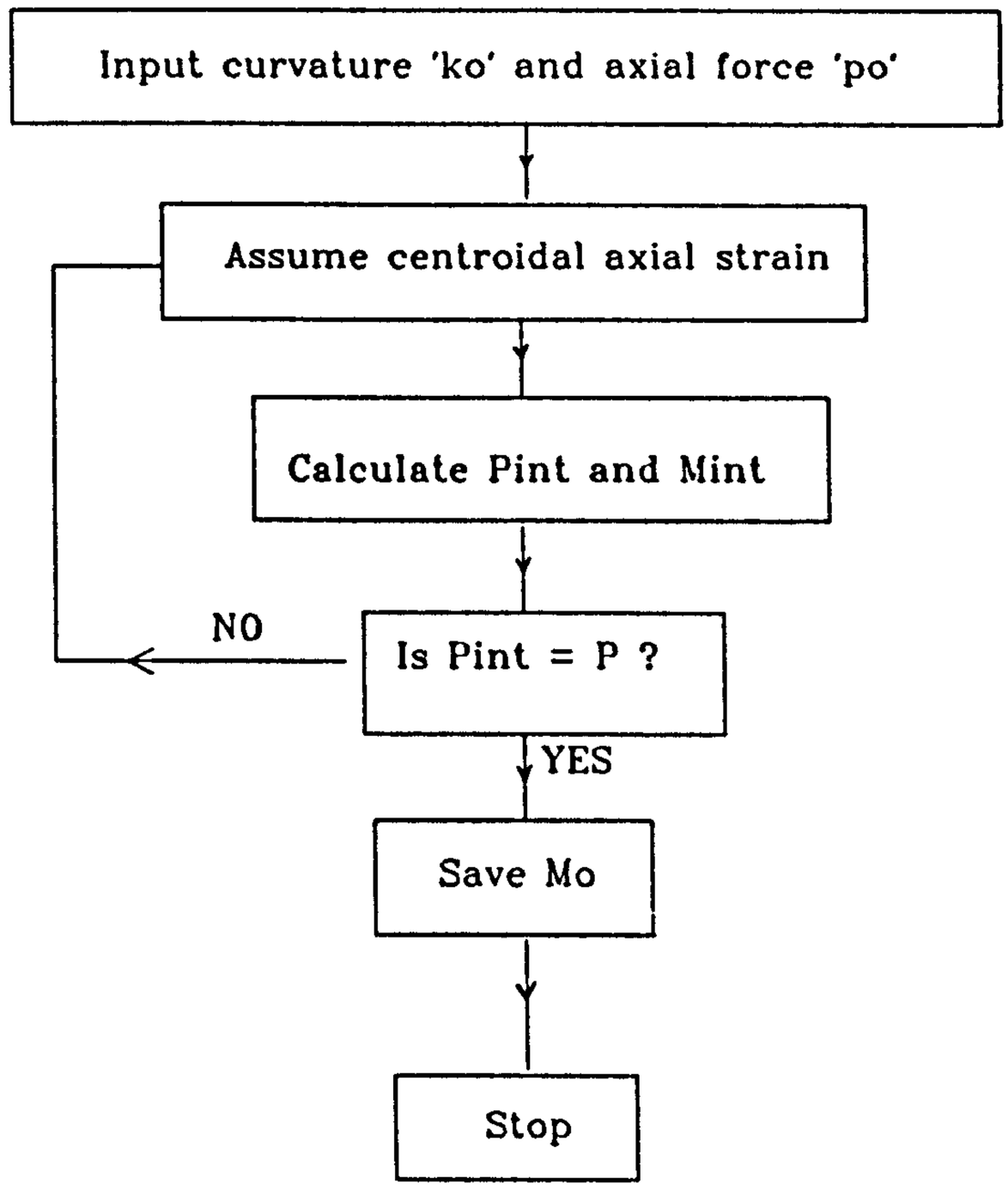

Figure 3.13: Logical sequence of operations in determining the moment 'Mo' for each element.

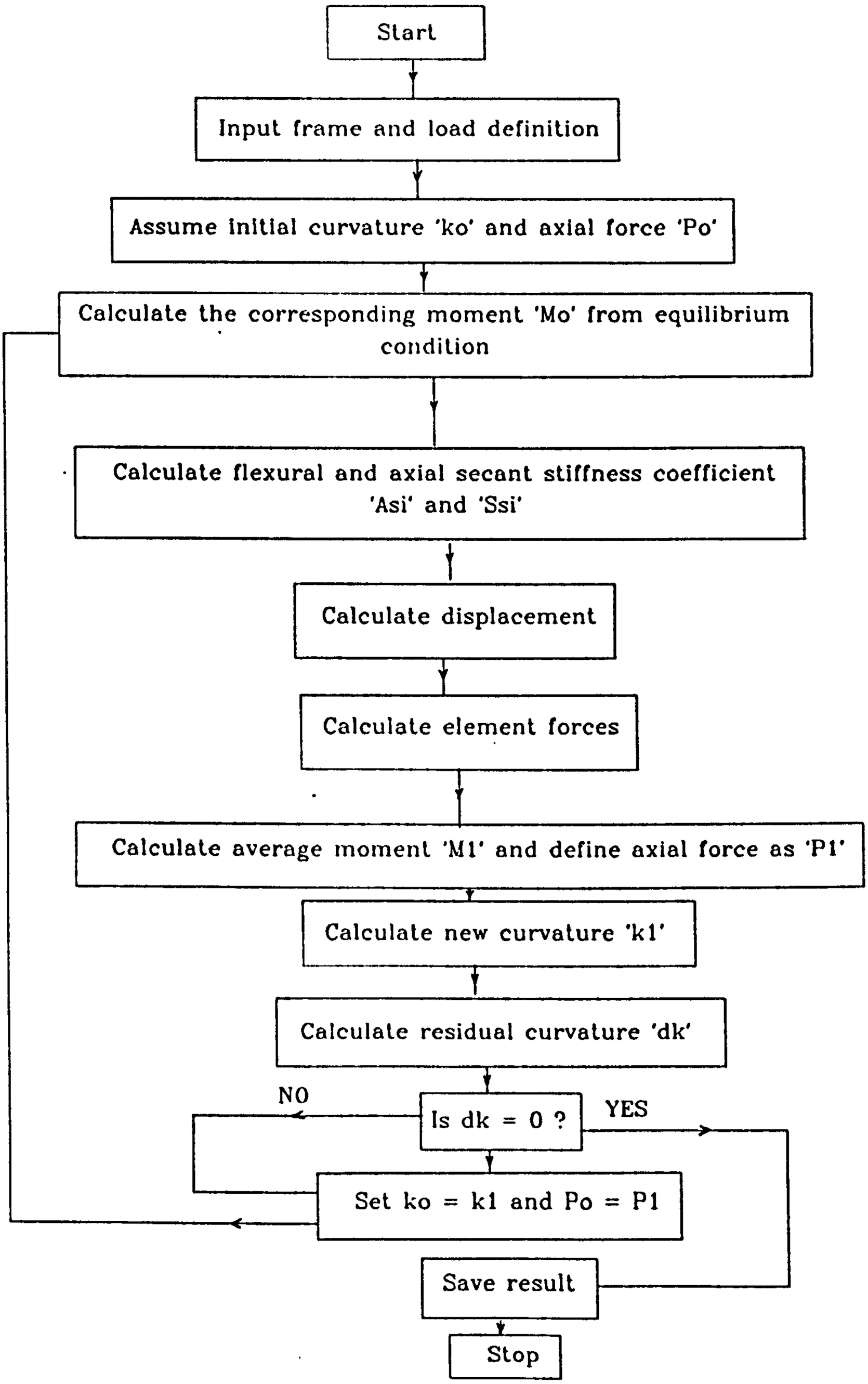

Figure 3.14: Logical sequence of operations for the frame analysis including the effect of material non-linearity

$\{d\}_m$ = node displacements in global terms.

$[T]_m$ = nondensed element transformation matrix.

Having determined the node displacements in this way, the differential displacement of the two ends of an element, $\delta_{v\,i}$ can be determined. The axial shortening due to bending for each element is then calculated using an Equation 3.21 and this is then used for the next cycle of iteration to determine the new axial secant stiffness coefficient.

A new curvature, k_1 for each element can be established by using the approach outlined in Figure 3.12. By projecting the secant line of the previous moment 'M_0' and curvature 'k_0' to the new value of bending moment 'M_1', a new curvature can be calculated according to:

$$k_1 = M_1 k_0 / M_0 \quad \ldots\ldots\ldots\ldots\ldots\ldots (3.27a)$$

where k_1 = new curvature in each element.

M_1 = new average moment in each element.

k_0 = previous curvature.

M_0 = previous average moment in each element.

The new value of moment in each element, M_1 is taken from the average of the values at its ends, and the new axial force in each element is defined as P_1. In general the new values of curvature (k_1), moment (M_1) and axial force (P_1) will not be the same as those assumed initially. Therefore

an iterative procedure must be adopted until there is sufficiently close agreement between the assumed and calculated values. El-Rimawi [5] used a similar approach when studying beam elements in the absence of axial load. He found that using the curvature as the basis for convergence was most secure, and therefore the same procedure has been adopted in the current analysis.

The difference between the current and previous curvatures can be written:

$$dk = |k_1 - k_0| \quad \text{.....(3.27b)}$$

where dk = residual curvature.

If this difference is not sufficiently small the calculated values of curvature k_1 and axial force P_1 are adopted as the initial values for the next iteration. The procedure is repeated until the difference between the current and previous curvatures in each element is sufficiently small.

It should be noted that the results obtained from any iteration are independent of those obtained from the previous iteration. Moreover, once the correct curvature profile has been found the calculated forces and displacements are the actual non-linear ones. For these reasons the iteration can be started using any initial values. However it is most convenient to assume values of

curvature sufficiently small that the secant stiffness coefficient equals the elastic stiffness coefficient. By doing this the number of iterations required for special cases such as a linear analysis will be minimised without changing the iteration process.

3.8 SECONDARY EFFECTS DUE TO AXIAL FORCE.

In the previous section the influence of axial load inducing additional bending, the so-called p-delta effect, was ignored in the analysis. To obtain a more accurate analysis, this influence will now be included.

3.8.1 Secondary moments due to axial force.

If a member is perfectly straight, the axial load P acting on its own would produce no lateral displacement. However, if the member is subject to bending, for instance due to lateral loads or eccentricity of loading, or if the column had an initial curvature, deflections are increased if the member is subjected to axial compressive load or decreased for a tensile load. This is caused by the secondary moments generated by the load acting on the deformed member and is called the p-delta effect. This can be important, particularly for high axial loads. To obtain a relationship between bending moment and lateral deflection, suppose a beam is displaced by some means from its initial position to

the configuration v(x), as shown in Figure 3.15.

At a position (x,y) the external bending moment $M_{(x,y)}$ is given by:

$$M_{(x,y)} = Pv \quad \text{.....(3.28)}$$

The increased bending moment due to P is resisted by the bending stiffness of the member. Since the member is in equilibrium the external and internal bending moments and axial forces must be equal. These conditions can be used to include the p-delta effect within the structural analysis.

3.8.2 Derivation of fixed end moments and forces due to p-delta effect.

To include the p-delta effect in the secant stiffness method, the moments and forces induced by the axial force must be included in the load vector. To start with, each element in the frame is assumed to be restrained against rotation and the element is then analysed incorporating the effect of the axial force as shown in Figure 3.15b. The element is assumed to be very small, and consequently has a high value of Euler load. Thus the ratio of the axial force to the Euler load is very small and the general element stiffness matrix shown in Equation 3.4 is almost unchanged.

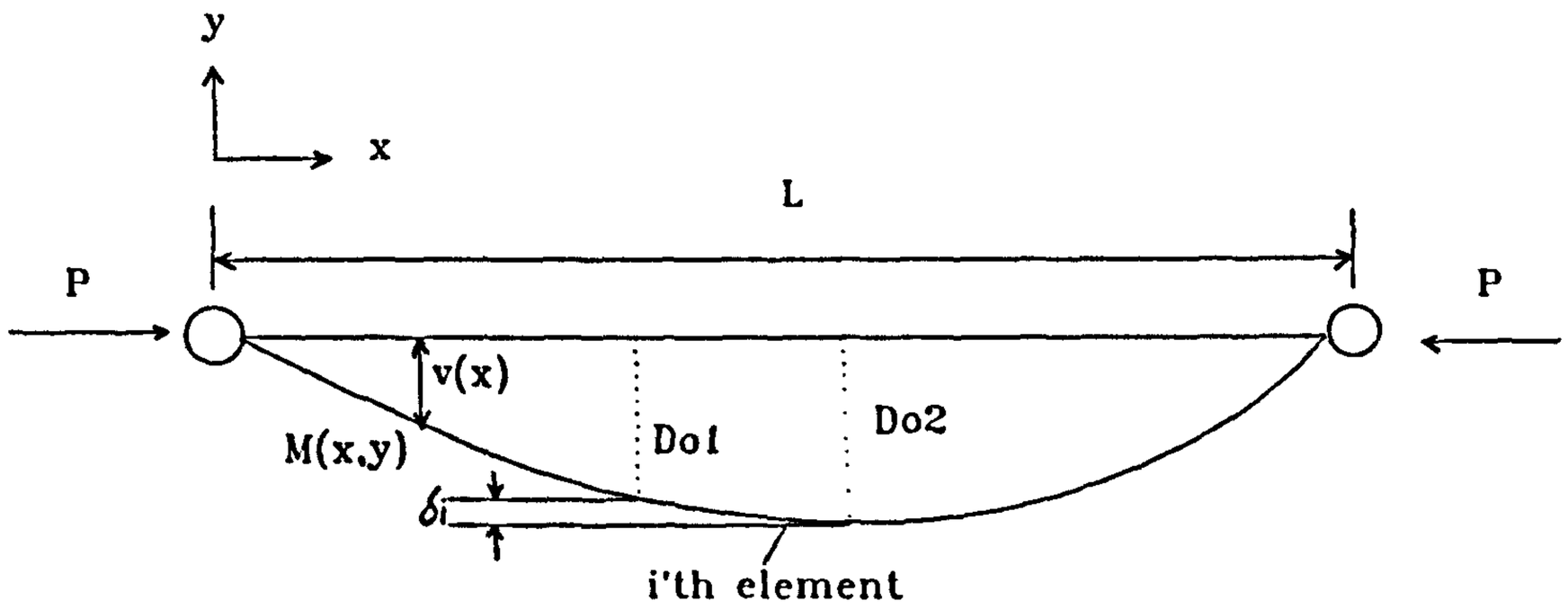

(a). Deflected shape of pin-ended column

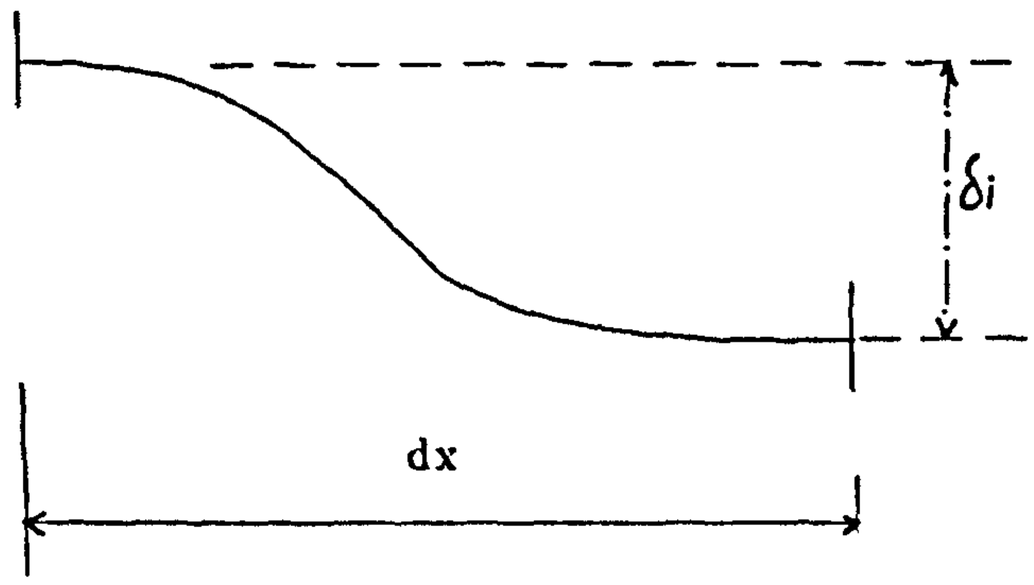

(b). Fixed ended condition of i'th element

Figure 3.15: Schematic representation in determining the fixed end forces of an element due to the p-delta effect.

Suppose a member is subjected to an axial load P and the corresponding deformation is shown in Figure 3.15a. The i'th element is analysed and Figure 3.15b shows the arrangement of the fixed-ended element. The difference between the vertical displacements of the two nodes in the element is given by δ_i. The forces at each end of the element are then determined using the differential deflection equation [116]. Table 3.1 shows the fixed end forces for the element subjected to axial compressive and tensile forces.

The terms $6EI\delta/L^2$ and $12EI\delta/L^3$ are in fact the fixed-end moment and shear force caused by the support displacements and these effects have already been included in the modified joint restraint conditions. Thus the modified fixed end forces for the element subjected to axial compressive and tensile forces are as shown in Table 3.2.

3.8.3 Analysis of frame structures including second-order geometric and material non-linearities.

The analysis which was described in Section 3.5.4 is now extended to include the p-delta effect. Since the analysis is non-linear, an iterative process is required to determine the final deflected shape. The analysis is summarised in Figure 3.16.

Initially the normal first-order analysis is carried out as

	Compressive Forces	Tensile Forces
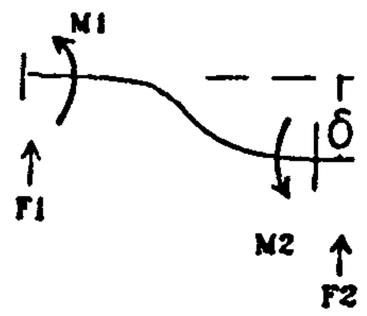	$M1=M2=6EI\,\delta/L^2$ $F1=-F2=12EI\,\delta/L^3$ $-P\,\delta/L$	$M1=M2=6EI\,\delta/L^2$ $F1=-F2=-12EI\,\delta/L^3$ $+P\,\delta/L$
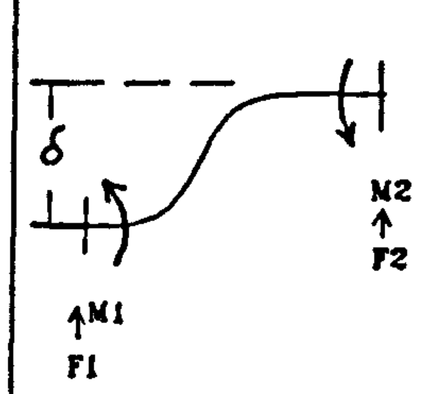	$M1=M2=-6EI\,\delta/L^2$ $F1=-F2=-12EI\,\delta/L^3$ $+P\,\delta/L$	$M1=M2=-6EI\,\delta/L^2$ $F1=-F2=12EI\,\delta/L^3$ $-P\,\delta/L$

Table 3.1: Fixed end moments and forces for uniform beam

	Compressive Force	Tensile Force
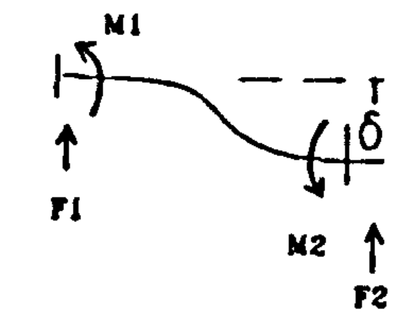	$M1=M2=0$ $F1=-F2=-P\delta/L$	$M1=M2=0$ $F1=-F2=P\delta/L$
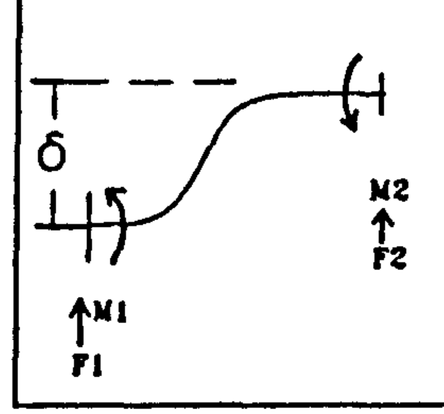	$M1=M2=0$ $F1=-F2=P\delta/L$	$M1=M2=0$ $F1=-F2=-P\delta/L$

Table 3.2: Modified fixed end moments and forces for uniform beam

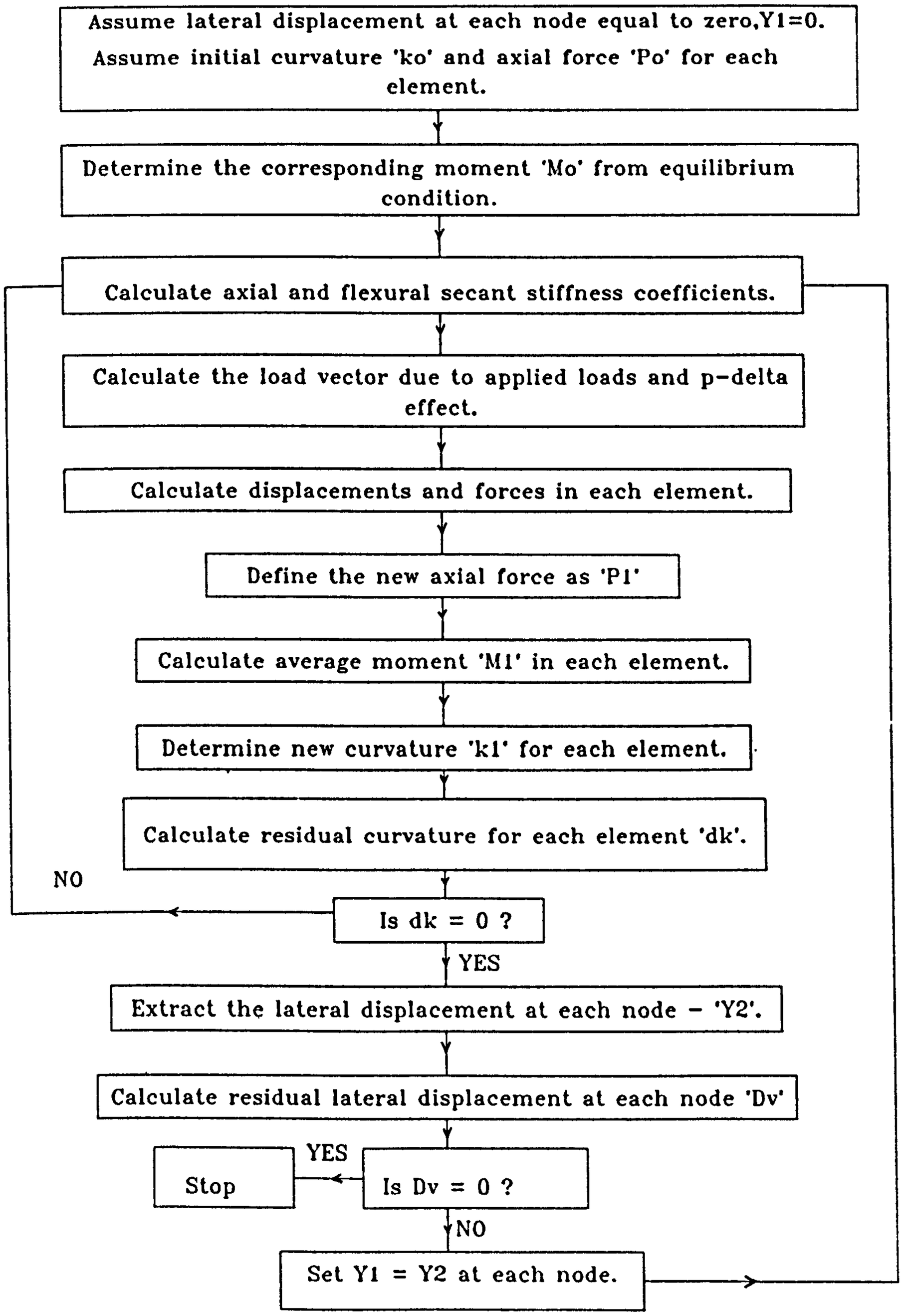

Figure 3.16: Computer chart for the analysis of frame structures including the effect of geometric and material non-linearities.

summarised in Figure 3.14 but with the lateral displacement for each node assumed zero, thus ignoring the influence of the p-delta effect. This provides values for displacement at each node and enables the additional fixed-end forces for each element to be calculated using the procedure described in Section 3.8.2. By performing a subsequent analysis in which the load vector is extended to incorporate these fixed-end forces, the p-delta effect can be included. This results in revised displacement values at each node. If these are not sufficiently close to the values assumed at the beginning of the calculation, the analysis must be repeated using the revised values. It should be noted that the fixed end forces due to the p-delta effect are assumed to remain constant during the iteration process until the residual curvature dk (see Equation 3.27b) for each element is within the tolerance limit. Although this is not strictly correct, any errors resulting from this assumption are likely to be very small, yet the savings in computation time are considerable.

The analysis is stopped when the difference between the current and previous values of lateral displacement is sufficiently small. If not, the process is repeated with the current values of lateral displacements used as the new initial values. This forms the basis for a computer program written in QuickBasic and running on an IBM PC286.

3.9 VALIDATION OF THE PRESENT THEORY.

The accuracy of the analysis is clearly dependent on the number of elements into which each member is divided, and the number of strips used to represent the cross-section as discussed in Section 3.4. With regard to the convergence of the results the influence of the number of elements and strips in the cross-section will be discussed fully in Chapter 5, which covers the analysis of frames both at ambient temperature and in fire. This shows that for 10 elements per-member and with each cross-section divided into 10 strips the results of the analysis give adequate accuracy.

In this section this representation will be used to compare the behaviour of isolated beams and columns with previously published results using the differential deflection equation derived by Chen and Lui [30] which is valid for members which behave in a linear elastic manner with constant flexural stiffness. For simplicity a rectangular cross section is used with breadth b = 100mm and height h = 200mm. The span of the member is taken as 8.66m, giving a slenderness ratio of 150 and ensuring a significant p-delta effect. The member is assumed to be simply supported and subjected to a combination of axial load and various types of lateral loads. Material properties are represented in a bi-linear elastic-perfectly plastic manner with Young's Modulus E = 205000 N/mm^2 and yield stress σ_y = 250 N/mm^2.

Unless otherwise stated the axial load P is 500 kN which is sufficiently small (i.e, $0.1P_y$) to avoid inelastic behaviour of the member, and the comparisons can be made in the linear elastic region only (Sections 3.9.1 to 3.9.3). In subsequent sections inelastic behaviour is considered.

3.9.1 Simply supported beam subject to a compression force P and end moment applied at both ends.

Consider the simply supported beam with a span of 8.66m, subjected to end moments M = 10 kNm ($0.04M_p$) and axial force P of 500 kN.

The bending moment and vertical deflection at any point along the span can be determined from the differential deflection equation [30] and the results from this are compared in Figures 3.17 and 3.18 with those obtained using the present method. These show very good agreement between the two methods. The p-delta effect can be seen to have a significant influence on the bending moment. If the effect is ignored the bending moment is clearly constant at 10 kNm, but the mid-span bending moment increases to about 15 kNm when it is included.

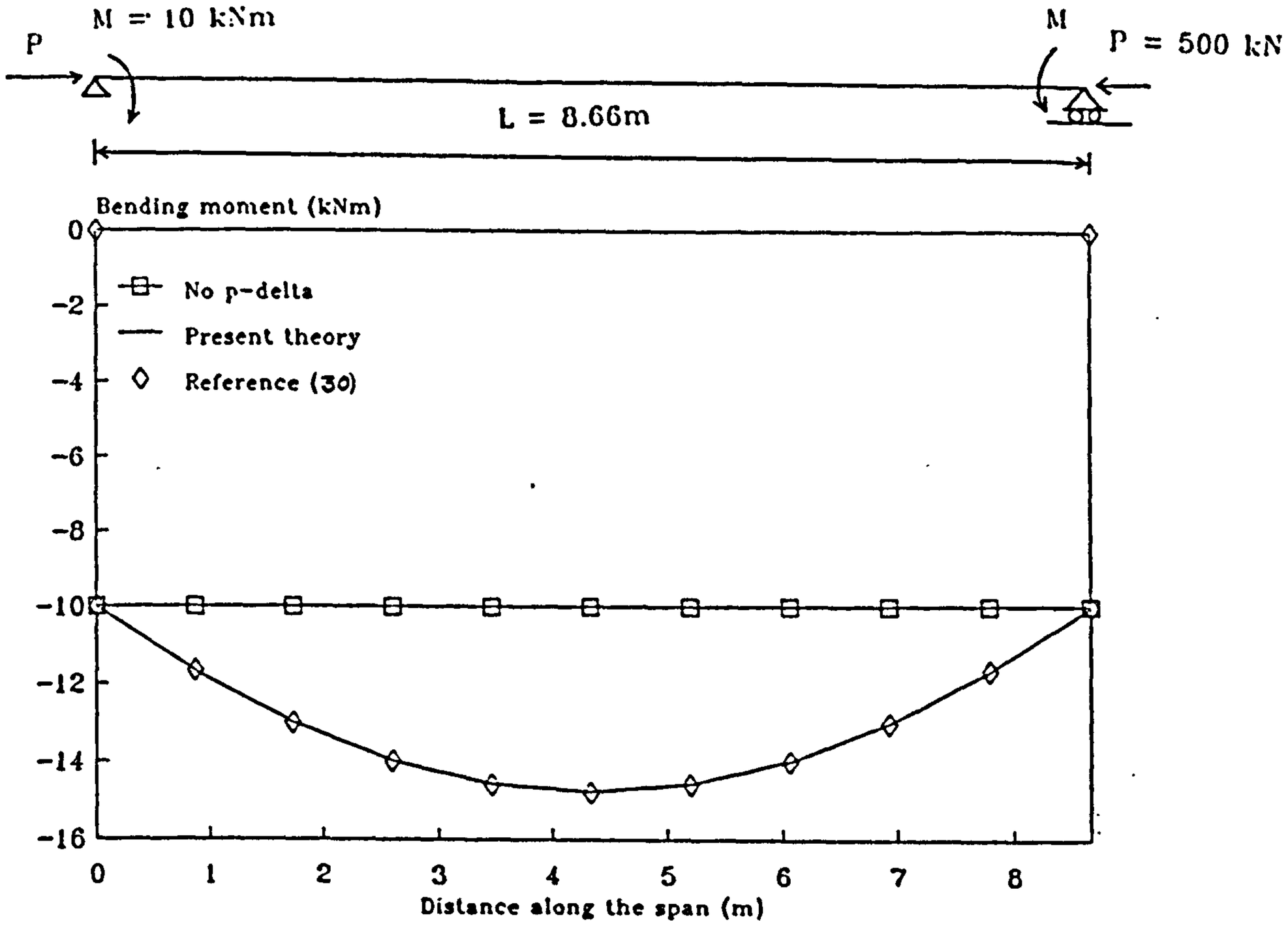

Fig.3.17: Bending moment of beam subjected to axial load and end moments.

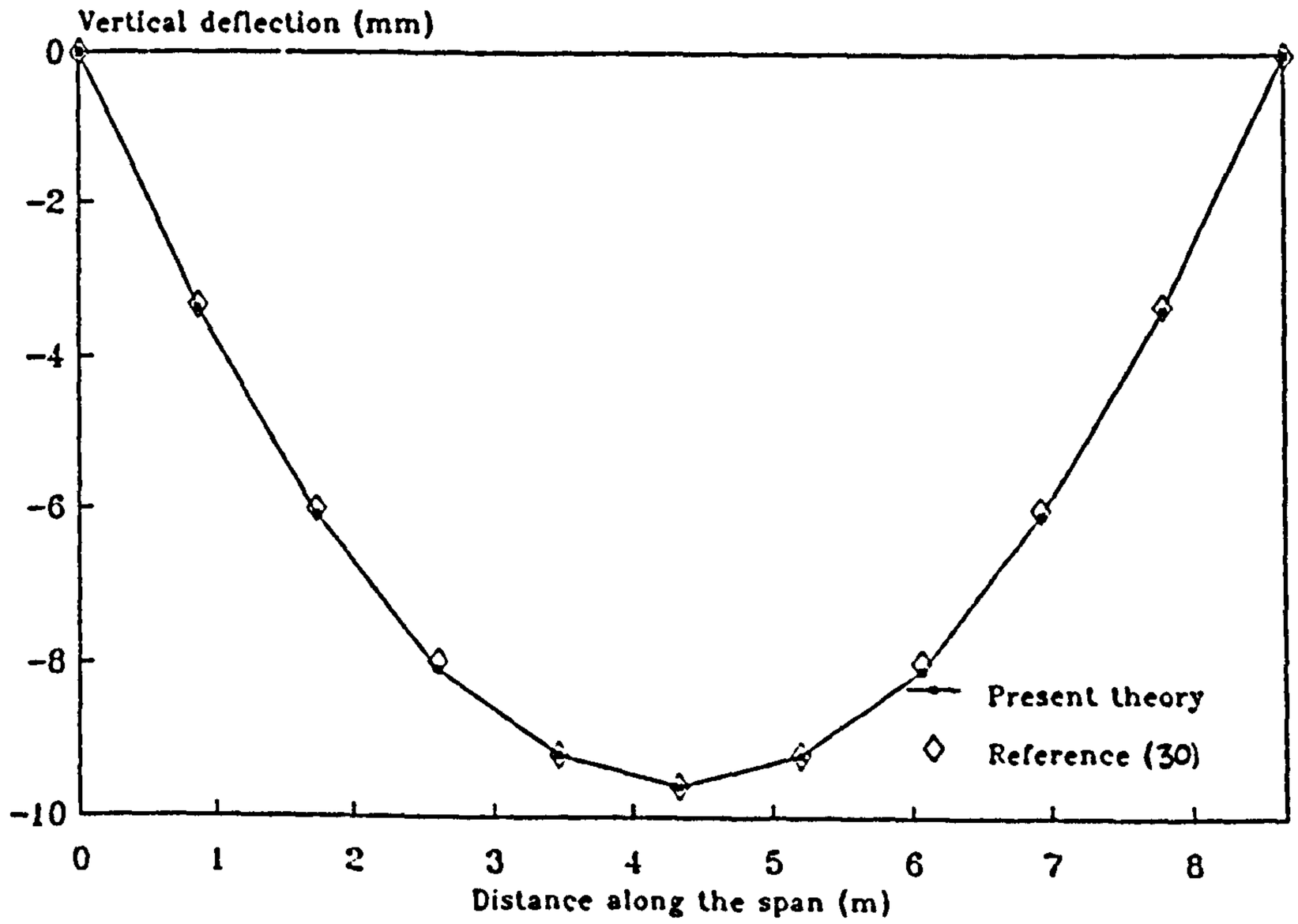

Fig.3.18: Vertical deflection of beam subjected to axial load and end moments (p-delta included).

3.9.2 Simply supported beam subject to a compression P and a uniformly distributed load applied along its span.

Consider the same beam subjected to the same amount of axial load (P = 500 kN) and a uniformly distributed load of 1 kN/m (giving a mid-span bending moment of $0.38M_p$ in the absence of the p-delta effect). Again, the bending moment and vertical deflection at any point along the span can be determined from the differential deflection equation [30] and the results from this are compared in Figures 3.19 and 3.20 with those obtained using the present method. The comparison shows very good agreement between the two methods.

3.9.3 Simply supported beam subject to a compression P and a concentrated load applied at mid span.

Consider the same beam subjected to the same magnitude of axial load (P=500 kN) and a concentrated load Q of 3 kN (giving a mid-span bending moment of $0.26M_p$ in the absence of the p-delta effect). The bending moment and vertical deflection at any point along the span can be calculated using the differential deflection equation [30] and the results from this are compared in Figures 3.21 and 3.22 with those obtained using the present method. The comparison again demonstrates very good agreement between the two methods.

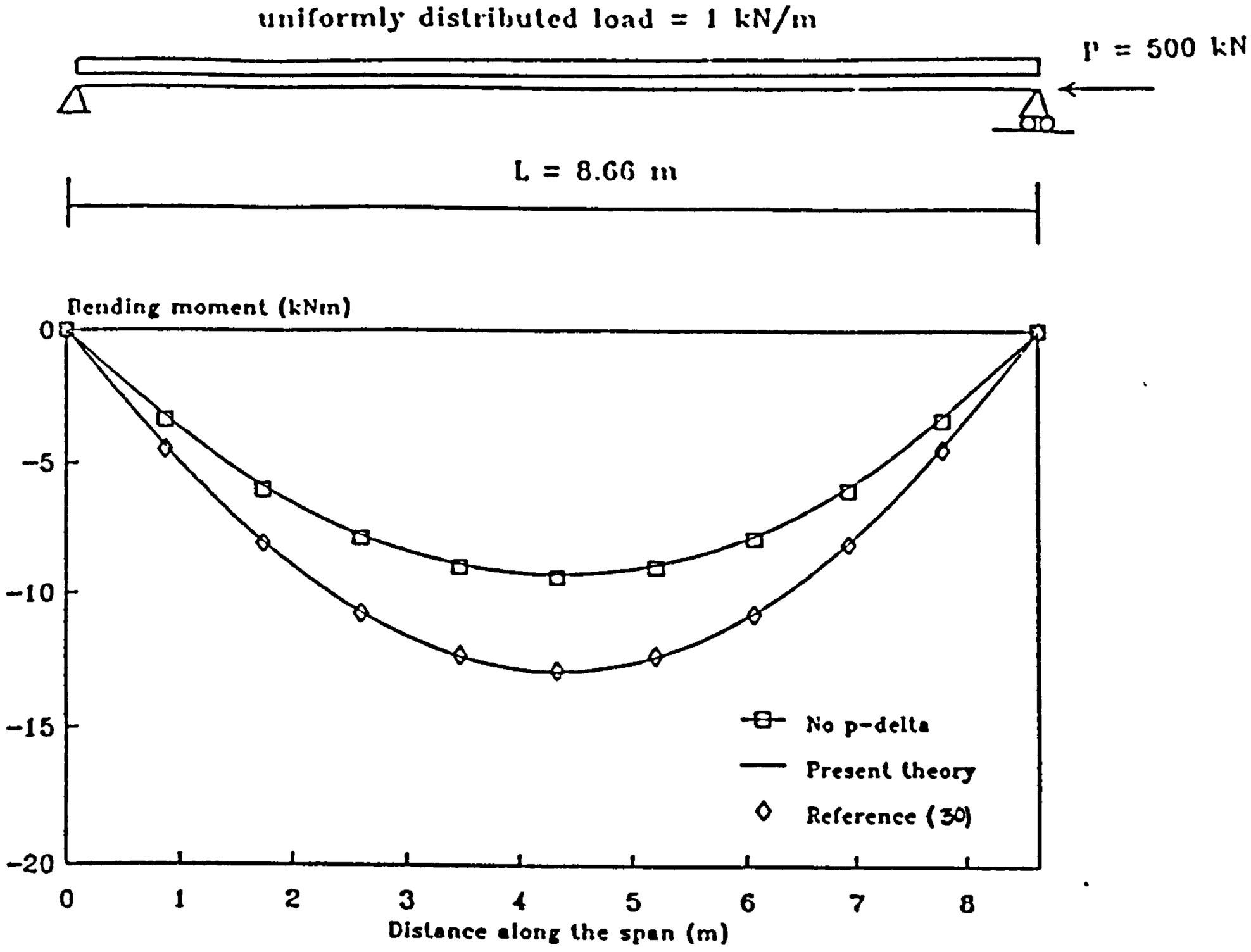

Figure 3.19: Bending moment of beam subjected to a uniformly distributed load and axial load.

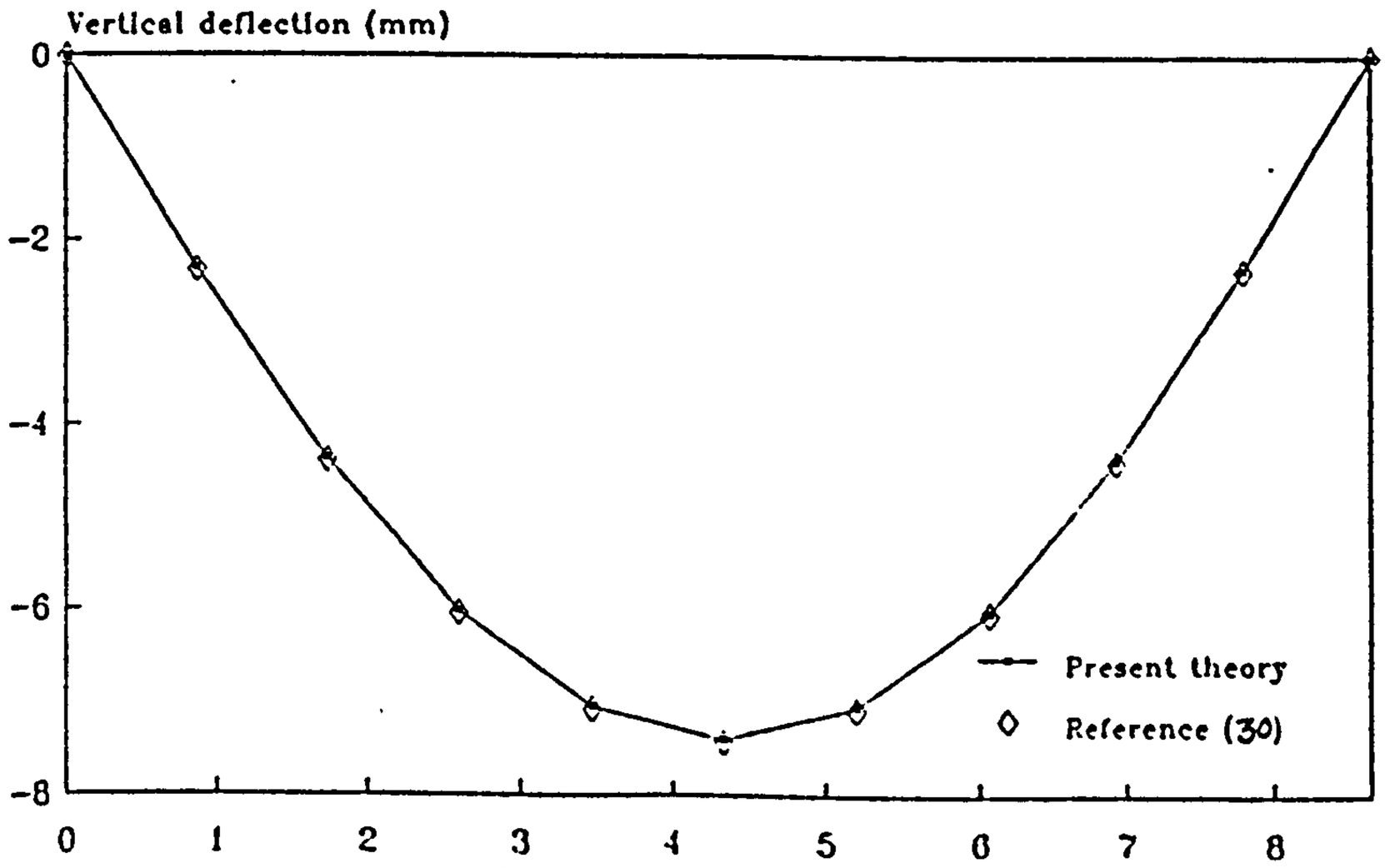

Figure 3.20: Vertical deflection of beam subjected to a uniformly distributed load and axial load (p-delta included).

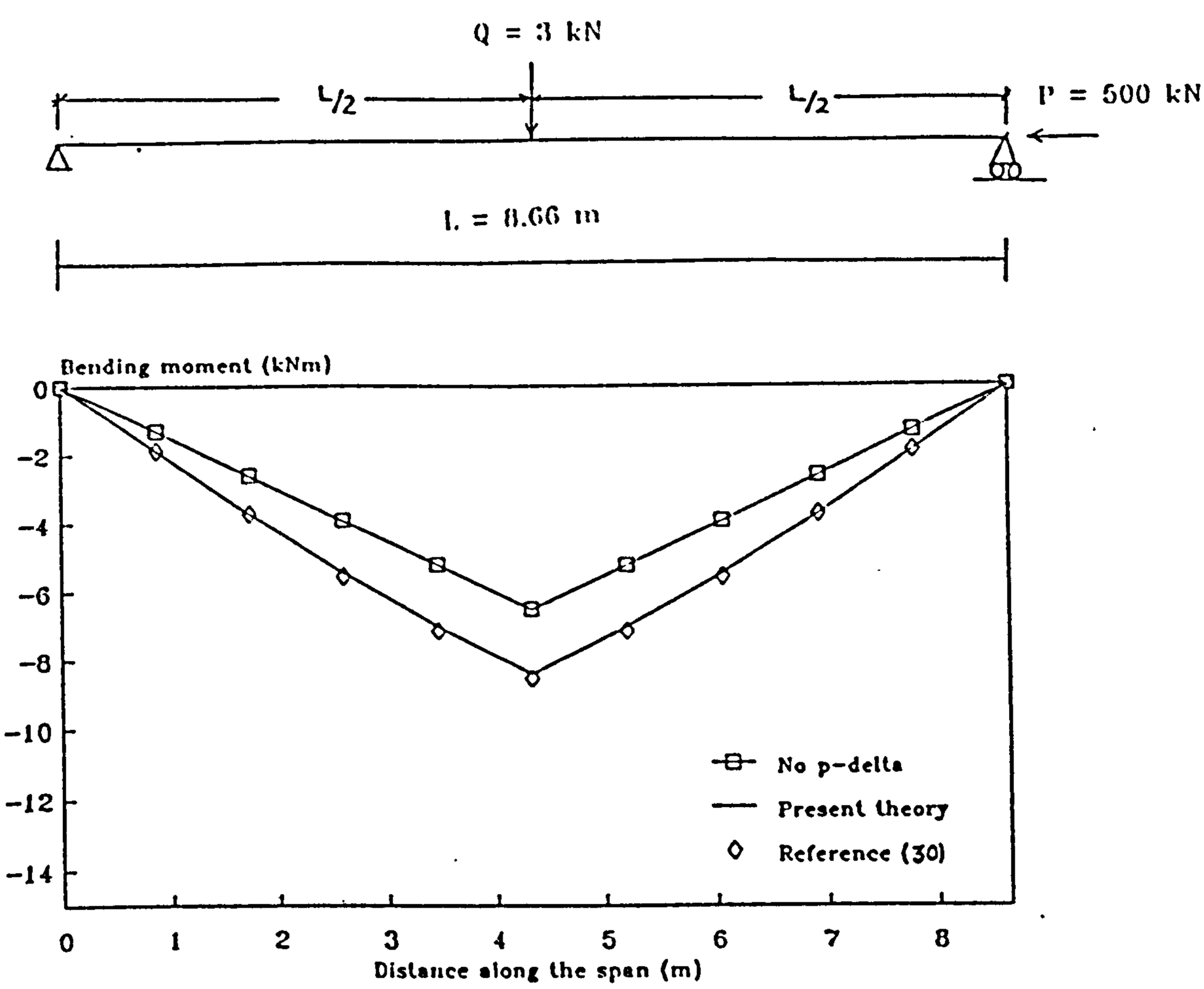

Figure 3.21: Bending moment of beam subjected to a point load and axial load.

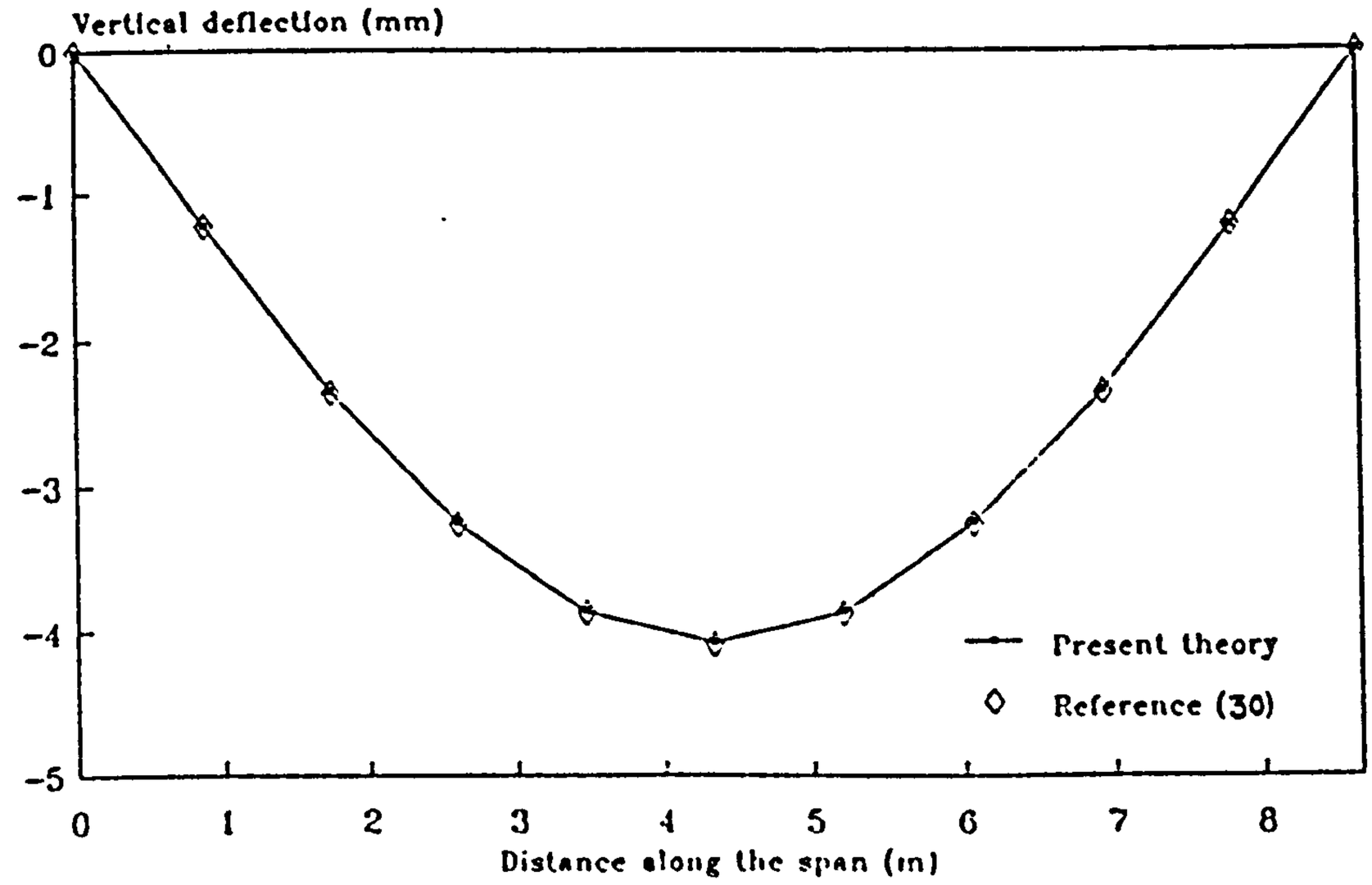

Figure 3.22: Vertical deflection of beam subjected to a point load and axial load (p-delta included).

The structural analyses carried out in Sections 3.9.1 to 3.9.3 demonstrate the potential significance of the p-delta effect on the deflected shape of steel members. Even with a fairly modest axial load, the bending moment at mid-span is increased by up to 50%. The very good comparison between the present method and the results of the differential equation approach [30] indicate that this aspect of the non-linear structural behaviour is being satisfactorily modelled in the current analysis.

3.9.4 Load deflection curve for pin-ended column.

Now consider the load-deflection behaviour of a pin-ended column subjected to various levels of end moment. Cross-section dimensions, length and slenderness ratio are as described in Section 3.9. An increasing value of axial load is applied and the corresponding lateral deflection is plotted in Figure 3.23 for a range of end moments from $0.01M_p$ to $0.4M_p$. This shows that the present theory predicts a load carrying capacity which is always less than the Euler load. In addition the load carrying capacity decreases as end moments increases.

The results for an end moment of 10 kNm ($0.04M_p$) are compared with those obtained from the column deflection curve (CDC) [53] in Figure 3.24 and demonstrate very good agreement between the two methods. This lends support to

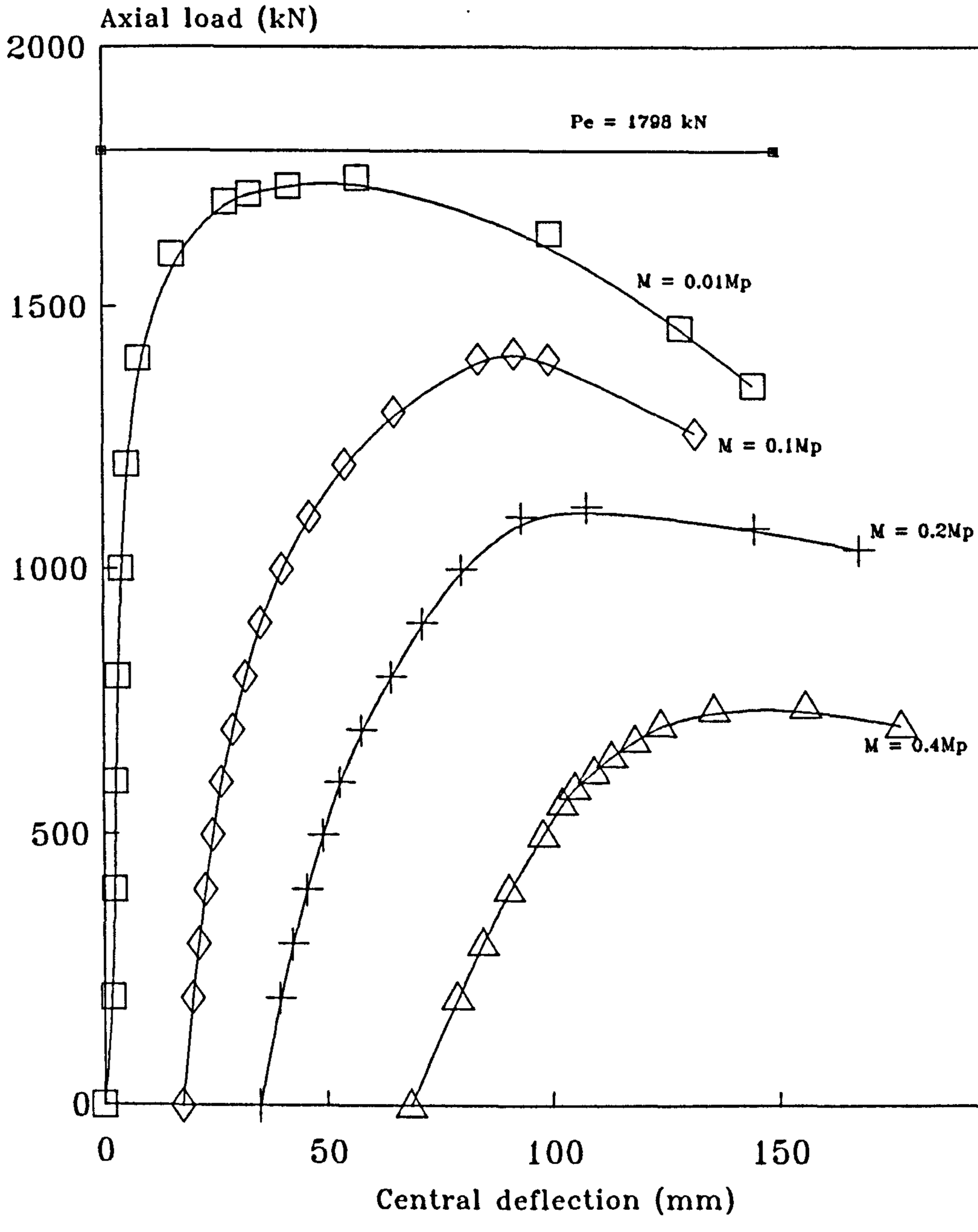

Figure 3.23: Load deflection curves for a pin-ended column with a rectangular cross-section (l/r = 150)

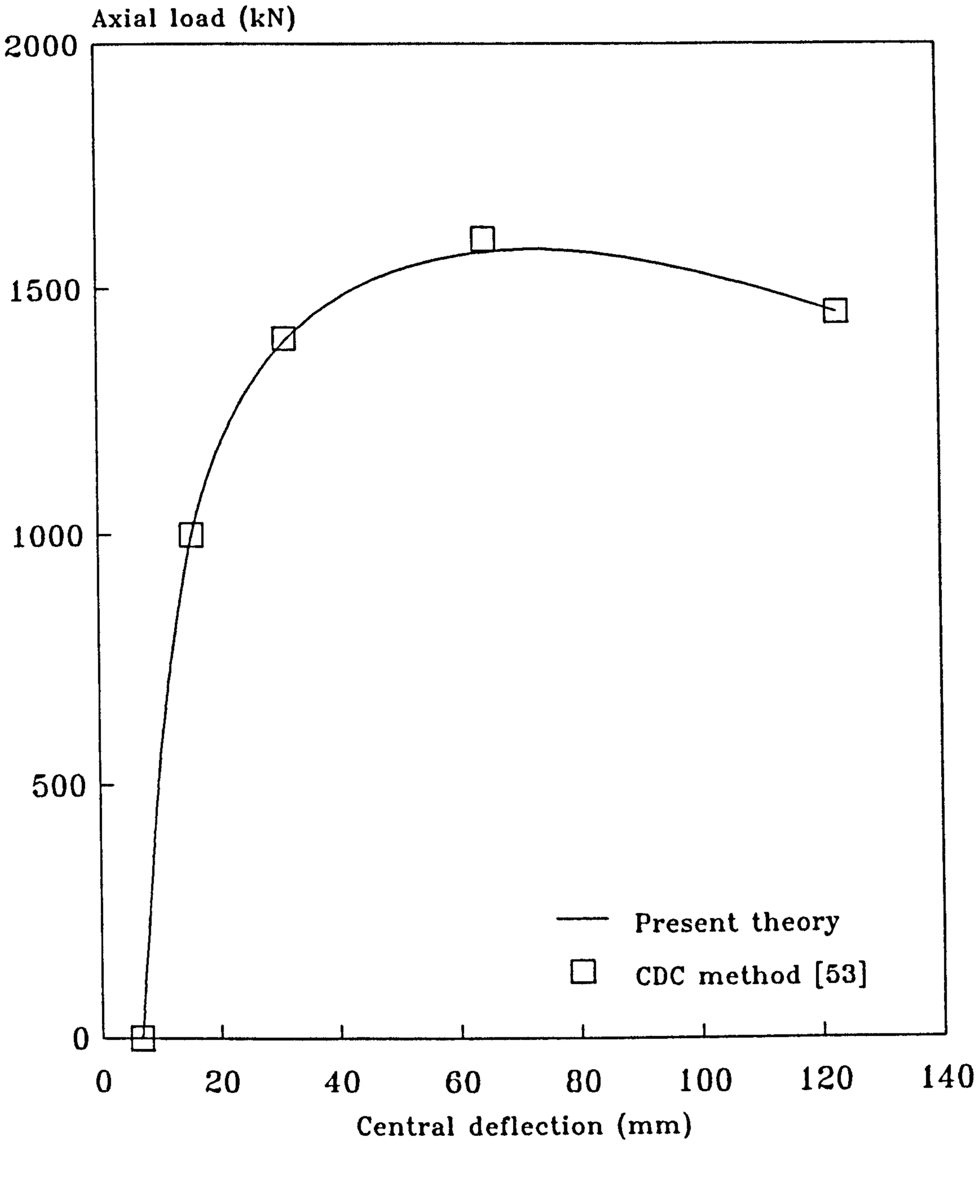

Figure 3.24: Comparison of load-deflection curves obtained by the present theory and the column deflection curve for a rectangular cross-section.

the present treatment of the moment-axial force-curvature relationship with respect to the p-delta effect.

3.9.5 Interaction curve for axial load and bending moment acting on pin-ended column.

The final comparison in this section is of the interaction curve for a pin-ended column of section 8WF31 and slenderness ratio of 120. The curve expresses the maximum axial load which the column can carry when subjected to a certain end moment. Figure 3.25 shows the results reported both by Chen and Atsutsa [53] and the present theory. These are clearly in very close agreement, indicating that both material and geometric non-linearities are treated in a satisfactory fashion in the current analysis.

3.9.6 Conclusion.

The comparisons outlined above demonstrate the accuracy of the present method for the analysis of individual structural members at ambient temperature. In particular the method has proved to be capable of handling material non-linearity and the p-delta effect on the structural analysis at ambient temperature. Although this is not an exhaustive validation it provides evidence that basic non-linear formulation of the element stiffness matrix is satisfactory and that the solution procedures are sound. This provides the basis for

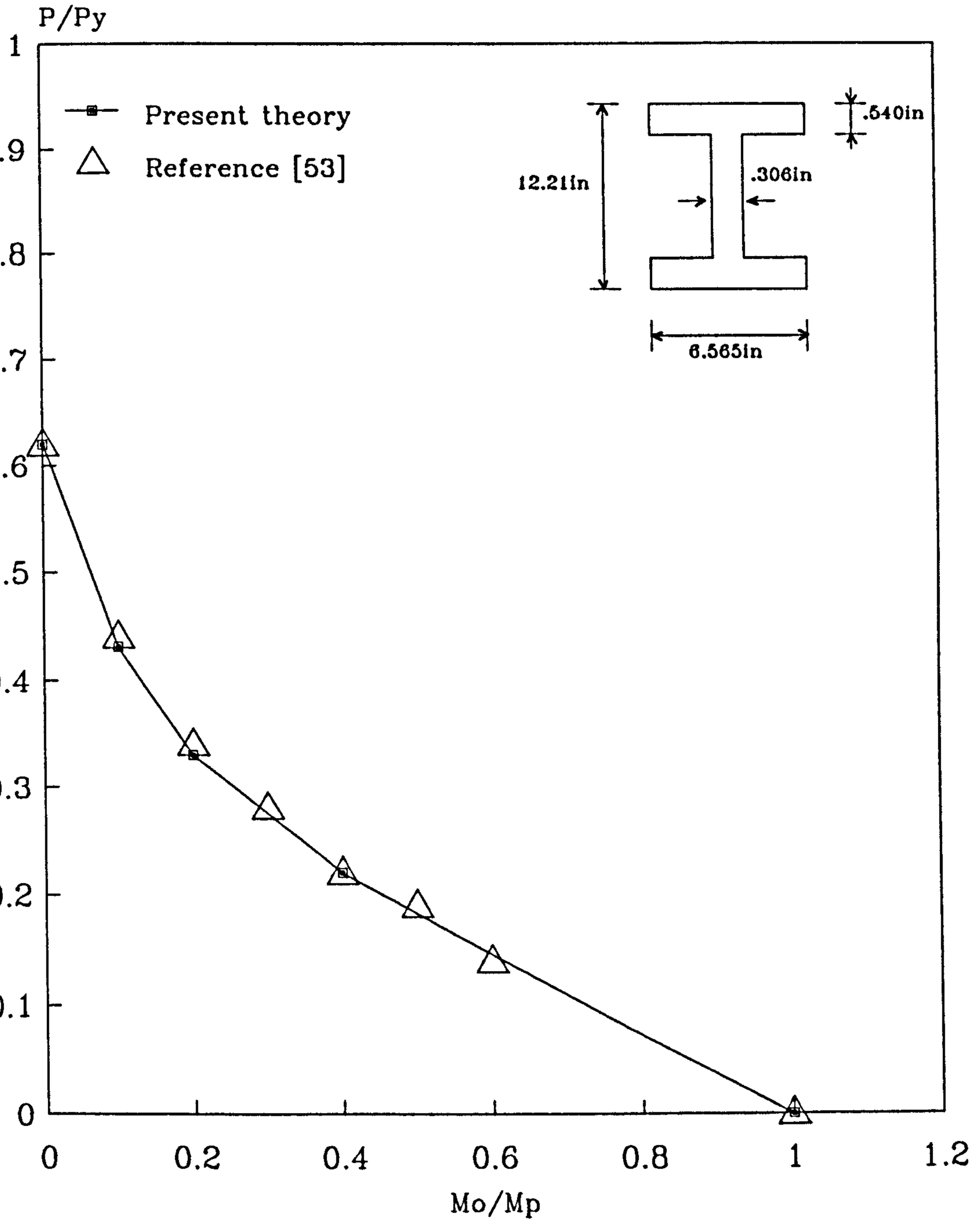

Figure 3.25: Comparison of interaction curves for an I–section pin–ended column (l/rx = 120)

the analysis of frame structures in fire, which effectively requires a series of non-linear solutions at progressively increasing temperature, although other effects such as expansion also need to be included. A more detailed validation of the current method will be given in Chapter 6.

CHAPTER FOUR

THE EFFECT OF MATERIAL UNLOADING ON MOMENT–AXIAL FORCE–CURVATURE RELATIONSHIP AT AMBIENT TEMPERATURE AND IN FIRE

4.1 INTRODUCTION.

In order to consider the subject of material unloading, it is necessary to trace the exact sequence of strain distribution produced as a cross-section is loaded. Strain reversal happens when the strain is reducing from a previous state and consequently induces unloading stress. If this happens to material in the elastic region there is a unique relationship between the stress and strain in which the loading and unloading paths are the same, but this is not the case in a plastic region. A non-unique relationship exists for the latter case due to the fact that the loading and unloading paths are different.

The potential implication of material unloading for frame analysis can be illustrated by considering a section under combined bending moment and axial force, and examining its final stress profiles, initially at ambient temperature.

To start with, a `strain controlled' loading system is discussed to show qualitatively the effect of material unloading on a beam-column cross-section by combining the axial and bending strain profiles corresponding to an independent axial force P and bending moment M. This is then developed towards a `load controlled' loading system, to illustrate that there is a range of possible means of achieving a final strain profile which create the required axial force P and bending moment M. This is followed by numerical determination of moment-axial force-curvature relationships for different cross-sections. The influence of material unloading on the final stress profile is then extended to the case of fire where the effects of material expansion and softening are included.

4.2 THE INFLUENCE OF MATERIAL UNLOADING ON THE FINAL STRESS PROFILE.

4.2.1 `Strain controlled' loading system.

The influence of material unloading on a stress profile can be examined by considering a `strain controlled' application of axial and bending strains on a cross-section, corresponding to an independent axial force P and bending moment M. The entirely elastic condition is discussed first, considering the strain at the extreme fibres of the cross-section.

From Figure 4.1a, suppose ε_a is the axial strain, and ε_{b1} and ε_{b2} are the bending strains at the top and bottom of the section, and both are in the elastic region. By combining these strain profiles in different orders (i.e. axial strain first, followed by bending strain, or vice versa) the stress and strain profiles are shown in Figures 4.1b and 4.1c respectively. It is evident that a unique relationship exists in which the final stresses for both cases are the same, so that superposition of stresses is valid.

The influence of material unloading in the plastic range is considered next. Suppose an initial bending strain profile is itself elasto-plastic. Combinations of axial and bending strains, applied in alternate order, are shown in Figures 4.2a and 4.2b. From the figures, it can be seen, even though the final strain profiles are the same, that due to different material unloading the final stress profiles are different, particularly in the tensile region. Figure 4.2b shows that, in the case where bending strain is applied first followed by an axial strain, material unloading happens in the tensile zone. This causes a different stress profile to that in which the strains are applied in the alternative order (Figure 4.2a). This demonstrates the non-uniqueness of stress states caused by material unloading in the plastic region. In addition, the final moment and axial force are clearly neither identical in the two cases nor to the required external forces.

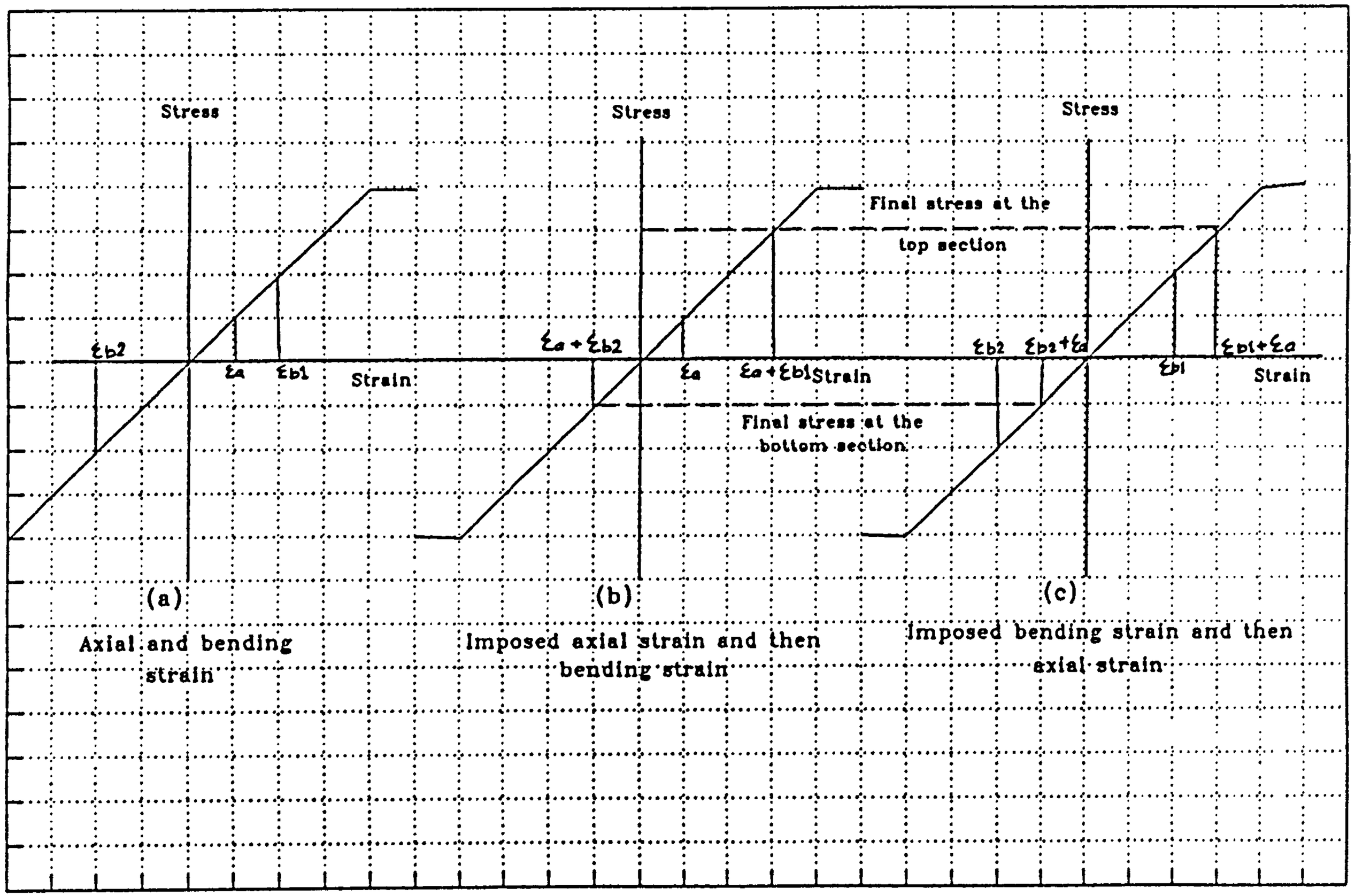

Figure 4.1: Influence of material unloading in the purely elastic region.

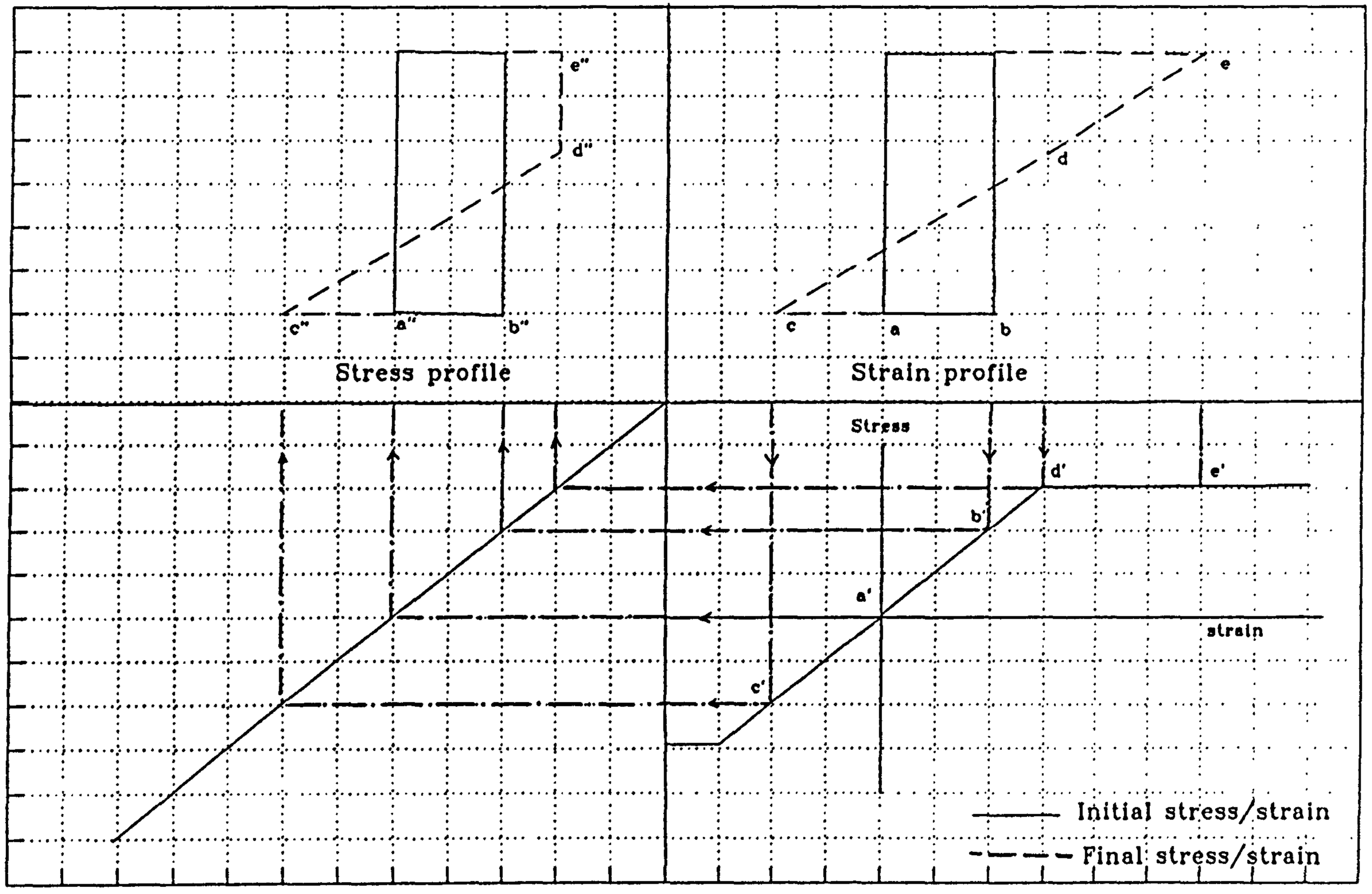

Figure 4.2a: Influence of material unloading when axial strain is applied first, followed by bending strain.

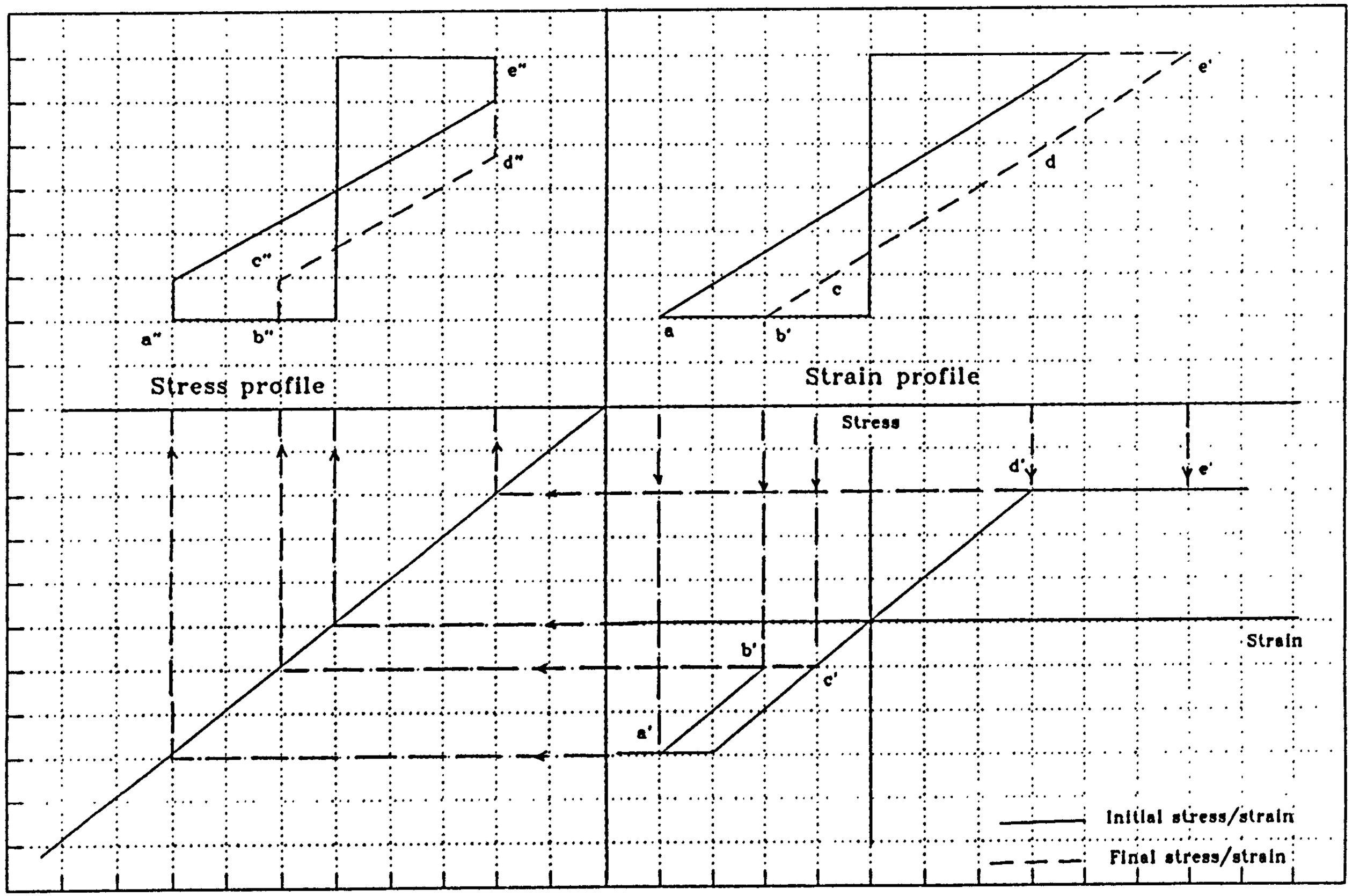

Figure 4.2b: Influence of material unloading when bending strain is applied first, followed by axial strain.

4.2.2 'Load controlled' loading system.

At all stages of equilibrium the internal force resultant must equate to the externally applied moment and thrust, but the final strain profile cannot simply be produced by superposing the strains as described in the previous section. Because of this, a 'load controlled' loading system is discussed to show a range of possible means of achieving a final strain profile which creates the required axial force P and bending moment M.

Consider first the final strain profile produced by superposing the strains caused independently by the force components (i.e bending moment M and axial force P). It is evident from the previous section that both the internal moment and thrust will be less than these external values. In order to bring the internal and external forces into balance it is necessary to increase both the mean strain and the strain gradient. Whichever external 'force' is to be applied 'first' must first be rebalanced by adjusting the appropriate component of the strain profile (see Figure 4.3). This will reduce the 'second' force component whose strain component must be increased. This process is clearly iterative, and shows that 'strain control' and 'load control' applications of axial force and bending moment do not necessarily result in the same final distribution of stress.

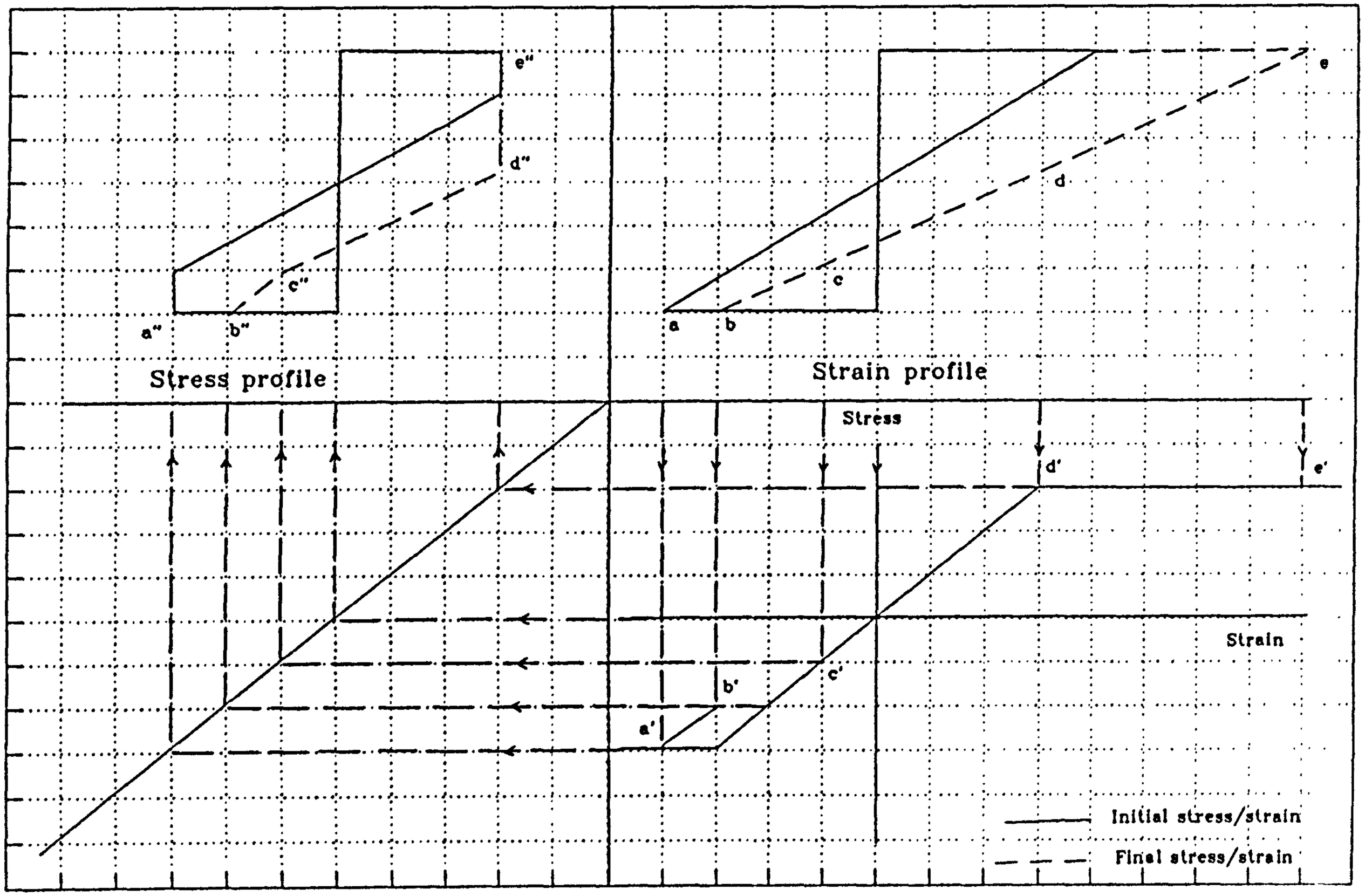

Figure 4.3: Influence of material unloading when bending moment is applied first, followed by axial force.

The main concern of this chapter is to identify the degree to which this non-uniqueness of the influence of material unloading affects the moment-axial force-curvature relationship.

4.3 DETERMINATION OF FINAL STRESS BY INCLUDING THE EFFECT OF MATERIAL UNLOADING AT AMBIENT TEMPERATURE.

The determination of the final stress distribution across a section due to the effect of material unloading is now discussed. It should be noted that, in order to quantify the effect of material unloading on the moment-axial force-curvature relationship, initial and final strain distributions must be known. Also the tension and compression zones must be clearly identified before proceeding to any further calculations, because in the presence of material unloading the condition of the material in a certain region may change from a tension zone to a compression zone or vice versa. The stress-strain curves in tension and compression are assumed to be identical, and a sign convention of tension positive and compression negative is adopted.

In deriving the moment-axial force-curvature relationship the cross-section is divided into strips, each at a uniform level of strain and stress over its depth, as described in Section 3.4. The final stress σ_f in each strip is determined according to the particular conditions applying

to the change of the initial strain ε_{1_0} as shown in Figure 4.4a. These show the logical sequence in determining the final stress due to loading and unloading conditions in the compression and tension zones of the cross-section respectively.

If the magnitude of the final strain ε_{1_1} is greater than the initial strain ε_{1_0} the strip has undergone a process of loading. The corresponding final stress is therefore equal to the Young's Modulus multiplied by the final strain or to the yield stress, whichever is the smaller. On the other hand, if the magnitude of the final strain is less than the initial strain, or it has reversed, then the strip has undergone a state of unloading. If the initial strain is less than the yield strain the corresponding final stress is therefore equal to the Young's Modulus times the final strain. However, if the initial strain is greater than the yield strain the unloading path is different from the loading path and the final stress is then given by Equation 4.1.

$$\sigma_{1_1} = \sigma_y - E(\varepsilon_{1_0} - \varepsilon_{1_1}) \quad \ldots\ldots\ldots\ldots (4.1)$$

where σ_{1_1} = final stress.

σ_y = yield stress.

Having determined the stress in each strip in this way, the internal bending moment and axial force in the cross-

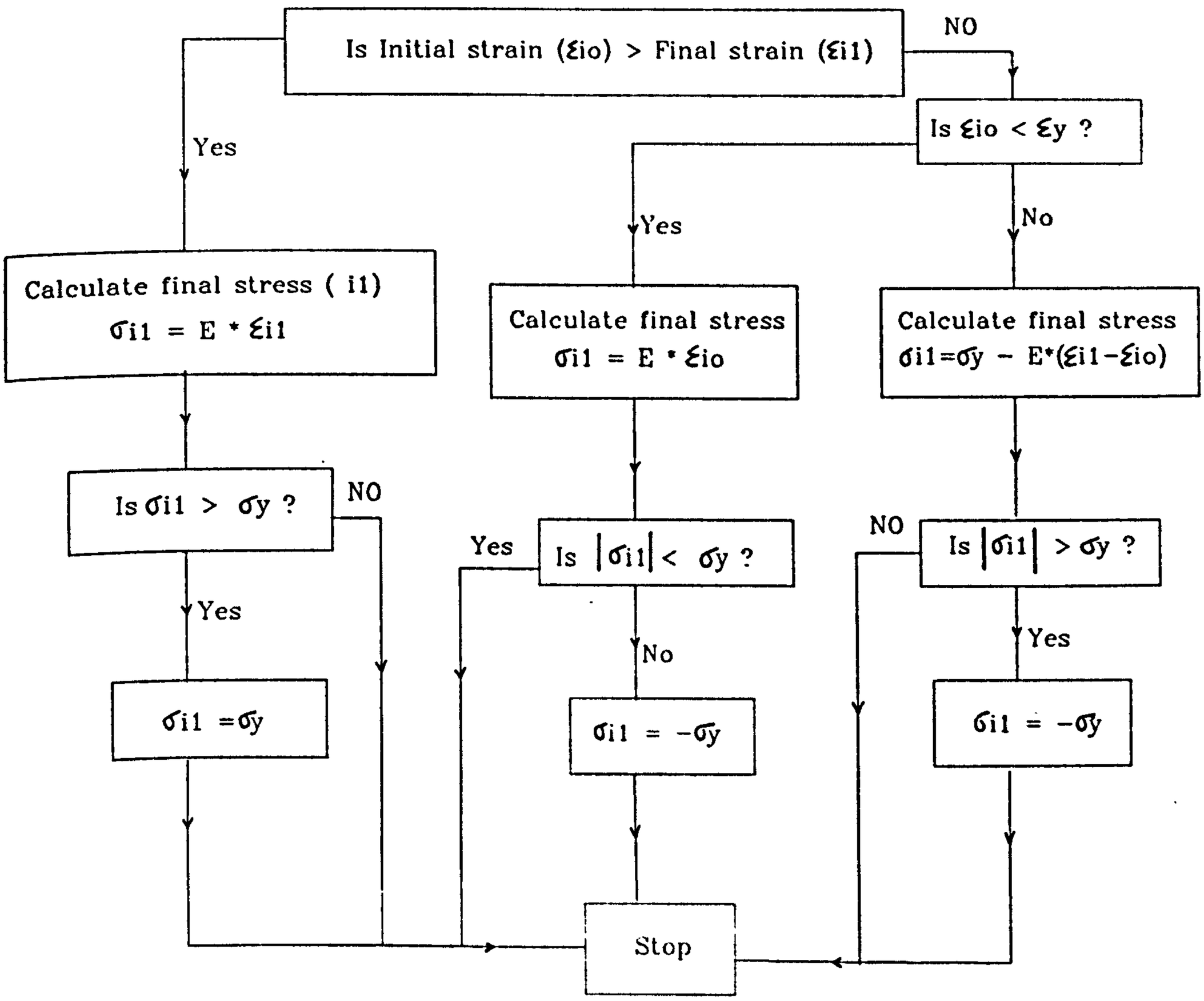

Figure 4.4a: Algorithm for calculating the final stress accounting for loading and unloading conditions.

[Note: the procedure described here relate specifically to an initial tensile stress state. An almost identical procedure applies for initiel compression]

section can be computed from Equations 3.13 and 3.14 respectively. The determination of the corresponding moment-axial force-curvature relationship based on this principle is described in detail in the following section.

4.4 THE DERIVATION OF MOMENT-AXIAL FORCE-CURVATURE RELATIONSHIP BY INCLUDING THE EFFECT OF MATERIAL UNLOADING AT AMBIENT TEMPERATURE.

The derivation of moment-axial force-curvature relationship described in Chapter 3 will now be extended to include the effect of material unloading. From the previous discussions this derivation clearly depends on how the axial force and bending moment are applied. To investigate this three cases are considered as follows:

Case 1. Bending moment is applied first and then an axial force.

Case 2. Bending moment and axial force are both applied simultaneously.

Case 3. Axial force is applied first and then bending moment.

The numerical determination of the curvature relationships due to the first and third cases will be discussed in the following section. The second, which implicitly ignores

the possibilities of material unloading, has been used by many authors in deriving moment-axial force-curvature relationships [45],[48],[53]. This will used as a comparison for the other two cases.

4.4.1 Determination of moment-axial force-curvature relationship by including the influence of material unloading.

A computer program was developed to investigate the effect of material unloading on the moment-axial force-curvature relationship. A rectangular section and an I-section will be considered. The influence of material unloading on a beam-column cross-section for case 1 is considered first. The logical sequence of operations involved in this case is divided into two stages as shown in Figure 4.4b. The first stage is to determine the final strain distribution during the first equilibrium condition (i.e $M_{int} = M_{ext} = M$ and $P_{int} = P_{ext} = 0$). This strain distribution is taken as the initial condition for the second stage, where an axial force is introduced and the new equilibrium condition must be determined (i.e $M_{int} = M_{ext} = M$ and $P_{int} = P_{ext} = P$). By comparing the initial and assumed values of the final strain distributions across the section, the loading and unloading regions can be identified. Thus, the internal axial force and bending moment of an element can be calculated. The normal process of iteration is then carried out until the second equilibrium condition is achieved.

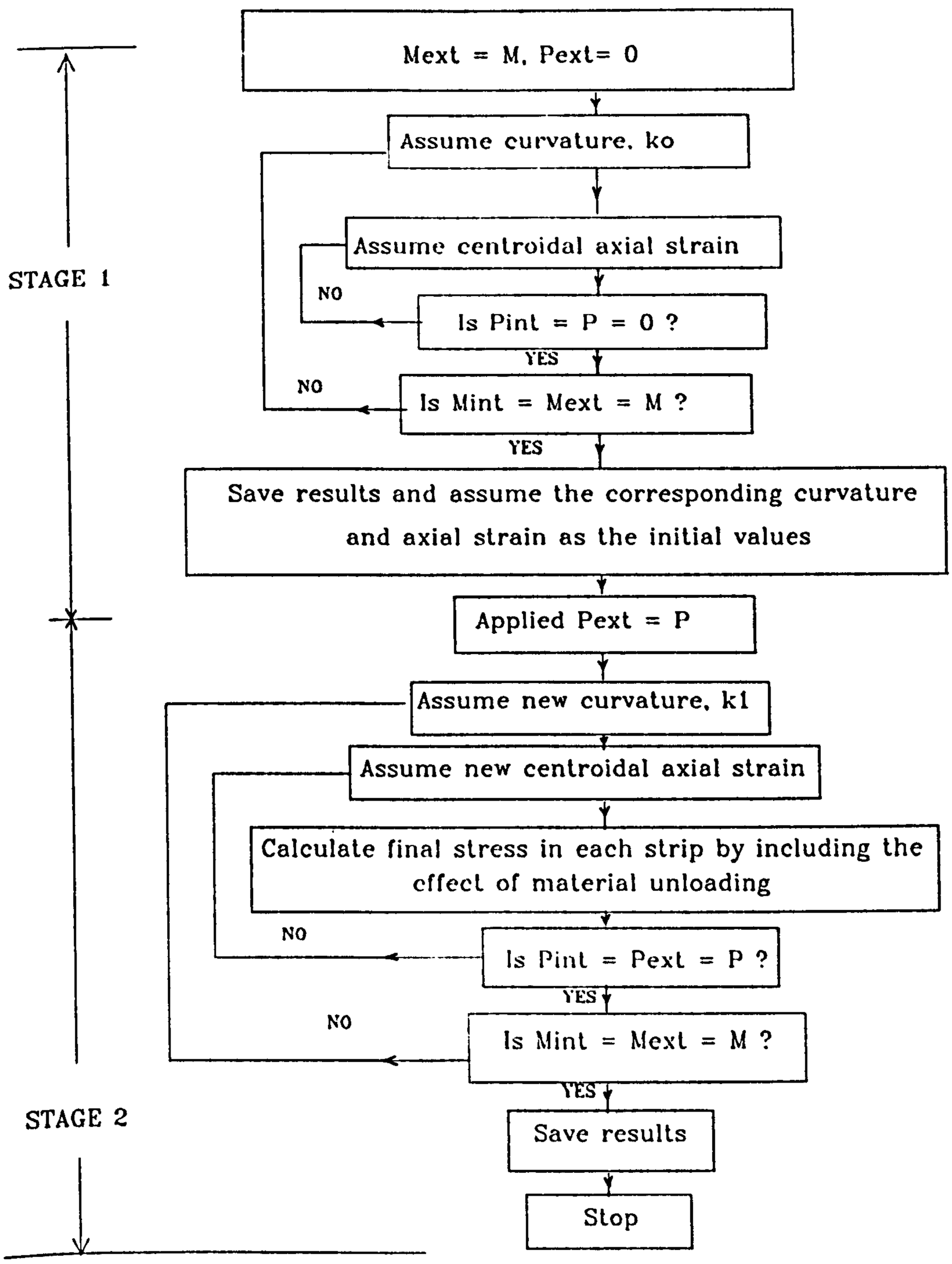

Figure 4.4(b): Logical sequence of operations in deriving moment–axial force–curvature relationship due for case 1 (bending applied first, followed by axial load).

The logical sequence of operations for case 3 is identical to the above except that the initial equilibrium condition has $P_{int} = P$ and $M_{int} = 0$. This is because axial force P is applied first without any bending moment. The corresponding strain distribution is then considered as the initial value for the second stage of the operation in which the bending moment M is applied. An iteration process is then carried out to determine the new curvature relationship which is similar to that shown in Figure 4.4b.

4.4.2 The effect of material unloading on a rectangular cross-section.

To illustrate the effect of material unloading on the moment-axial force-curvature relationship consider a rectangular cross-section with dimensions of depth h = 400mm, width b = 200mm, Young's Modulus E = 205000 N/mm² and yield stress σ_y = 250 N/mm². Figure 4.5 shows a comparison of the curvature relationships between case 1, case 2 and case 3. It is clear that curvatures calculated for case 2 and case 3 are exactly the same. This is because, for an elastic-perfectly plastic material, unloading for case 3 is always within the elastic region and consequently has no effect on the moment-axial force-curvature relationship.

Comparing case 1 and case 2 when the axial load is relatively small ($P = 0.2P_y$) there is a small difference in the curvature relationship. However when the axial load

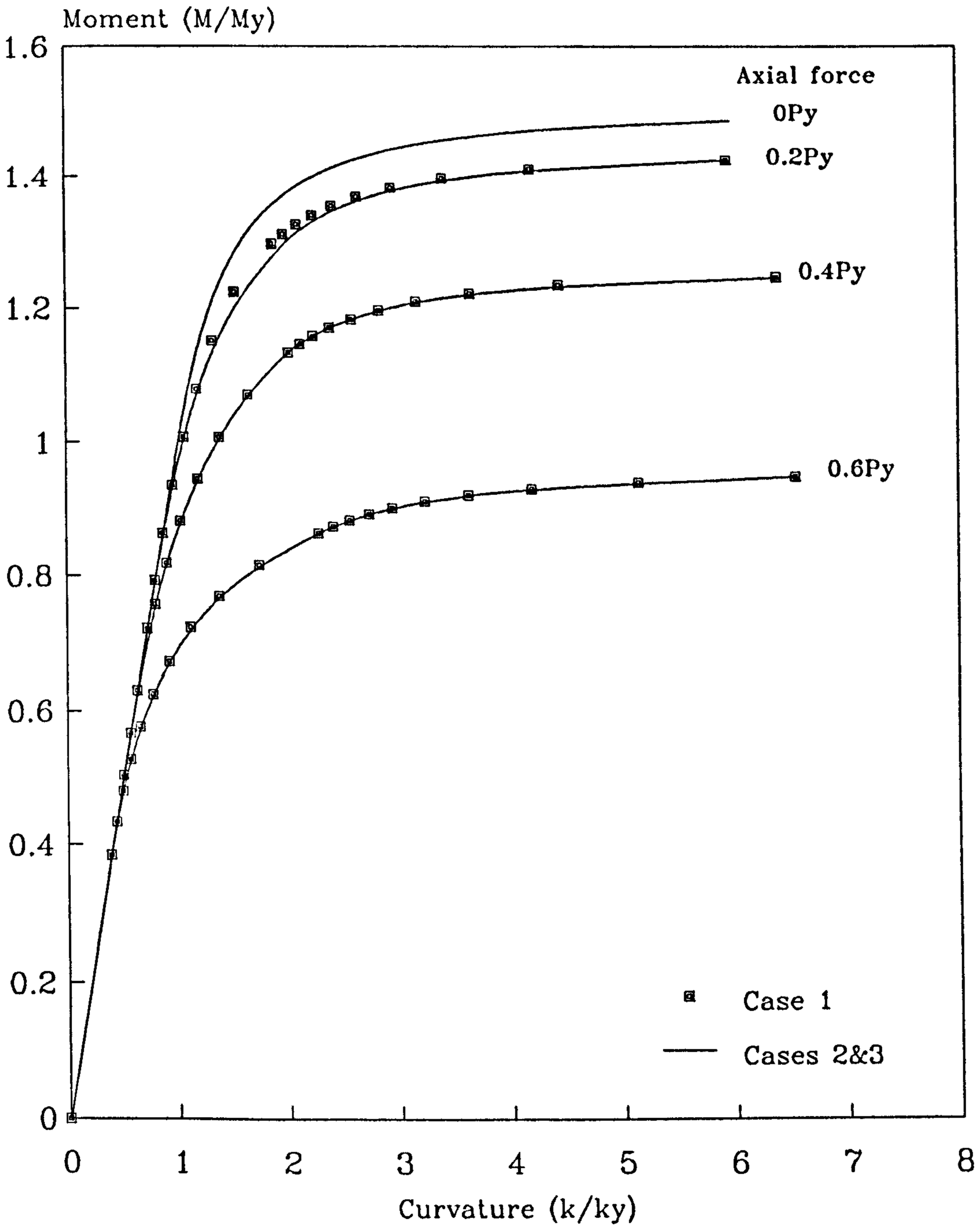

Figure 4.5: Moment–axial force–curvature relationship for rectangular cross–section.

increases ($P = 0.4P_y$ or $P = 0.6P_y$) this difference is no longer apparent.

Figure 4.6 shows the moment-curvature relationship for case 1 and case 2 for $P=0.2P_y$ and Figure 4.7 shows the corresponding stress profiles for increasing moment in case 1. The continuous line represents the initial stress distribution due to the effect of bending moment M while the dotted line represents the final stress block diagram when an axial force is subsequently applied to the element. For bending moments up to about $1.00M_y$ ($0.67M_p$), these two curvatures are the same. This is due to the fact that material unloading is entirely within the elastic range as shown in Figure 4.7. This is confirmed in Figure 4.8 which shows that during this period the final stress profile for cases 1 and 2 are exactly the same.

When the bending moment M is increased to a value greater than $1.00M_y$, the curvature for case 1 (in which the unloading effect is considered) is greater than the curvature obtained in case 2. This difference is due to the fact that material unloading is now occurring in the plastic range, as shown in the stress block diagrams of Figure 4.7. Further increase in bending moment up to about $1.32M_y$ ($0.92M_p$) results in a more marked difference between the two cases. This is due to the fact that the region subjected to material unloading in the plastic range increases as shown in Figure 4.7. However when the bending

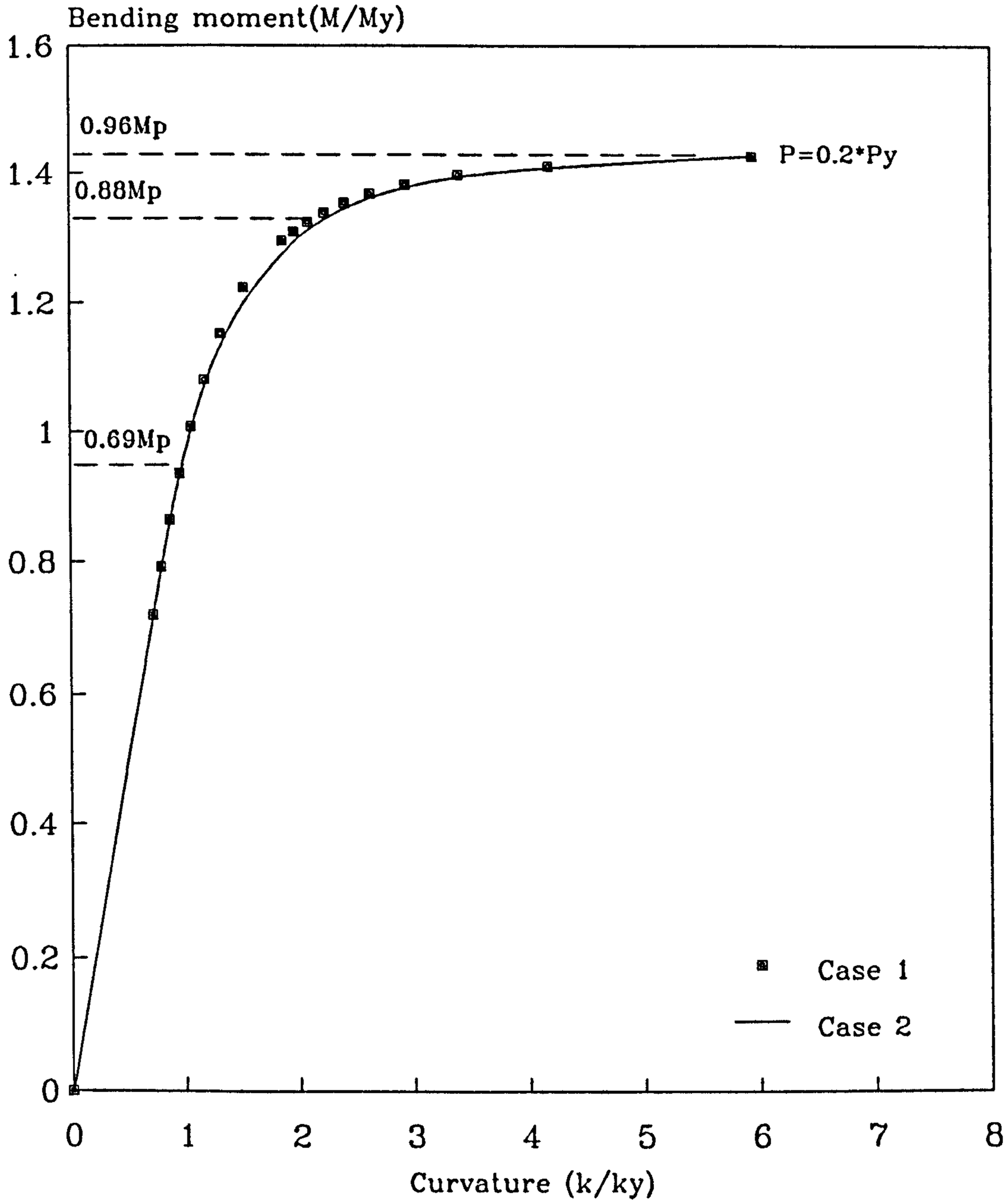

Figure 4.6: Moment–curvature relationship for a rectangular cross–section when P=0.2Py.

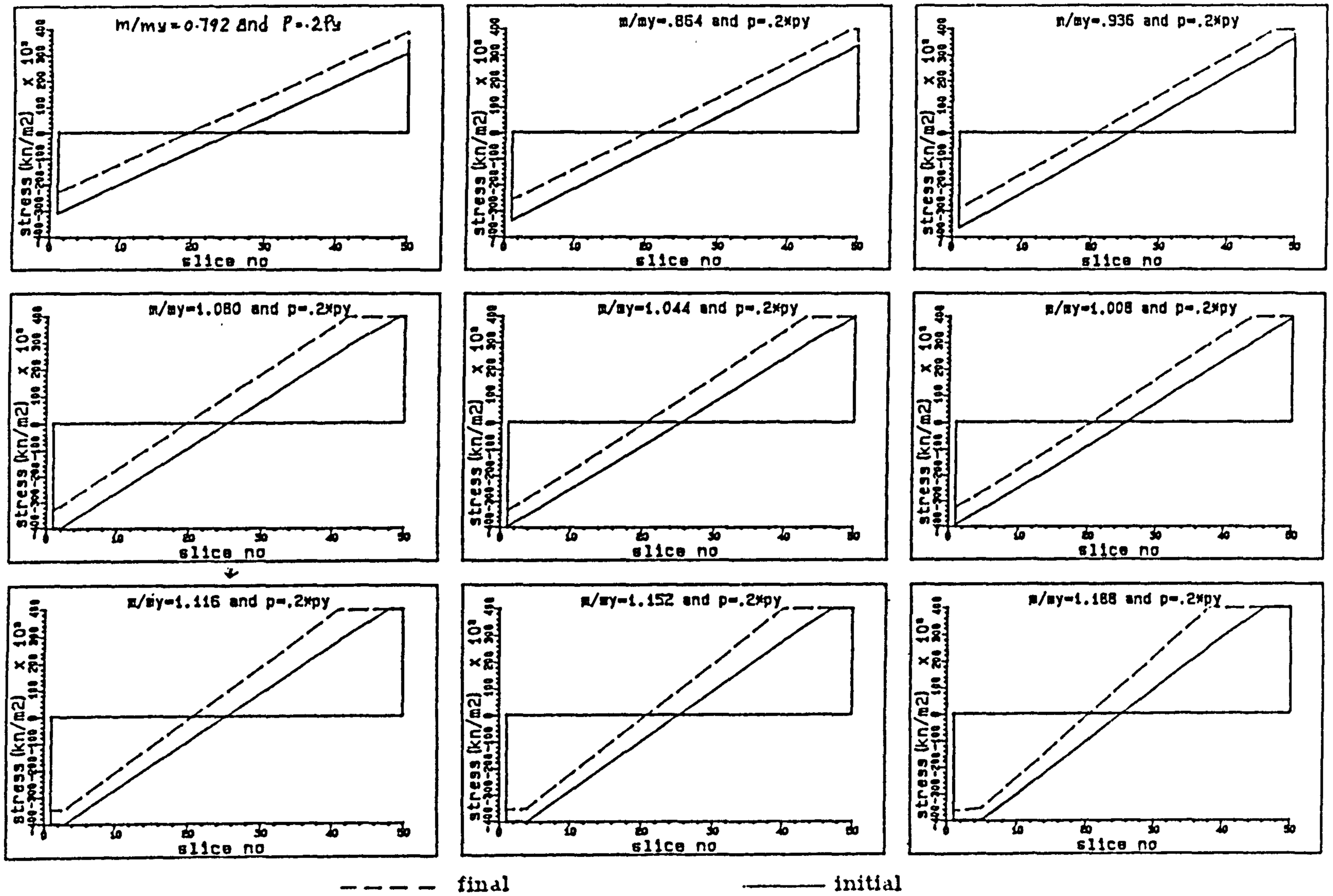

Figure 4.7: Initial and final stress block diagrams for a rectangular beam-column element for increasing moments when P=0.2Py - case 1.

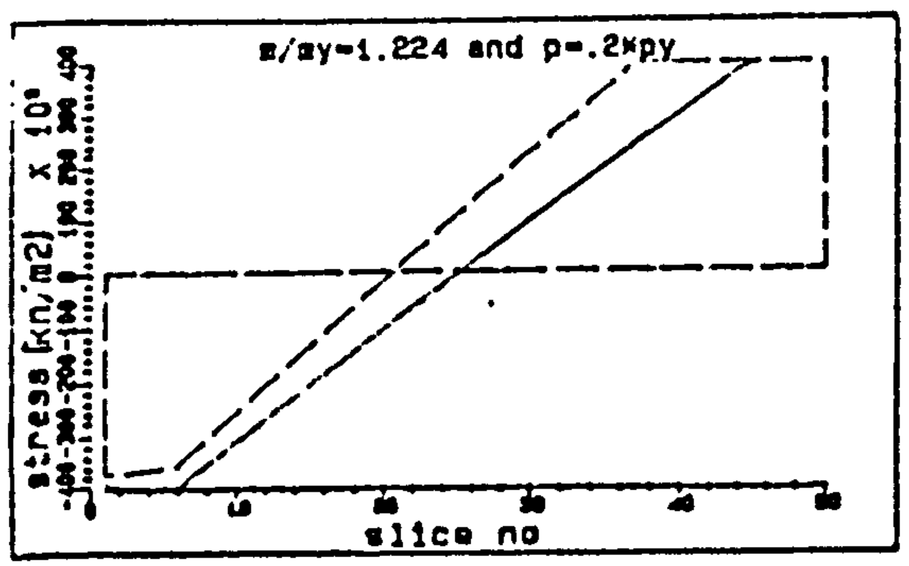

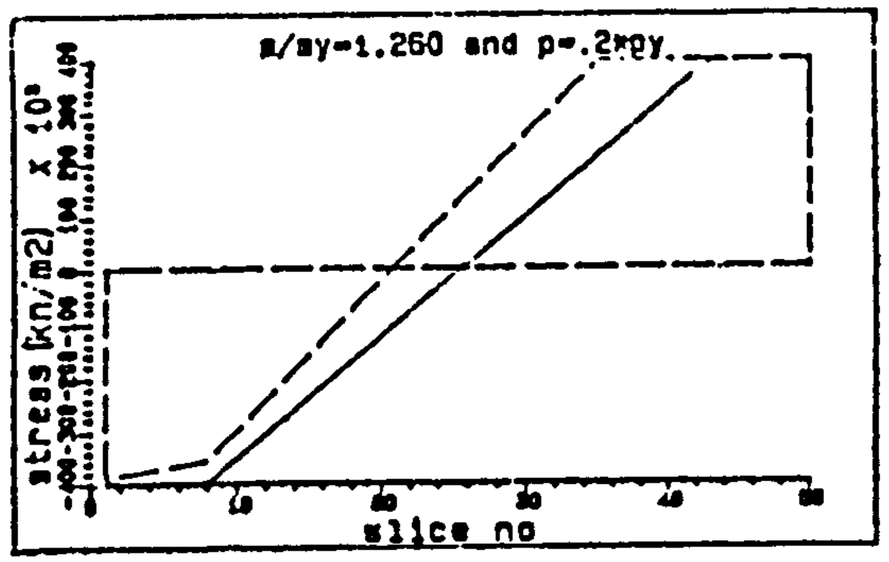

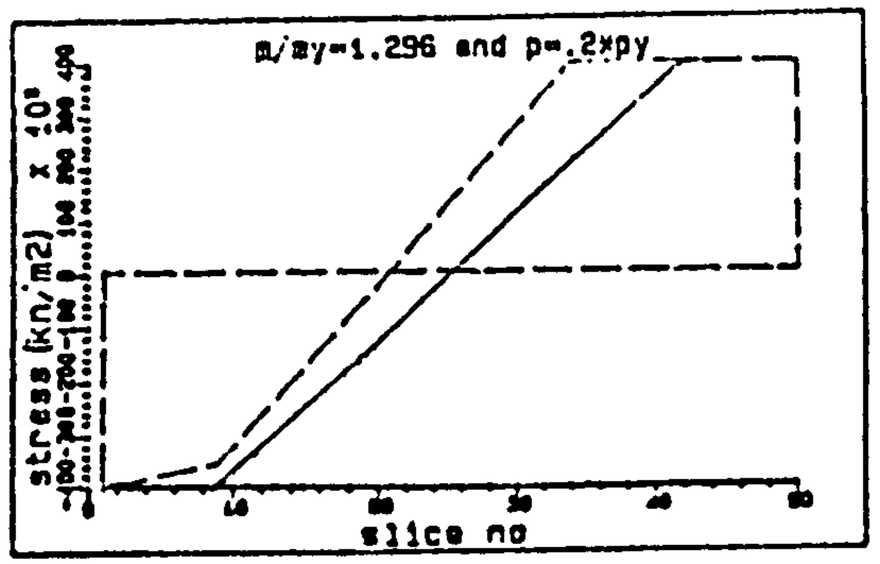

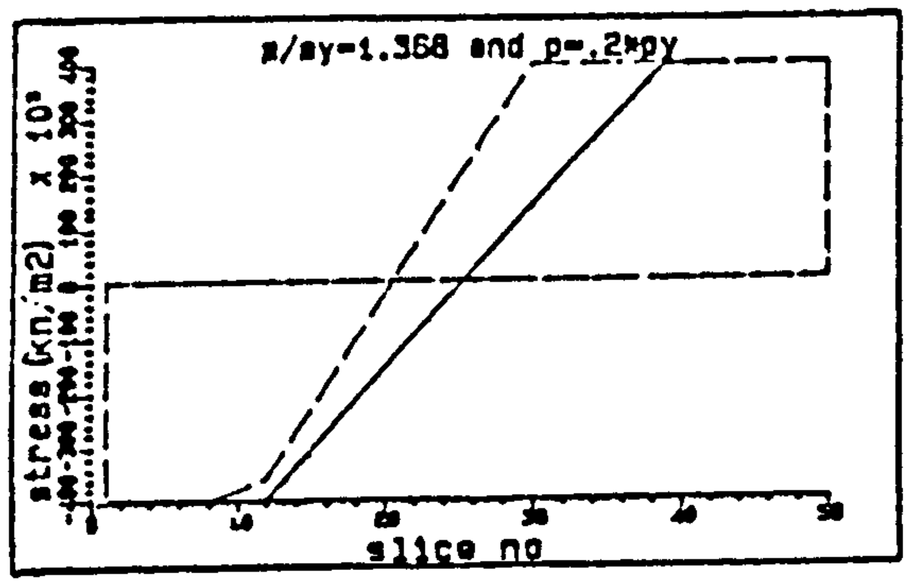

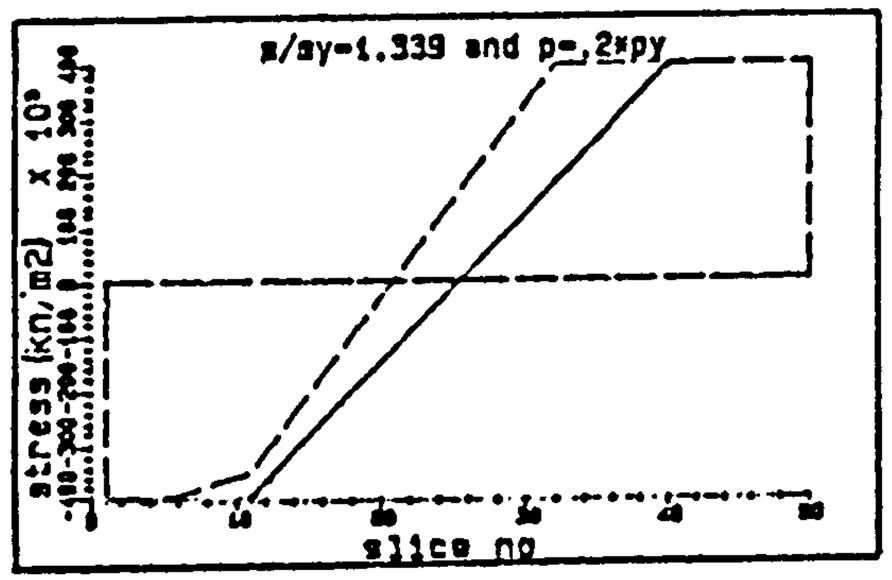

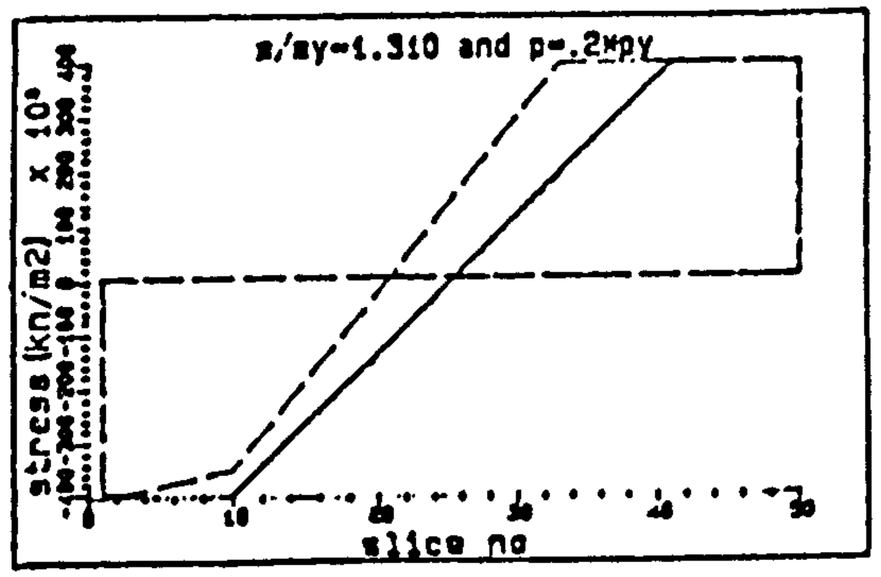

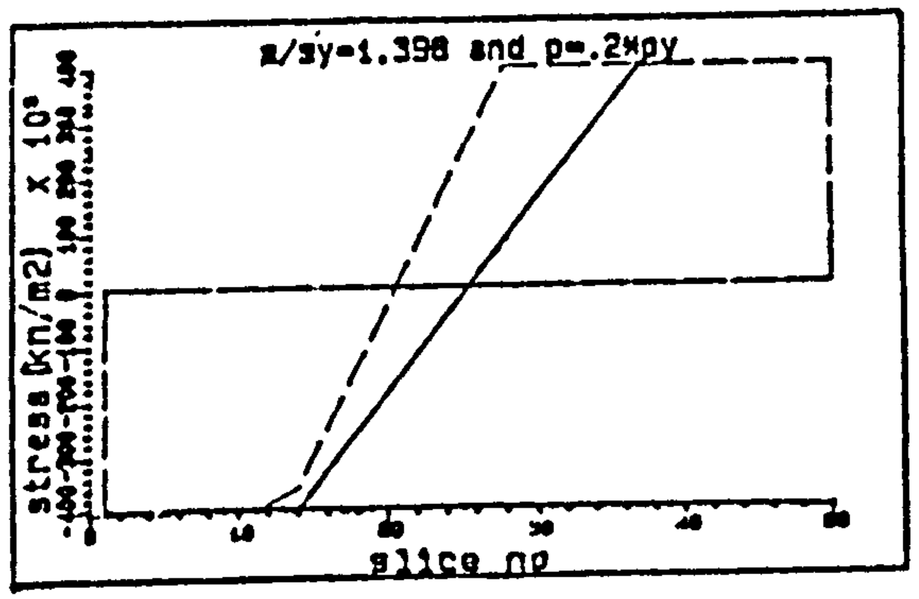

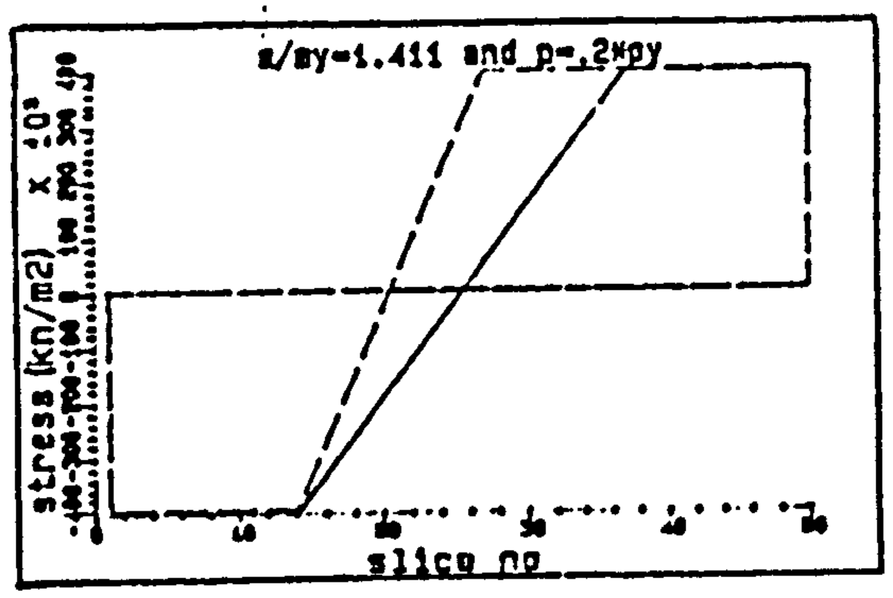

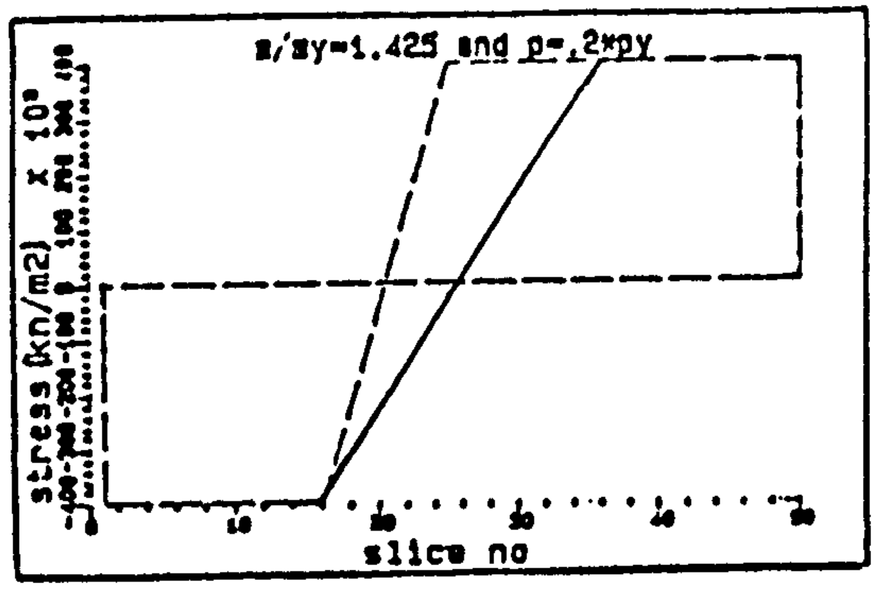

Figure 4.7 (continued)

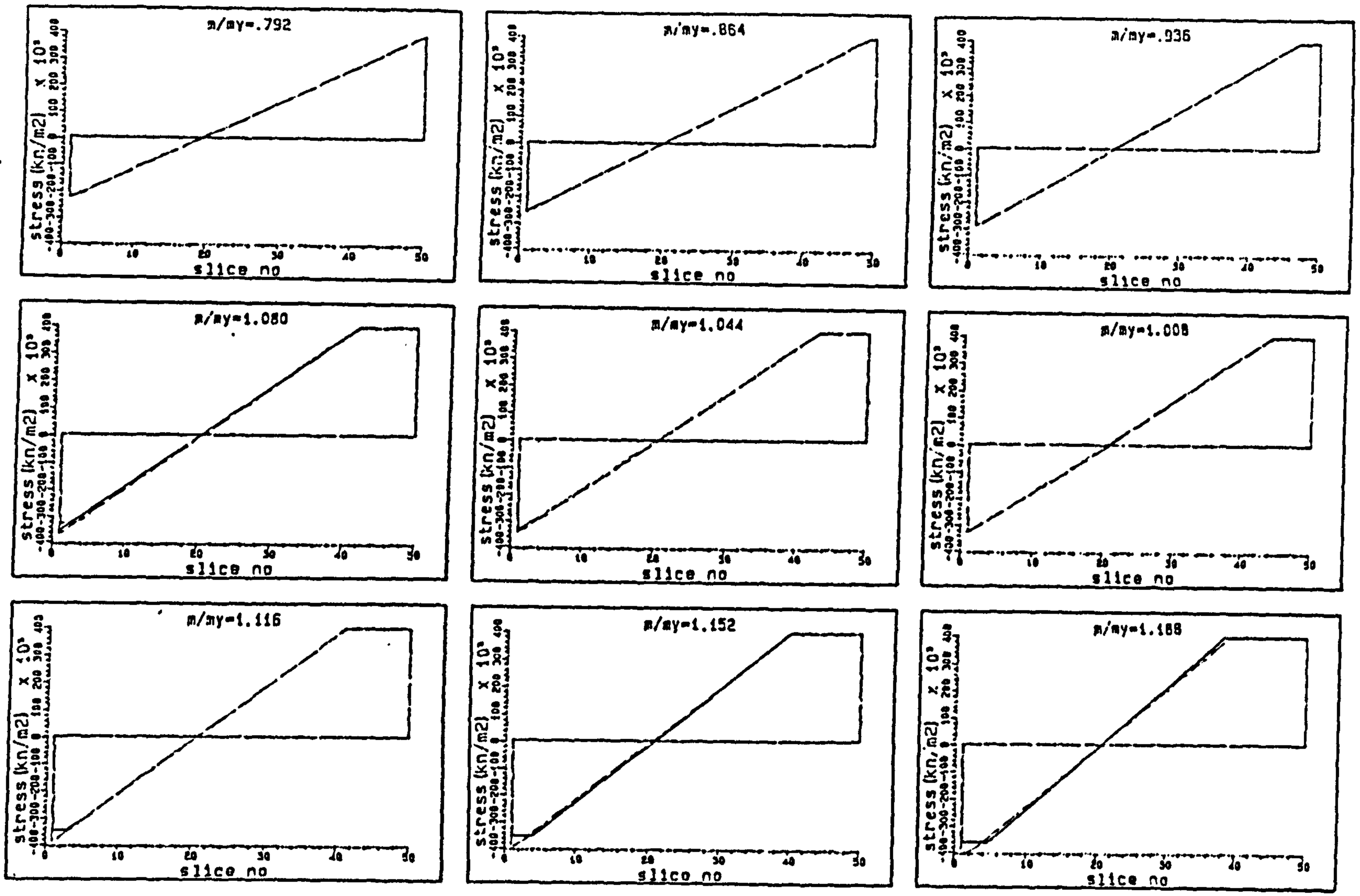

Figure 4.8: Final stress profiles in case 1 and case 2 of beam-column element with increasing moments when P=0.2Py.

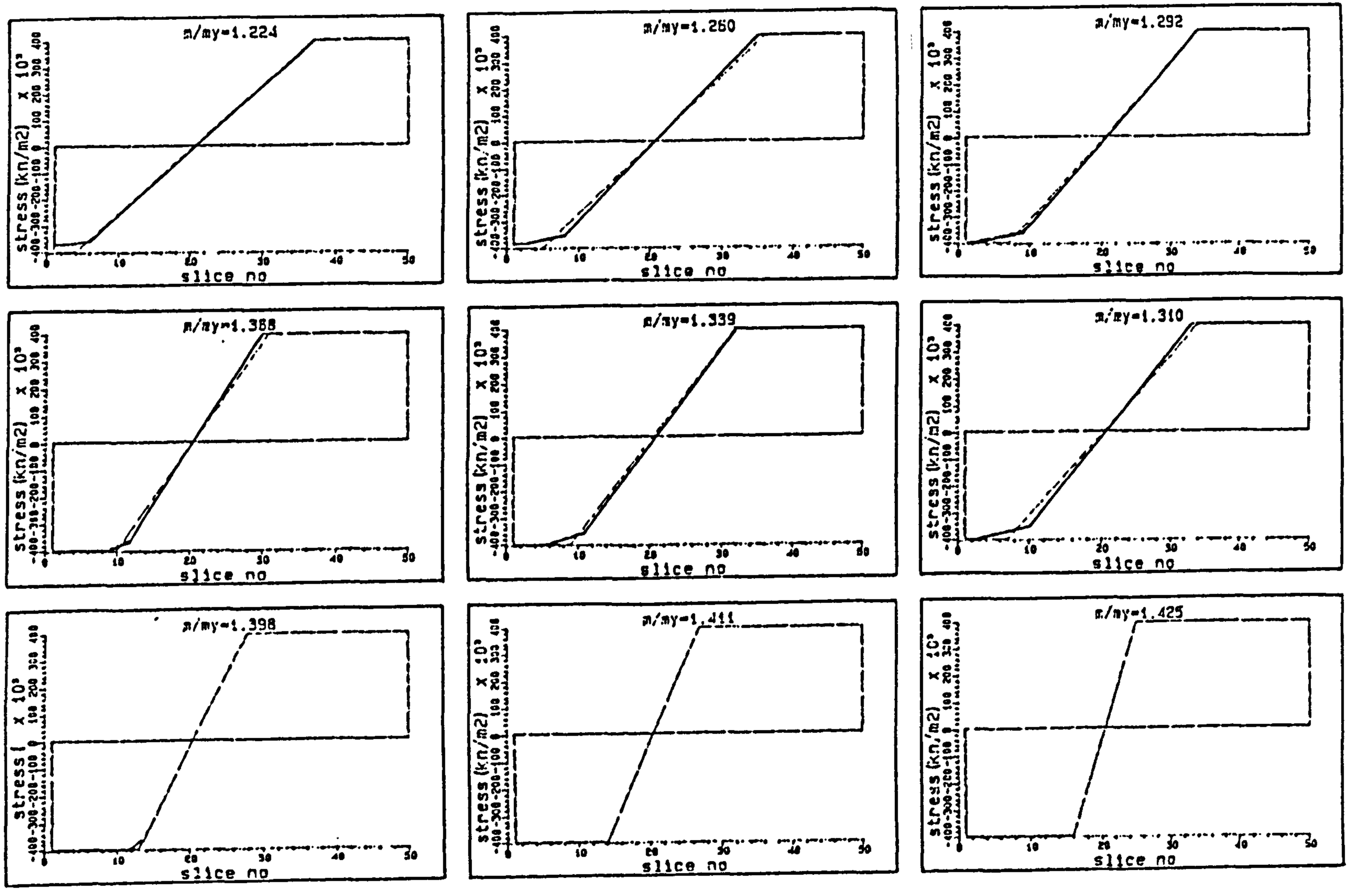

Figure 4.8 (continued)

moment M is increased above $1.32M_y$ ($0.92M_p$) the difference between the two curvatures decreases. This is because material unloading in the plastic range reduces. Even though a large bending moment is applied, initially causing a large plastic region, the final process of balancing the internal and external forces and moments results in a change in stress distribution in which very little unloading is occurring within the plastic region.

Similar comparisons are made in Figures 4.9 to 4.14 for axial loads $P=0.4P_y$ and $P=0.6P_y$. Figure 4.9 shows a comparison between the moment-curvature relationships for case 1 and case 2 for $P=0.4P_y$. A series of stress block diagrams is presented in Figure 4.10 showing initial and final stresses for case 1 and a comparison of the final stress levels for the two cases is shown in Figure 4.11.

Figure 4.10 shows that material unloading in the plastic range is still occurring for bending in the range $1.071M_y$ to about $1.134M_y$. However, the affected area is very small and hence the difference in the curvature relationships between case 1 and case 2 is negligible. Figure 4.10 also shows that even though most of the section in the element is strained into the plastic region, the final process of balancing the internal and external forces and moments results in no material unloading in the plastic region. A similar pattern of behaviour was observed for higher axial loads as shown in Figures 4.12 to 4.14 for $P=0.6P_y$.

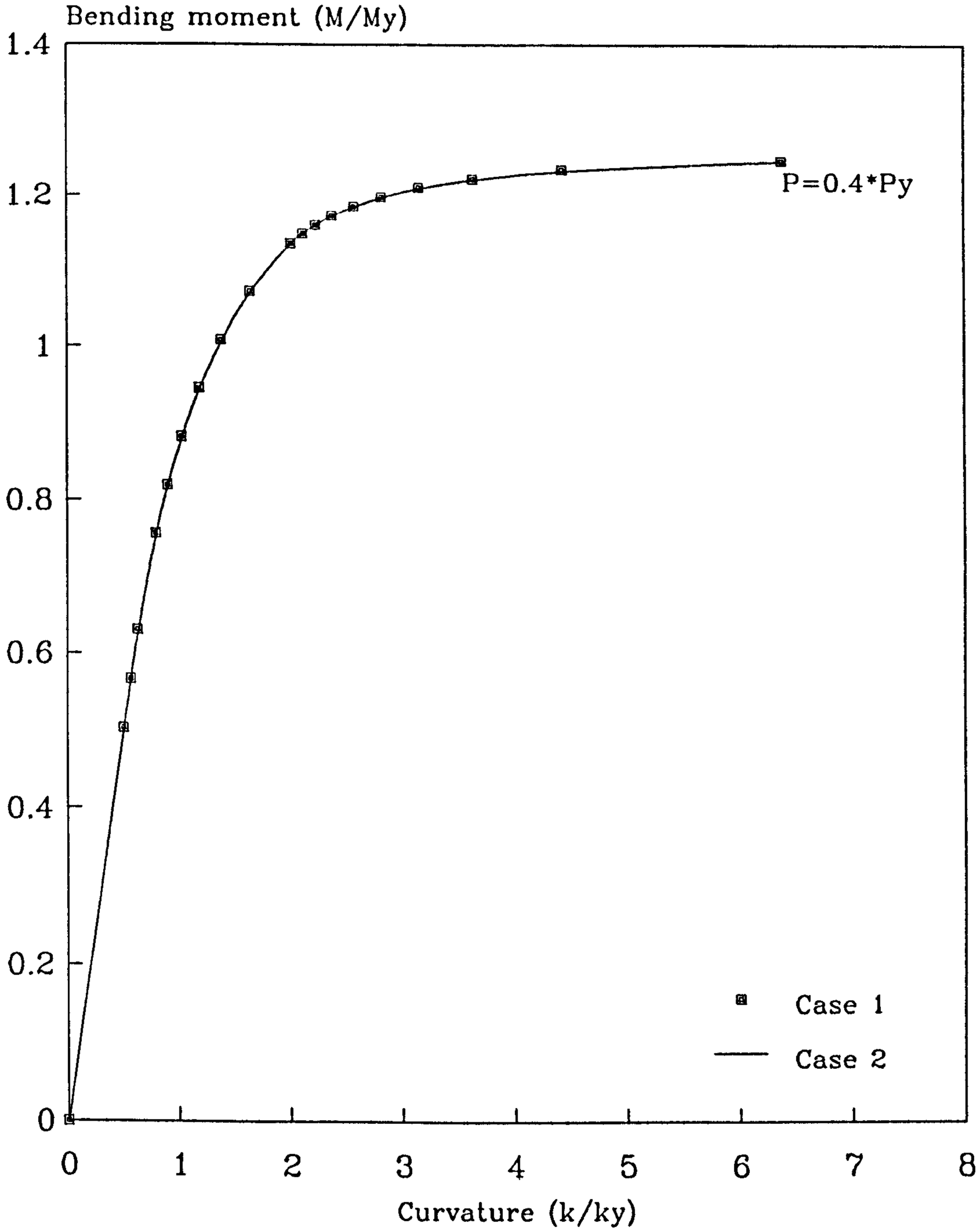

Figure 4.9: Moment–curvature relationship for a rectangular cross–section when P=0.4Py.

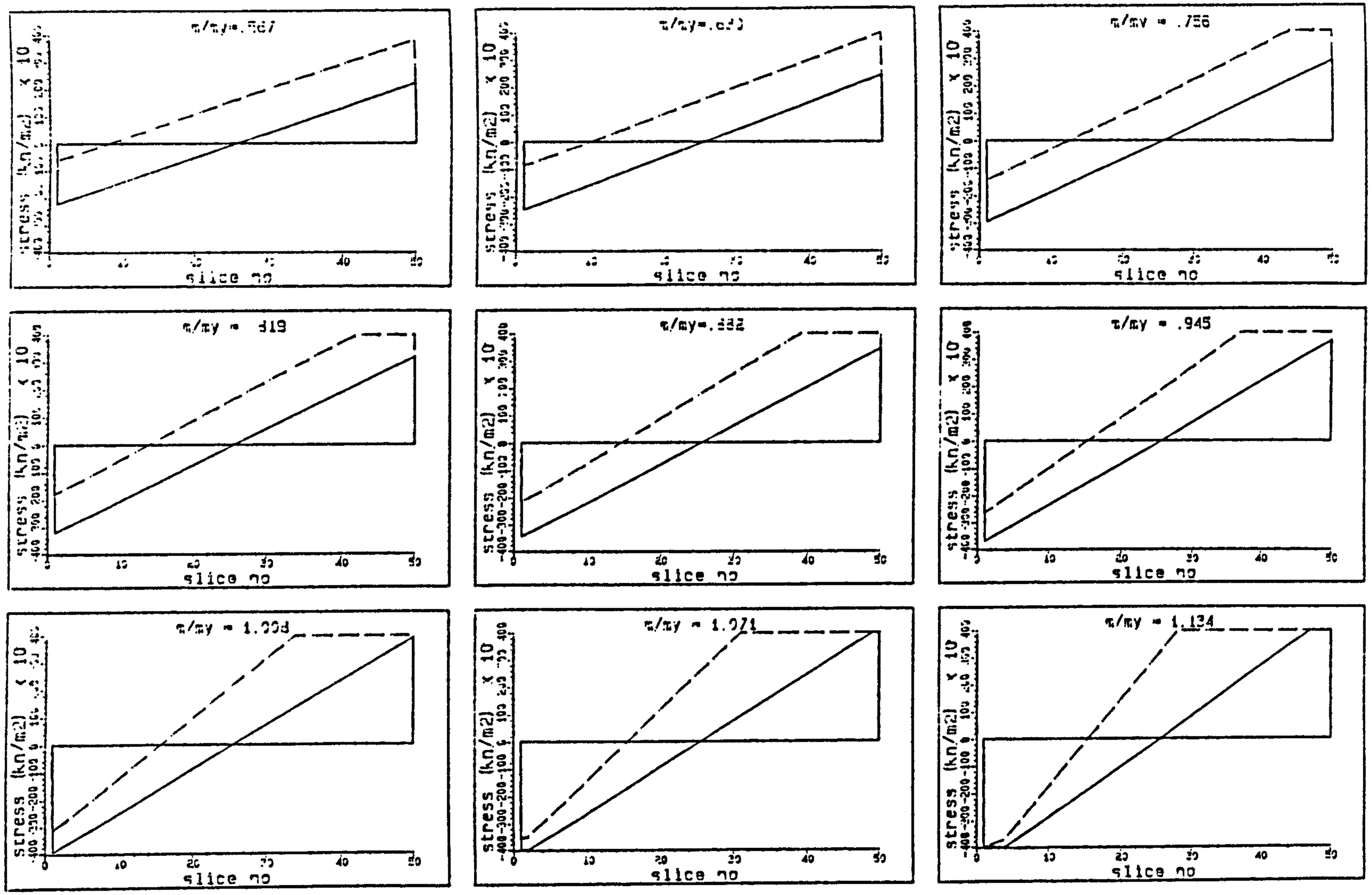

——— Initial stress - - - - Final stress

Figure 4.10: Initial and final stress profiles for a rectangular beam-column element for increasing moments when P=0.4Py.

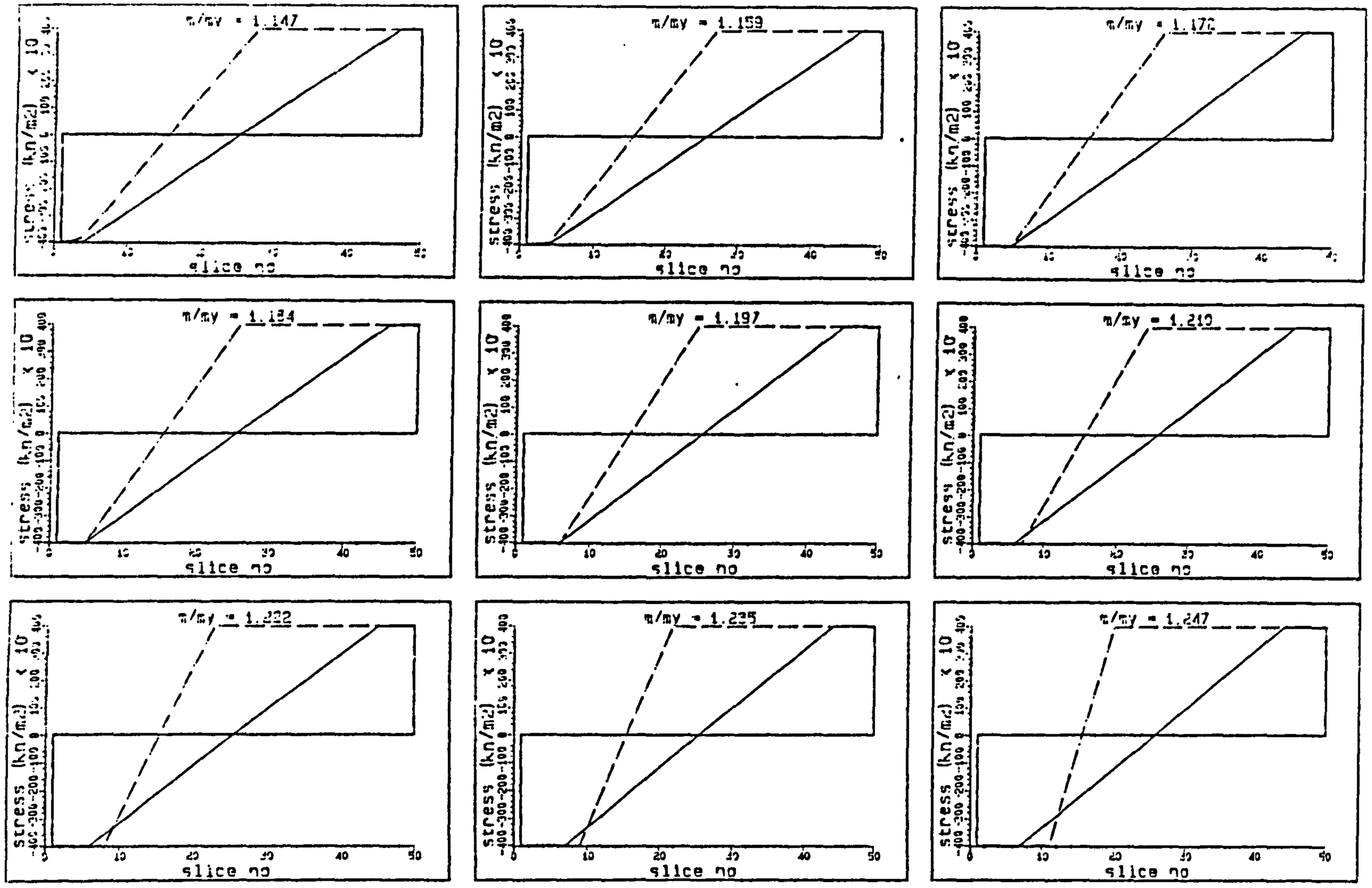

Figure 4.10 (continued)

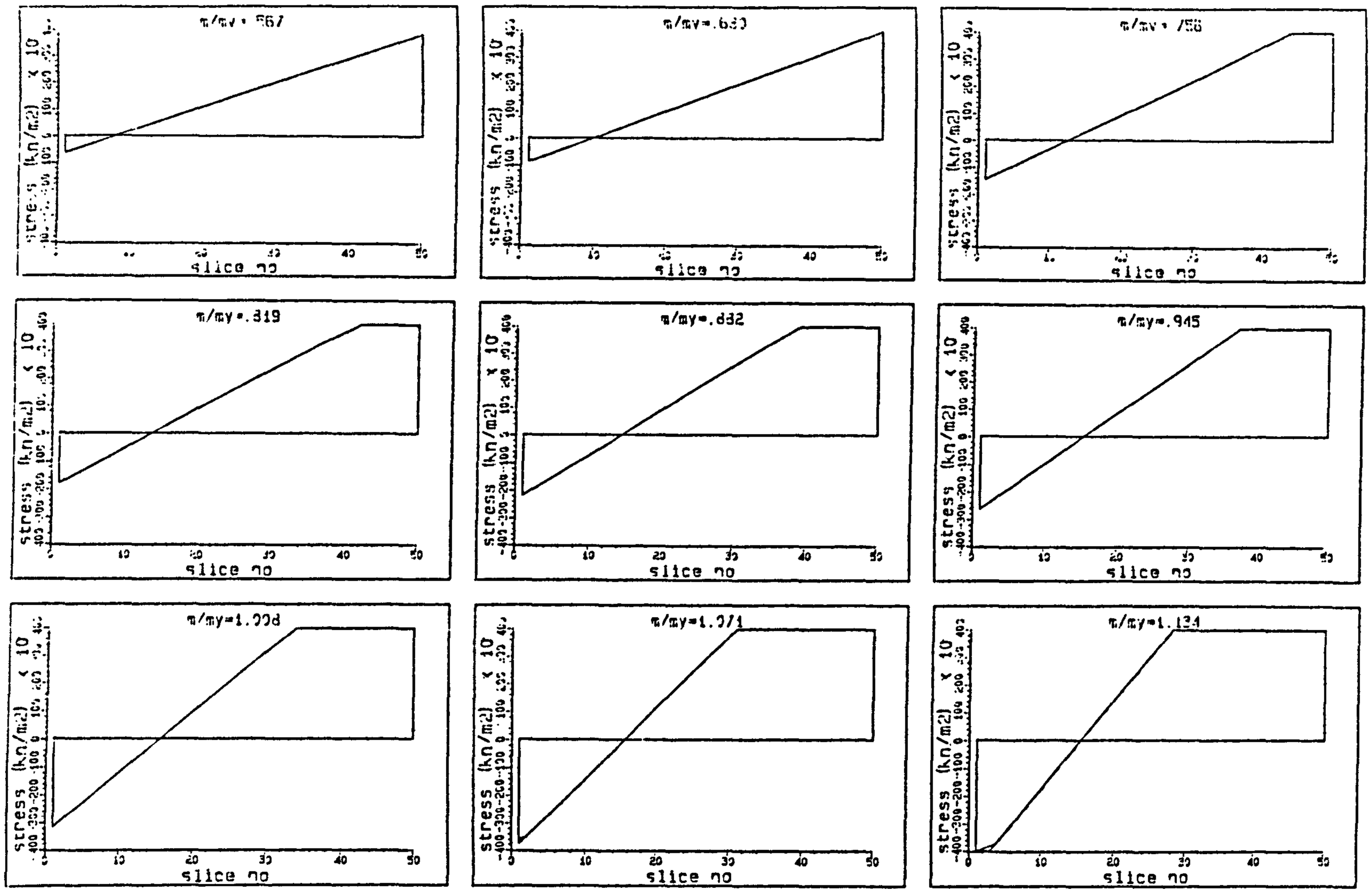

------ Case 1 ——— Case 2

Figure 4.11: Final stress profiles in case 1 and case 2 of rectangular beam–column element when P=0.4Py.

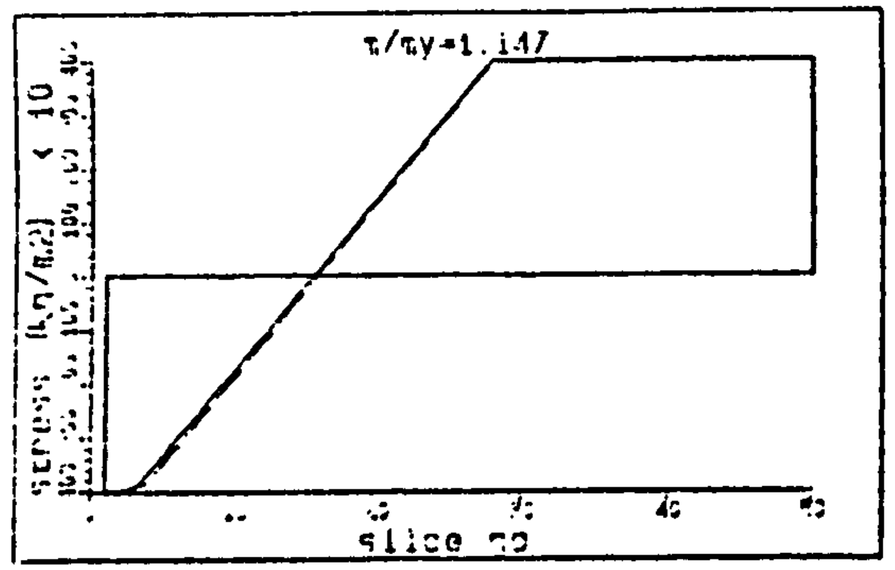

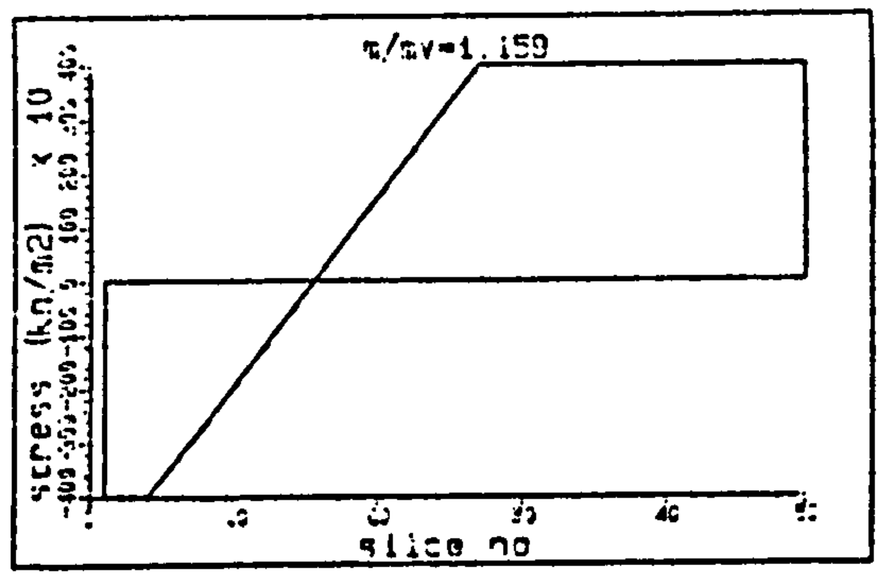

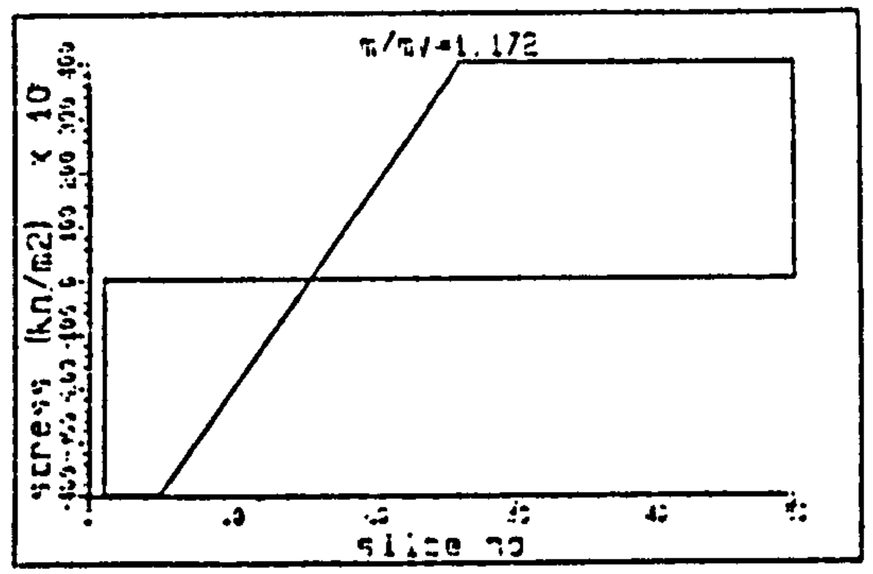

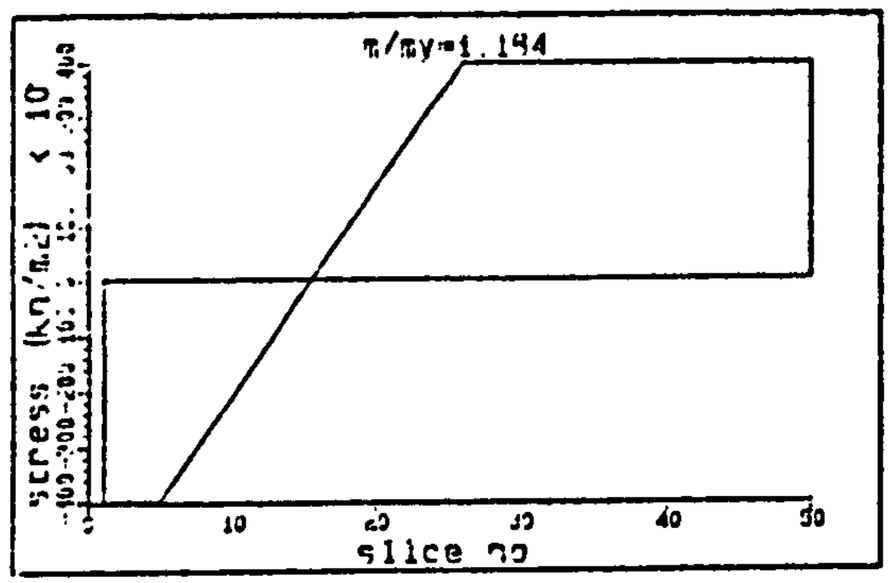

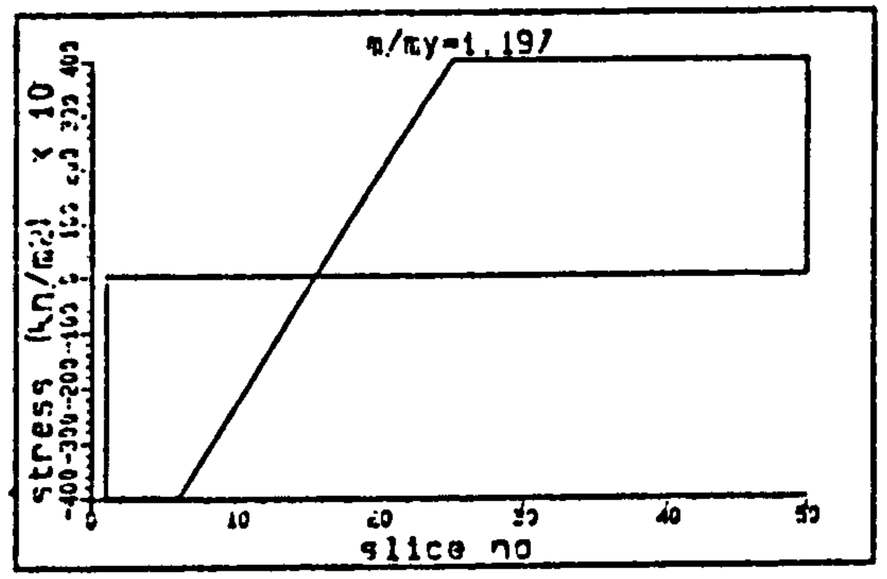

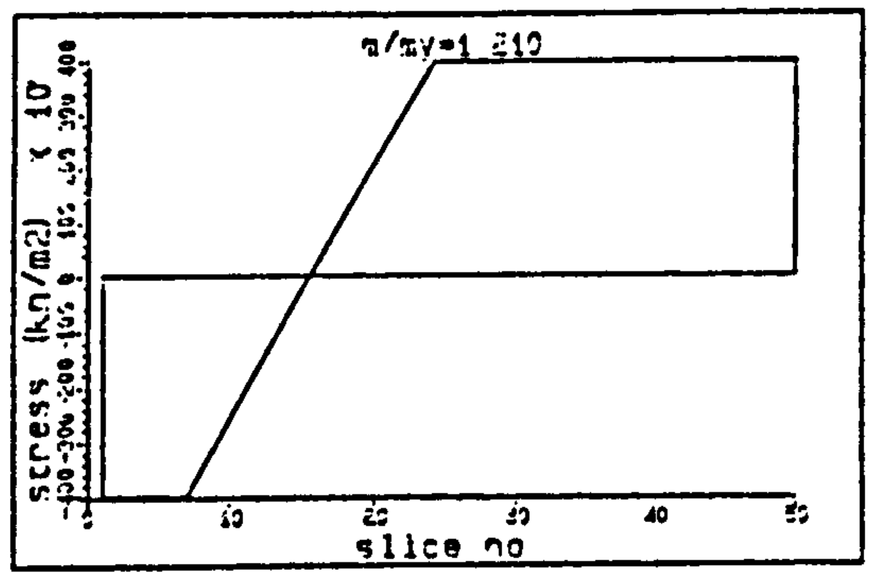

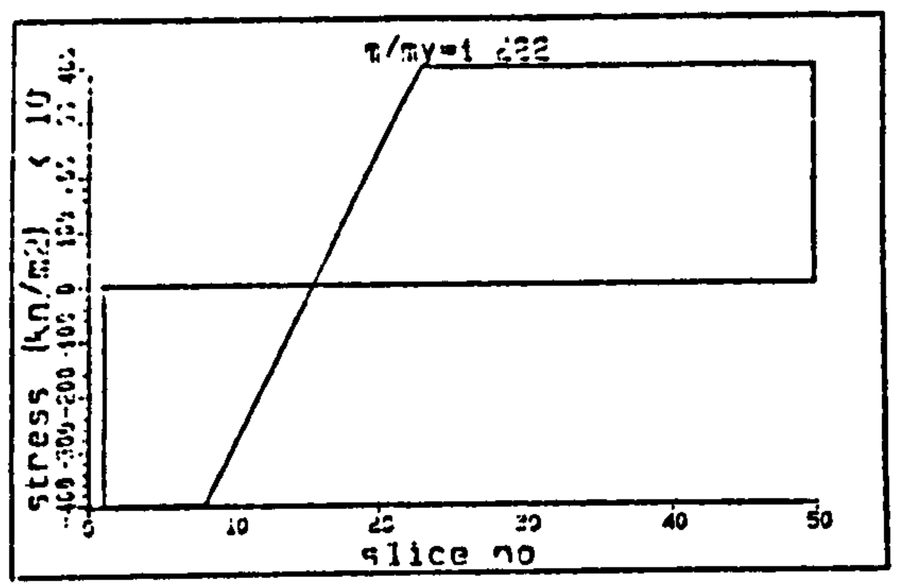

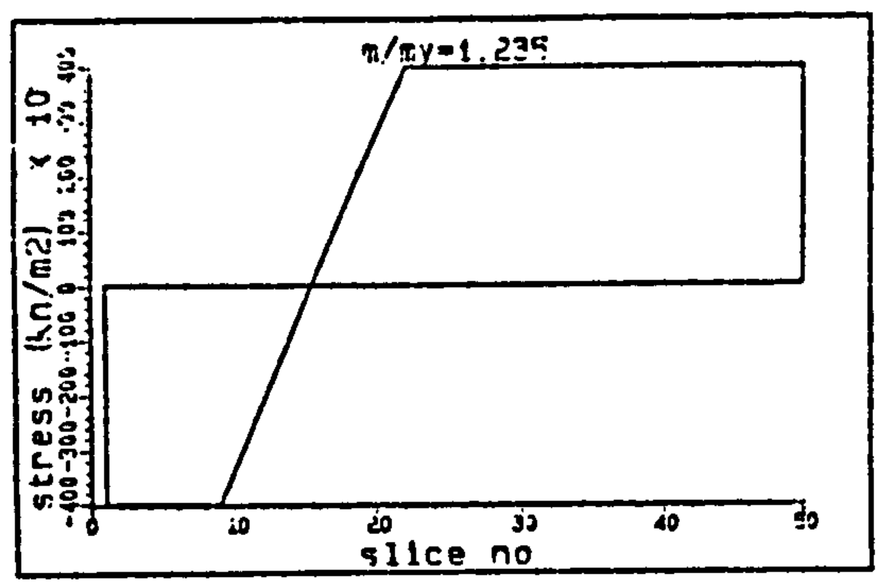

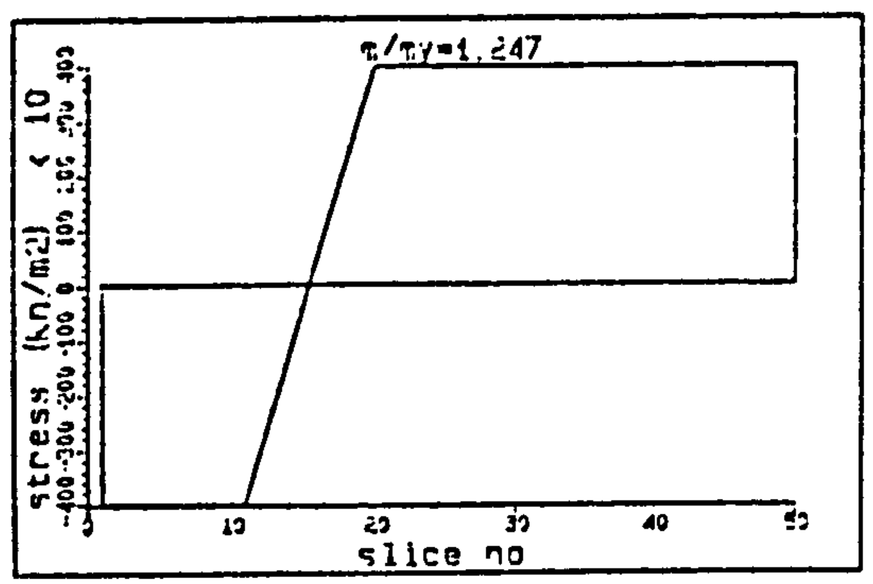

Figure 4.11 (continued)

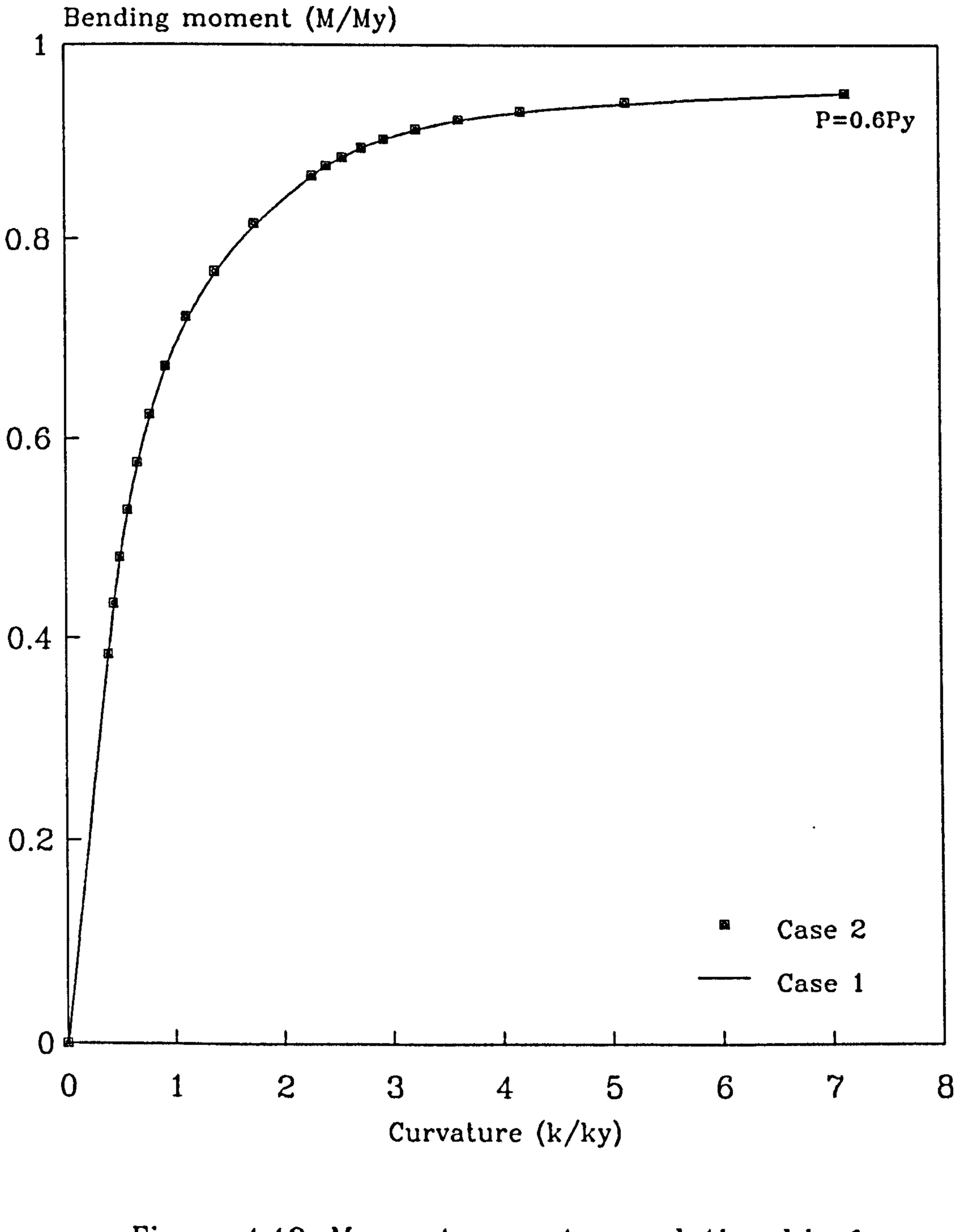

Figure 4.12: Moment-curvature relationship for a rectangular cross-section when P=0.6Py.

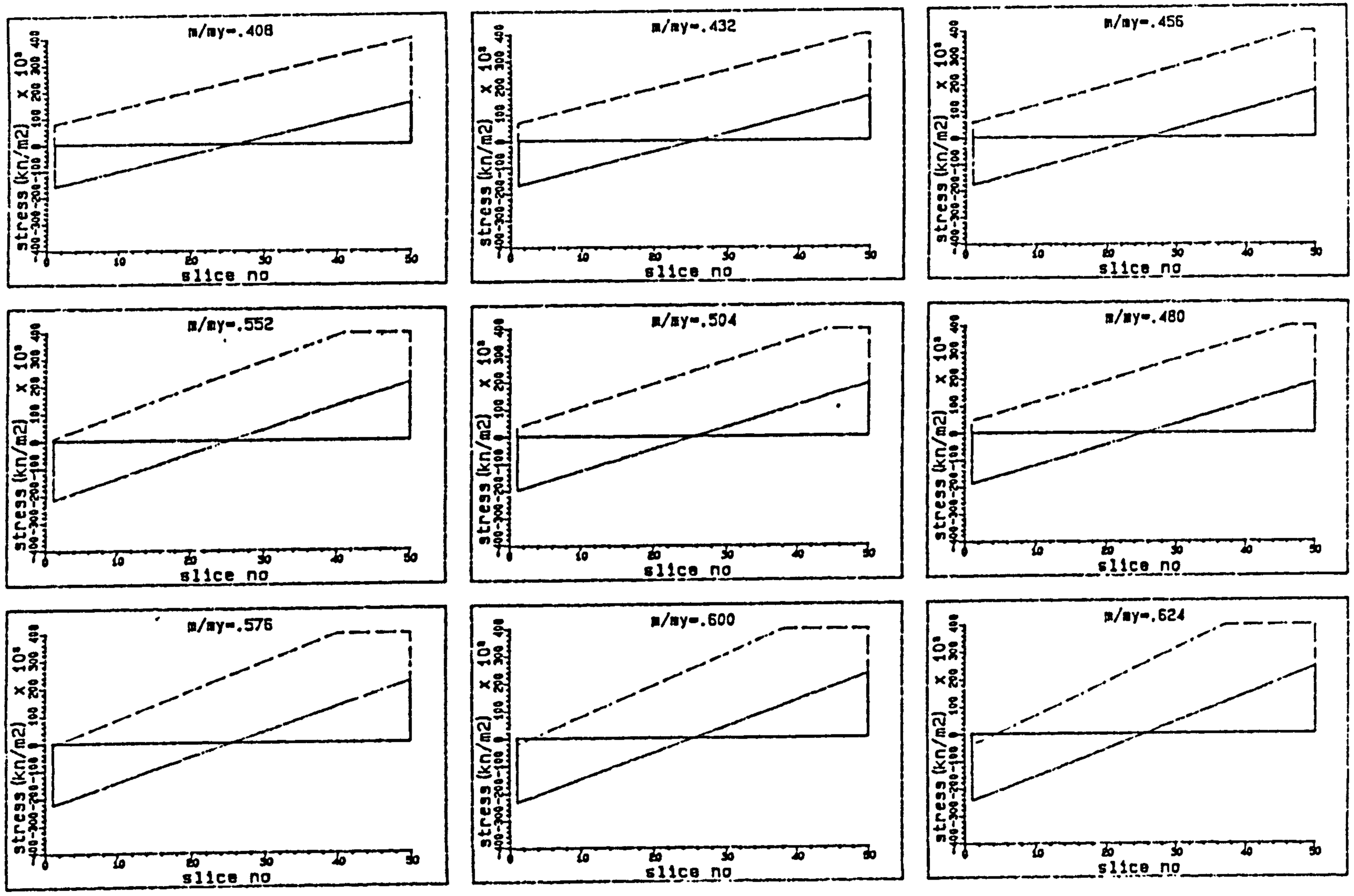

Figure 4.13: Initial and final stress block diagrams of a rectangular beam-column element for increasing moment when P=0.6Py.

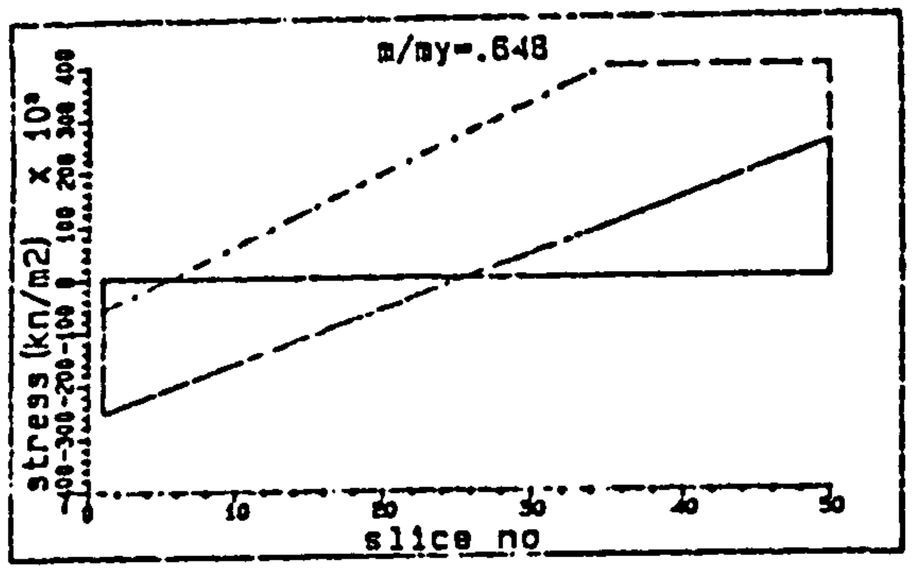

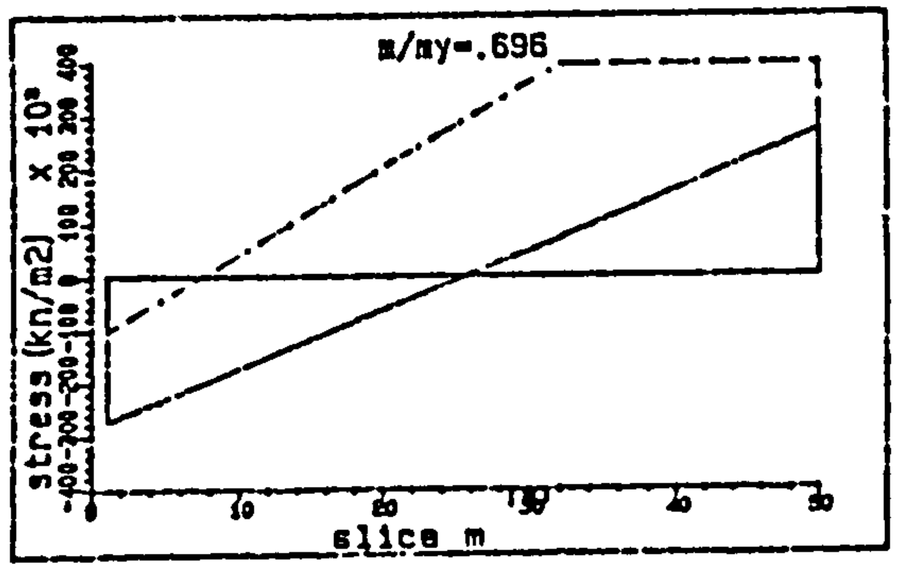

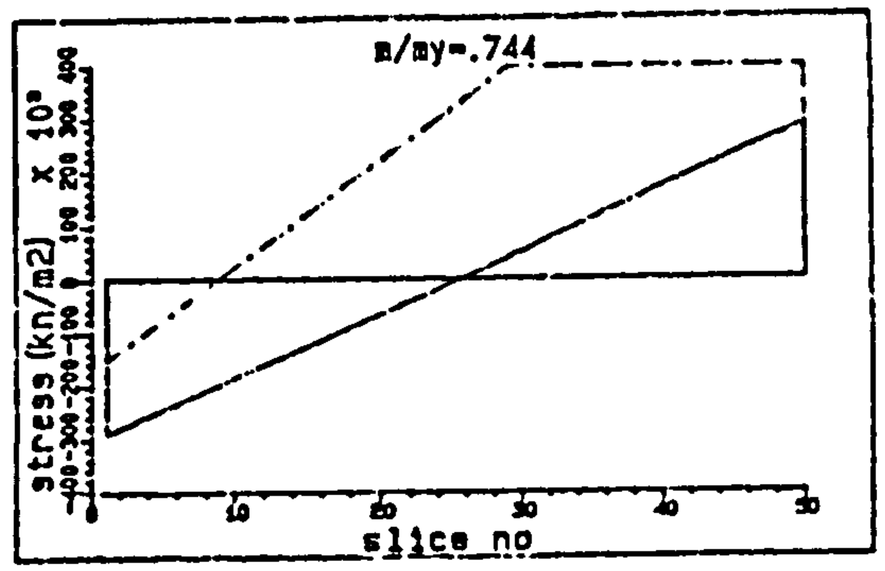

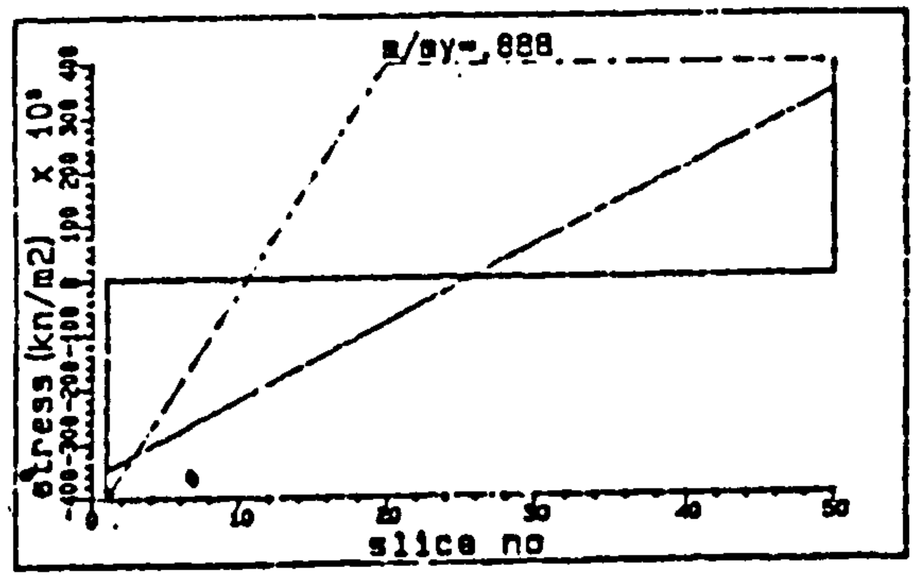

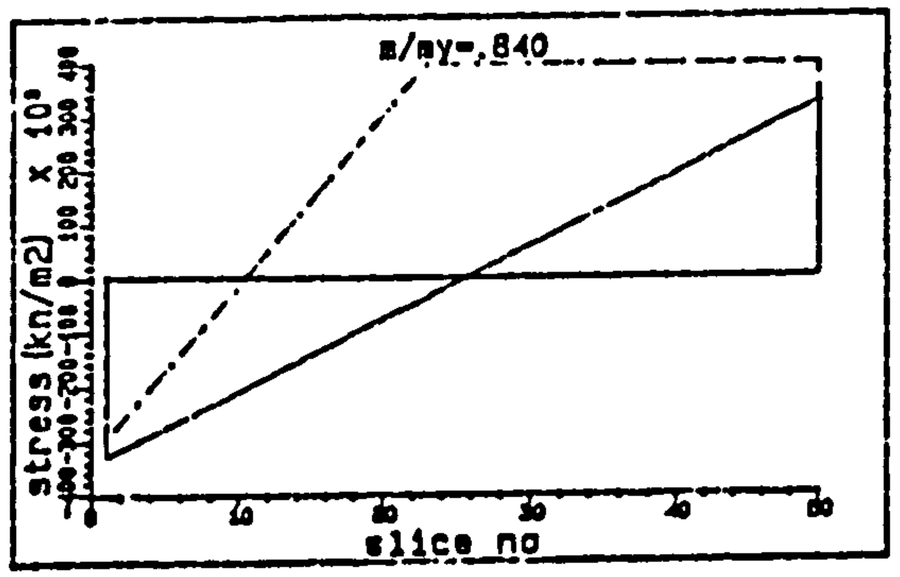

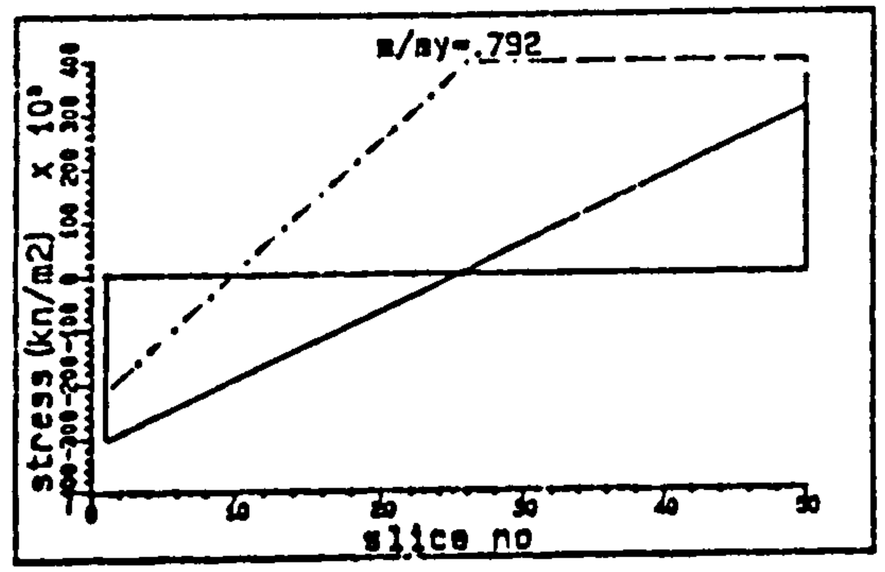

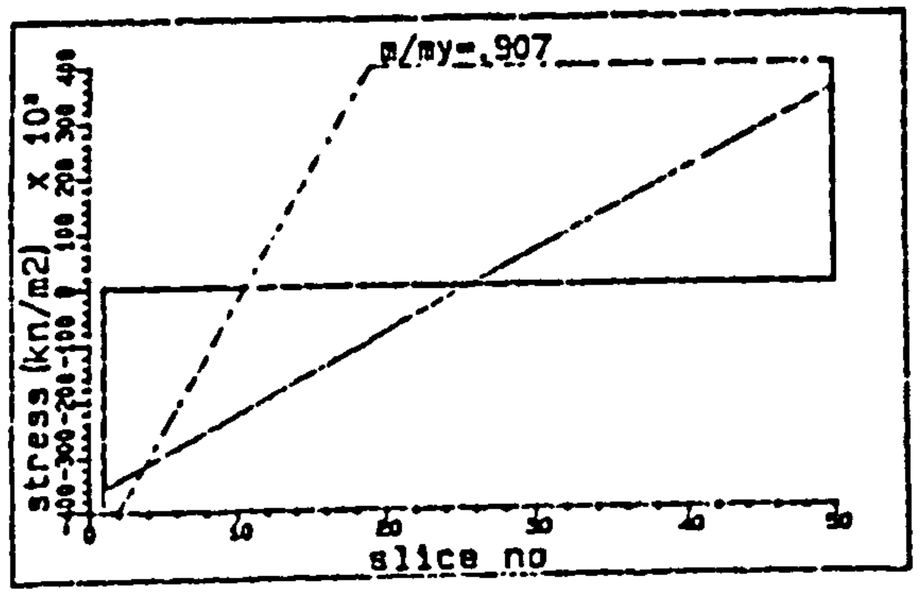

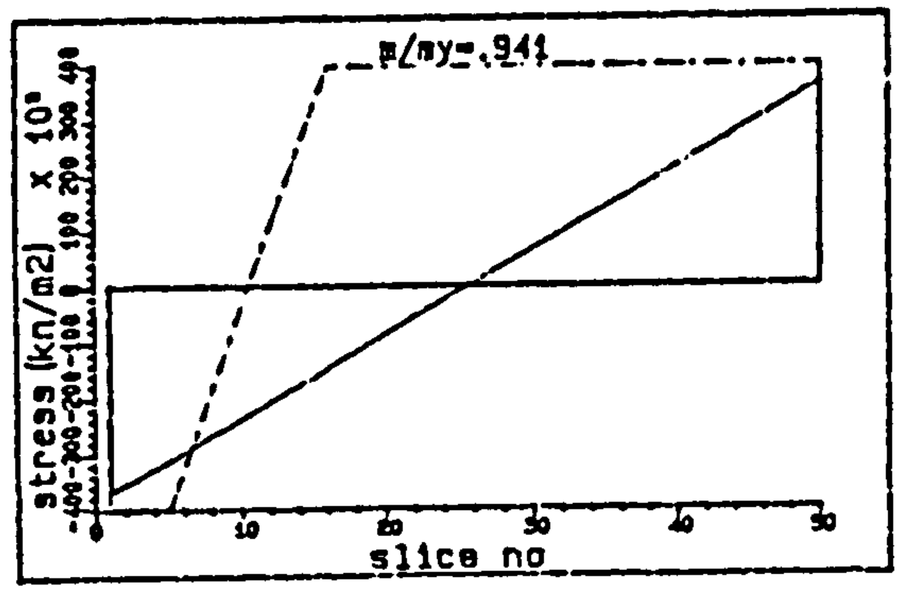

Figure 4.13 (continued)

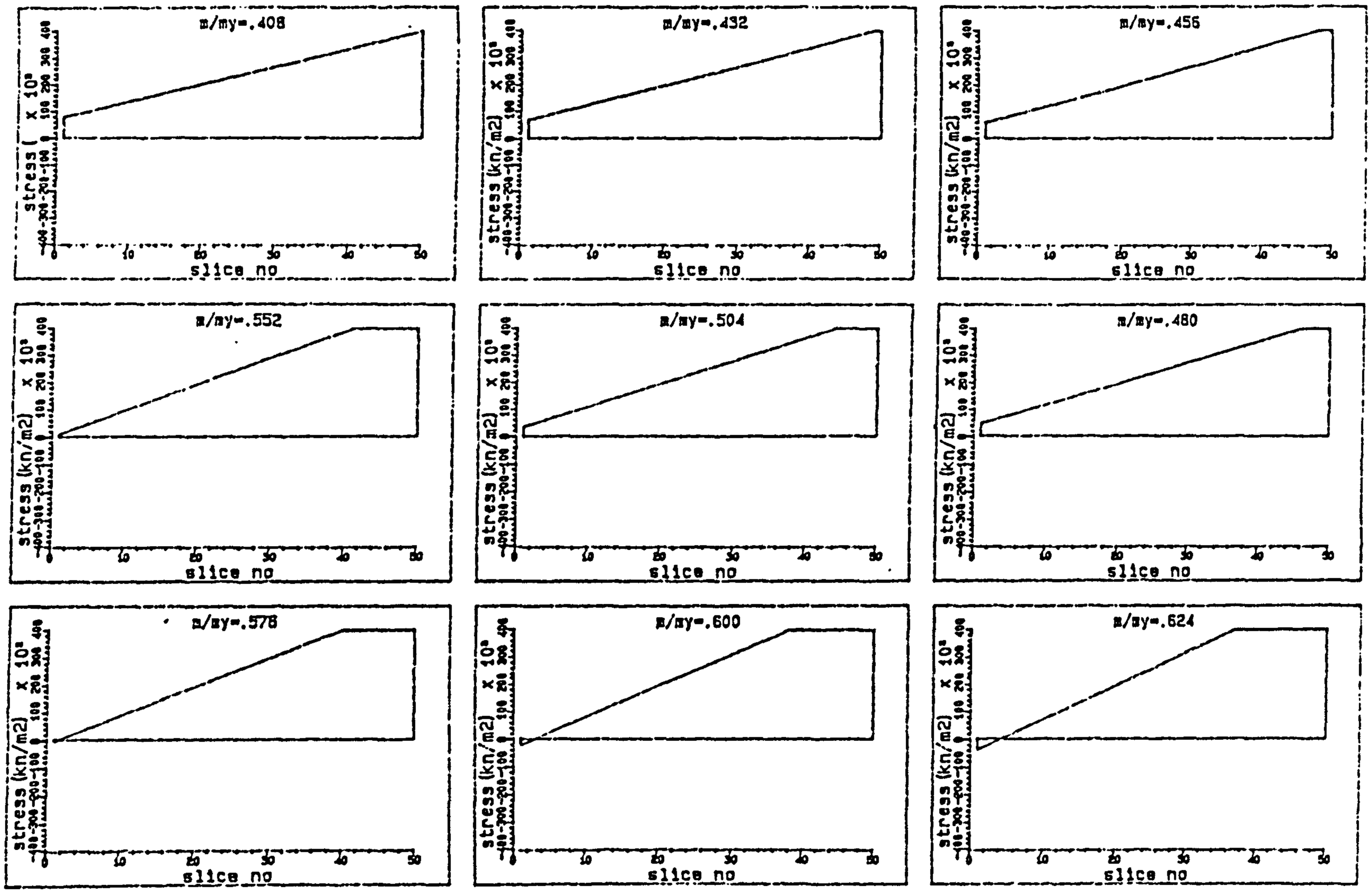

Figure 4.14: Final stress profiles in case 1 and case 2 of rectangular beam-column element when P=0.6Py.

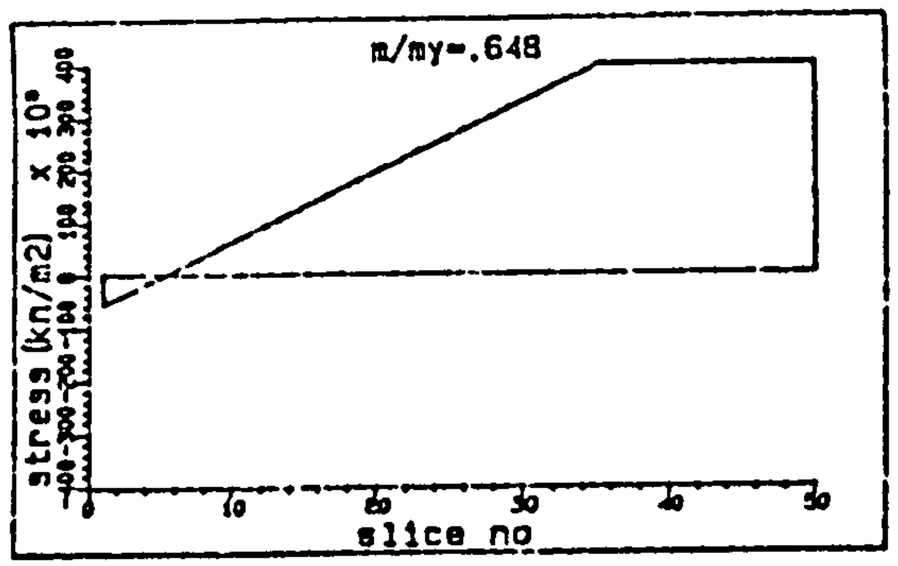

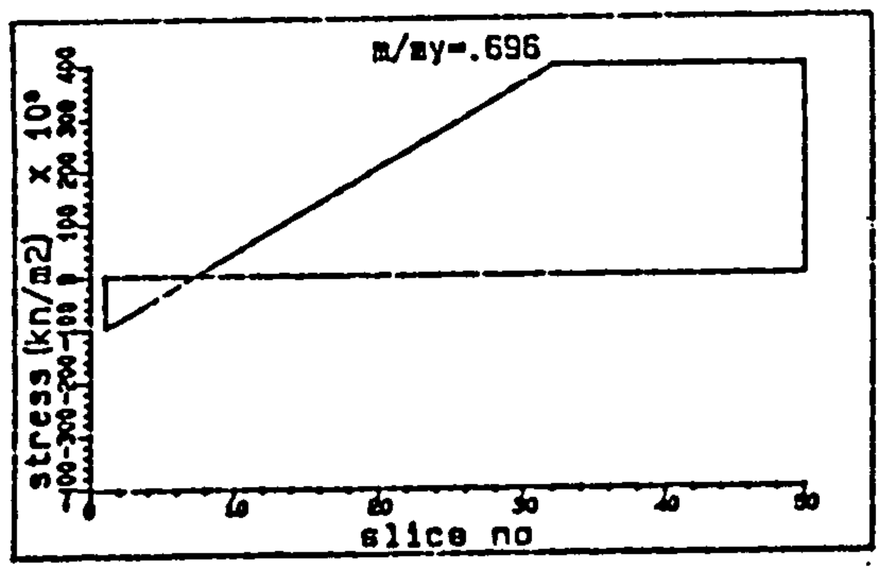

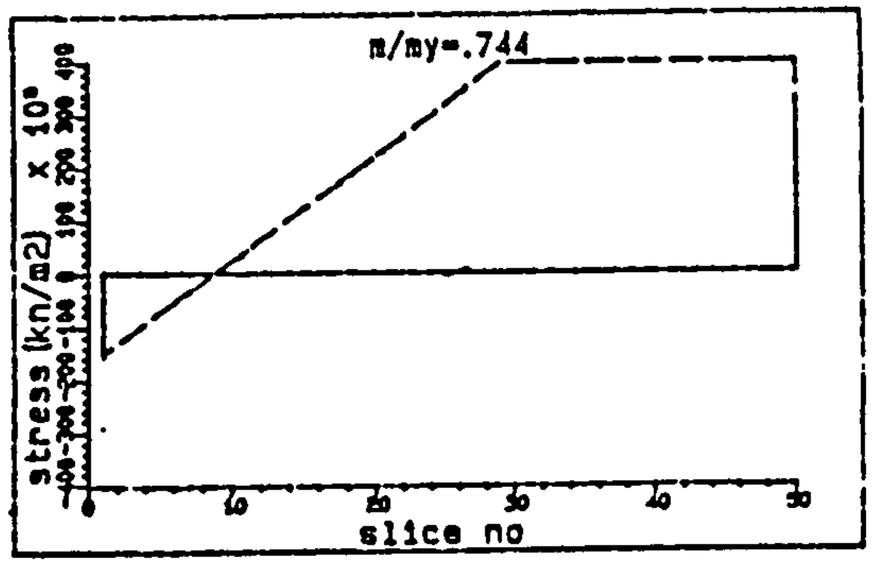

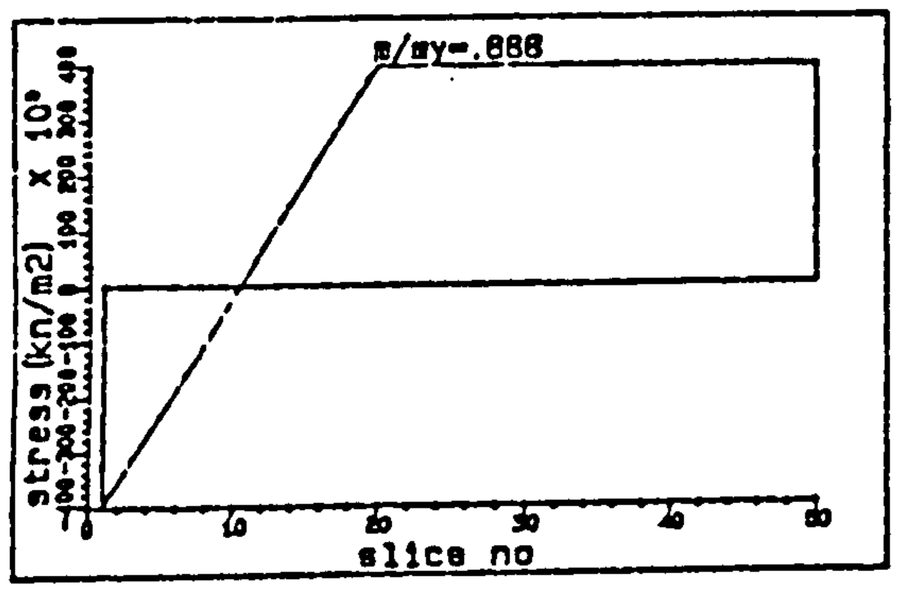

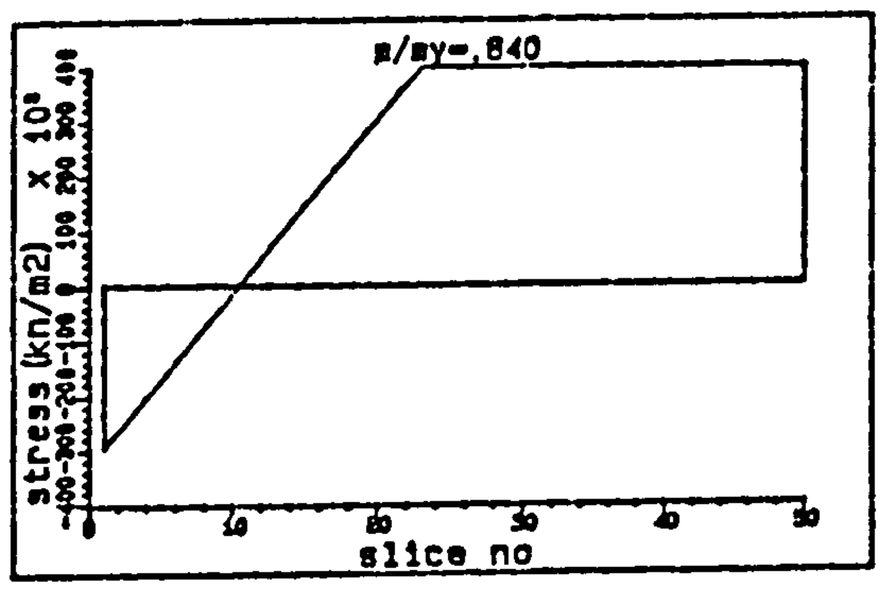

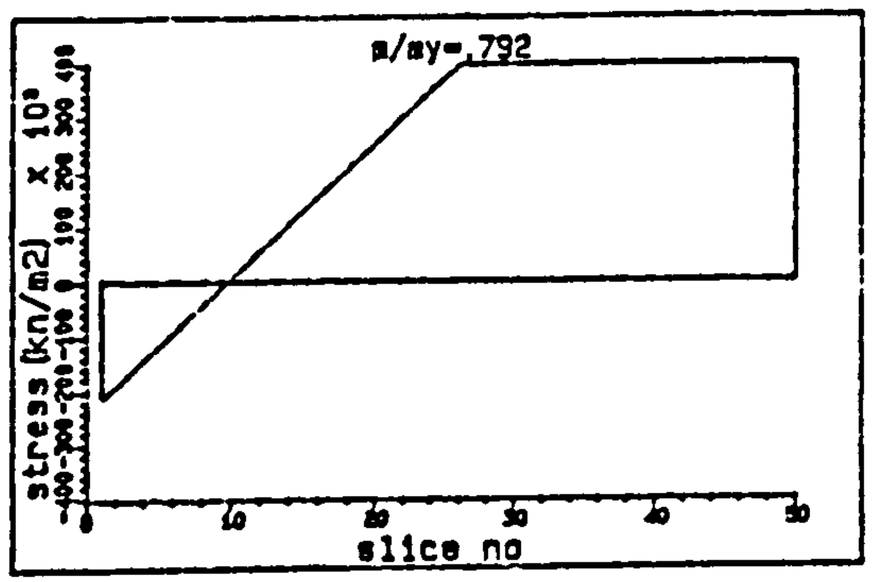

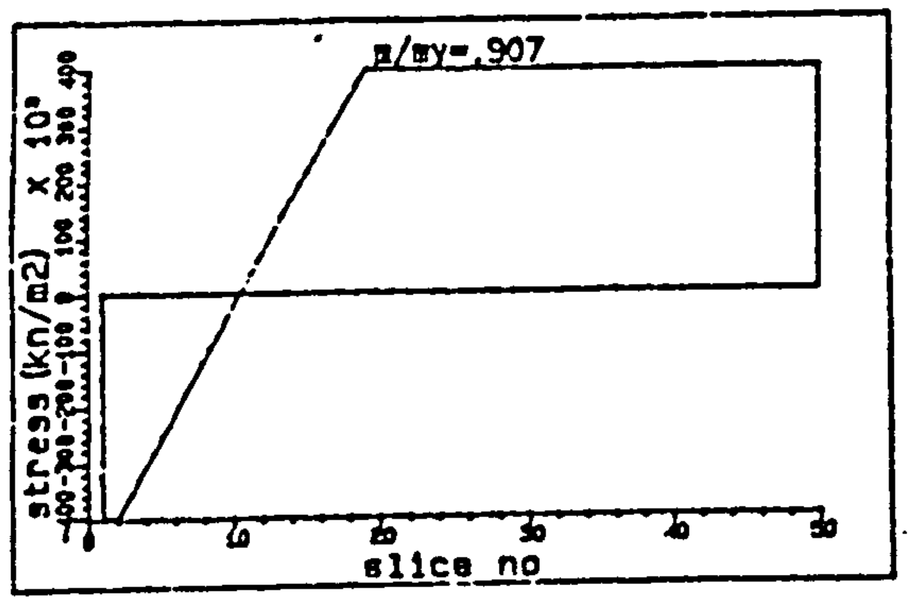

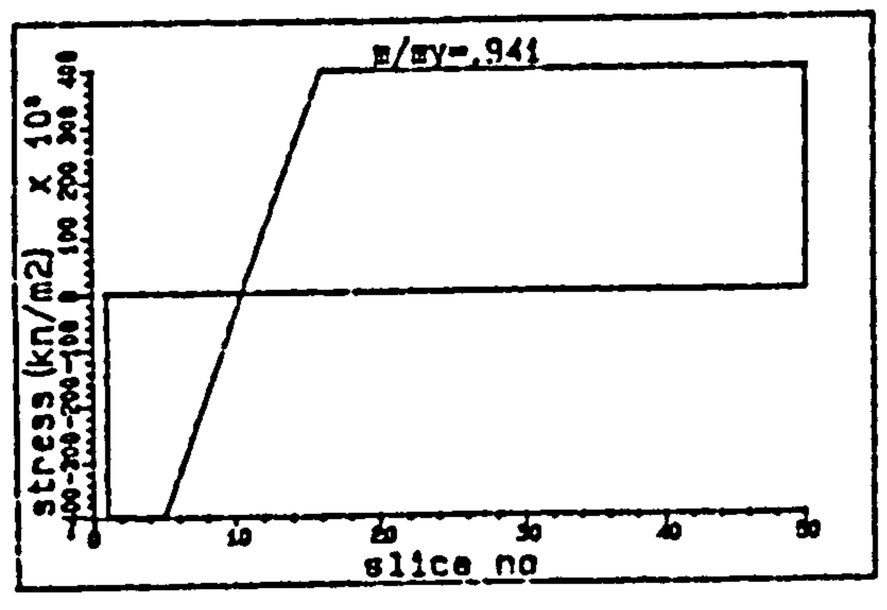

Figure 4.14 (continued)

This suggests that for rectangular cross-sections material unloading is a negligible effect. In the study of structural steelwork, other cross-sectional shapes, principally I sections, are normally used, and these are studied in the next section.

4.4.3 The effect of material unloading on moment-axial force-curvature relationship for an I section.

From the previous discussions material unloading in the plastic range is largely concentrated at the extremities of the cross-section. In the case of I sections, this is precisely where most material is concentrated, and it may therefore be that material unloading will have a more marked effect than for rectangular cross-sections. As an example consider a UC section 356x406x467 kg/m. Such a large section was chosen because of its bigger flanges and hence the greater possibility of material unloading affecting the moment-axial force-curvature relationship.

Figure 4.15 shows a comparison of the moment-axial force-curvature relationships for different levels of axial force and indicates no perceptible difference between the two cases. A series of stress block diagrams is presented in Figure 4.16 for an axial force of P=0.2Py. These compare the behaviour of a beam-column element for cases 1 and 2.

An important conclusion from this investigation is that even

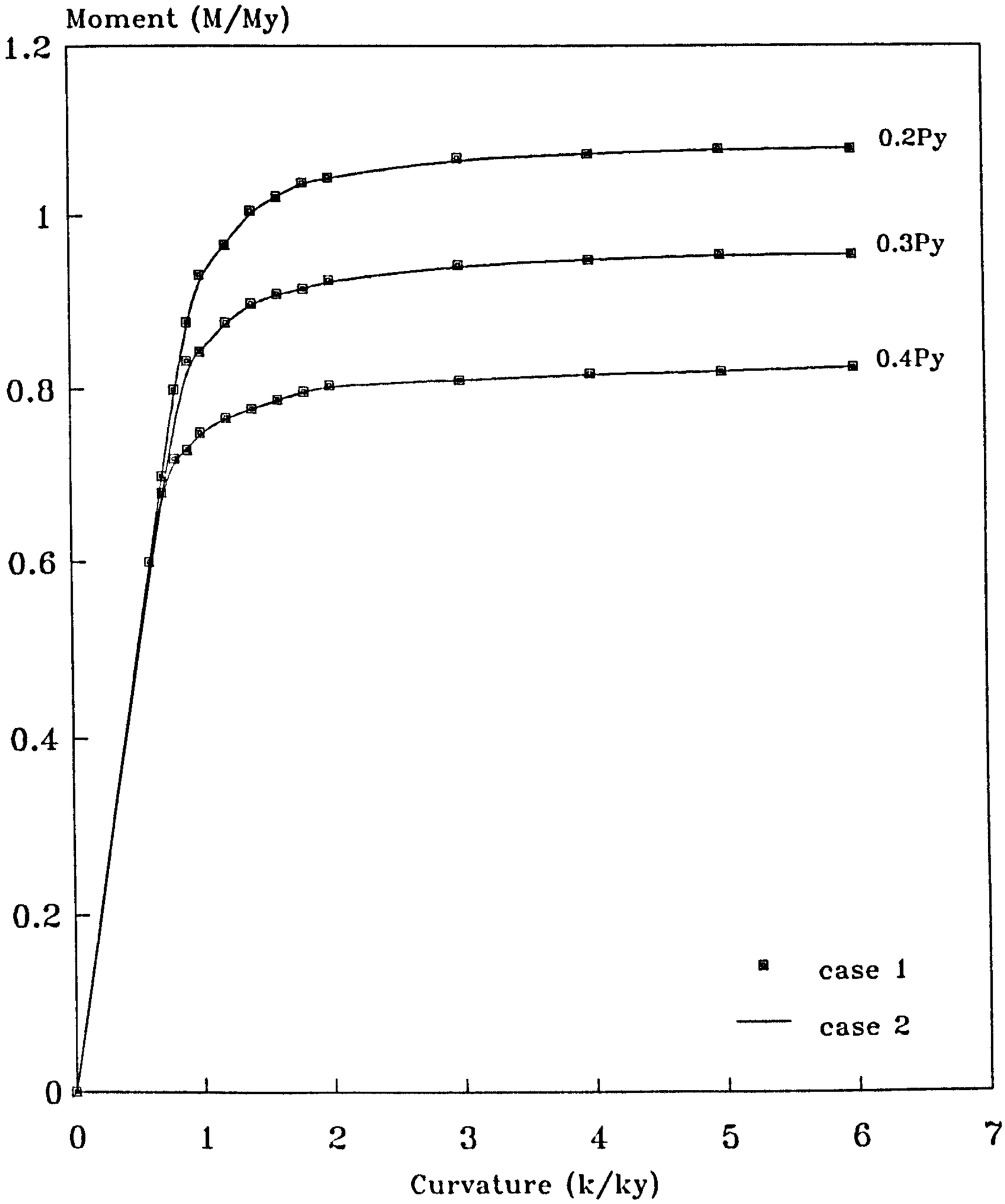

Figure 4.15: Moment–axial force–curvature relationship of an I–section for cases 1 and 2.

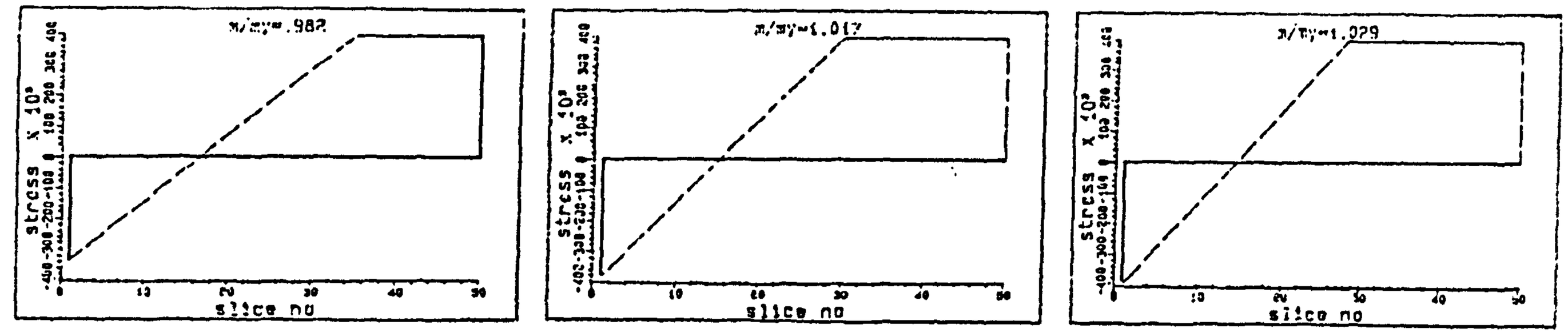

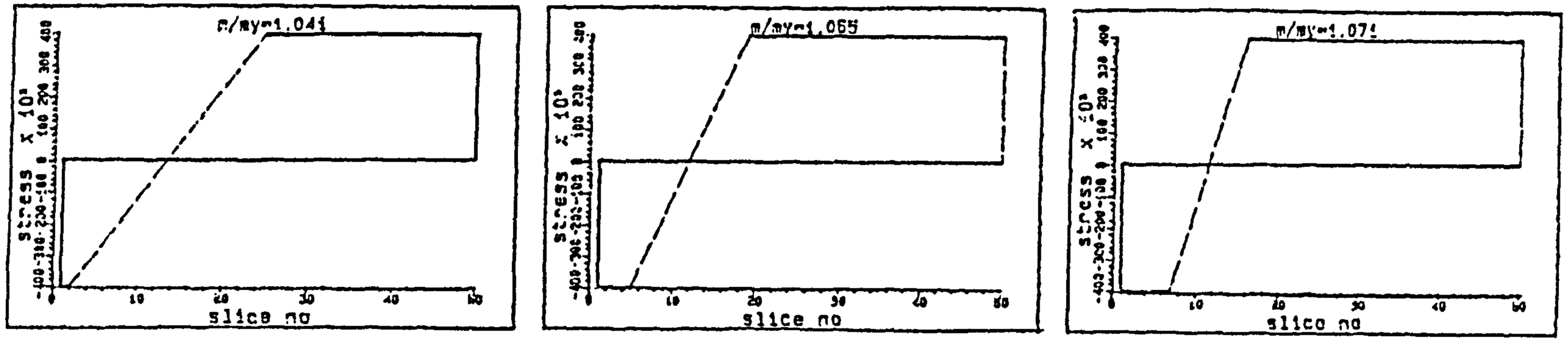

— — — — Case 1 ——— Case 2

Figure 4.16: Final stress profiles in case 1 and case 2 of an I–section beam–column element at increasing moments when P=0.2Py.

though material unloading has the potential to affect the curvature relationship, this effect is very small and can safely be ignored. This study will be extended to the case of sections subject to increasing temperature in the following section.

4.5 THE EFFECT OF MATERIAL UNLOADING ON MOMENT-AXIAL FORCE-CURVATURE RELATIONSHIP IN FIRE.

The effect of material unloading on the moment-axial force-curvature relationship becomes more complicated for fire conditions because it involves another parameter, that is temperature. This results in modified stress-strain curves which, even for a constant bending moment M and axial force P, can lead to a change in strain distribution within the cross-section. The position of neutral axis may change and consequently material unloading may occur.

Another possible cause of material unloading is when the member is restrained against longitudinal expansion. If it is exposed to fire, an axial force will be induced in the element and this, together with any bending stresses due to applied loads, may cause material unloading over parts of the cross-section.

In this study the bending moment M and axial force P are assumed to remain constant as the temperature is increased. The cross-section is assumed to be uniformly heated and the

stress-strain curves based on the ECCS recommendation as described in Chapter 2 are used.

4.5.1 Derivation of moment-axial force-curvature relationship in fire including the effect of material unloading.

The analysis is similar to that for the ambient temperature study (Section 4.3) but at increasing temperature. A step temperature increase is adopted to calculate the current temperature level:

$$T2 = T1 + dT \quad \text{.....(4.2)}$$

where T2 = new temperature.

T1 = previous temperature.

dT = temperature increment.

To include the effect of material unloading in this case the strain distribution at the previous temperature level must be recorded. This is then used as the initial strain value ε_{T1} when the new temperature level is considered. Material unloading happens when the strain at the current temperature level ε_{T2} is less than at the previous temperature.

The determination of the stress at the new temperature level σ_{T2} is based on the same conditions as for the ambient

temperature study, except that the yield stress and Young's Modulus are now functions of temperature as shown in Figure 4.17. The procedure described in Figure 4.4 still applies but with Young's Modulus E and yield stress σ_y replaced by their values E_{t2} and σ_{yt2} at the new temperature T2.

A computer program was developed to investigate the effect of material unloading on the moment-axial force-curvature relationship in fire. Figure 4.18 illustrates the logical sequence of the operations involved. To start with the effect of material unloading at room temperature due to case 1 and case 2 are considered based on Figure 4.4. The strain distribution is then considered as the initial value when the next temperature increase is introduced. Since the stress-strain curve is no longer the same an iteration process must be adopted in order to achieve the new equilibrium condition equating the internal and external bending moment and axial force. Material unloading is included in this process.

4.5.2 The effect of material unloading on moment-axial force-curvature relationship in fire.

From Figure 4.6 it was noted that the influence of material unloading can clearly be recognised for an axial force and bending moment equal to $0.2P_y$ and $1.26M_y$ ($0.84M_p$) respectively, and hence these values are used in this section. It should be noted that the loads are assumed to

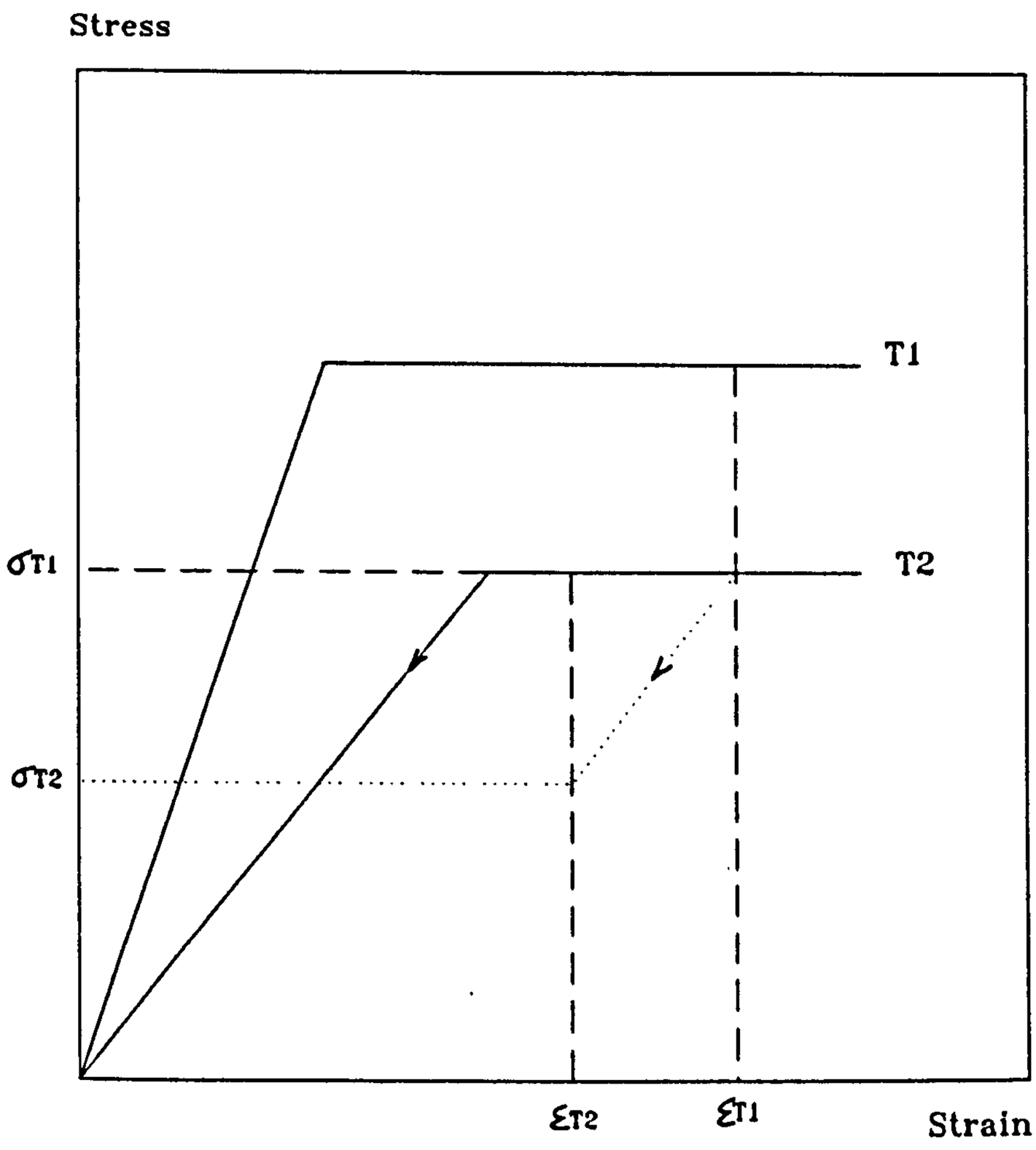

Loading and unloading path of stress-strain curve are assumed to be identical in tension and compression.

Figure 4.17: Illustration of the effect of material unloading in the plastic region at elevated temperature.

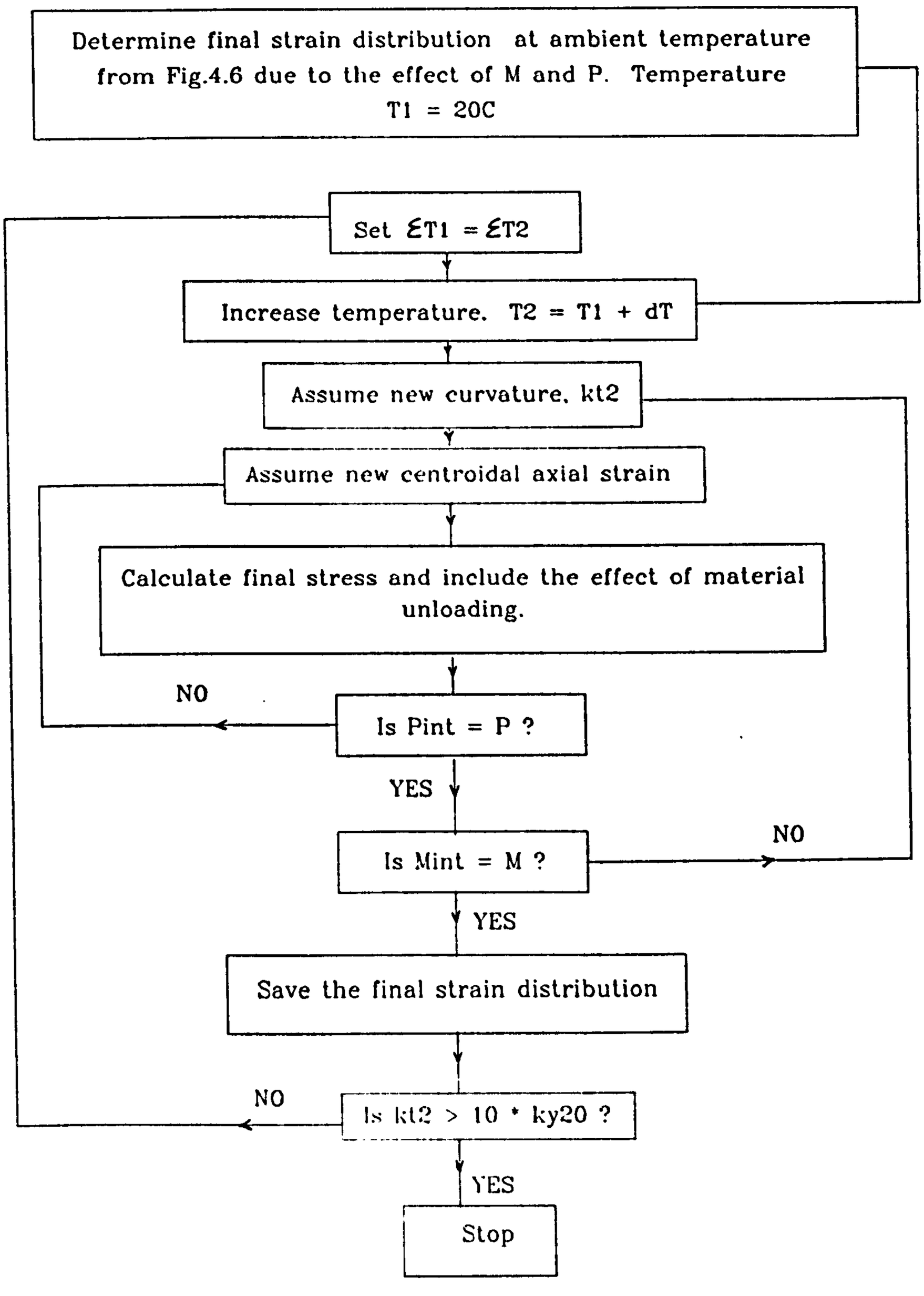

Figure 4.18: Logical sequence of the algorithm for deriving moment–axial force–curvature–temperature relationship including the effect of material unloading.

remain constant while temperature increases and a rectangular cross-section will be examined first. The derivation of the curvature relationship is based on the logical sequence described in Figure 4.18.

Figure 4.19 shows the moment-curvature-temperature relationship in fire for the rectangular cross-section. A series of final stress profiles is presented in Figure 4.20. This shows that even at low temperatures material unloading occurs in the plastic range resulting in the difference in curvature relationships shown in Figure 4.19 for case 1 and case 2.

However, the difference between these two curvatures decreases slowly for temperatures above about 100°C. Even though material unloading still occurs at the higher temperatures, as shown in Figure 4.20 the affected area is very small and hence the difference between the moment-axial force-curvature relationships for case 1 and case 2 becomes negligible.

To study the effect of material unloading in fire for an I section consider a UC section 356x406x467 kg/m subject to bending moment M and axial force P of $1.00M_y$ ($0.87M_p$) and $0.2P_y$ respectively. Figure 4.21 shows the corresponding curvature-temperature relationship and a series of stress block diagrams is shown in Figure 4.22 for increasing temperature. These figures show that the effect of material

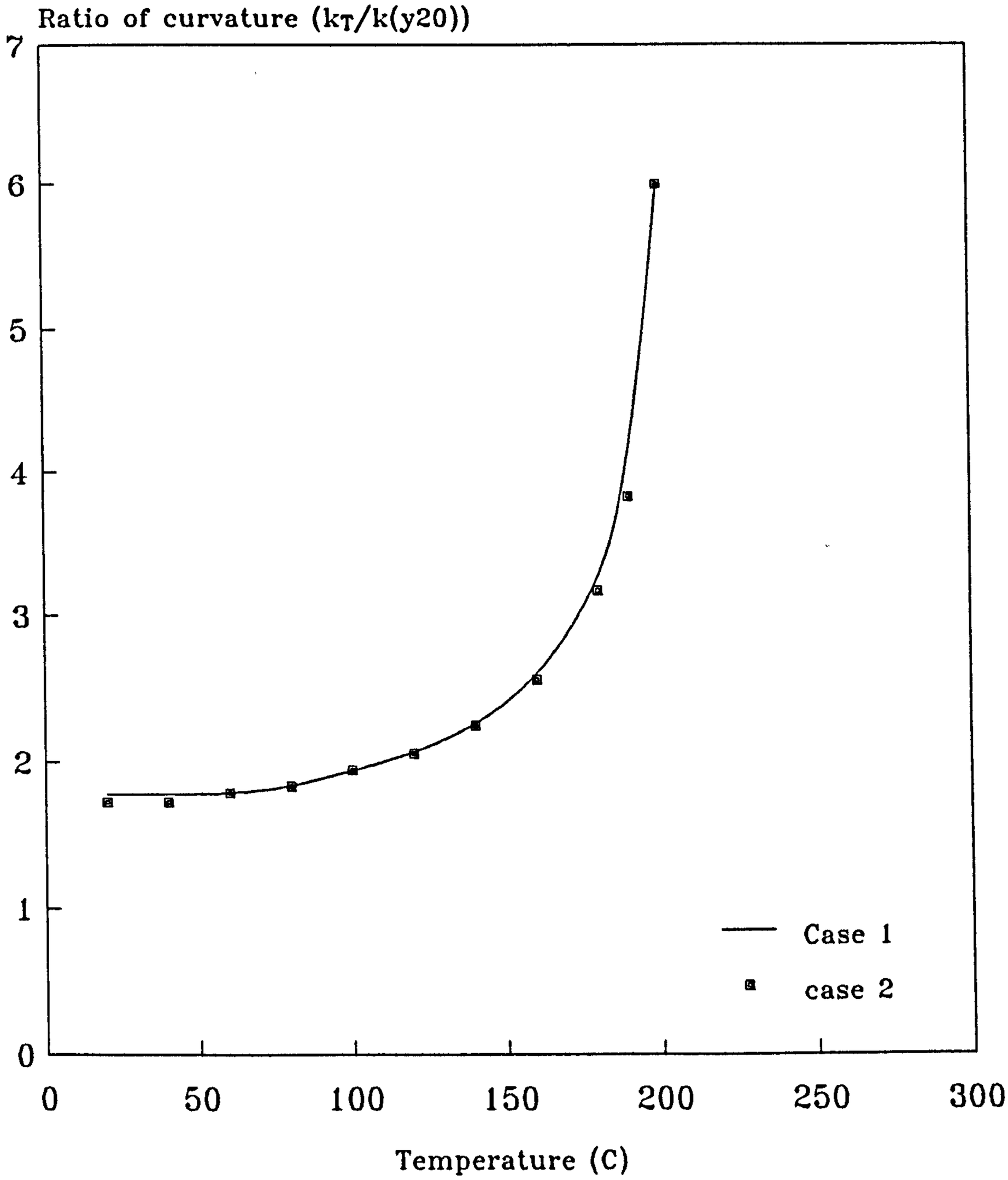

Figure 4.19: Moment-curvature-temperature relationship for P=0.2Py and M=0.84Mp (rectangular cross-section).

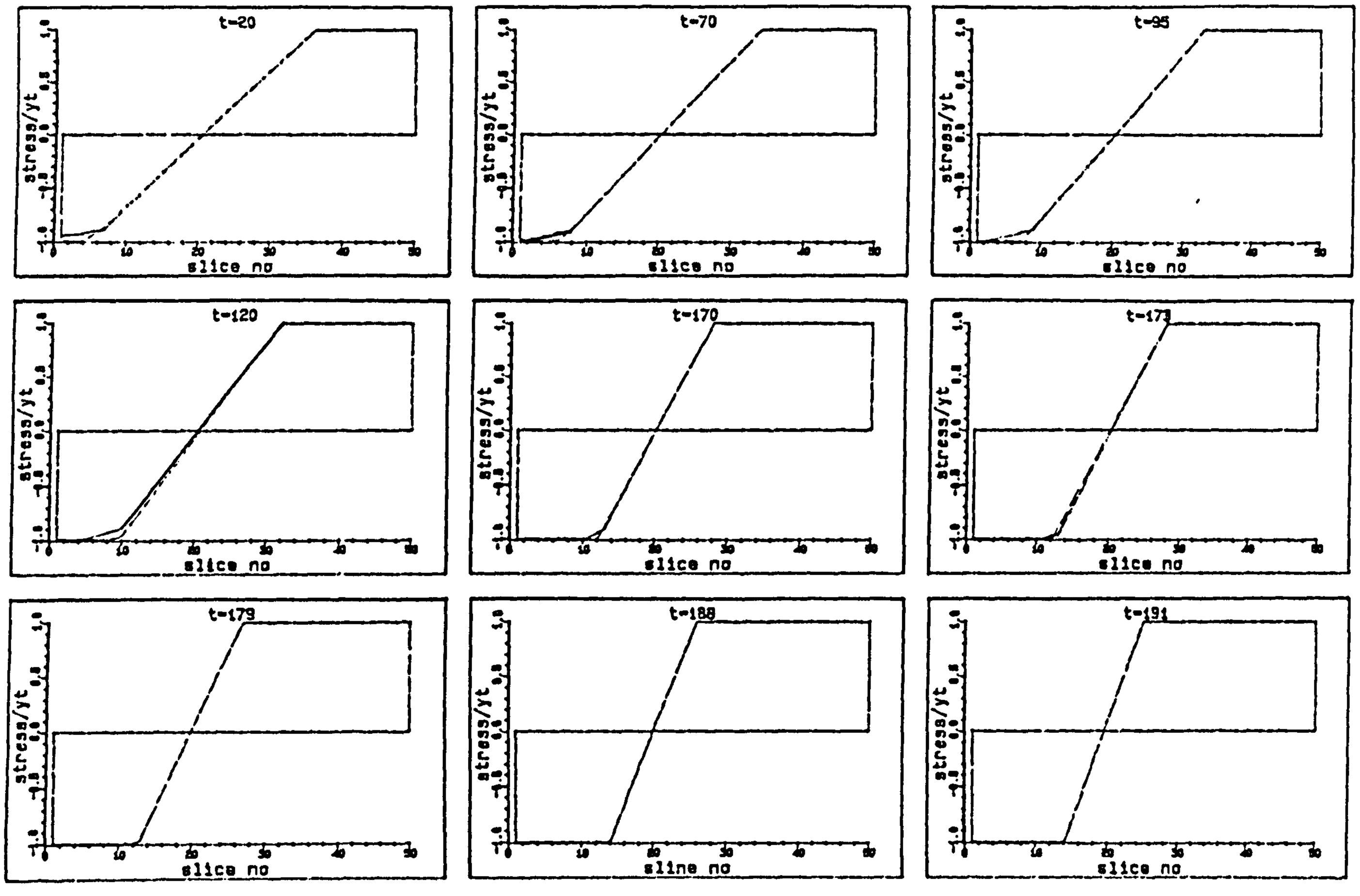

Figure 4.20: Final stress profiles for case 1 and case 2 of a rectangular beam–column element when P=0.2Py and M=0.84Mp.

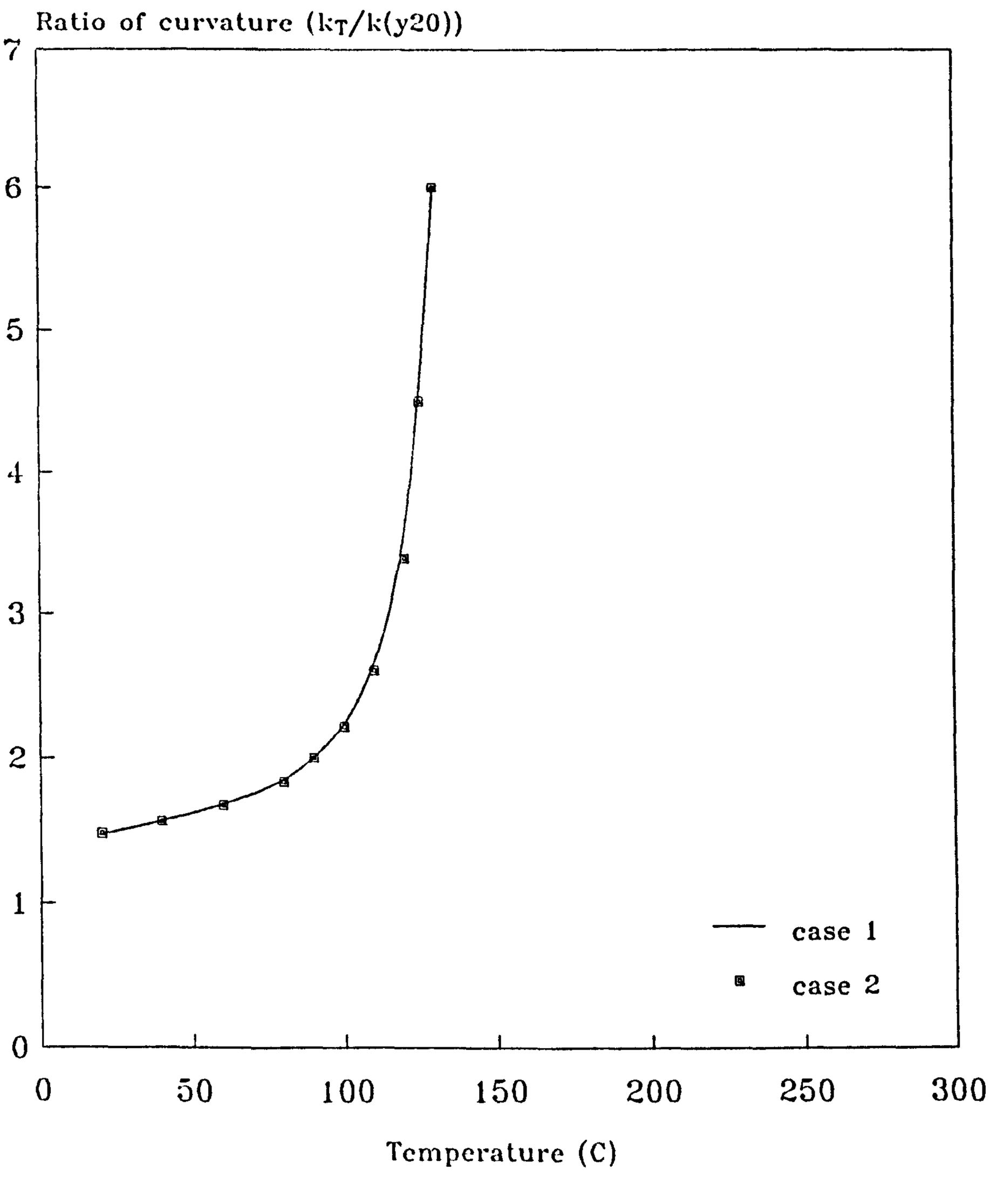

Figure 4.21: Moment-curvature-temperature relationship for cases 1 and 2 when P=0.2Py and M=0.87Mp (I-section)

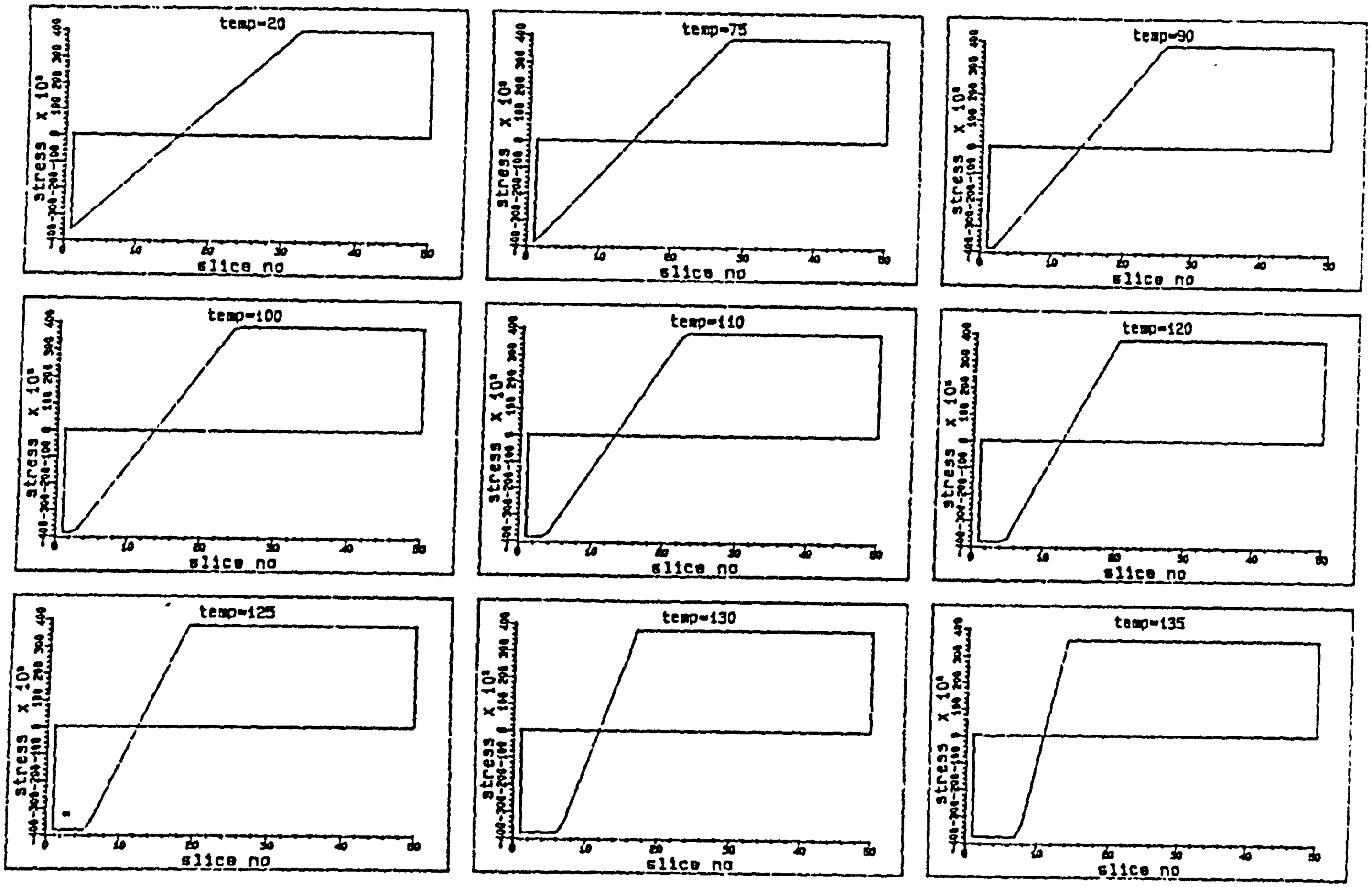

Case 1 ——— Case 2

Figure 4.22: Final stress profiles for case 1 and case 2 of a beam-column element when P=0.2Py and M=0.87Mp (I-section)

unloading on the curvature-temperature relationship is negligible. The same pattern of behaviour was also observed for smaller sizes of I section as shown in Figures 4.23 and 4.24.

4.6 CONCLUSION.

From the above investigation it is clear that material unloading can give rise to a non-unique stress distribution where sections are subject to a combination of axial load and bending moment. This occurs both at constant (ambient) temperature when the sequence of loading is the controlling factor, and at increasing temperature when the initial stress state is fixed. However from the comparisons made it can be concluded that the effect of material unloading is negligible and can be safely ignored both at ambient temperature and in fire for the determination of moment-axial force-curvature relationships. In the present research the effect of material unloading in fire will therefore be ignored in the analysis of frame structures.

The present work is concerned with sections subject to uniform temperature only. It may be that the effect of non-uniform temperature distributions in fire could create different conditions due to differential softening of the material causing a shift in the position of neutral axis. In addition, non-uniform heating patterns often lead to internal stresses which, although self equilibrating, could

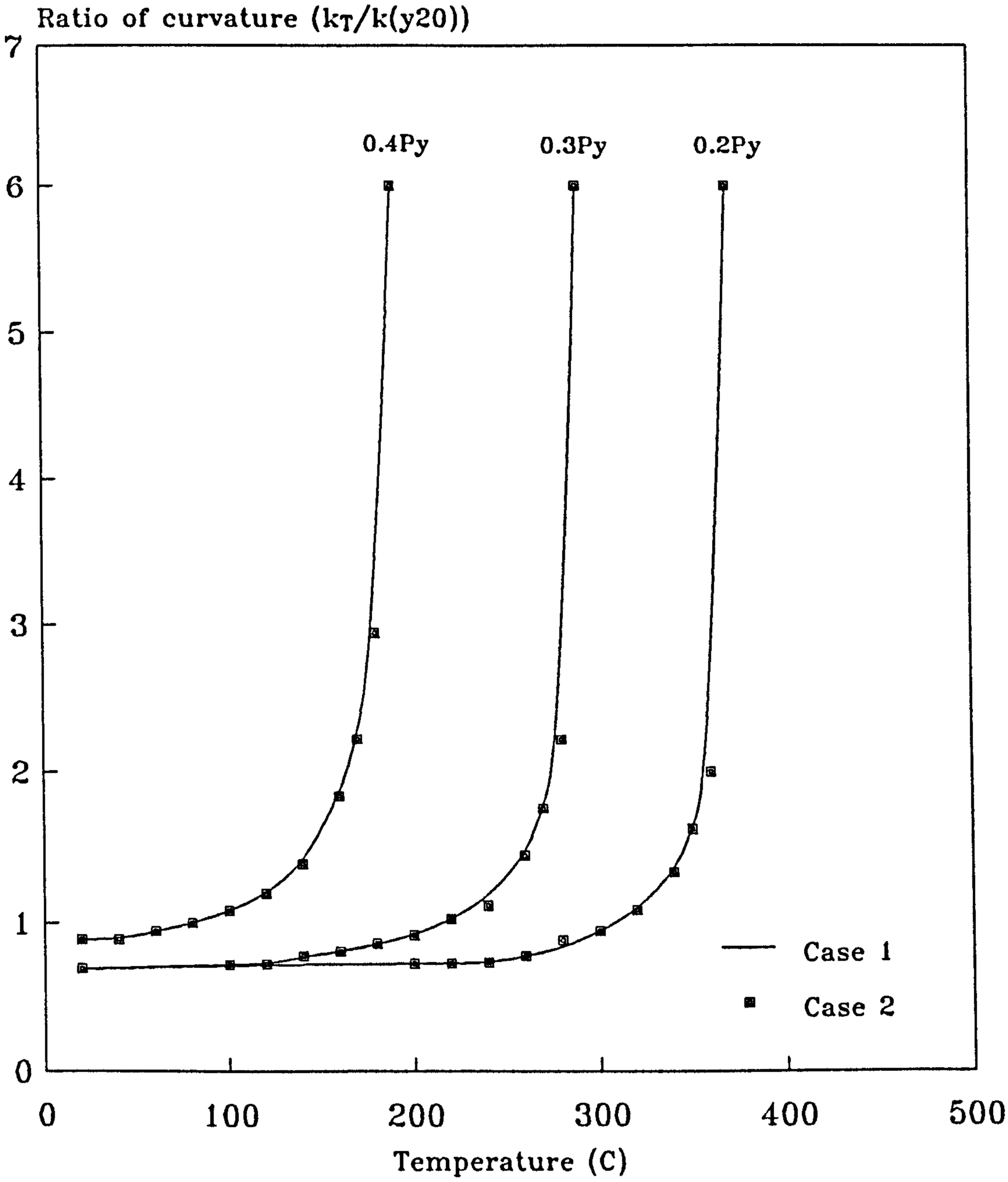

Figure 4.23: Change of curvature with temperature for different axial loads for cases 1 and 2 when M=0.6Mp (I–section).

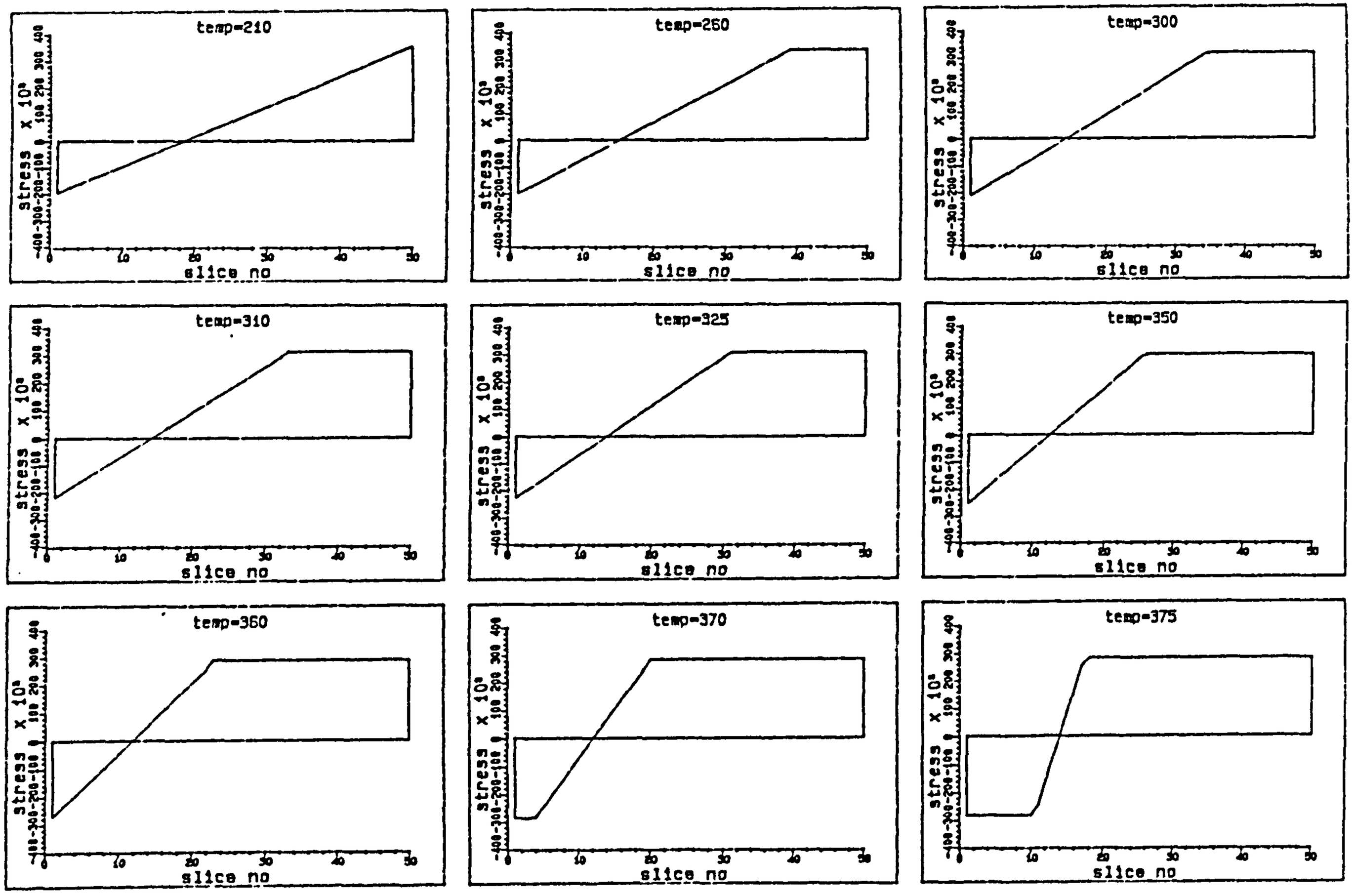

Case 1 Case 2

Figure 4.24: Final stress profiles for case 1 and case 2 of a beam-column element when P=0.2Py and M=0.6Mp (I-section)

also cause material unloading. However, such conditions have not been included in the scope of the present study of the effects of material unloading.

CHAPTER FIVE

ANALYSIS OF FRAME STRUCTURES

IN FIRE

5.1 INTRODUCTION.

The secant stiffness method described in Chapter 3 for the analysis of frame structures at ambient temperature is now extended and will be used to investigate the behaviour of steel frames in fire. The behaviour of such frames generally depends on both the thermal and structural response to an increasing temperature. Assuming that the problem of the thermal analysis can be treated separately, the work of the present research will be concentrated on the structural response of steel frames in fire.

The analysis of frame structures in fire is a complicated process because of the many variables involved. These variables include temperature distribution in the structural elements, interaction between individual structural components, changes in material properties, and the influence of loads on the structural system. All of these effects will be discussed and included in the present analysis.

At elevated temperatures the mechanical properties of structural steel change dramatically with loss in both strength and stiffness, and this can be represented by a series of multi-linear stress-strain curves as described in Chapter 2. In addition the steel will expand, characterised by the coefficient of thermal expansion α_T. For realistic analysis of frame structures in fire, both of these effects should be included in the analysis.

The analysis of frames under fire conditions generally assumes a constant level of load, but at increasing temperature. The approach is therefore equivalent to performing a series of analyses with modified material relationships, taking account of imposed deformations due to thermal expansion. As discussed in previous chapters, the secant stiffness approach provides an efficient means for doing this. This is based on a moment-axial force-curvature relationship, and the derivation of this relationship at increasing temperature is discussed in the following section. The effect of geometric non-linearity, uniform and non-uniform expansion are then considered. Finally a computer program for the analysis of frames in fire is described and validated.

5.2 DERIVATION OF MOMENT-AXIAL FORCE-CURVATURE-TEMPERATURE RELATIONSHIP FOR UNIFORM TEMPERATURE PROFILES.

Several recommendations for the determination of the

structural performance in fire are still based on a uniform temperature profile [17],[19],[89],[90] even though this may rarely occur in real conditions. In the case of unprotected steel columns heated on all sides the temperature profile may be approximately uniform, but in many cases beams and columns will receive partial protection from floor slabs and walls.

The derivation of the moment-axial force-curvature relationship which is basic to the structural analysis is now extended to the case of fire. In this case the derivation is basically the same as described in Section 3.4 but becomes more complicated because it involves another parameter, the steel temperature. The section is again divided into strips, each of which is assumed to be at a uniform temperature.

The stress $\sigma_{T\,i}$ corresponding to the strain in each strip can be calculated from the stress-strain curve according to its temperature level. Thus, the stress σ_i stated in Equation 3.7 is equal to $\sigma_{T\,i}$. The iterative process described in Section 3.4 and Figure 3.6 is then followed in order to bring the internal and external axial force and bending moment into balance.

When a steel cross-section is uniformly heated, the material properties within the section (i.e for each strip) can be represented by a single stress-strain curve at any given

temperature. In this case the determination of the moment-axial force-curvature relationship is based on the same conditions as for the ambient temperature study except that the stress-strain curves are now functions of temperature.

The structural analysis therefore follows the procedures developed previously for general non-linear behaviour. To give an indication of the effects of expansion, material softening and geometric non-linearity these are considered separately in the following sections.

5.3 THE INFLUENCE OF UNIFORM EXPANSION AND RESTRAINT TO EXPANSION.

In the case of steel elements heated uniformly within their cross-section, the expansion is uniform and thermal bowing does not occur since there is no differential expansion of the steel element. When the ends of the member are free to expand the structural behaviour is unaffected, but if the expansion is restrained in any way significant stresses can be induced in the section. This is illustrated in Figures 5.1 and 5.2 which can be used to compare the behaviour of restrained and unrestrained UB 305x165x54 kg/m beams.

The significance of this for frame structures restrained against free expansion is now considered. The behaviour of frame structures in fire is complicated due partly to the fact that the axial displacement and rotation of individual

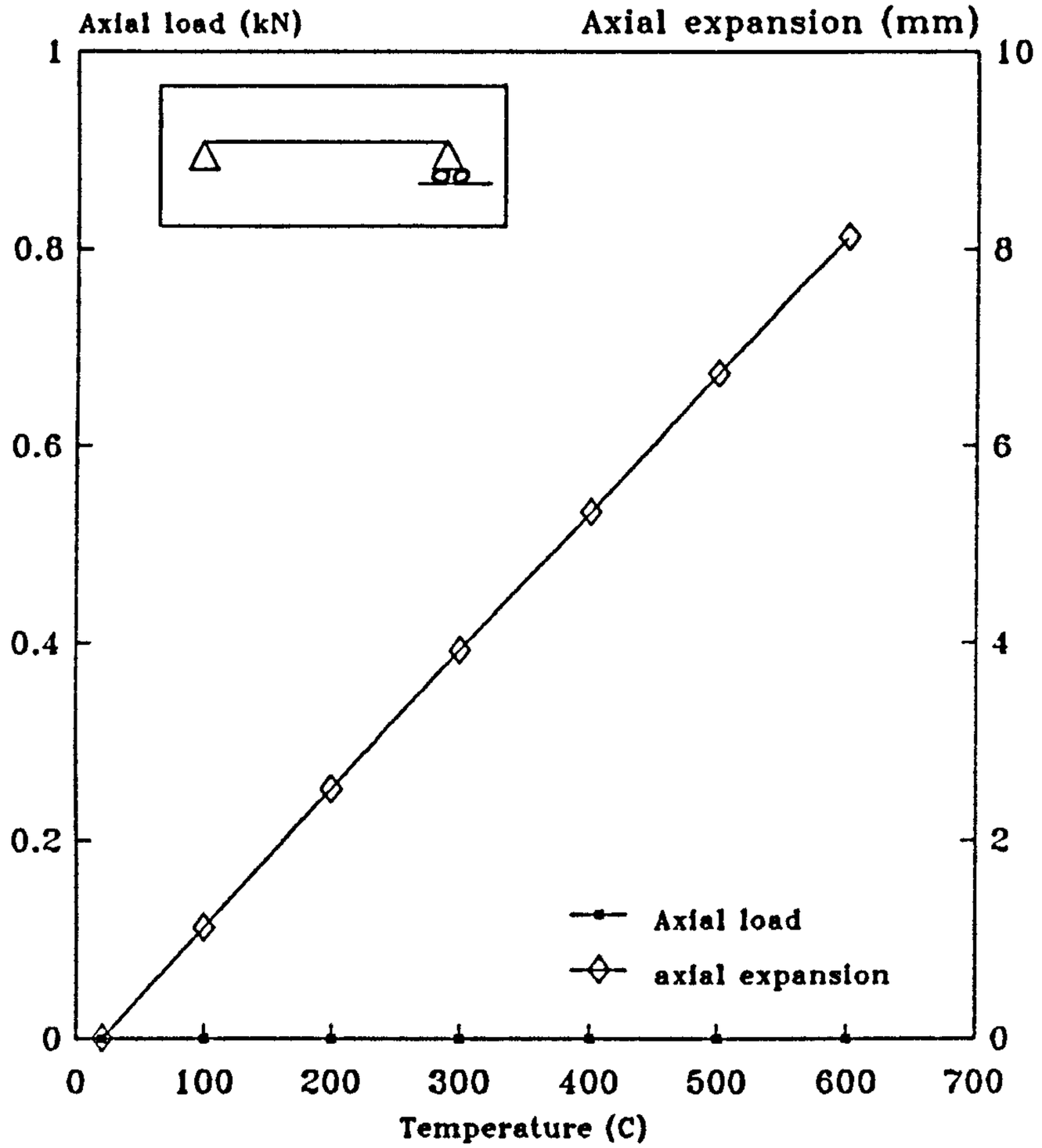

Figure 5.1: Free thermal expansion due to temperature increase.

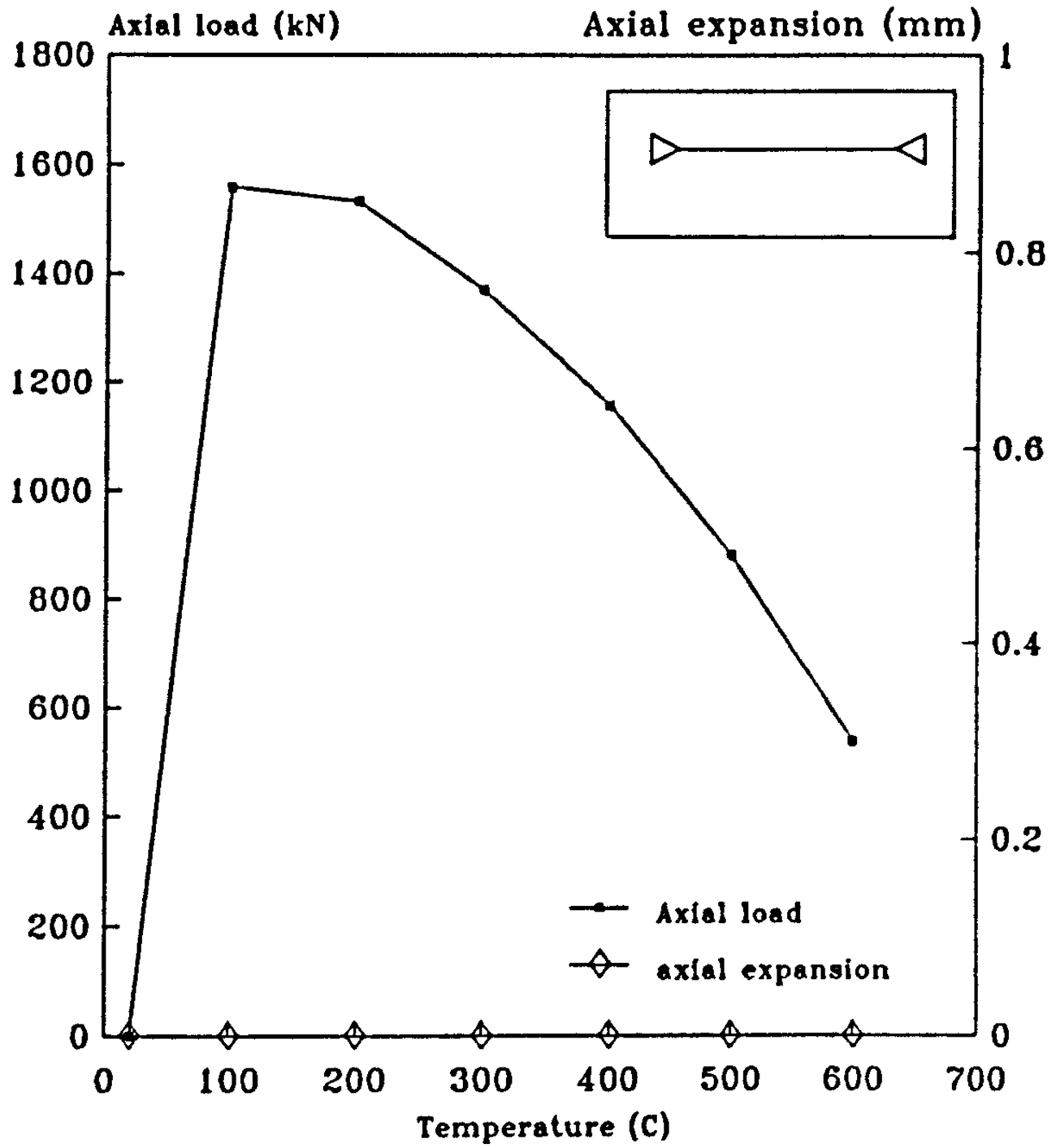

Figure 5.2: Axial force induced due to full restraint against longitudinal expansion.

members are influenced by the degree of restraint at the member ends, for instance where beams are connected to columns.

The influence of thermal expansion on frame structures can be considered by examining a simple portal frame with pinned bases as shown in Figure 5.3. The structure is assumed to be free from external load and the stress-strain curve of steel is assumed to remain constant at its ambient temperature. The reason for this rather artificial condition is to demonstrate the effect of thermal expansion alone on the structural behaviour of frames in fire. The column and beam are of UB 305x102x33 kg/m sections. The frame is analysed for steel temperatures equal to first 200°C and then 300°C. To do this supports A and D (Fig.5.3) are initially assumed to be able to slide allowing the frame to expand freely such as from A to A' and D to D'. The structural analysis is then performed by introducing support displacements equal to $\Delta/2$ at each support due to the fact that both joints should remain in their original position (Figure 5.3). The support displacements at each base can be determined from:

$$\Delta/2 = \alpha_T L(T-20) \quad \ldots\ldots\ldots\ldots\ldots\ldots (5.1)$$

where L = span of beam.

T = temperature.

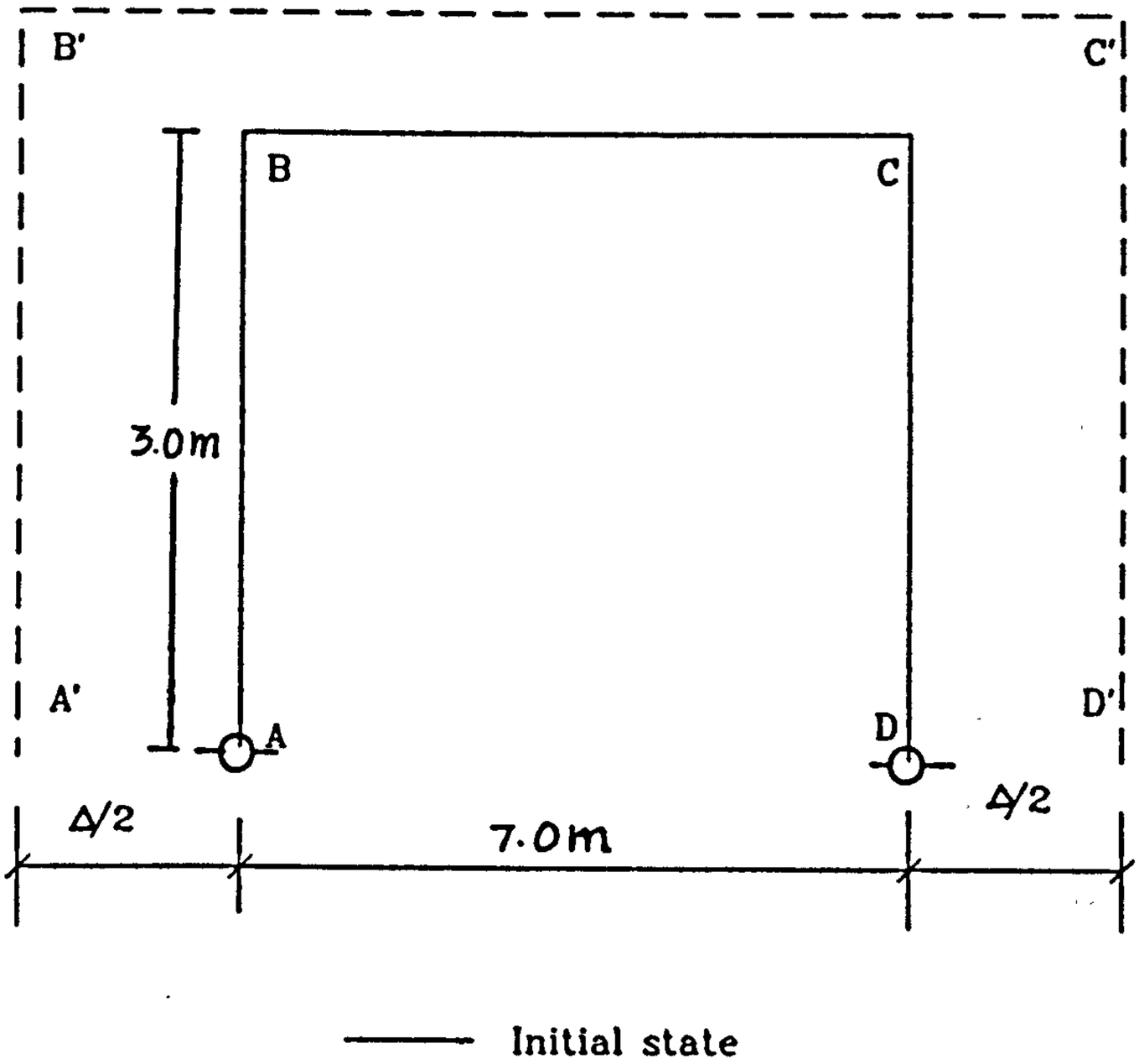

Figure 5.3: Free thermal expansion of frame structure due to temperature increase.

The resulting deflected shape and bending moment diagram for the column are shown in Figures 5.4a and 5.4b. These show that restraint to free expansion could have a very significant effect on the overall behaviour of steel portal frames in fire. Not only are bending moments induced in the unloaded frame, but considerable deformations are imposed on the structure. In the presence of axial loads these will create important additional bending effects.

5.4 THE INFLUENCE OF MATERIAL SOFTENING AND AXIAL SHORTENING.

The influence of material softening on structural analysis in fire is now discussed. Consider a simply supported beam of span 7.0m with a section size of UB 305x165x54 kg/m and a uniformly distributed load of 20 kN/m, equivalent to a maximum design stress of 165 N/mm^2. The stress-strain curves for steel are based on the idealised curves shown in Figure 2.13. The beam was analysed at different temperatures using the corresponding curve, but ignoring any other temperature effects.

Figure 5.5a shows the relationship between the central deflection of the beam and the steel temperature. The figure shows that by including the influence of material non-linearity in the analysis, the critical temperature of the beam is about 550°C for a limiting deflection of span/20 (350mm). This is in keeping with test results [1],[20].

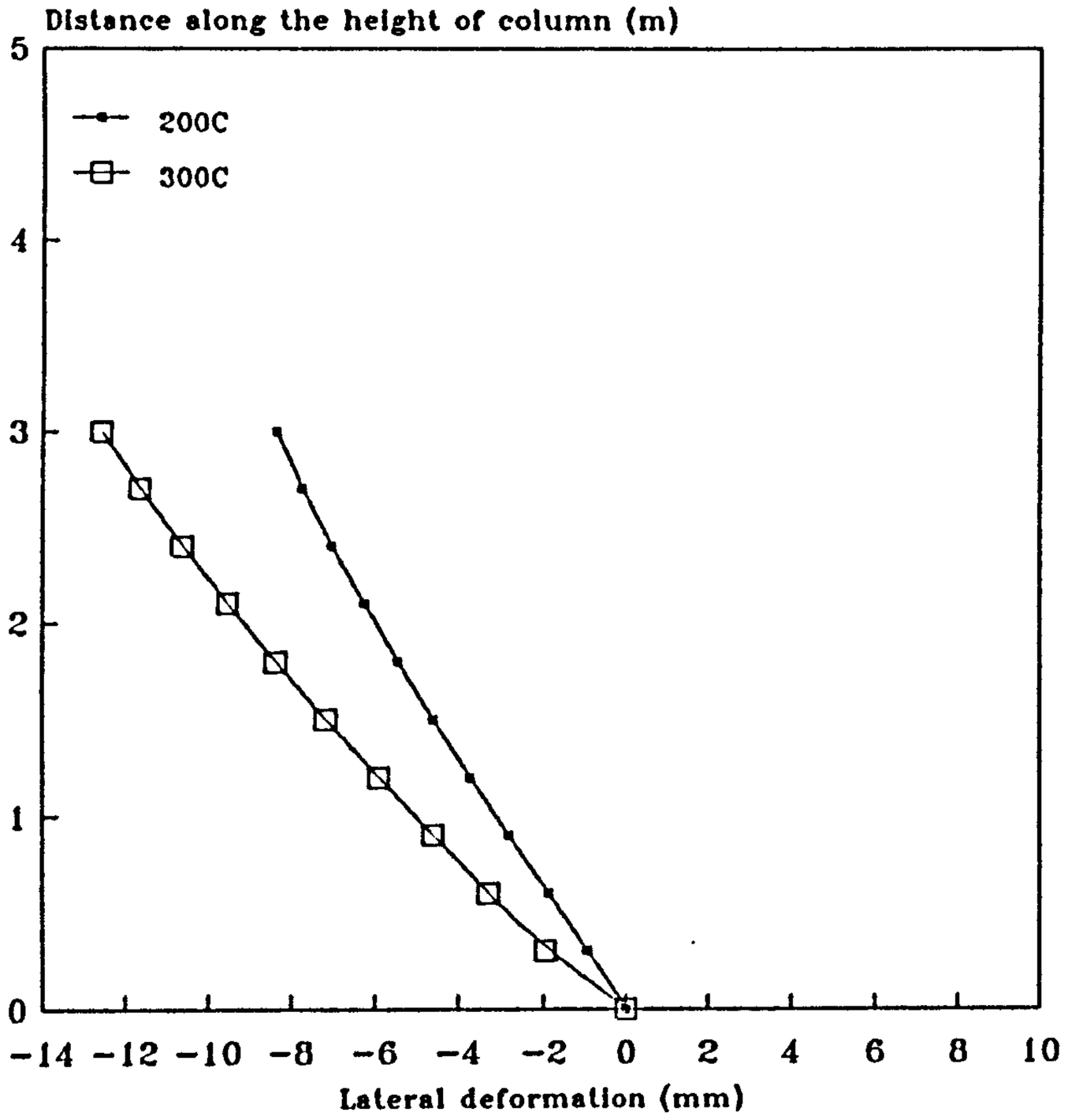

Figure 5.4a: Lateral deformation of column of frame due to thermal expansion only.

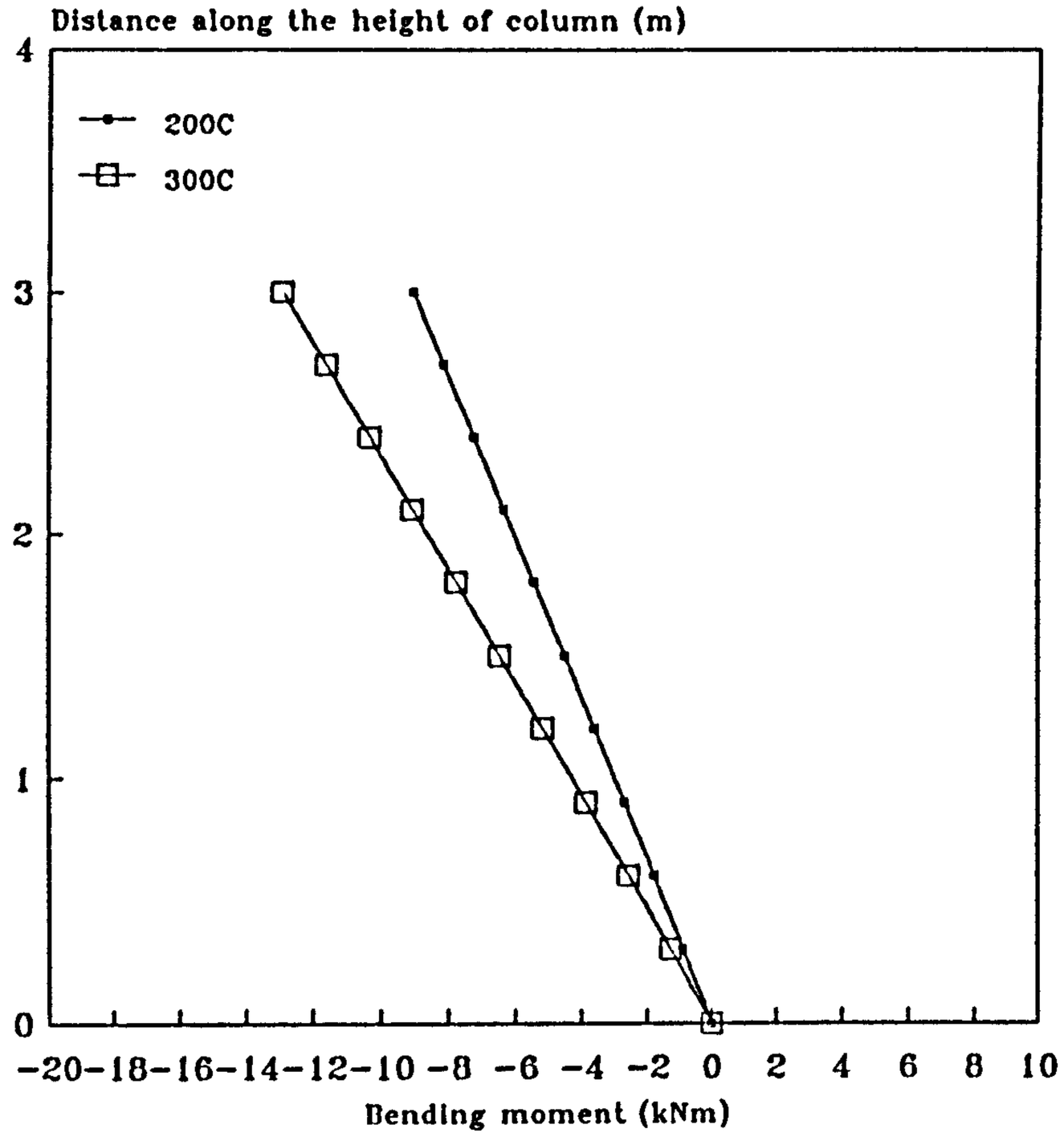

Figure 5.4b: Bending moment of column of frame due to thermal expansion only.

Figure 5.5b shows the effect of excluding and including axial shortening due to bending on the horizontal (axial) deformation of the beam in fire. The curves start to deviate at temperatures beyond about 400°C. It should be noted that by including this effect the axial expansion is reduced, consequently reducing the potential axial force induced in the element due to restraint to expansion. The effect of this is likely to be smaller predicted deformations and hence higher predicted failure temperatures.

5.5 INFLUENCE OF THE P-DELTA EFFECT.

As discussed in Chapter 3, the presence of compressive or tensile axial force on a steel beam will change the bending moment and also the deformed shape. This p-delta effect is likely to be more significant at higher temperatures since the stress-strain curves are progressively reducing, and its influence on a simply supported beam in fire is discussed in this section.

Consider a beam of section UB 305x165x54 kg/m with a span of 15.71m giving a span/r_x ratio of 120. A uniformly distributed load of 0.702 kN/m (equivalent to a bending stress at mid-span of 28.75 N/mm^2) and a compressive force of 410.4 kN ($0.24P_y$) are applied. The beam is analysed at temperatures of 20°C and 300°C, both with and without the p-delta effect. Figures 5.6a and 5.6b show the deflection and

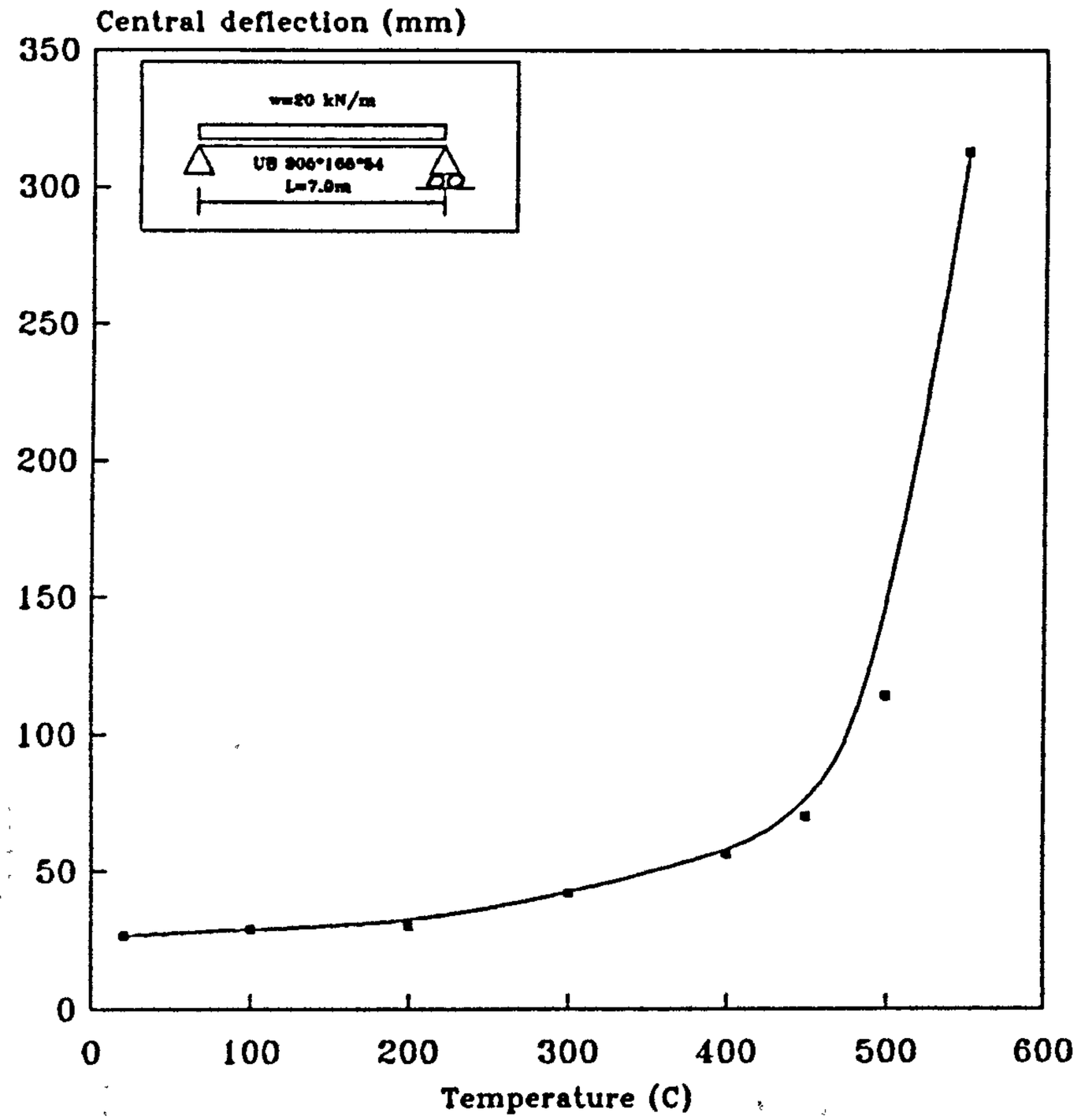

Figure 5.5a: Central deflection of a simply supported beam in fire.

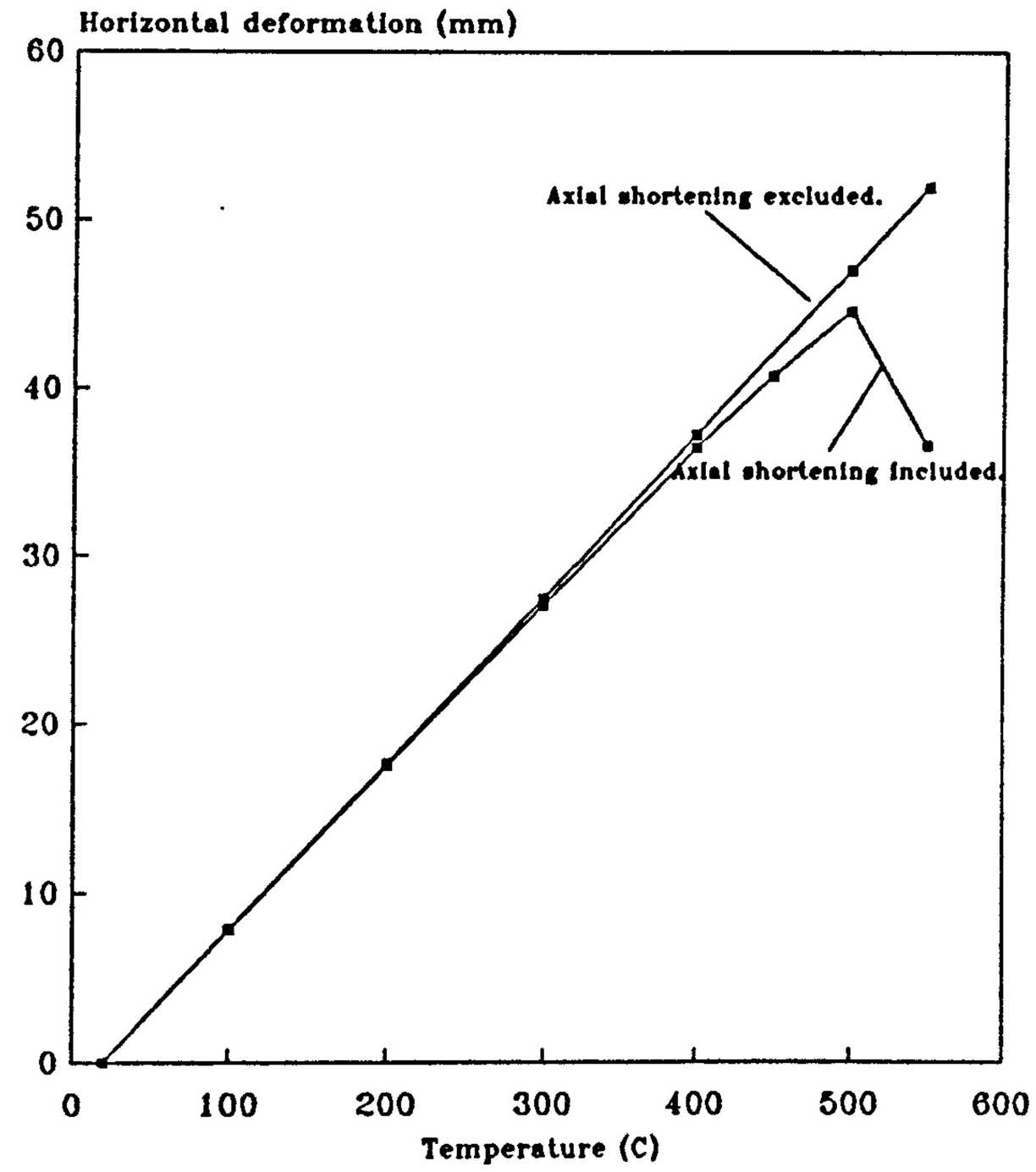

Figure 5.5b: Horizontal deformation of a simply supported beam in fire illustrating the effect of axial shortening due to curvature.

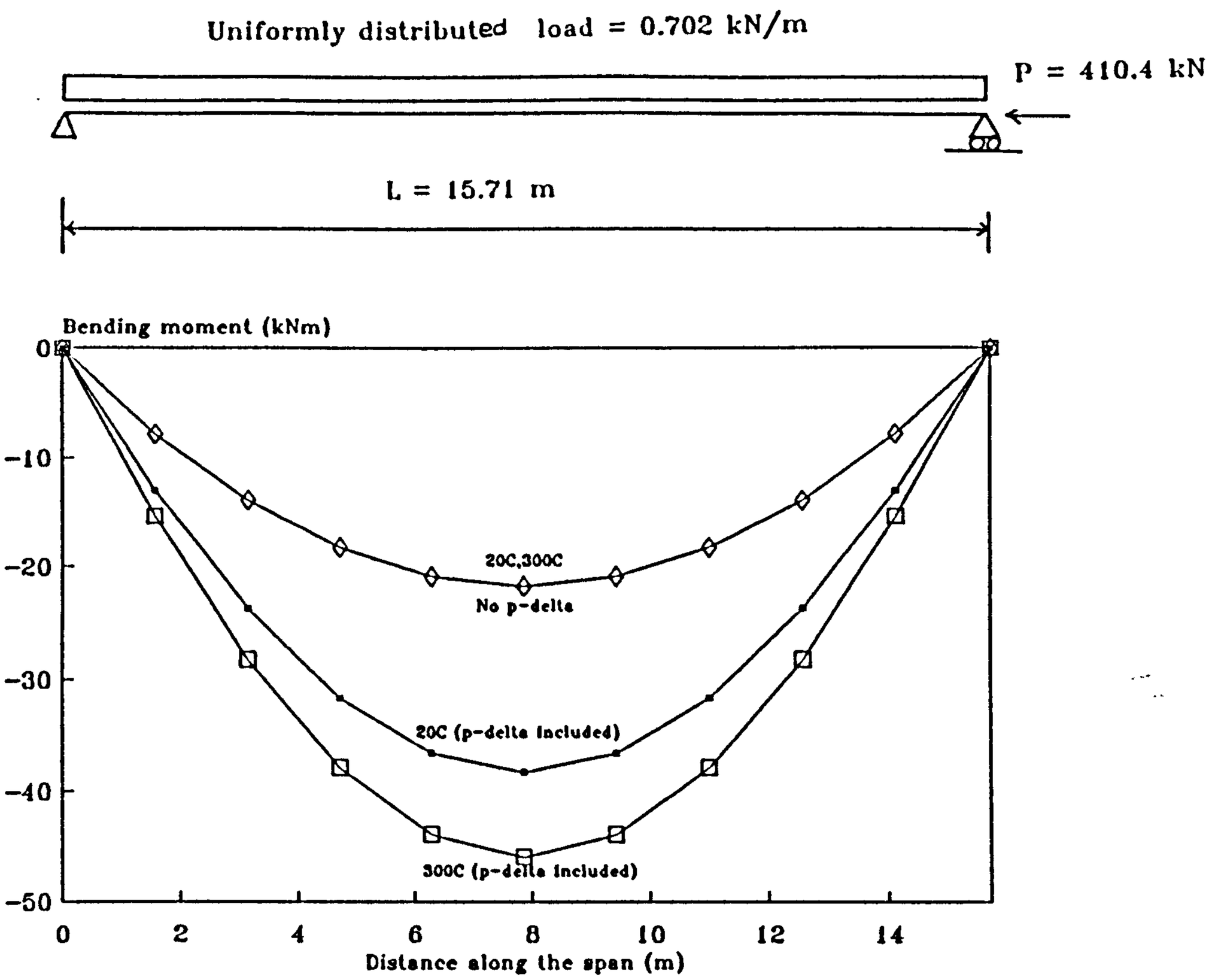

Fig.5.6a: Bending moment of simply supported beam subjected to a uniformly distributed load and axial load.

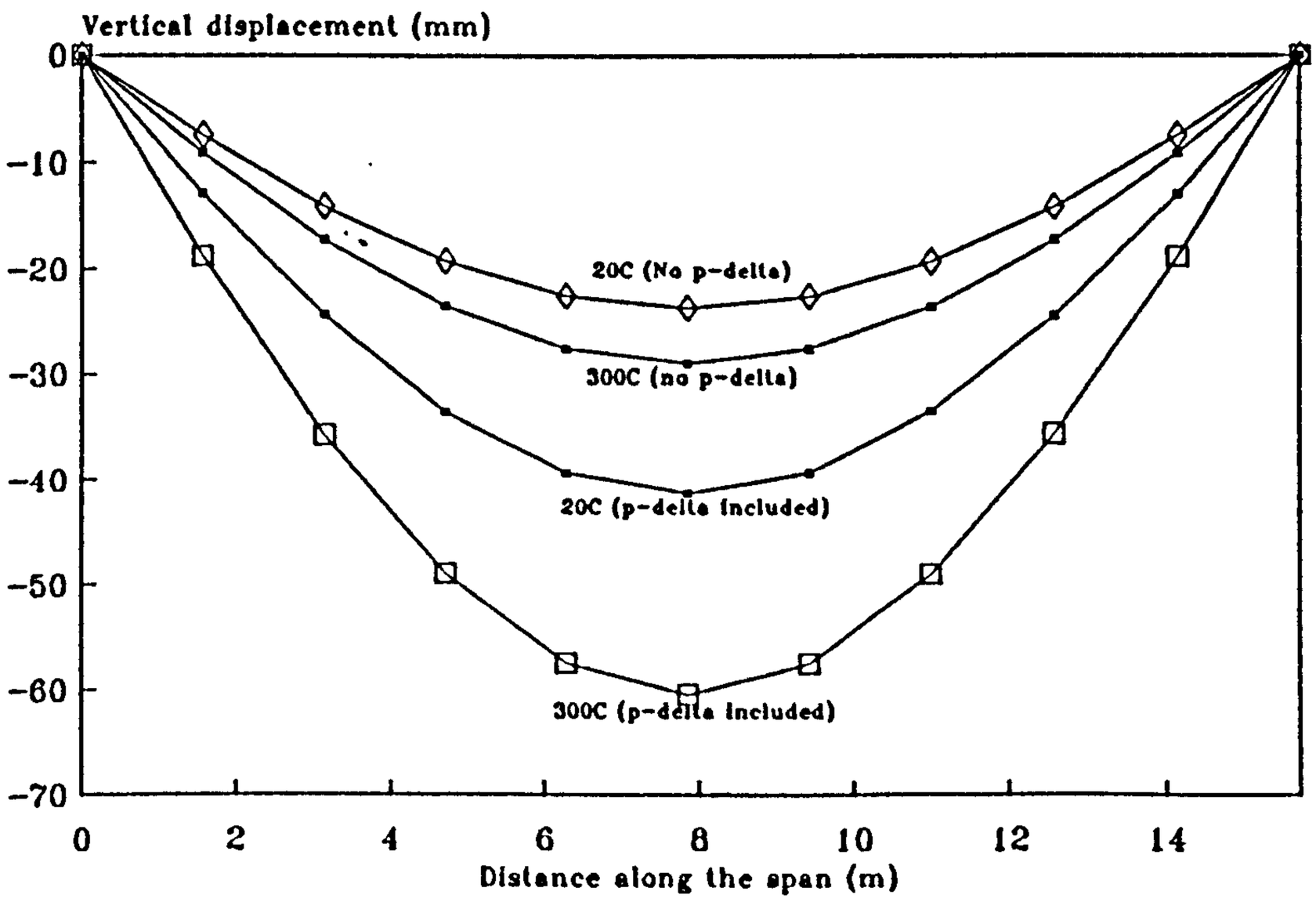

Fig.5.6b: Vertical deflections of simply supported beam subjected to a uniformly distributed load and axial load.

bending moment respectively. These indicate that at 20°C the inclusion of the p-delta effect increases the mid-span bending moment and deflection by about 80% and 67% respectively. This effect is even more significant at the higher temperature of 300°C, in which case the bending moment and deflection are increased by 114% and 150% respectively. Although this is a very slender member, and beams and columns of more realistic proportions may not respond in a such a dramatic fashion, it nevertheless indicates the increased influence of geometric non-linearity even at 300°C. Of course, in fire analysis very much higher temperatures will often need to be considered and the inclusion of the p-delta effect would then seem very important.

5.6 THE INFLUENCE OF NON-UNIFORM TEMPERATURE PROFILE WITHIN THE CROSS-SECTION.

In reality the temperature within the cross-section of a steel element is often non-uniform due to the nature of the construction details such as:

1. Where a concrete slab is placed on top of a steel beam, in which case the temperature at the bottom flange and web is often much greater than the temperature of the top flange.

2. In shelf angle floor and slim floor construction, where a

considerable part of the beam is shielded from fire.

3. When a wall is built into the web of a column again causing considerable shielding of the steel cross-section.

In such cases the non-uniform temperature profile within the cross-section results in a variation in the strength of the steel, and the structural analysis becomes more complicated than for uniform heating. In addition thermal bowing will occur due to differential expansion within the cross-section. It should be noted that the deflection due to thermal bowing alone, excluding the external imposed loads, may exceed the limiting deflection stated in BS 476: Part 8. On the other hand, this could induce eccentric loading, particularly when a steel member is subjected to a compressive force. Because of this, the effect of non-uniform temperature profile within the cross-section has been included in the present analysis.

5.6.1 Idealisation of temperature profile.

The non-uniform temperature profile within the cross-section can be complex, and for simplification it is represented in an idealised fashion in the present analysis.

As described in Chapter 3 the cross-section is divided into a number of strips for the purpose of structural analysis. The temperature in each strip is assumed to be constant and

equal to the value at its mid depth based on the idealised temperature profile. Clearly the more strips used the more accurate can be the representation of the steel temperature profile within the section. However in the present analysis a cross-section consisting of 10 strips will be used reflecting the study described in Section 5.9 which shows that this will provide adequate accuracy in frame analysis in fire.

Different types of idealised temperature profile have been adopted in the present analysis and these are shown in Figure 5.7. In the case of a linear temperature variation over the cross-section as shown in types 3 and 4 the temperature used is that at mid-height of the strip, determined by interpolation.

5.6.2 Derivation of free thermal curvature.

When a cross-section is subjected to non-uniform heating differential expansion will occur. If strips of the cross-section were allowed to deform independently, free thermal expansion would occur as shown in Figure 5.8. However, shear bonding between the strips will prevent such expansion, and rotation will take place. Assuming that plane sections remain plane during bending, this can create internal stresses in each strip. This is illustrated in Figure 5.8 which shows the free thermal expansion in each strip and the corresponding final distribution of thermal

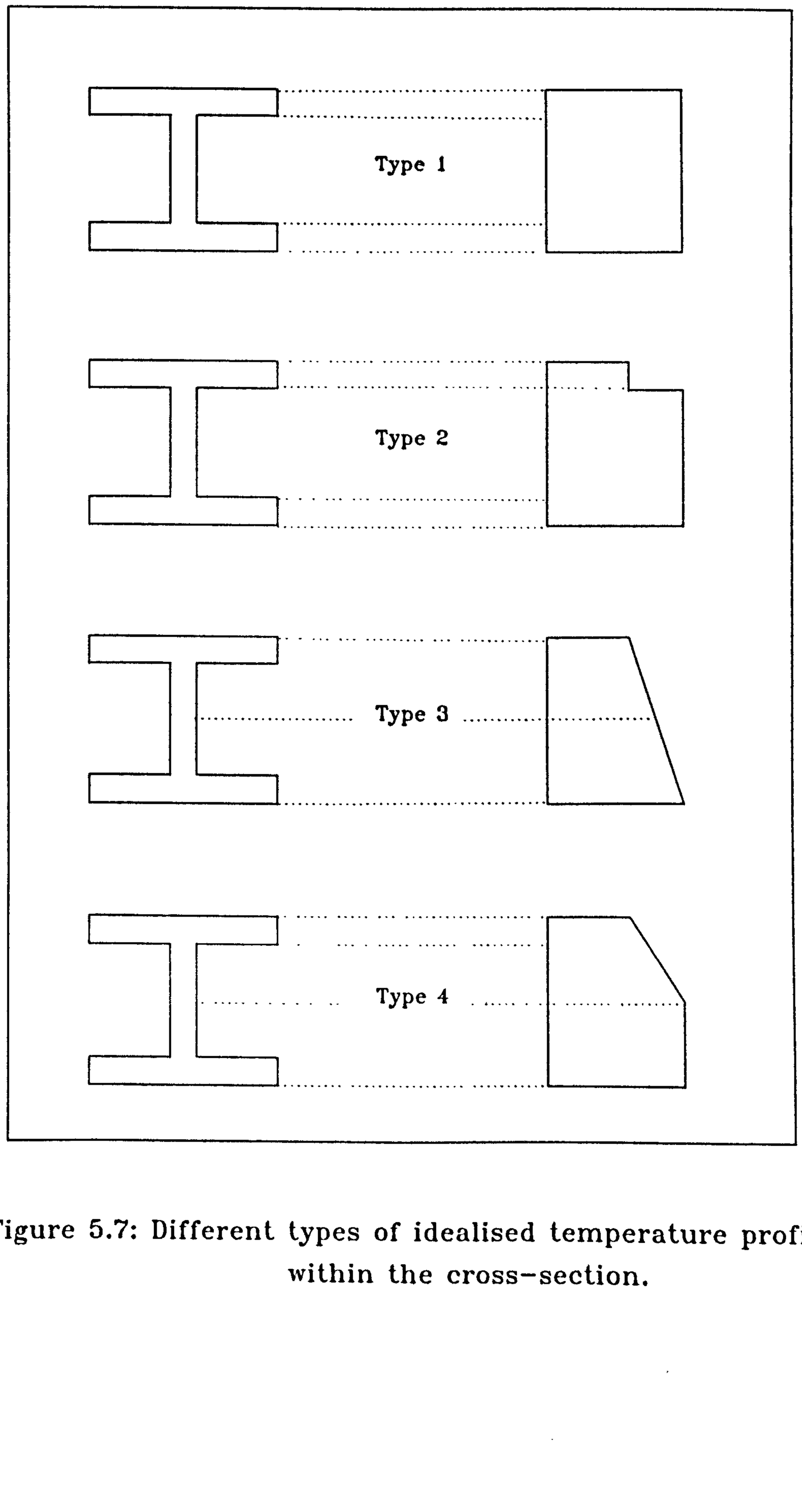

Figure 5.7: Different types of idealised temperature profile within the cross-section.

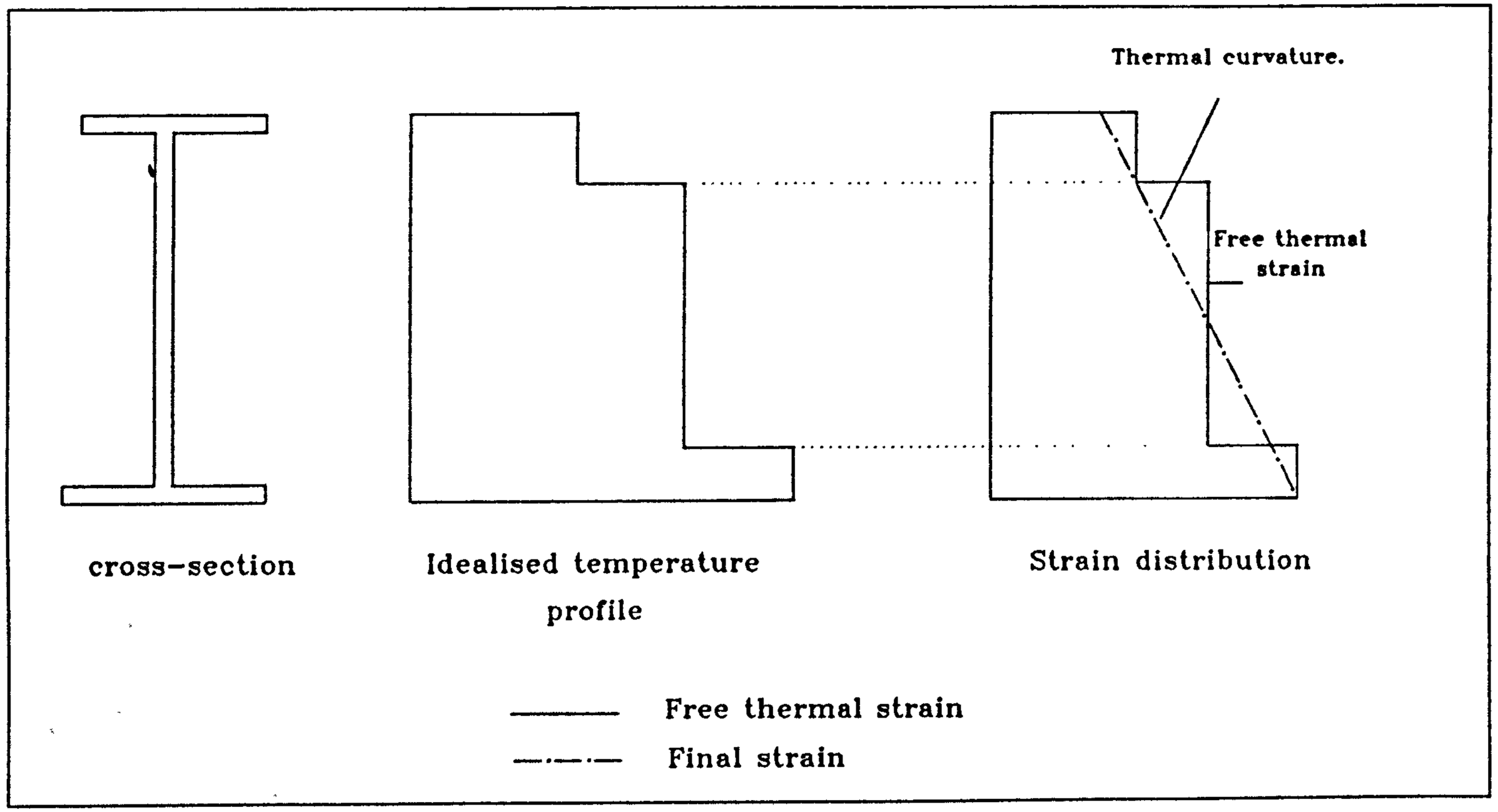

Figure 5.8: The influence of non-uniform temperature profile on the strain distribution of a crosss-section

expansion across the section. It can be seen that some of the strips are in compression while the rest are in tension.

The process of determining the free thermal curvature is in fact the same as was described in Section 5.2 except that the effect of thermal expansion is included. The analysis starts by assuming that each strip will expand freely according to its temperature level and is given by;

$$\varepsilon_{T\,i} = \alpha_T T_i \quad \ldots\ldots\ldots\ldots\ldots\ldots (5.2)$$

where $\varepsilon_{T\,i}$ = Free thermal strain of i'th strip.

T_i = Temperature of i'th strip based on the idealised temperature profile.

α_T = coefficient of thermal expansion.

A free thermal curvature k_{th} is then assumed and the elongation or contraction of any strip can be calculated from Equation 5.3 as illustrated in Figure 5.9a.

$$\varepsilon_i = \varepsilon_o + (k_{th} y_i) - \varepsilon_{T\,i} \quad \ldots\ldots\ldots\ldots (5.3)$$

where ε_i = resultant strain of i'th strip.

$\varepsilon_{T\,i}$ = free thermal strain of i'th strip.

ε_o = centroidal axial strain.

The stress $\sigma_{T\,i}$ corresponding to the resultant strain in each strip ε_i can be calculated from the stress-strain curve

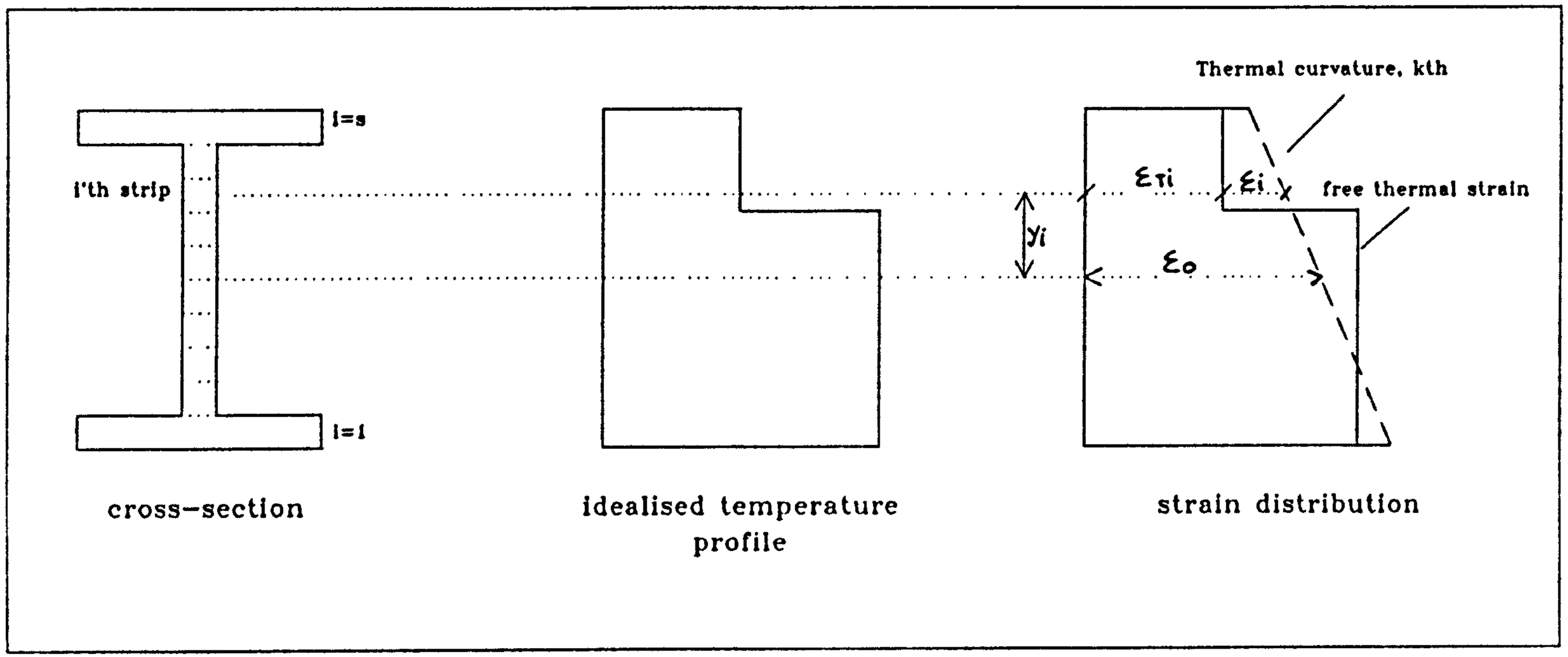

Figure 5.9a: Schematic representation for determining the resultant strain at each strip.

corresponding to the temperature level. Then the internal axial force dP_i and bending moment dM_i for each strip can be computed from Equations 3.7 and 3.8. The internal axial force and bending moment for the complete cross-section can be calculated from Equations 3.9 and 3.10 respectively. An iteration process is then required to bring the internal and external axial force and bending moment into balance (Figure 5.9b). In this case the external axial force P and bending moment M are equal to zero due to the fact that no external forces are applied on the element. Having determined the free thermal curvature k_{th} in this way provides a basis for the inclusion of thermal bowing in the present analysis, as is discussed in the following section.

5.6.3 Derivation of fixed end moment due to thermal curvature.

In the secant stiffness method the flexural stiffness coefficient is represented by S_{si}. The effect of thermal curvature on the secant stiffness is included by treating it as an equivalent external load. To start with, consider a simply supported beam with a constant flexural stiffness along the span. If a non-uniform temperature profile is introduced over the cross-section thermal bowing will occur (Figure 5.10a). The free thermal curvature k_{th} can be determined according to section 5.6.2. The same amount of curvature can also be achieved if end moments are applied to the element (Figure 5.10b). The equivalent external moment

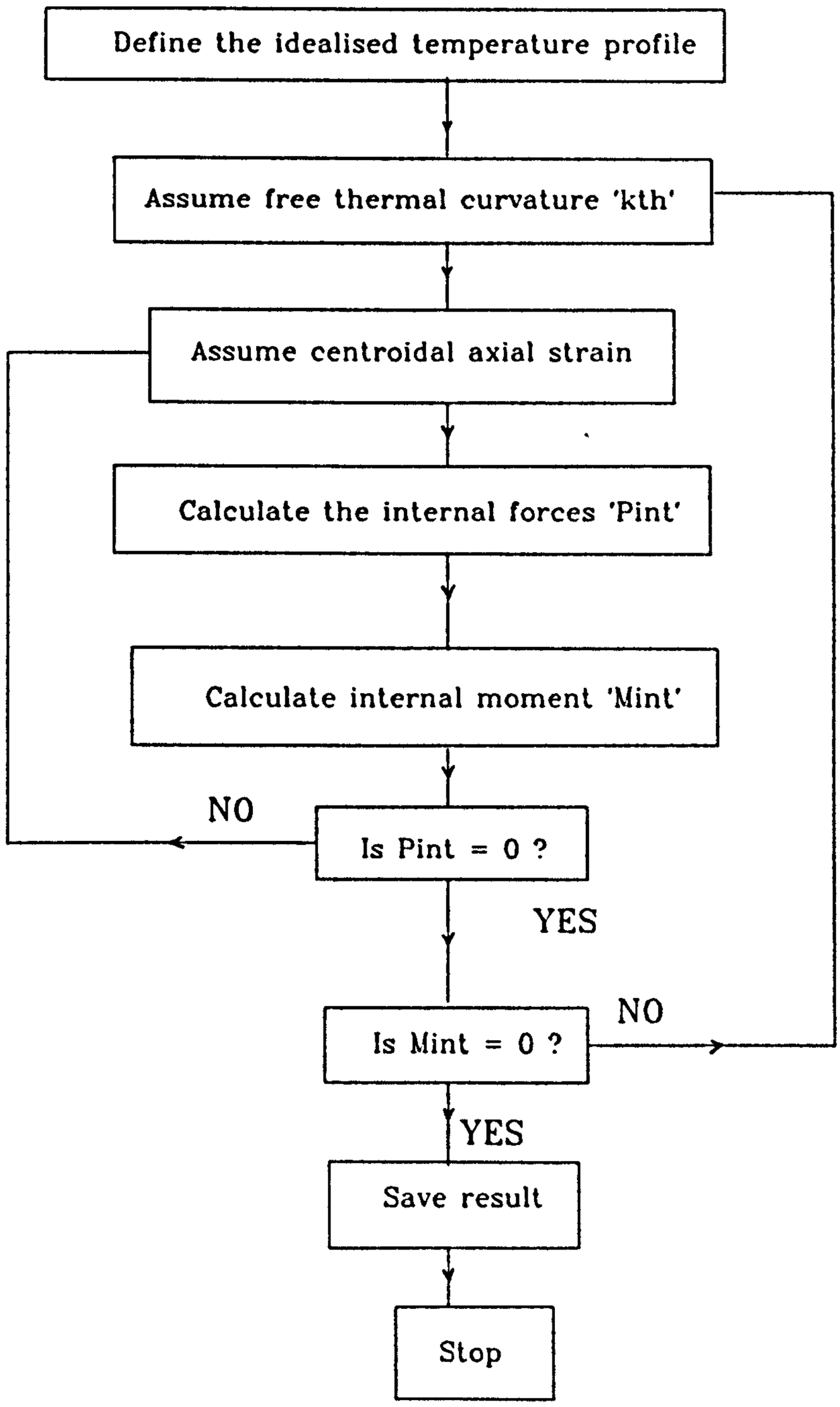

Fig. 5.9b: Logical sequence of the operations in obtaining the free thermal curvature.

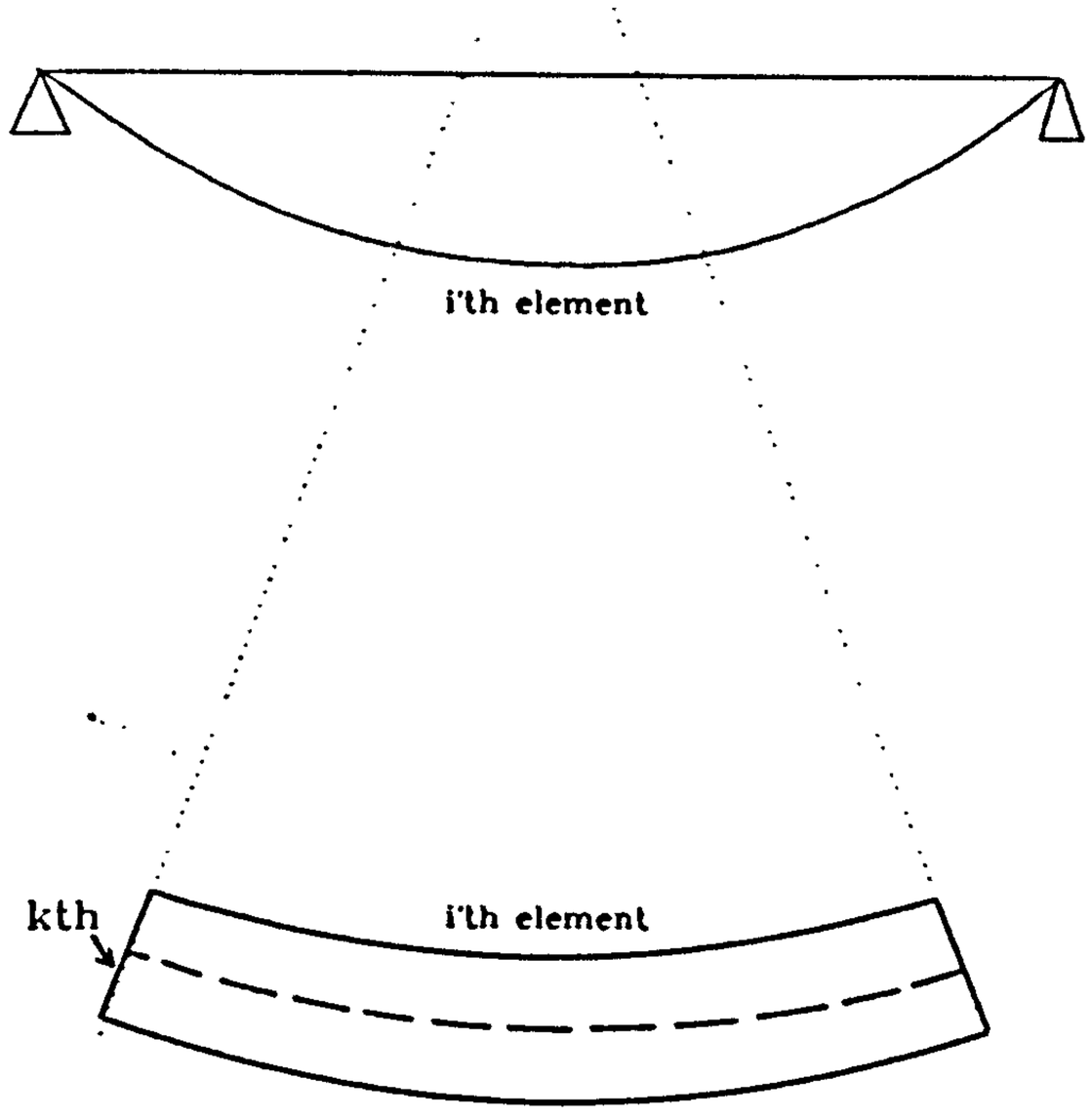

(a) Deflection due to thermal bowing.

(b) Enlargement of the i'th element showing the thermal curvature.

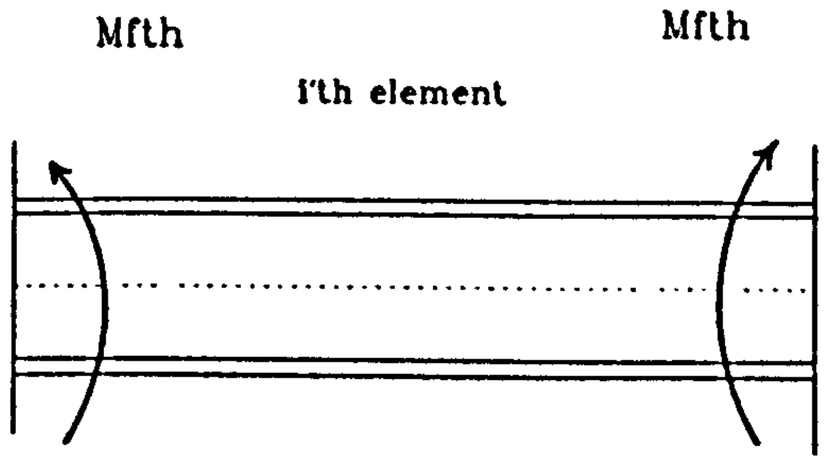

(c) Fixed end moments used to restrain the thermal curvature.

Figure 5.10: Schematic representation for determining the fixed end moments due to thermal curvature.

can be calculated from the relationship of the free thermal curvature k_{th} to the flexural secant stiffness coefficient S_{s1}. The equation takes the form:

$$M_{eq} = S_{s1} k_{th} \quad \ldots\ldots\ldots\ldots\ldots\ldots (5.4)$$

where M_{eq} = Equivalent external moment.

If end restraint is introduced, by the ends of the element being fixed preventing rotation as shown in Figure 5.10c, the moment restraint M_{fth} must be equal to this equivalent external moment. In frame analysis in fire this value M_{fth} is then considered as a fixed end moment due to thermal curvature in determining the total load vector.

5.7 COMPUTER PROGRAM.

The secant stiffness method described in Chapter 3 has been extended to include the analysis of statically determinate and indeterminate steel frame structures in fire. This has been developed into computer program called NASBIF for predicting the deformation history of such structures.

The logical sequence of the analysis is shown in Figure 5.11 which is in fact an extension of the flow chart described in Figure 3.18. The normal secant stiffness analysis is adopted but in addition the temperature is required in order to calculate the free thermal curvature k_{th}, for inclusion

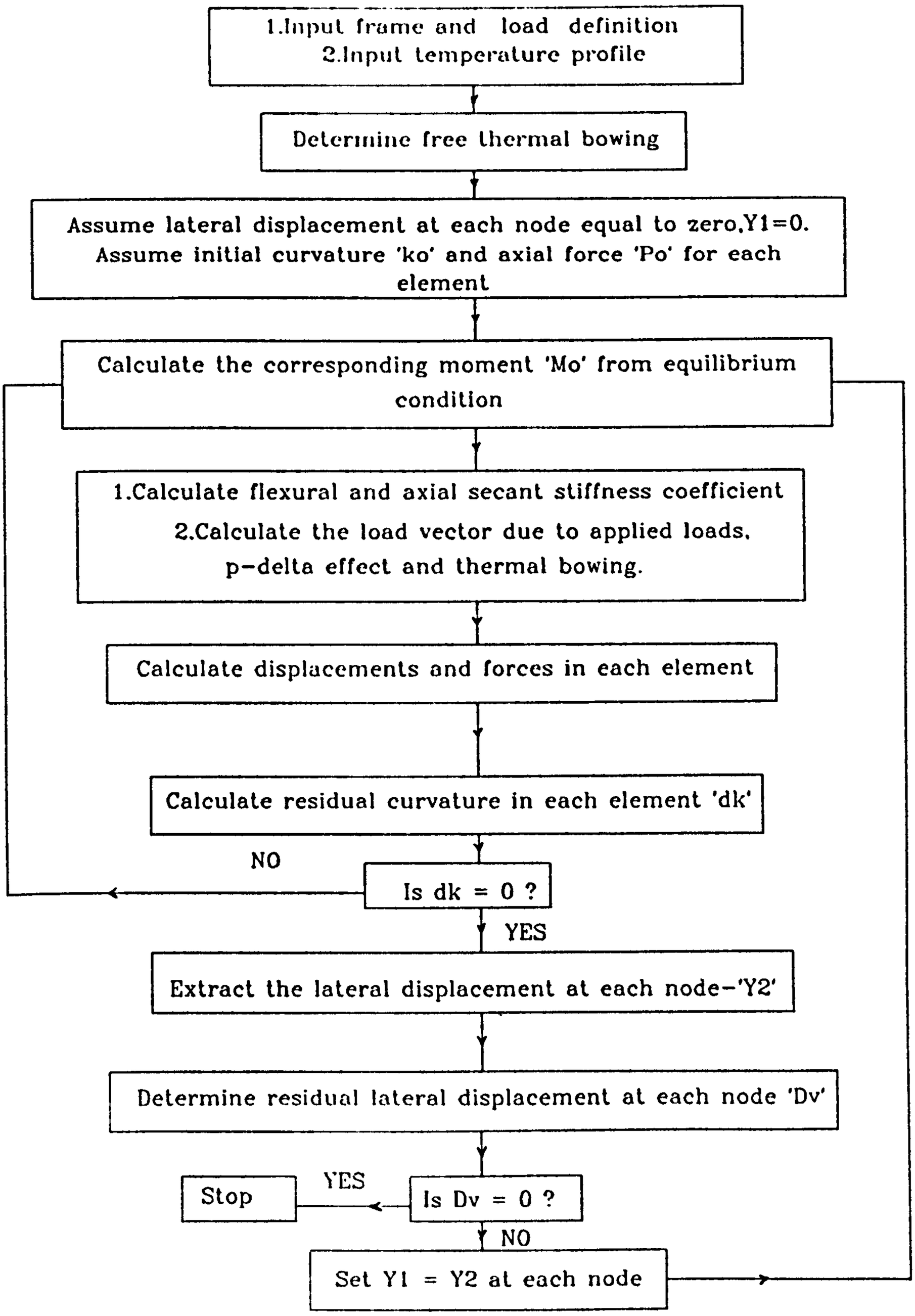

Figure 5.11: Computer chart for the analysis of frame structures in fire.

in the load vector and the appropriate material properties in each strip in the cross-section.

From Figure 5.11, the frame, loading and temperature profiles are first defined. The free thermal curvature 'k_{th}' for each element is then determined according to Section 5.6.3. This is used to calculate the fixed end moments due to thermal bowing which are then included in the load vector. The frame analysis described in Section 3.8.3 can then be performed.

As was described in Section 3.7 a curvature k_o and axial force P_o for each element are first assumed. The corresponding moment M_o is calculated from a consideration of equilibrium equating the internal and external axial forces P_o as shown in Figure 5.12. The flexural secant stiffness coefficient S_{s1} is then determined by dividing the moment M_o by the assumed curvature k_o. This is used in calculating the fixed end moment due to thermal bowing.

The flexural secant stiffness coefficient S_{s1}, which is independent of thermal expansion, is determined separately from the axial secant stiffness coefficient A_{s1}, which varies with thermal expansion. The determination of the latter coefficient is considered next. The values of axial force P_o and bending moment M_o for each element, as defined at the beginning of the cycle are used to determine the average axial strain ε_o. This is based on consideration of

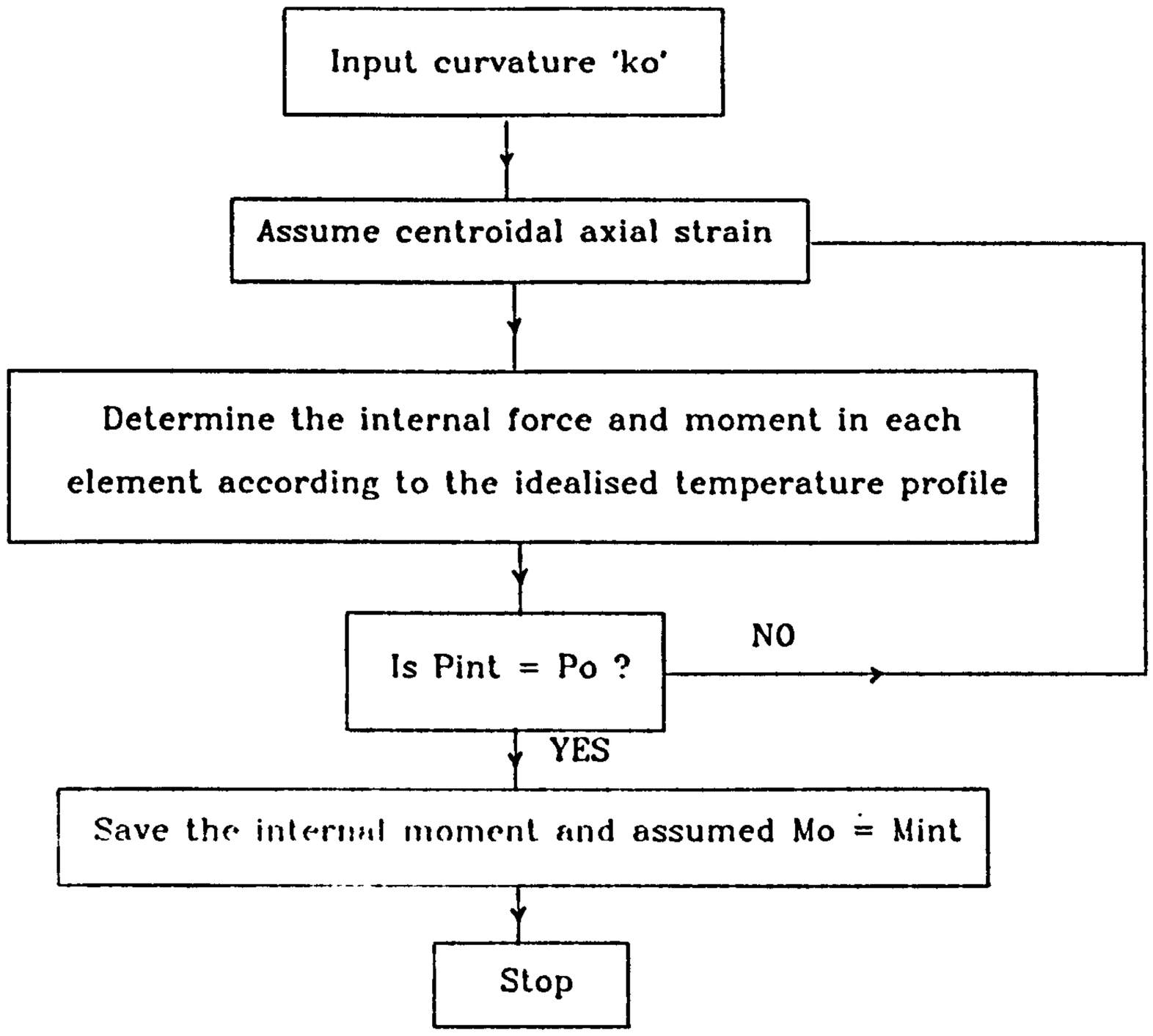

Figure 5.12: Logical sequence of the operations for determining the internal moment 'Mo' of each element.

equilibrium, equating the internal axial force and bending moment with P_o and M_o respectively. The procedure is basically the same as described in Section 5.6.2, for free thermal curvature but must now be modified to account for restraint to this. In this case a total curvature k_t due to both loading and thermal effects is assumed for each element. The elongation or contraction of any strip is then given by Equation 5.3 but with the free thermal curvature k_{th} replaced by the total curvature k_t.

Having determined the strain in each strip in this way, the internal axial force and bending moment for each strip and the complete cross-section is determined in accordance with Section 5.6.2. An iteration process is then carried out in order to balance the internal axial force and bending moment with P_o and M_o respectively. If the difference between the internal and external forces as described in Equations 3.11 and 3.12 is sufficiently small the average axial strain ε_o (at the centroid of the cross-section) is then recorded. This is then combined with the axial strain due to axial shortening to generate a resultant axial strain ε_t (see Equations 3.21 and 3.22). By doing this the axial secant stiffness coefficient for each element can be determined according to Equation 3.23.

Having determined the axial and flexural secant stiffness coefficients, the load vector is then calculated. This includes the effect of applied loads, thermal bowing and the

p-delta effect. Equations 3.24 and 3.25 are then used to calculate the nodal displacements and element forces.

As mentioned in Section 3.8.3 the analysis is iterative and repeats until the previous and current displacements of each node are within the specified tolerance limit.

5.8 ANALYSIS OF FRAME STRUCTURES WITHIN A TEMPERATURE RANGE.

The non-linear stress-strain curves of steel at increasing temperature do not exhibit a clear yield stress and hence a collapse criterion cannot normally be used. Instead the failure condition can be related to a limit state of deformation. This is in keeping with the standard fire test which prescribes deformation limits to avoid damage to the furnace. Because of this the analysis needs to be performed over a temperature range in order to obtain the deformation histories up to the point of failure.

In the secant stiffness method the curvature relationship is independent of any previous analysis. However to minimise computation time the calculated value of curvature in each element at one temperature is taken as an initial value when the next temperature increase is considered. This is shown diagrammatically in Figure 5.13.

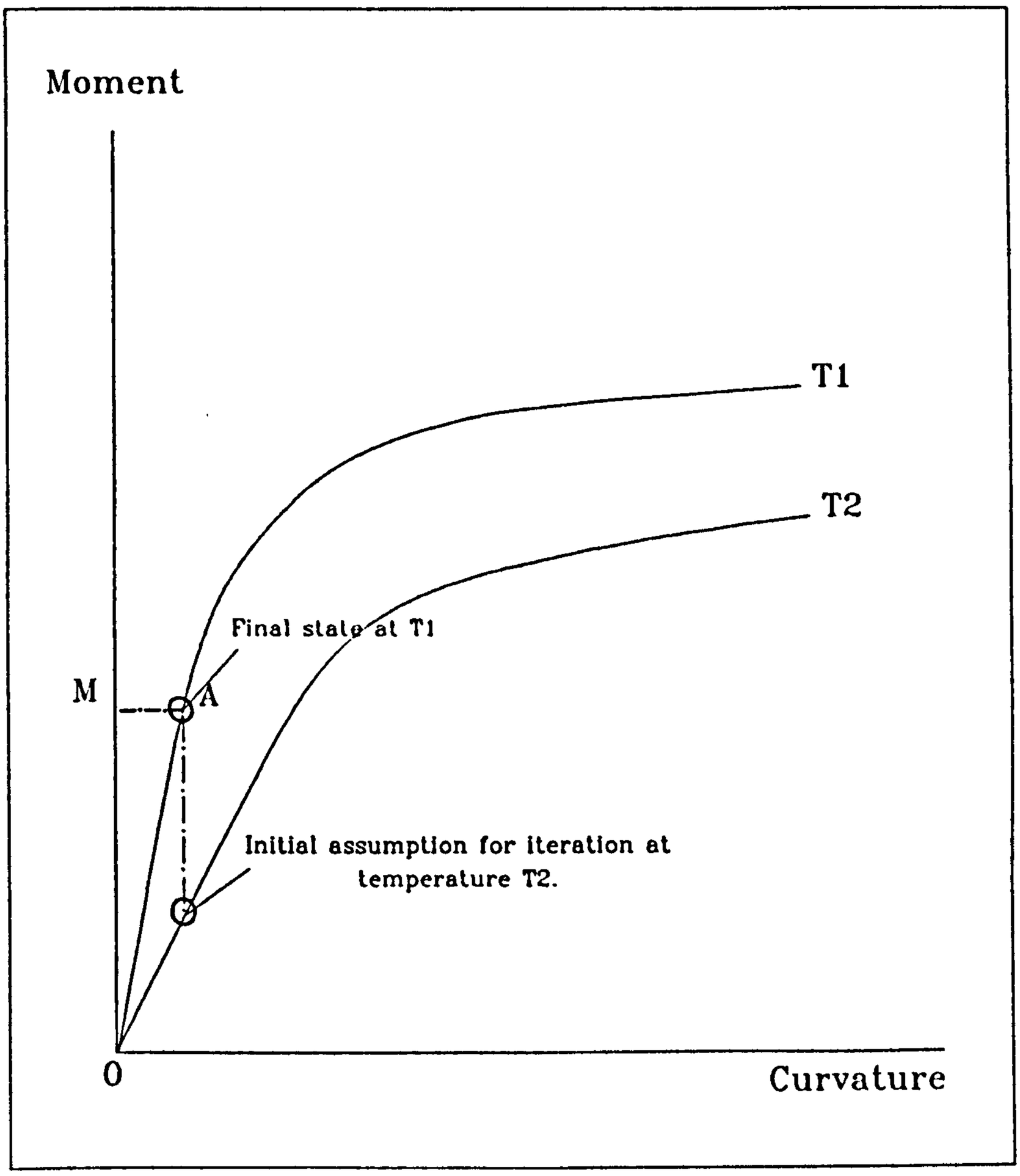

Figure 5.13: Schematic representation of frame analysis whithin a temperature range T1 to T2.

5.9 FACTORS AFFECTING THE ACCURACY OF THE RESULTS.

The effect of the number of beam-column elements and cross-section strips on the accuracy of analysis of frame structures is now studied. In the secant stiffness method the stiffness coefficient of each element is based on the average moment taken between the two ends of an element. Thus the accuracy of the result of the frame analysis is affected by the number of elements used. The smaller the size of the elements, the more accurate the results of analysis.

One other factor which affects the accuracy of the results of the analysis is the number of strips into which the cross-section is divided. This is because the determination of the moment-axial force-curvature relationship depends on the size of the strips. The smaller the size of the strip, the closer the representation of strain distribution and the idealised temperature profile over the cross-section. The minimum number of elements and strips consistent with accuracy of results should be used to minimise computational time. Different types of beams and loads were chosen for this investigation. The cross-section is shown in Figure 5.14, which also includes the effect of non-uniform temperature profile within the section. The Young's Modulus and yield stress at ambient temperature are assumed to be 205000 N/mm^2 and 328 N/mm^2 respectively, with high-temperature properties based on the multi-linear stress-

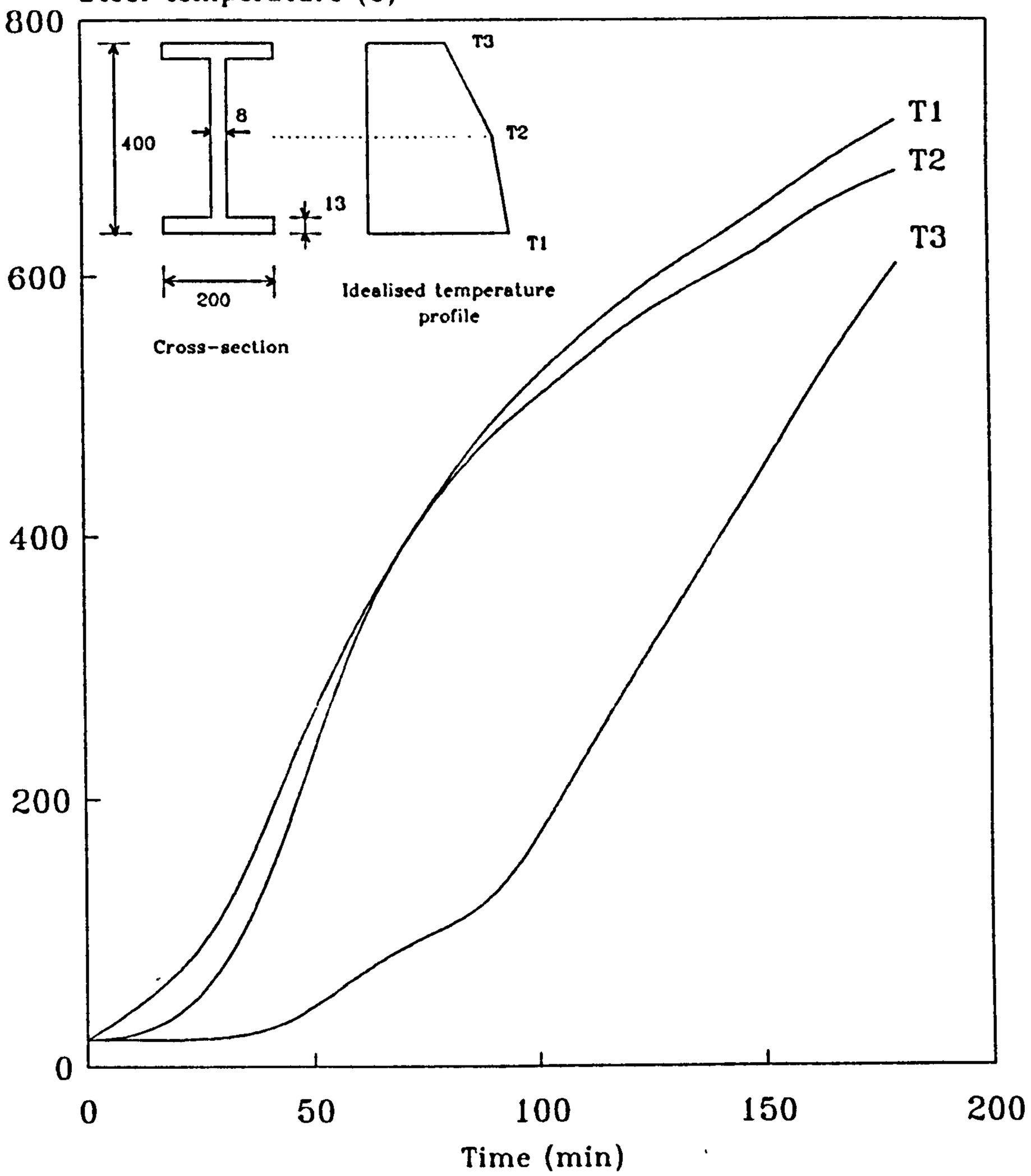

Figure 5.14: Steel temperature history for an I-section [11]

strain curves described in Chapter 2.

A simply supported beam of 7m span subjected to a uniformly distributed load of 41 kN/m is considered first. Figure 5.15a demonstrates the temperature-deflection relationship when the member and cross-section are divided into 10 elements and 10 strips respectively. The influence of numbers of elements and strips is then examined by considering a bottom flange temperature of 540°C corresponding to an elasto-plastic condition. Figure 5.15b summarises the difference in the calculated deflection for different combinations of strips and elements. It should be noted that the results for 30 elements and 40 strips will be used as a comparison. The figure shows that when 10 elements and 10 strips are used the error in the calculated deflection is less than 2%, and this number of strips will be used in the subsequent study on the influence of the number of elements on different forms of beams.

A simply supported beam of 7m span and subjected to a point load of 142 kN is considered next (Figure 5.16a). Figure 5.16a shows the temperature-deflection relationship for 10 elements and 10 strips. The influence of the number of elements is then studied when the bottom flange temperature is equal to 568°C - that is within the elasto-plastic range. Figure 5.16b shows that the error in the calculated deflection is less than 2% for the elements is more than 10.

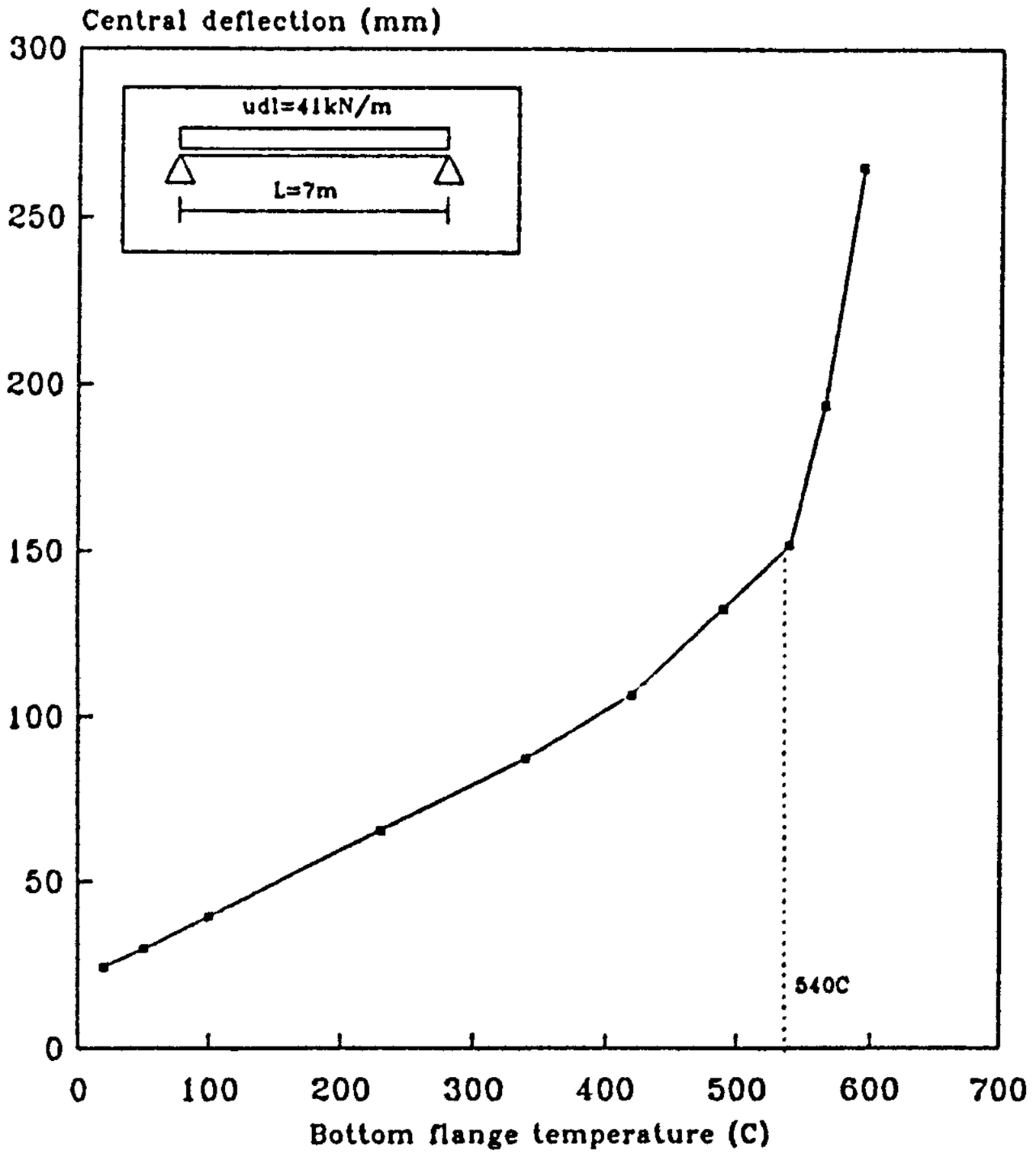

Figure 5.15a: Central deflection of a simply supported beam in fire.

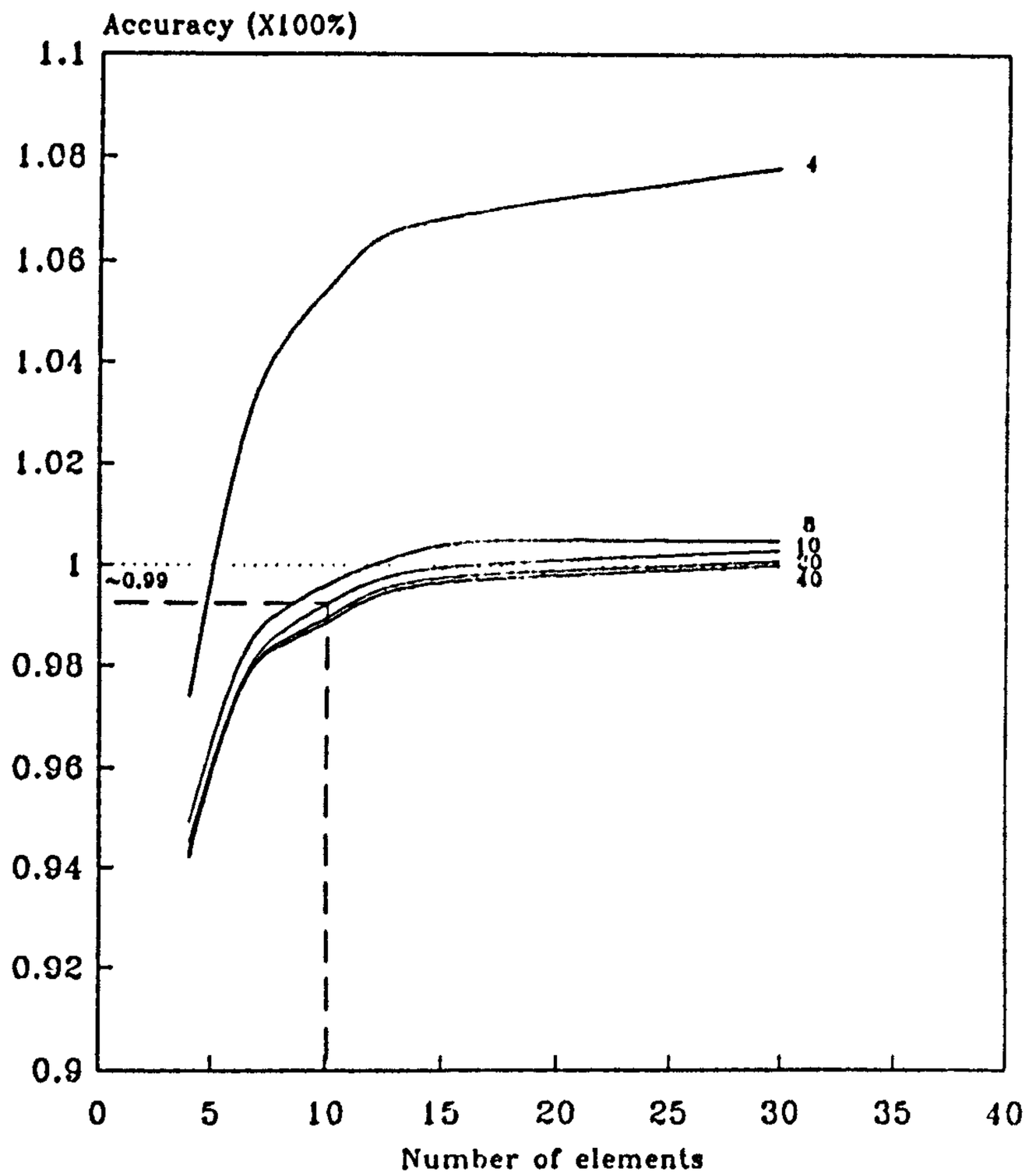

Figure 5.15b: The influence of the number of strips and elements on the accuracy of the results for the central deflection of a simply supported beam.

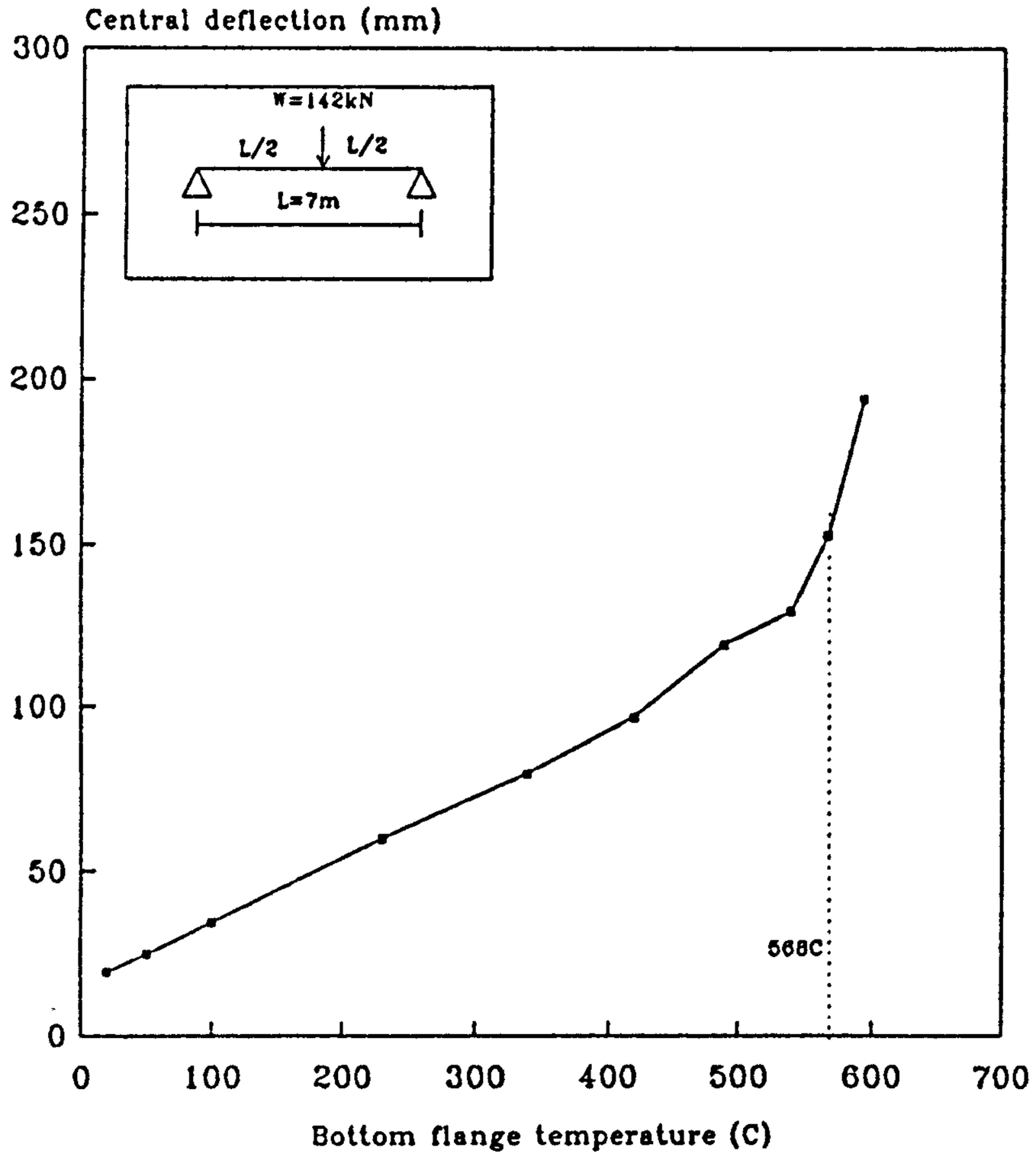

Figure 5.16a: Central deflection of simply supported beam in fire.

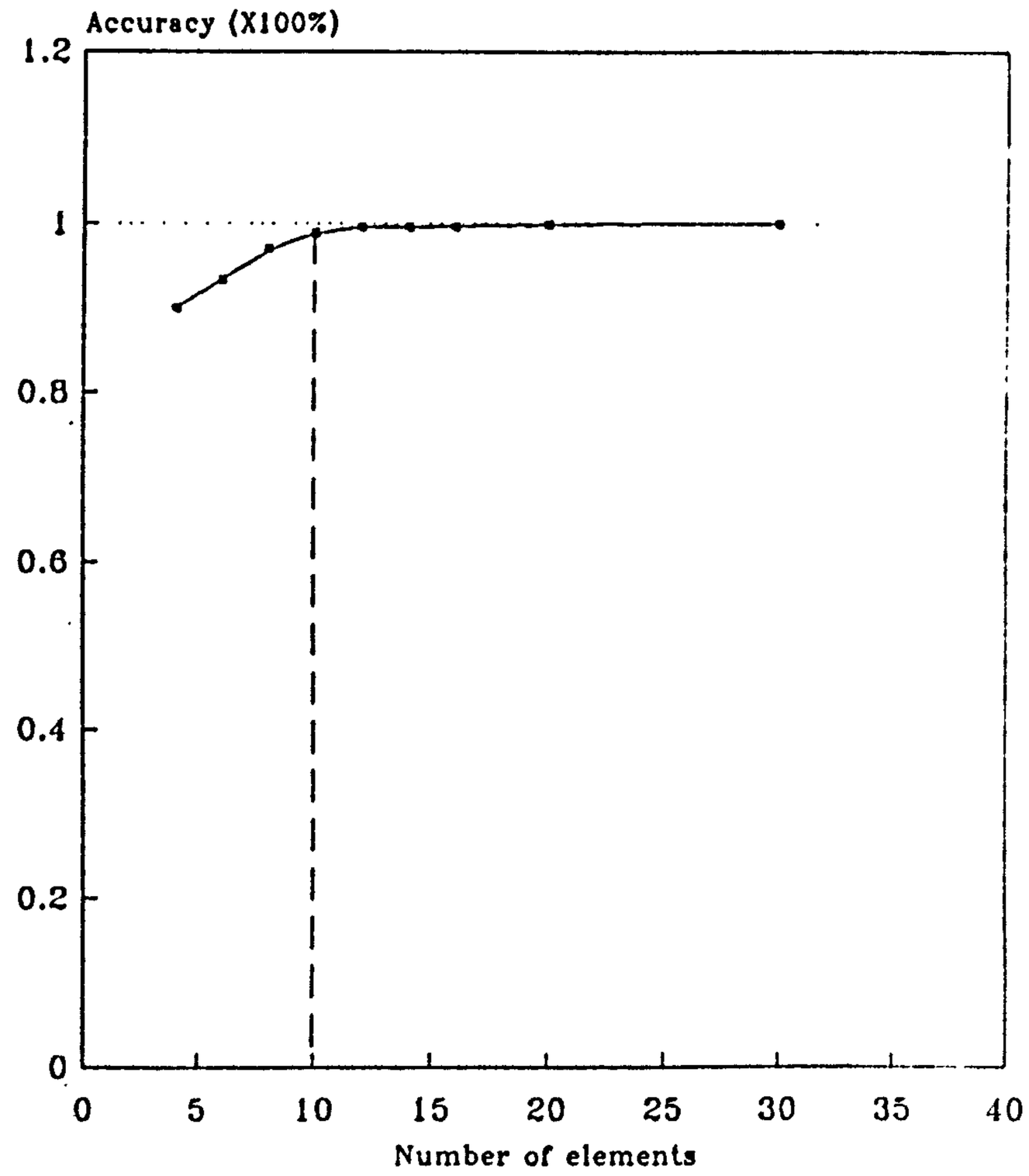

Figure 5.16b: The influence of the number of elements on the accuracy of the results for the central deflection of a simply supported beam subjected to a point load.

The influence of the number of elements on a fixed ended beam of 7m span, subjected to a uniformly distributed load of 61 kN/m (see Figure 5.17a) is also studied. Figure 5.17a shows the temperature-deflection relationship for 10 elements and 10 strips. The influence of the number of elements on the results for a bottom flange temperature of 690°C is shown in Figure 5.17b. The figure shows that when 10 elements are used the error in calculated deflection is less than 5%.

The influence of the number of strips and elements on the analysis including the presence of axial force will now be discussed. The temperature profile is assumed uniform within the cross-section. The Young's Modulus and yield stress are equal to 205000 N/mm² and 250 N/mm² respectively. The influence of number of elements will be considered first while the number of strips will be taken as 10.

A simply supported beam of UB 305x165x54 kg/m subjected to a uniformly distributed load of 0.702 kN/m (equivalent to a mid-span bending stress of 28.75 N/mm²) and a span of 15.71m (L/r_x = 120) is considered. An axial force of 410.4 kN ($0.24P_y$) is applied to the member. The beam is analysed when the steel temperature is equal to 300°C. Figure 5.18 shows the influence of number of elements on the results of the analysis. The figure shows that the error in the calculated deflection is less than 2% for the number of elements greater or equal to 10.

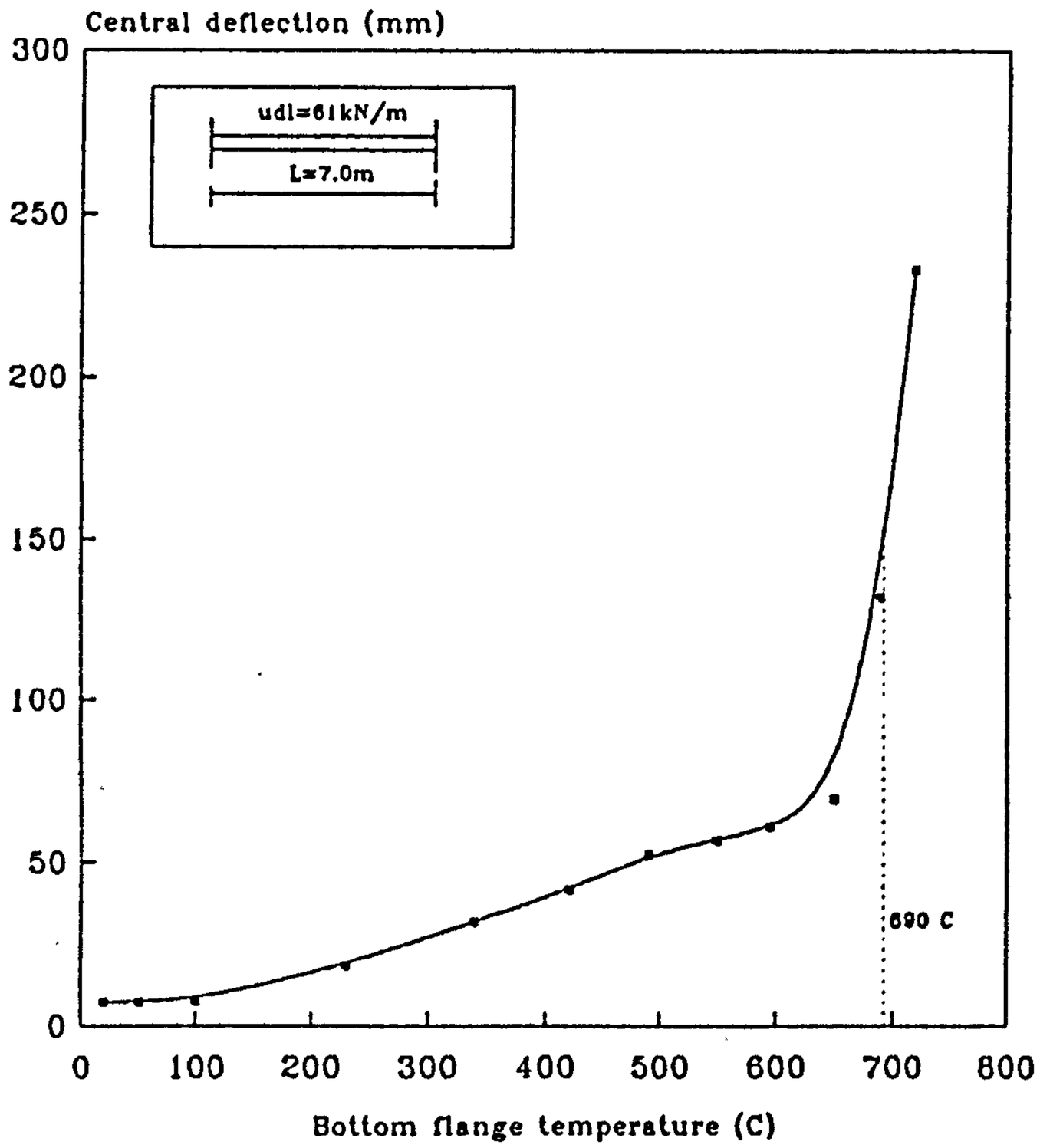

Figure 5.17a: Central deflection of fixed ended beam (restrained against rotation) in fire.

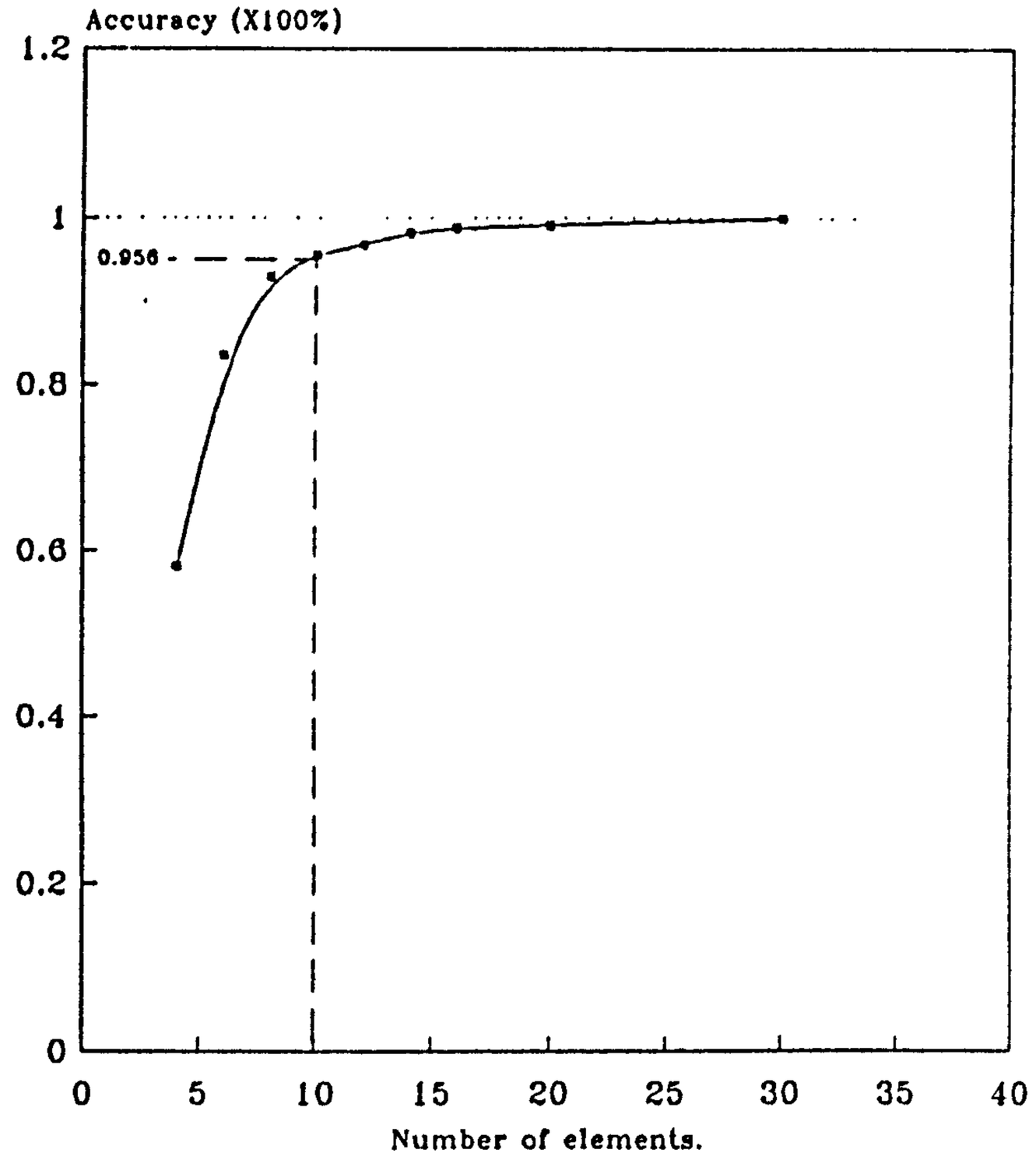

Figure 5.17b: The influence of the number of elements on the accuracy of the results for the central deflection of fixed ended beam in fire.

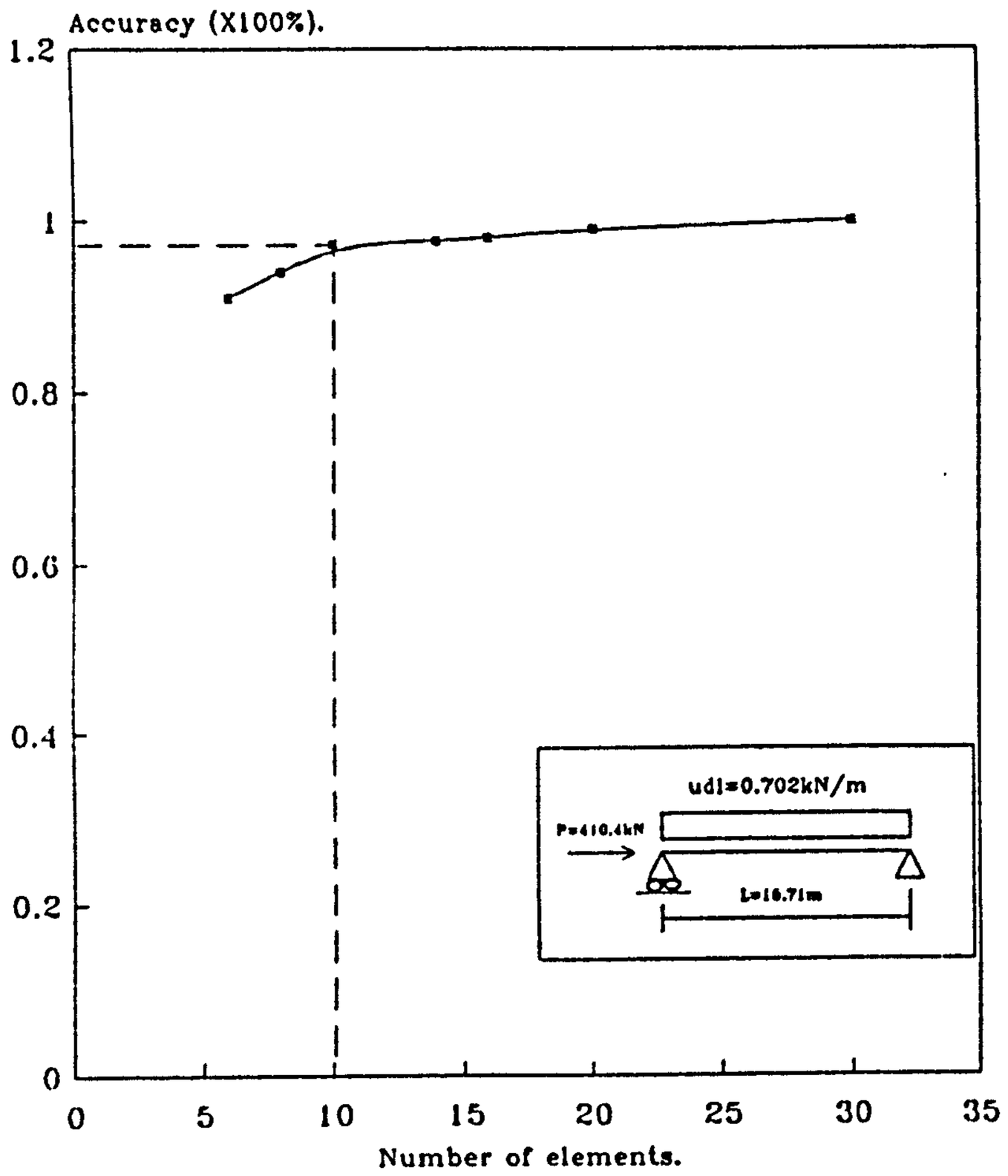

Figure 5.18: Influence of number of elements on the accuracy of the results for the central deflection of a simply supported beam subjected to a udl and an axial load.

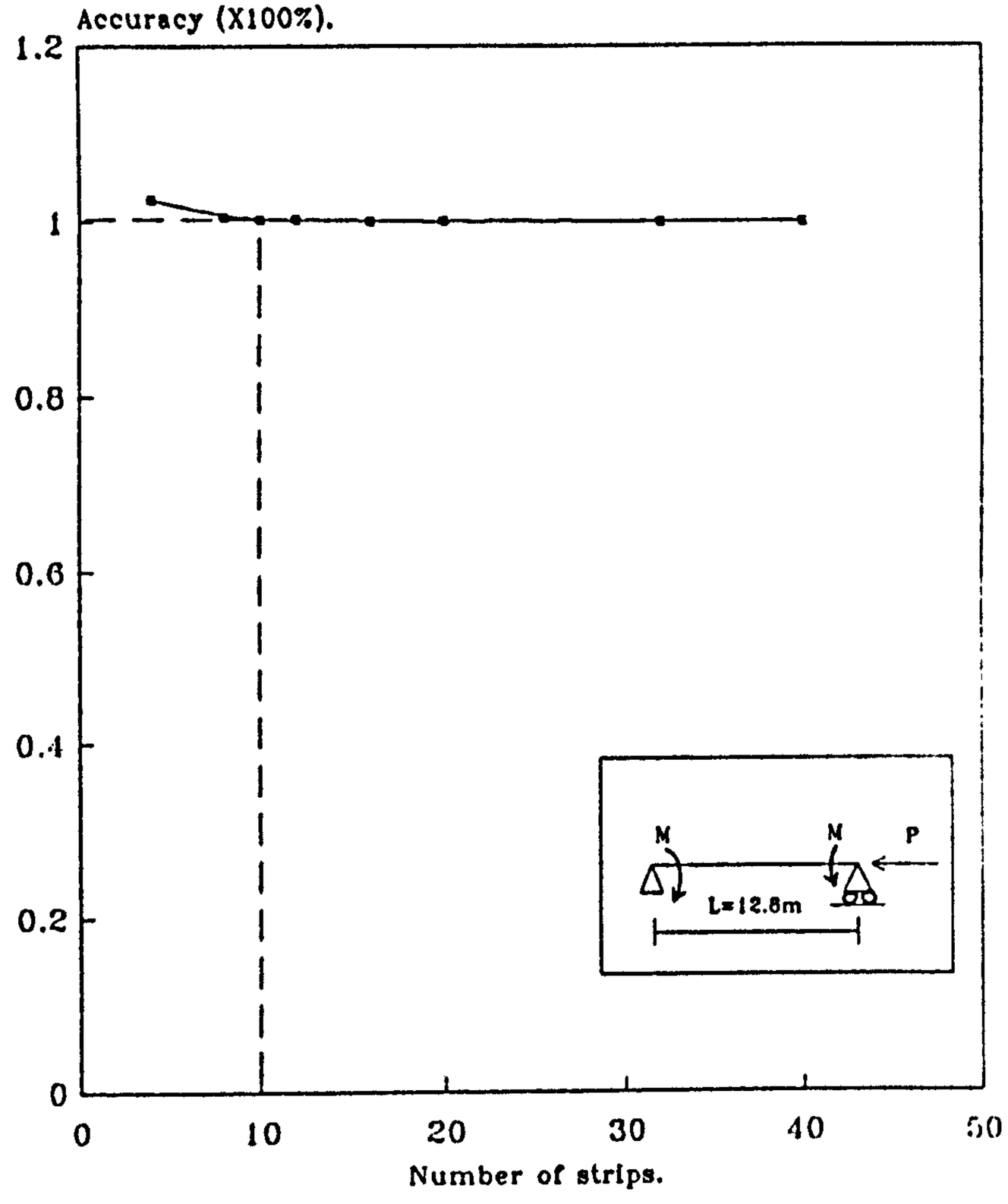

Figure 5.19: Influence of number of strips on the accuracy of results for the central deflection of a pin-ended column subjected to end moments and an axial load.

The influence of the number of strips is considered next. A pin-ended column of UC 356x368x202 kg/m with a span of 12.8 m (L/r_x = 80) is chosen for the analysis. An axial force of $0.2P_y$ (1289 kN) and end moments of $0.1M_p$ (101.8 kNm) are applied on the member. The column is analysed when the steel temperature is equal to 400°C. The material properties are as before and the number of elements is assumed to remain constant (i.e equal to 10). Figure 5.19 shows the influence of the number of strips on the results of the analysis. The figure shows that for 10 strips the error in the calculated deflection is less than 1%.

From these investigations it can be concluded that the results of the analysis are sufficiently accurate when the number of cross-section strips and elements are each equal to 10, and these will be used in the subsequent analysis.

CHAPTER SIX

COMPARISON BETWEEN THEORETICAL AND EXPERIMENTAL RESULTS

6.1 INTRODUCTION.

The aim of this chapter is to demonstrate the degree of accuracy that can be achieved using the secant stiffness method in the analysis of frame structures in fire. To achieve this a series of comparisons are made with results reported from previous experimental and theoretical studies.

6.2 SIMPLY SUPPORTED BEAM WITH ROLLER AT ONE END.

6.2.1 Comparison with test results.

A series of tests on simply supported beams has been carried out by British Steel [109] and the results will be used as a comparison for the results obtained from the present theory.

The present results are also compared with those obtained analytically by El-Rimawi [5].

It should be noted that the central deflections of the test beams were measured after an initial deflection had taken

place at ambient temperature. Thus, to obtain the total deflection as calculated by the present method at a certain temperature level the deflection at ambient temperature must be added to the measured deflection at that corresponding temperature.

Four simply supported beams with a span of 4.5 m have been used for comparison. During the test the beams were loaded through four point loads on the slab at the 1/8, 3/8, 5/8, 7/8 points of the span. The loads were applied through the supported slab and were consequently distributed along the span. The tests were stopped when the central deflections were equal to L/30, corresponding to the failure condition specified in BS 476: Part 8.

In the analysis the load acting on the beam is assumed to be a uniformly distributed load equal in magnitude to the total load acting during the test. The test parameters used in the furnace tests are shown in Table 6.1. The beams are denoted as SS1, SS2, SS3 and SS4. During the test the steel temperature in each of the beams was measured at the locations of the thermocouples as shown in Tables 6.2 to 6.5. The steel temperature and the central deflection of the beam were recorded at a time interval of three minutes.

In the present analysis a three-step temperature profile was adopted as shown in Figure 6.1. The temperature is assumed uniform in the web and each flanges of the cross-section.

Beam	Size	Ambient Temperature Yield stress (N/mm2)		Udl (kN/m)
		Web	Flange	
SS1	254*146 UB43	297	297	16.34
SS2	254*146 UB43	304	300	31.92
SS3	356*171 UB67	395	392	68.95
SS4	356*171 UB67	280	240	67.30

Table 6.1: Test parameters used in BSC furnace tests on floor beams [109].

THERMOCOUPLE POSITIONS

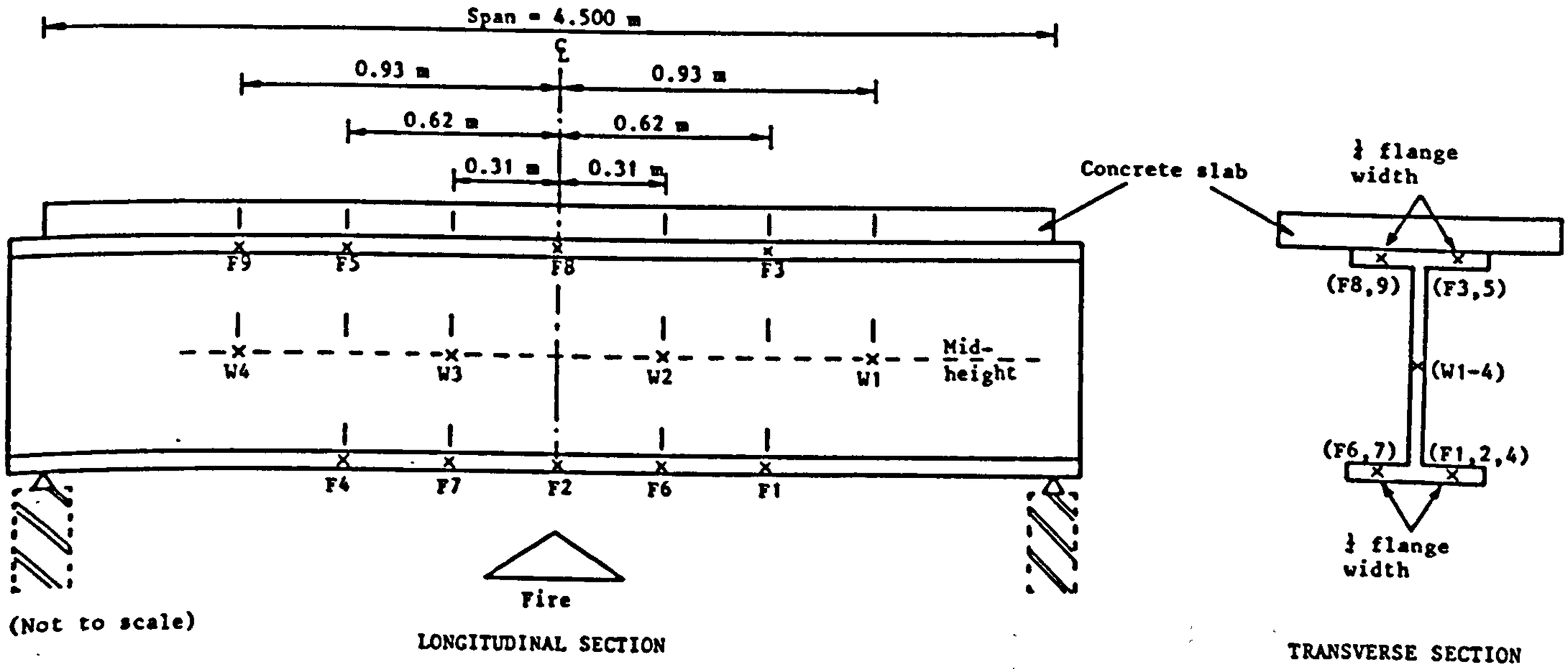

(Not to scale)

LONGITUDINAL SECTION

TRANSVERSE SECTION

Thermocouple Position		Temperature (C) After various times (min)								
		3	6	9	12	15	18	21	24	27
Lower flange	1	116	221	335	467	560	625	671	714	742
	2	119	228	342	483	579	645	691	731	756
	4	117	223	333	468	567	632	679	722	742
	6	124	228	337	472	567	633	680	722	743
	7	124	234	343	470	565	631	679	721	741
Mean lower flange		120	227	338	472	568	633	680	722	745
Web	1	145	255	357	475	561	612	653	697	731
	2	150	267	380	508	594	642	681	720	741
	3	152	277	387	512	598	646	683	725	746
	4	142	250	350	464	547	597	638	682	719
Mean web		147	262	368	490	575	624	664	706	734
Upper flange	3	69	112	156	224	282	341	398	457	525
	5	80	129	174	249	311	370	425	482	546
	8	81	133	183	270	344	415	477	532	581
	9	74	115	155	214	267	320	375	431	490
Mean upper flange		76	122	167	239	301	361	419	475	535

Table 6.2: Steel temperature data for beam SS1

Thermocouple Position		Temperature (C) After various times (min)						
		3	6	9	12	15	18	21
Lower flange	1	84	186	308	431	526	598	653
	2	126	220	329	442	529	604	654
	4	109	216	333	448	536	606	651
	6	110	213	330	456	535	605	653
	7	125	220	338	468	550	619	665
Mean lower flange		111	211	328	449	535	606	655
Web	1	114	223	340	457	533	594	640
	2	113	228	349	467	541	605	649
	3	130	244	368	490	560	621	661
	4	144	251	367	488	558	619	659
Mean web		125	236	356	475	548	610	652
Upper flange	3	73	136	185	246	303	362	426
	5	63	115	175	241	307	371	434
	8	72	124	177	240	300	369	433
	9	64	115	169	242	301	365	430
Mean upper flange		68	122	176	242	303	367	431

Table 6.3: Steel temperature data for beam SS2

Thermocouple Position		Temperature (C) After various times (min)								
		3	6	9	12	15	18	21	24	24.5
Lower flange	1	110	211	324	436	531	606	658	698	702
	2	120	221	342	458	553	624	673	711	717
	4	97	199	325	449	548	619	668	705	711
	6	132	244	363	468	558	626	675	712	718
	7	106	220	353	469	564	632	680	716	721
Mean lower flange		113	219	341	456	551	621	671	700	714
Web	1	124	246	377	483	563	623	665	695	701
	2	142	273	410	517	596	652	690	721	724
	3	151	290	436	542	612	657	692	721	725
	4	136	258	392	501	578	630	666	698	703
	5	143	256	390	491	559	608	644	677	684
	6	129	253	372	468	542	601	643	676	652
Mean web		138	267	404	511	587	641	678	709	713
Upper flange	3	76	120	167	218	275	334	367	438	447
	5	79	129	188	255	318	380	437	496	507
Mean upper flange		78	125	178	237	297	357	412	467	477

Table 6.4: Steel temperature data for beam SS3

Thermocouple Position		Temperature (C) After various times (min)								
		3	6	9	12	15	18	21	24	27
Lower flange	1	81	156	248	340	425	496	553	602	637
	2	76	157	256	352	438	510	569	618	653
	4	77	157	252	343	432	509	569	618	652
	6	72	147	235	327	418	494	553	604	639
	7	79	157	257	355	445	517	575	623	655
Mean lower flange		77	157	250	344	432	505	564	613	647
Web	1	114	205	295	384	460	520	567	604	630
	2	122	214	319	417	494	549	595	633	658
	3	127	228	337	429	502	556	600	636	663
	4	128	216	312	397	470	527	574	611	640
	5	130	211	297	371	437	492	535	576	607
	6	118	201	292	371	438	492	539	578	612
Mean web		123	212	310	395	467	523	568	606	635
Upper flange	3	76	91	137	173	214	259	303	354	399
	5	77	90	137	179	226	277	328	380	436
Mean upper flange		77	91	137	176	220	268	316	367	418

Table 6.5: Steel temperature data for beam SS4

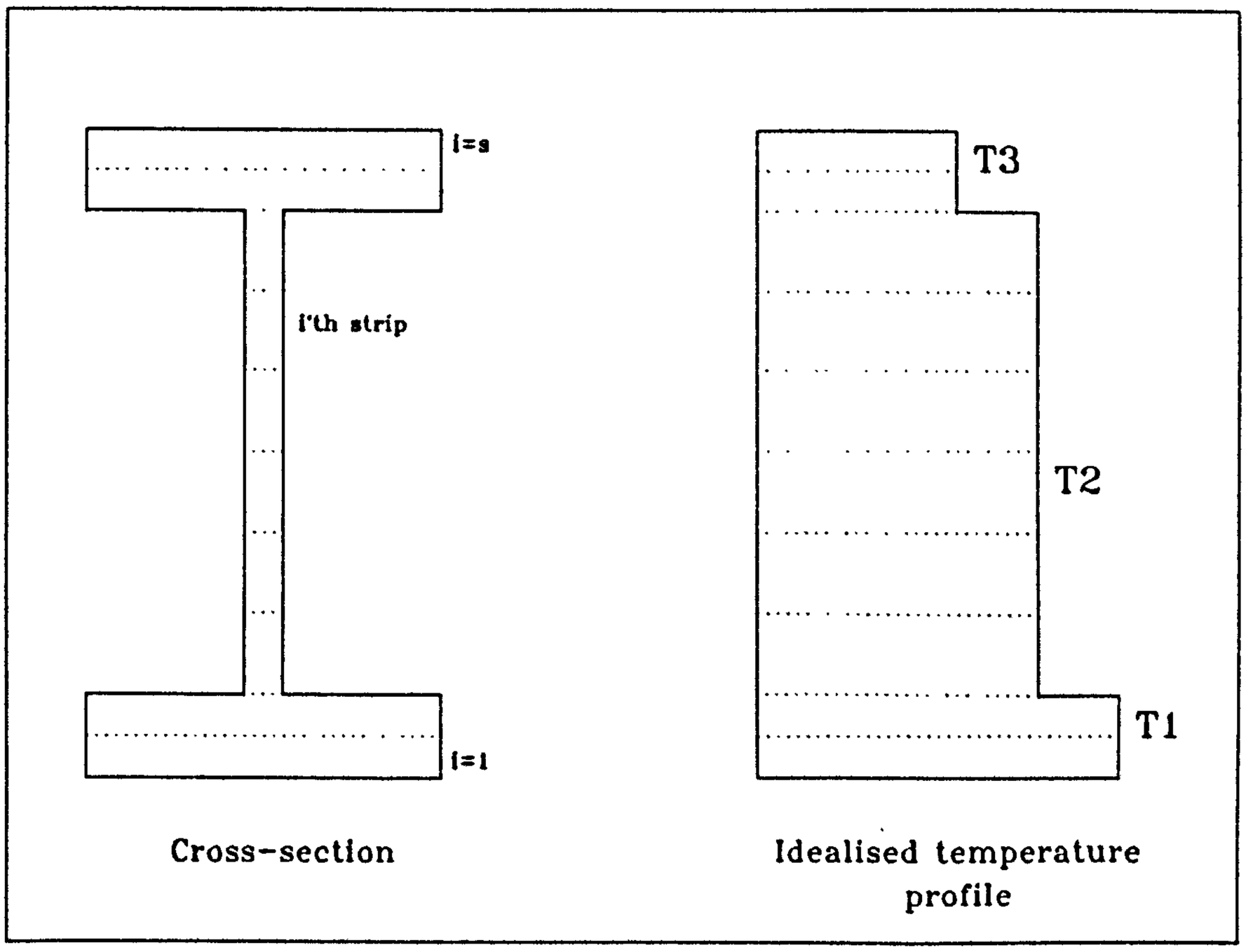

Figure 6.1: Idealised temperature profile and subdivision of the section used to analyse the furnace tests [109].

The average steel temperatures of the web and both flanges are also plotted against time as shown in Figures 6.2 to 6.5.

Figures 6.6 to 6.9 show a comparison between the analytical and test results for the central deflections of the beams. The figures show that for each beam there is a very good agreement up to a certain temperature level, beyond which the curves diverge. In all cases the analytical results predict early collapse compared with the test, although the difference is very small. Table 6.6 shows the `collapse temperature' for each beam indicating a difference between test and theory of up to 40°C.

To highlight the difference between the analytical and test results, Figure 6.6 is considered in more detail. The curves show very good agreement up to a temperature of 700°C, diverging beyond this point. A possible explanation is that the stress-strain curves used in the present analysis might be conservative. Slightly higher stress-strain curves, especially in the range of strain hardening, could result in closer agreement.

The other possible reason is that in the present theory the temperature is assumed to be constant along the span. It is probable that the temperature was in fact somewhat lower near the supports which could result in less deformation.

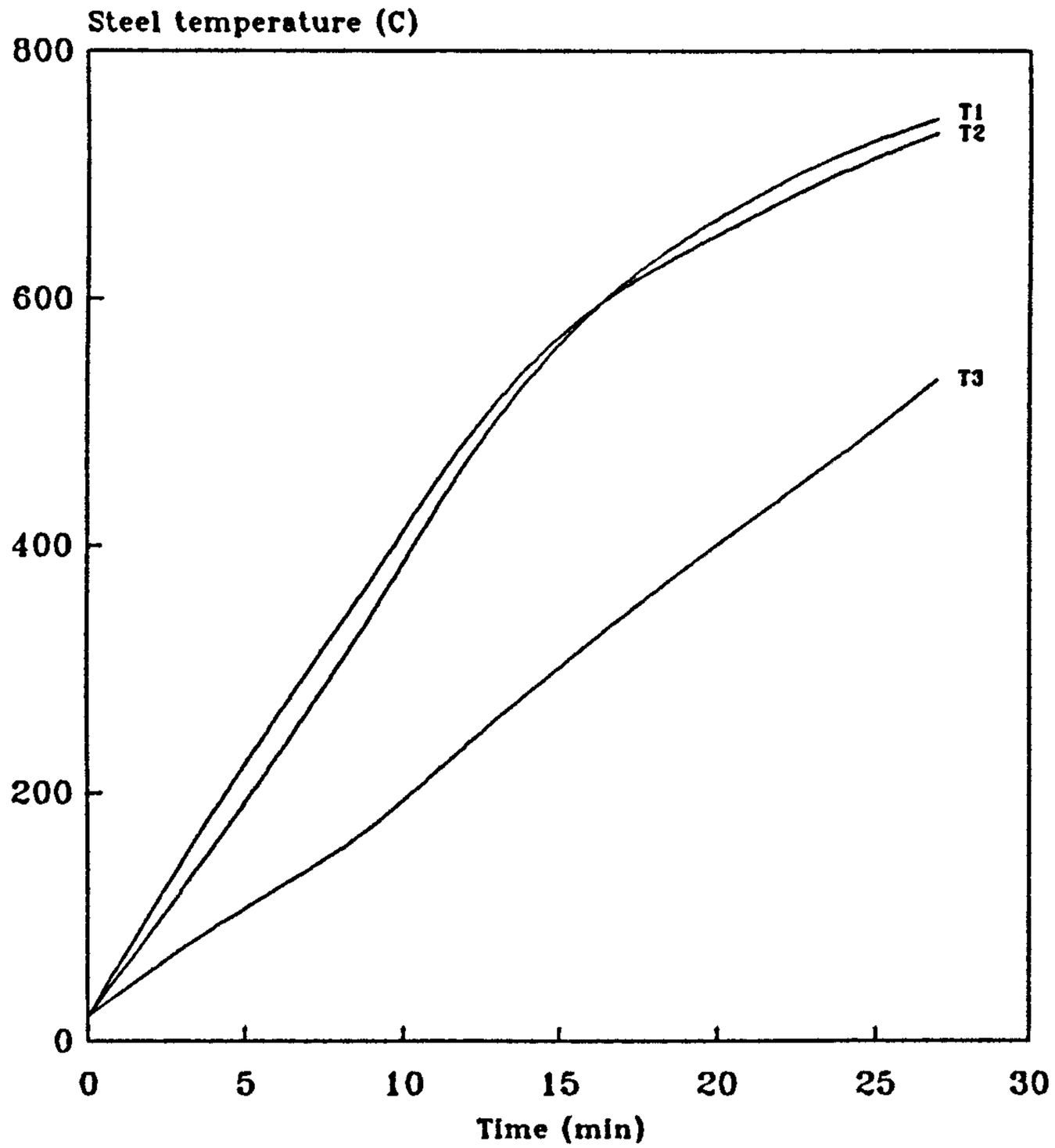

Figure 6.2: Steel temperature history of beam SS1.

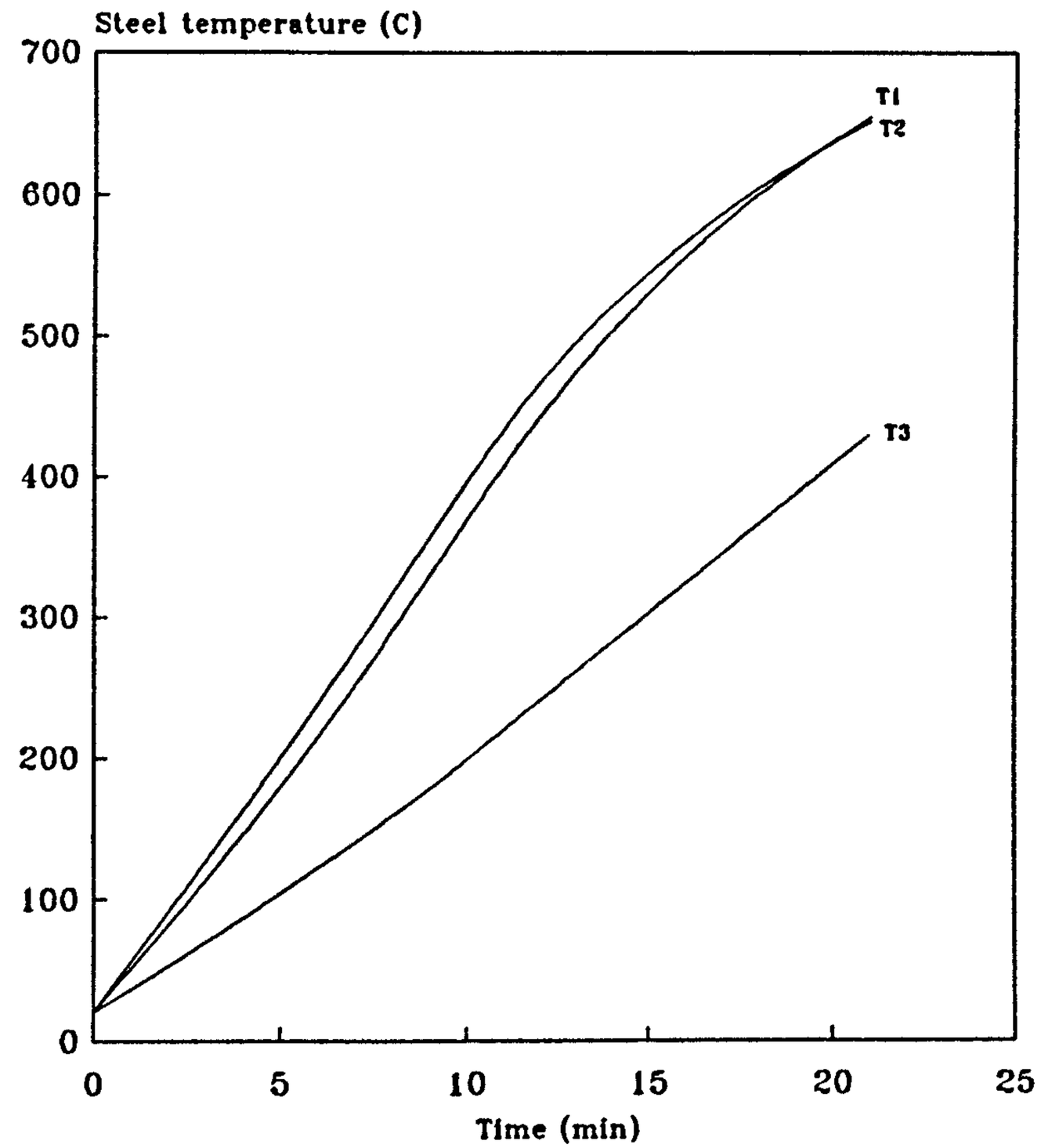

Figure 6.3: Steel temperature history of beam SS2.

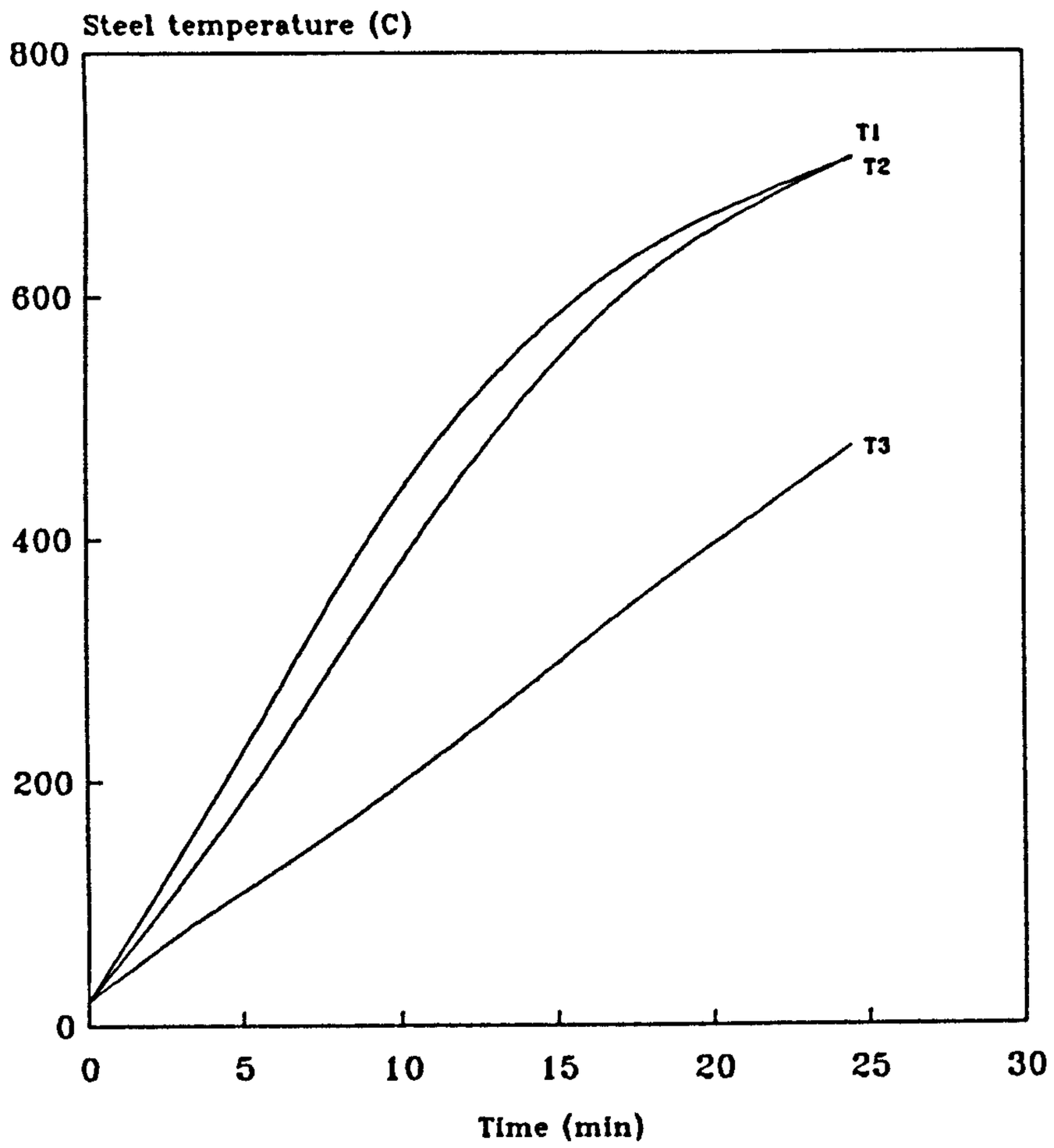

Figure 6.4: Steel temperature history of beam SS3.

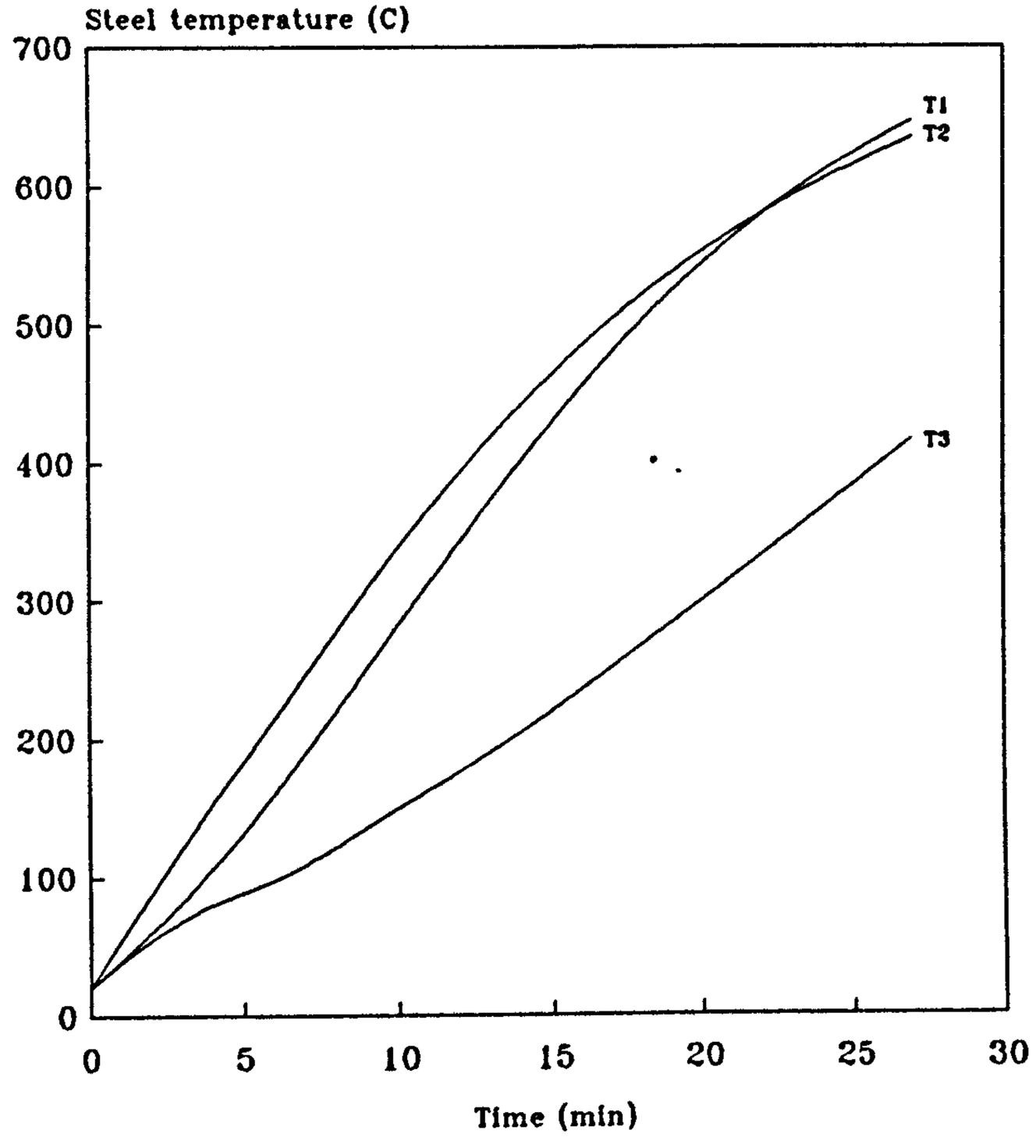

Figure 6.5: Steel temperature history of beam SS4.

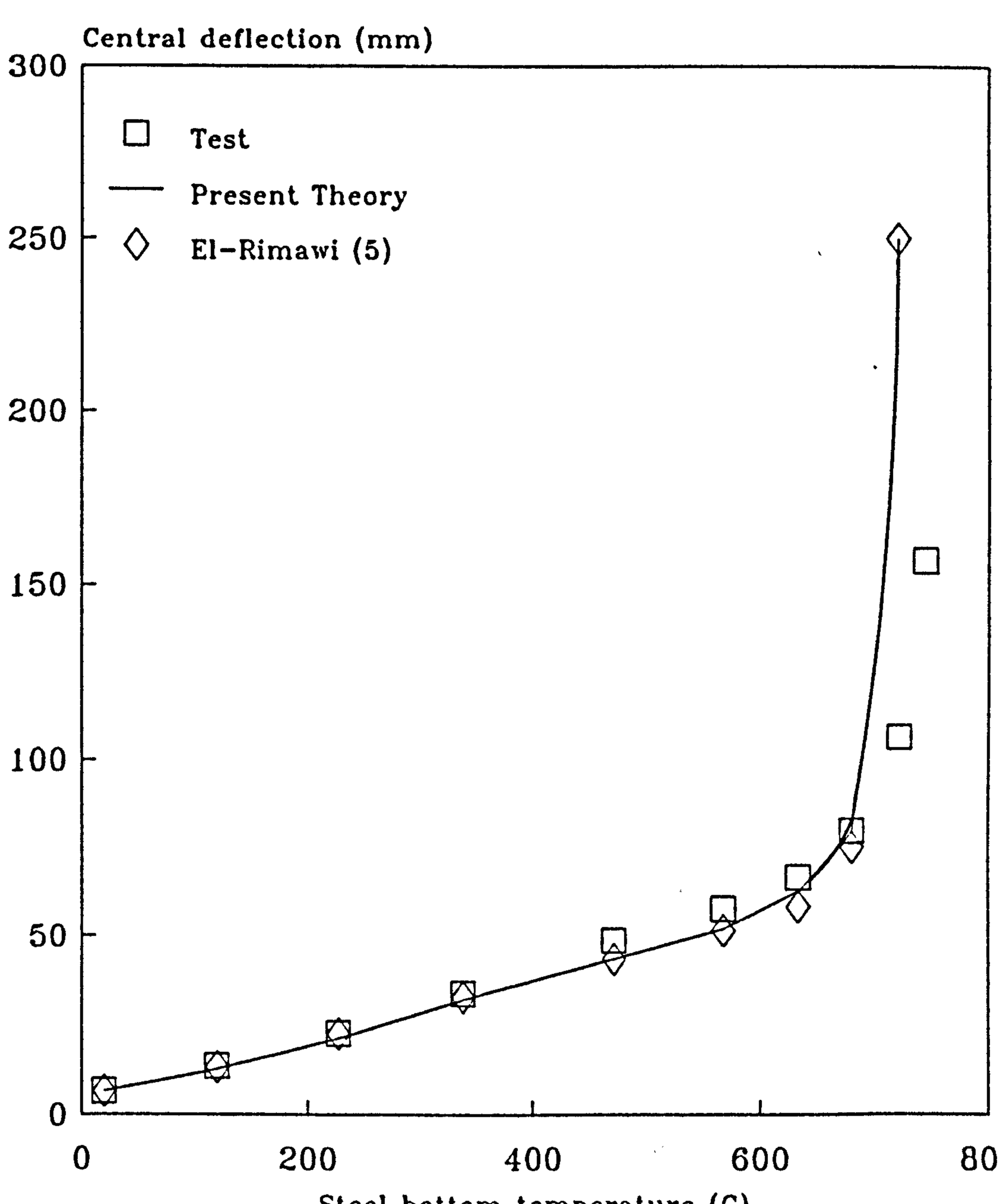

Figure 6.6: Central deflection of beam SS1 in test.

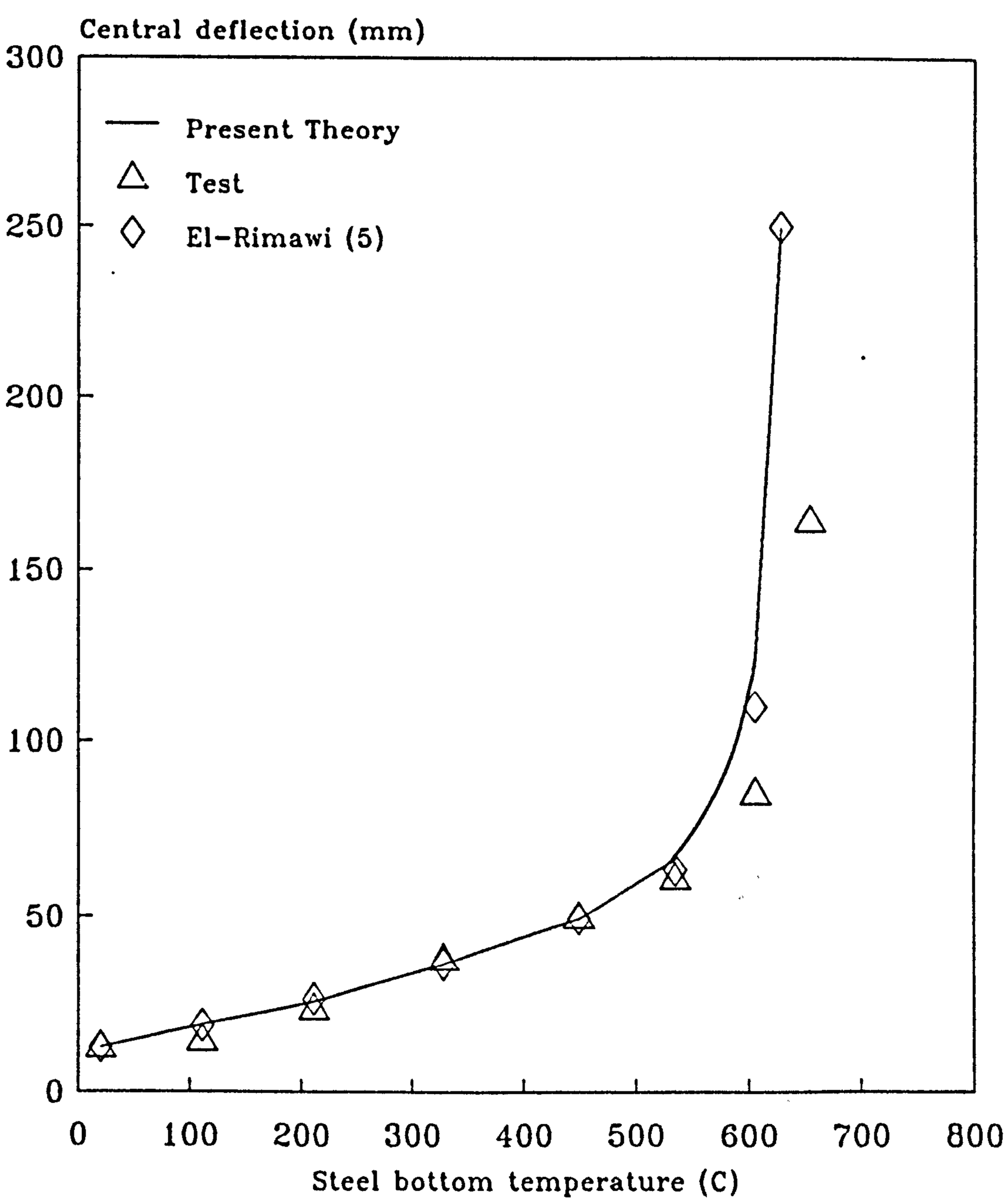

Figure 6.7: Central deflection of beam SS2 in test.

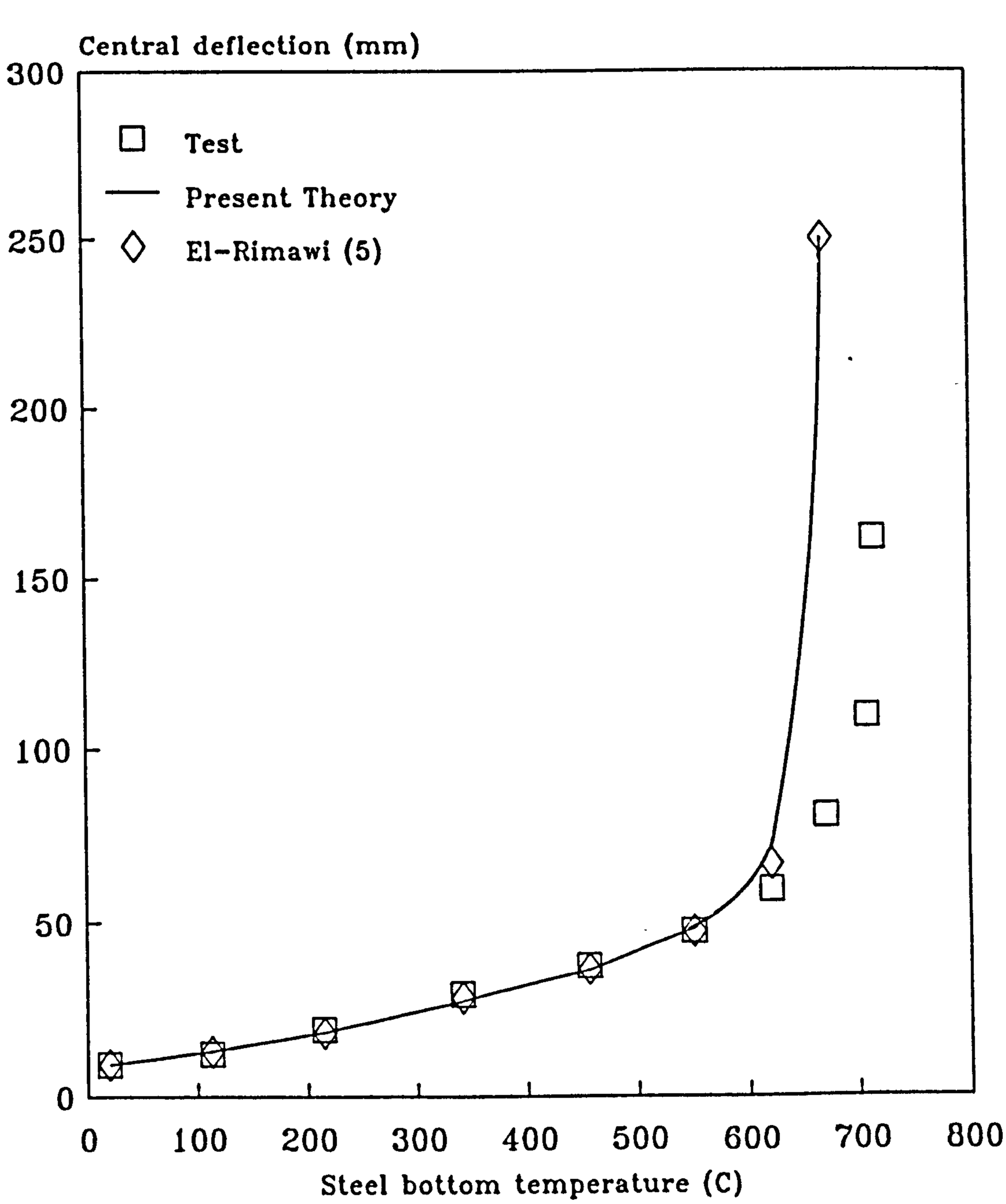

Figure 6.8: Central deflection of beam SS3 in test.

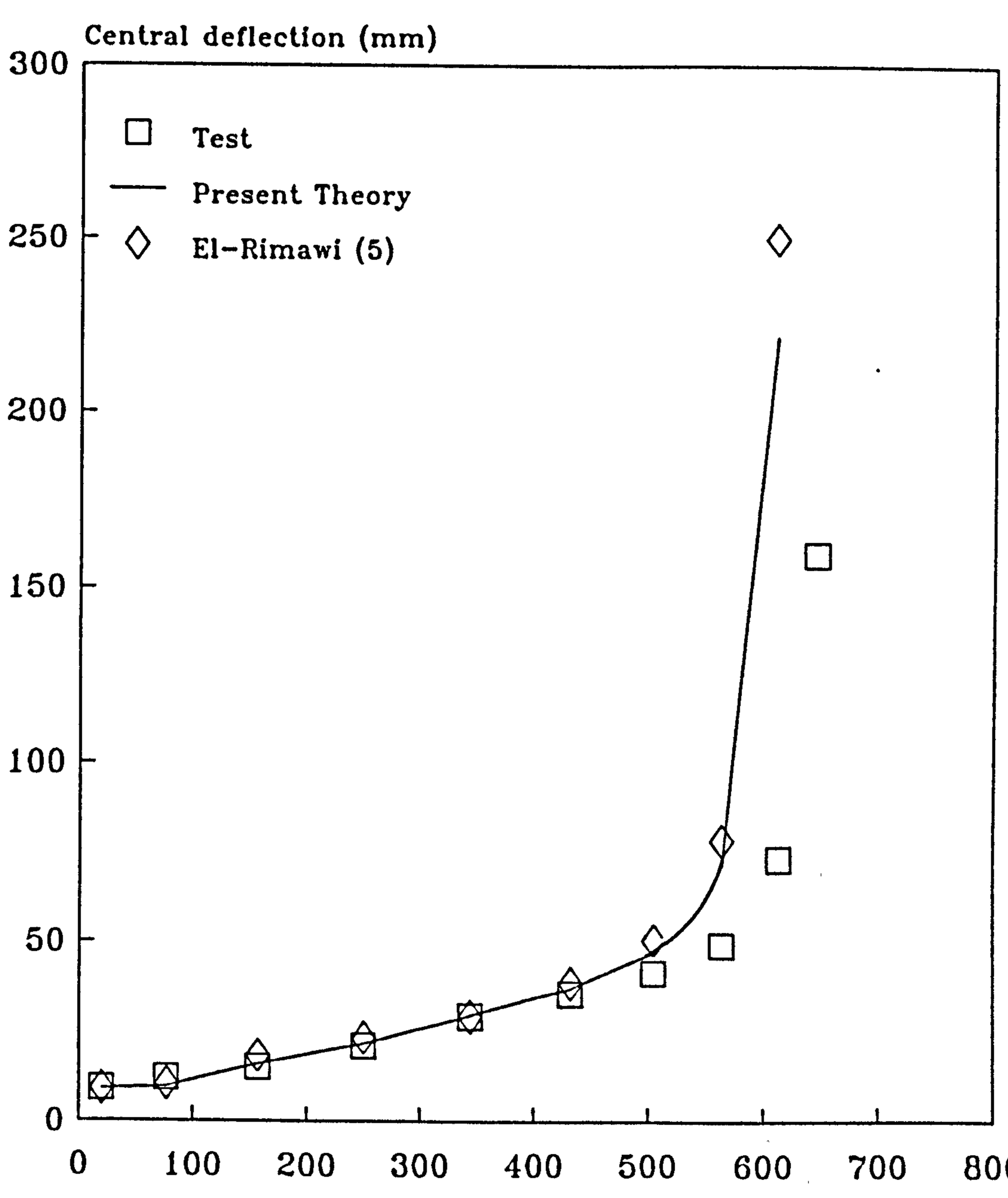

Figure 6.9: Central deflection of beam SS4 in test.

Beam	Size	Critical temperature (C)		
		Theory	Test	Ref [5]
SS1	254*146 UB43	722	745	722
SS2	254*146 UB43	630	655	630
SS3	356*171 UB67	671	714	671
SS4	356*171 UB67	613	647	613

Table 6.6: Comparison of predicted and experimental critical temperatures of the steel beams in fire tests.

In comparison with the analytical results obtained by El-Rimawi [5], very good agreement is obtained.

6.2.2 Comparison with theoretical result.

For comparison with a completely unrelated theoretical study, results obtained from the present formulation are compared with work carried out by Furumura and Shinohara [11].

A simply supported beam with a span of 7.0m is subjected to a uniformly distributed load equal to 29.43 kN/m. The cross-section is H400x200x13x8 as shown in Figure 6.10. The mechanical properties of steel in fire and the free thermal strains are based on reference [11]. The steel temperature measured during the fire is shown in Figure 6.10 and is represented for the present analysis by the idealised temperature profile (Figure 6.10). It should be noted that in reference [11] the steel temperature is only recorded up to 120 minutes, at which the maximum steel temperature is only 585°C. Because of this, an assumed steel temperature profile beyond 120 minutes has been introduced in the present work in order to determine the deformation history for steel temperatures greater than 600°C.

The results of the comparison are presented in Figures 6.11 and 6.12 which show the horizontal end displacement and central deflection of the beam respectively. The results

Time (min)	Steel bottom Temperature T1 (C)	Temperature difference between top and bottom flanges (T1–T3) (C)
0	20	0
15	50	30
30	100	80
45	230	200
60	340	270
75	420	320
90	490	370
105	540	340
120	590	300
135	620	250
150	650	200
165	690	150
180	720	110
195	760	70

Table 6.7: Temperature details for the beam cross–section.

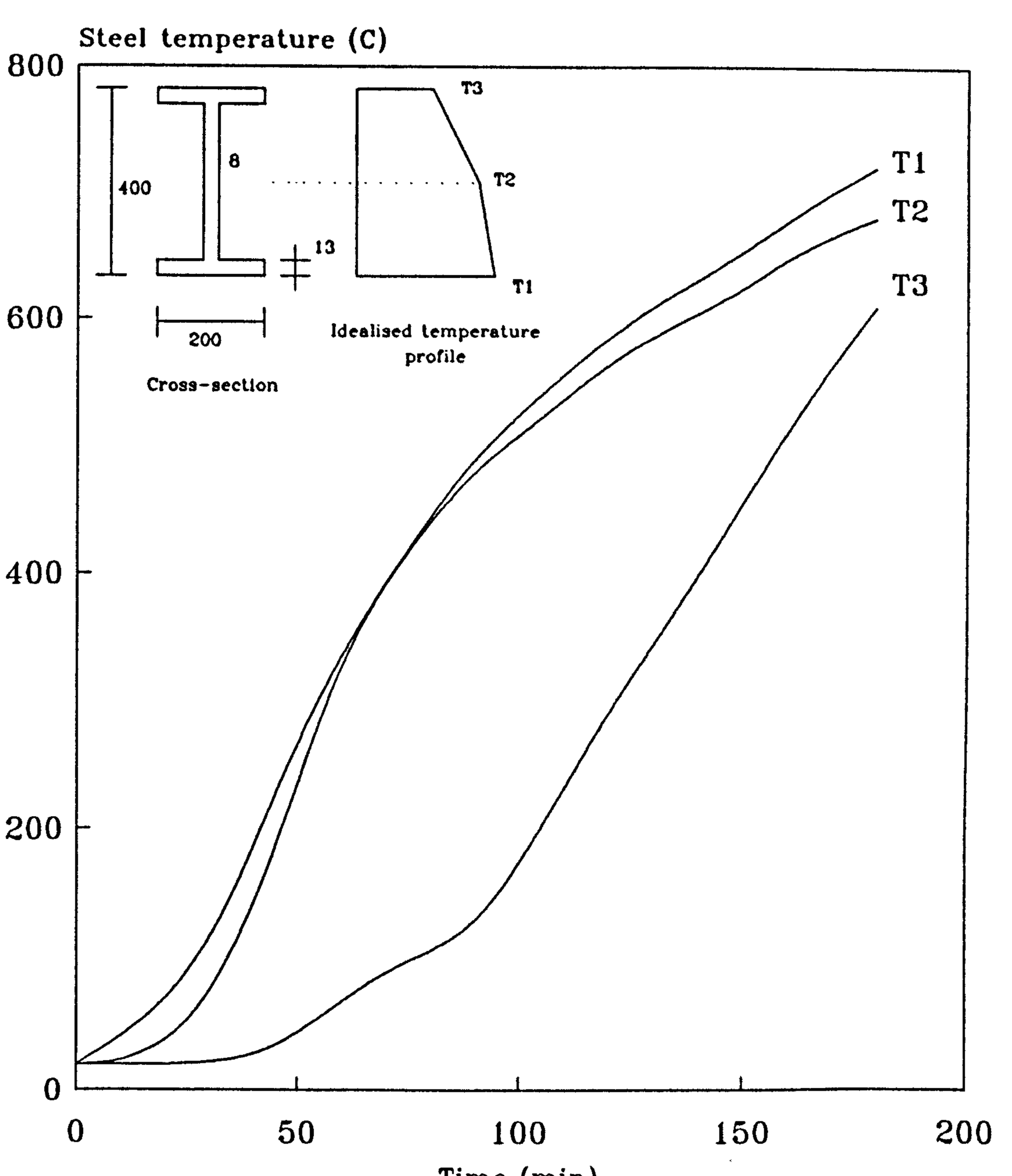

Figure 6.10: Steel temperature history of a simply supported beam [11].

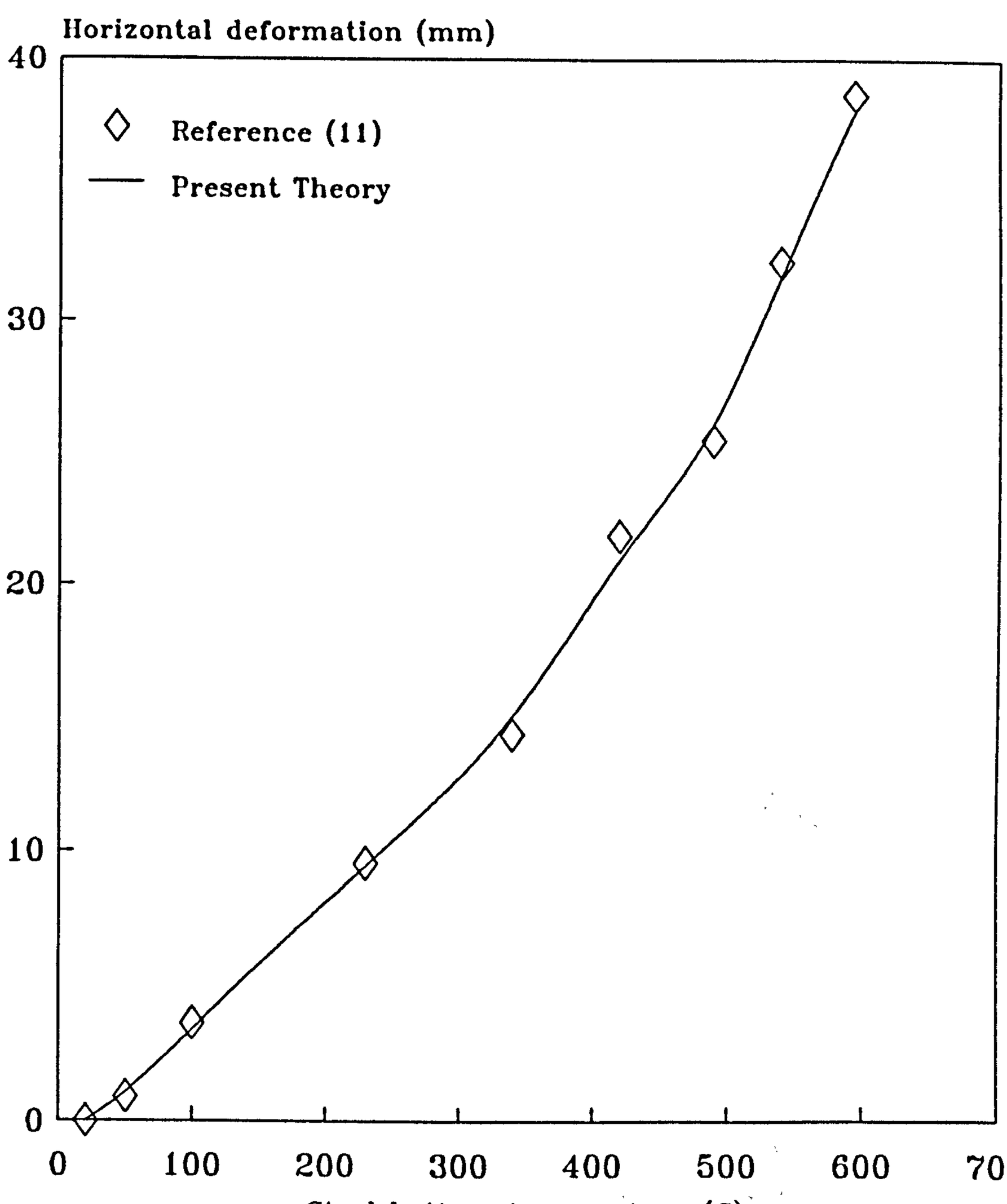

Figure 6.11: Comparison of calculated horizontal deformatios of a simply supported beam [11].

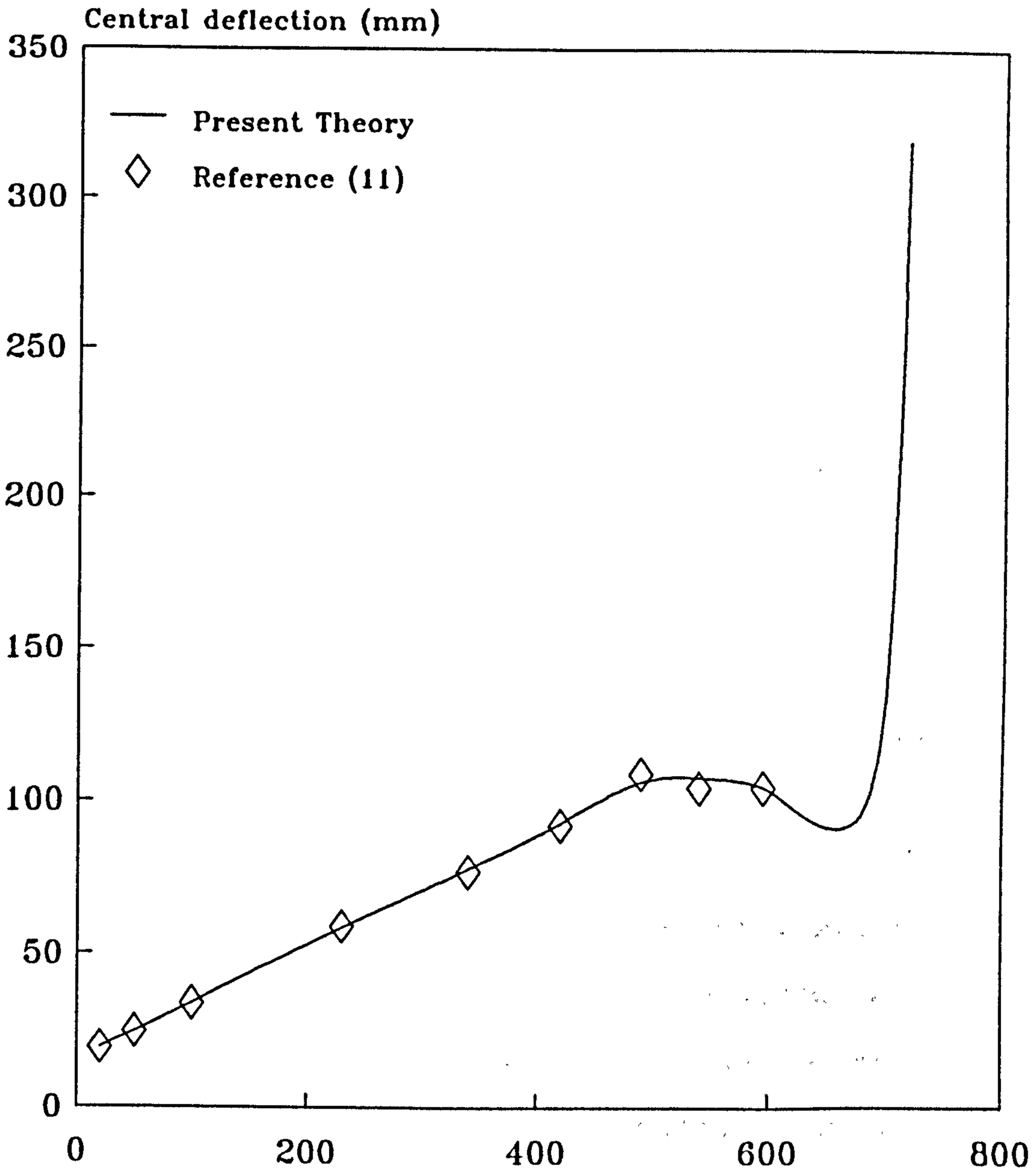

Figure 6.12: Comparison of calculated central deflections of a simply supported beam.

from the present theory show very good agreement with Furumura and Shinohara [11].

Figure 6.12 shows that the central deflection steadily increases with temperature up to about 540°C. This suggests that the effect of thermal bowing is predominant since the central part of the beam is still in an elastic condition as shown in the strain block diagrams in Figure 6.13. From Table 6.7 it can be seen that the temperature difference between the top and bottom flanges of the cross-section increases in this range, and the thermal bowing effect is dominant. For higher temperatures the central deflection shows a slight decrease up to 650°C. This behaviour is due to the temperature difference between the top and bottom flange of the cross-section decreasing as shown in Table 6.7, resulting in less thermal bowing. During this period the central part of the beam is still elastic as shown in Figure 6.13 and the central deflection therefore decreases. It should be noted that the influence of Young's Modulus over this temperature range is relatively small. A rapid increase in deflection occurs for temperatures beyond 650°C. At this point the central part of the beam develops partial plasticity as shown in the strain block diagrams in Figure 6.13. Even though the temperature difference between the top and bottom flanges of the cross-section is decreasing during this period and hence reducing the thermal bowing, the effect of plasticity clearly causes the beam to deflect very rapidly.

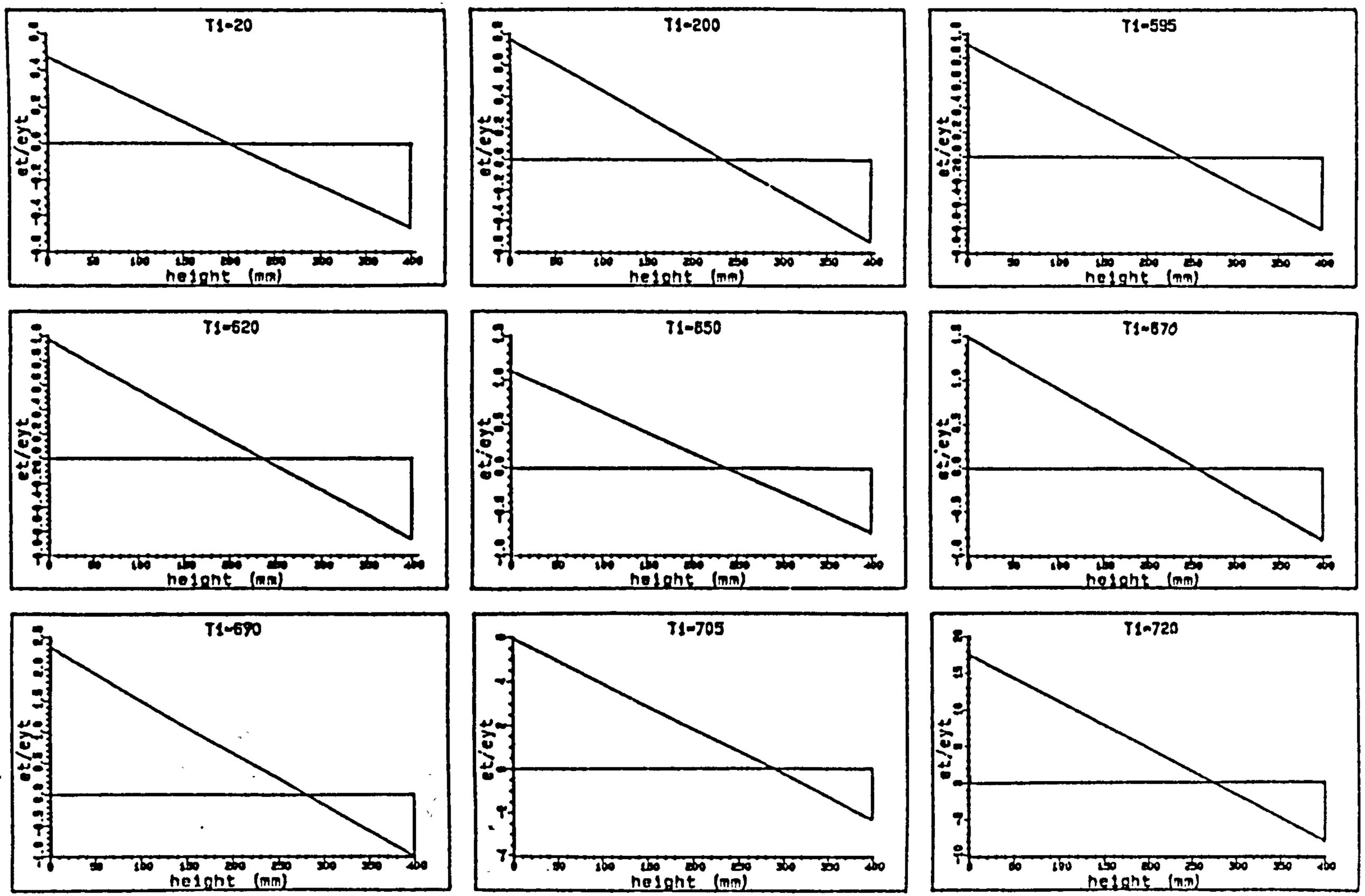

Figure 6.13: The development of the strain profile of the beam at mid-span.

6.3 PIN-ENDED BEAM WITH FULL RESTRAINT AGAINST LONGITUDINAL EXPANSION.

6.3.1 Comparison with theoretical results.

A comparison of the present analysis will now be made with further finite element analysis results obtained by Furumura and Shinohara [11]. An analysis was carried out on a pin-ended beam of 7.0m span subjected as before to a uniformly distributed load of 29.43 kN/m. The cross-section, mechanical properties of steel, and the heating sequence are as presented in Section 6.2. The essential difference is that the roller under the right-hand support in Figure 6.12 is eliminated, so that horizontal motion is prevented.

The change of axial load induced at the joint due to the effect of this restraint condition at increasing temperature is illustrated in Figure 6.14. This shows that the axial load obtained from the present theory is in very good agreement with the result obtained by Furumura and Shinohara. For example when the bottom flange temperature reaches 420°C the difference between those two results is about 5%.

The central deflection of the beam at increasing temperature is plotted in Figure 6.15. It can be seen that the central deflection obtained from the present theory is in very close

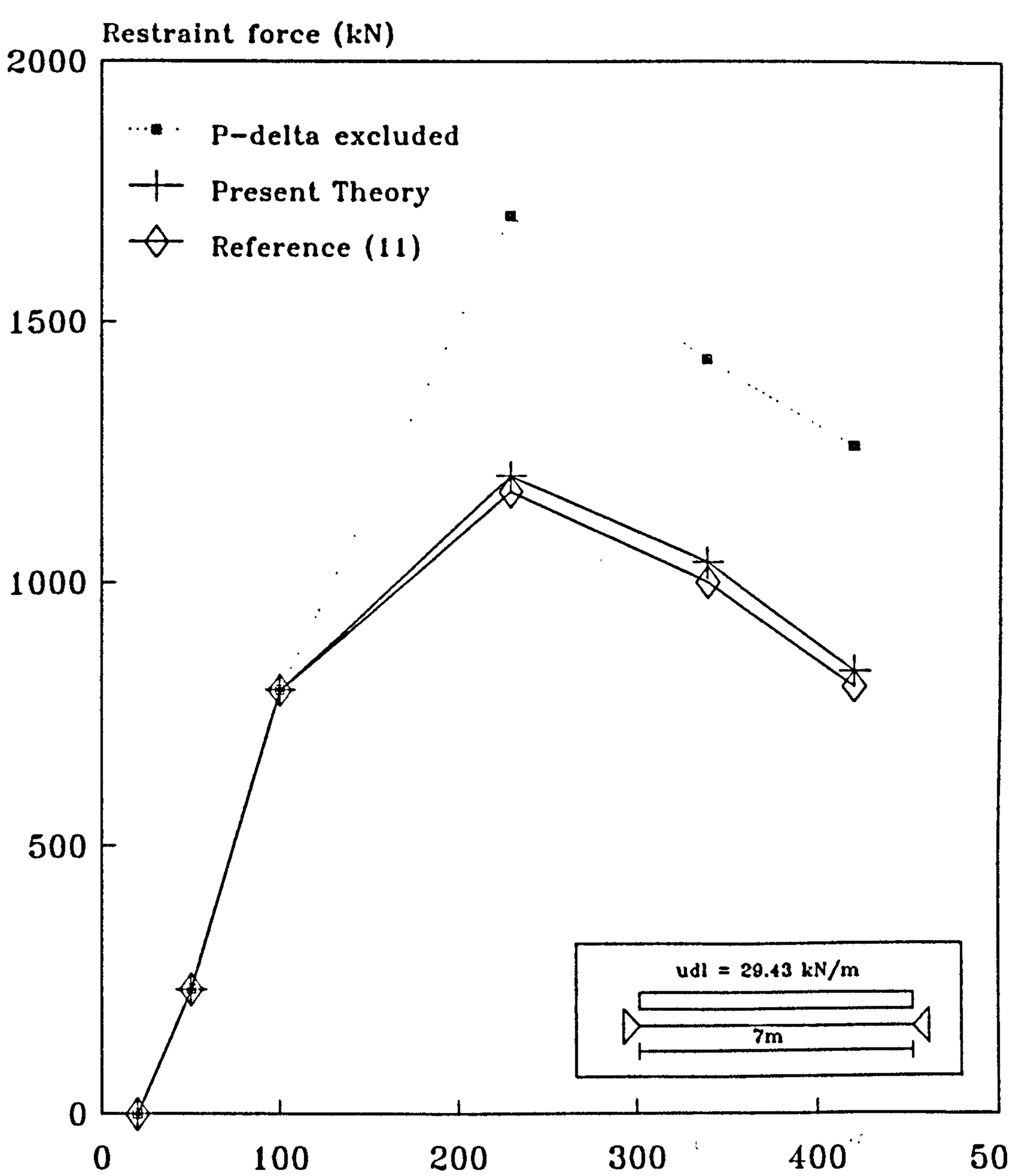

Figure 6.14: Comparison of end force for a restrained pin-ended beam showing the influence of p-delta effect.

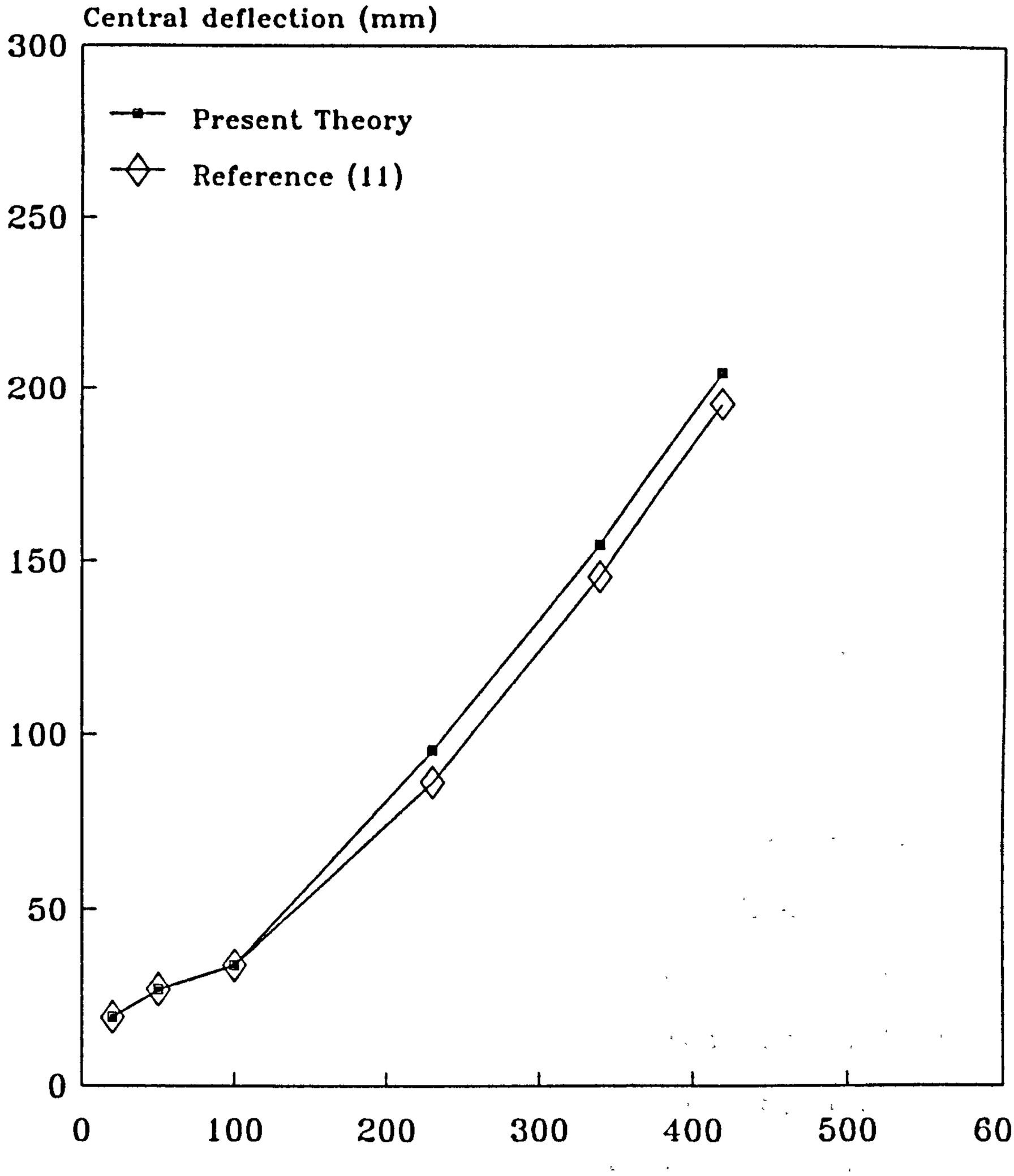

Figure 6.15: Comparison of central deflection of a restrained pin-ended beam.

agreement with the result from reference [11]. Once again, when the bottom flange temperature reaches 420°C the difference between these two results is about 4%. A similar comparison was also made with the mid-span bending moment as shown in Figure 6.16 and these are also in very good agreement.

6.4 SIMPLE PORTAL FRAME.

6.4.1 Comparison with theoretical results.

Furumura and Shinohara [11] also carried out an analyis on a simple portal frame with fixed bases and uniformly distributed roof load of 29.43 kN/m as shown in Figure 6.17. The steel temperatures of the beam and columns are shown in Figure 6.18.

Figures 6.19 and 6.20 respectively show the central deflection and axial force of the beam at increasing temperature. The bending moments at joints A, B and the mid-span of the beam are plotted against steel bottom flange temperature in Figures 6.21, 6.22 and 6.23 respectively. Figures 6.19 to 6.23 show that the two analyses are in very good agreement.

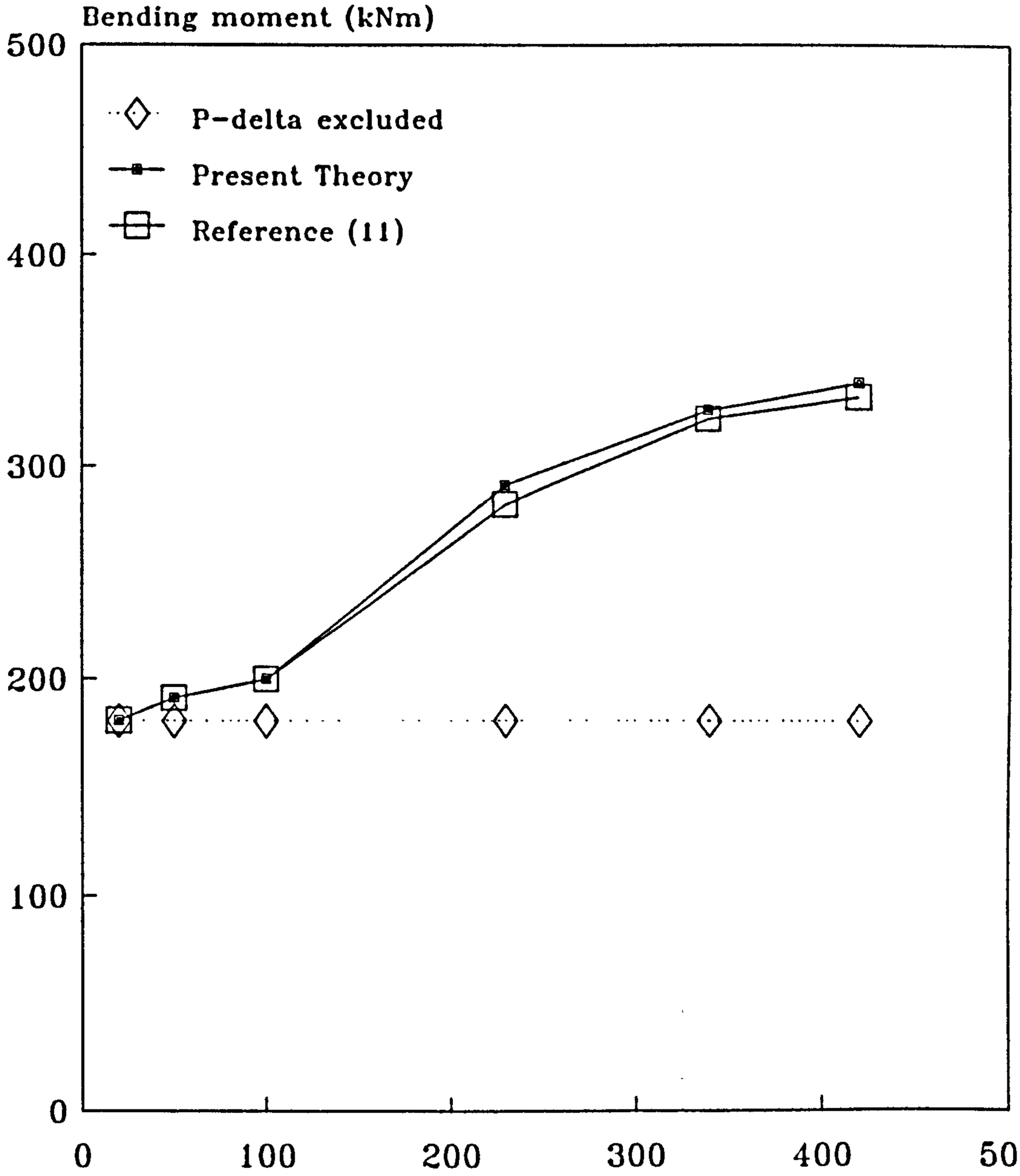

Figure 6.16: Comparison of mid-span bending moment of a restrained pin-ended beam showing the influence of p-delta effect.

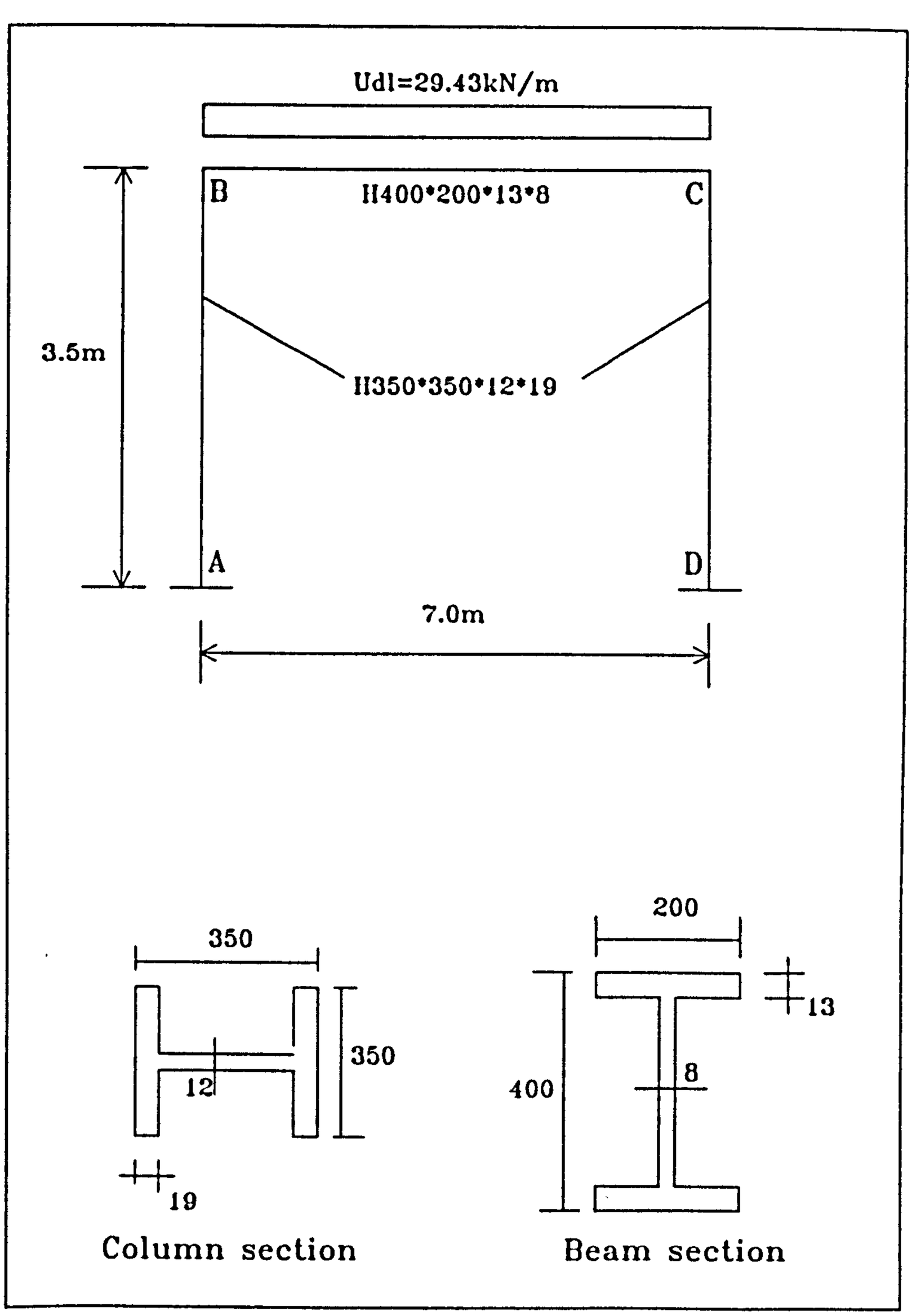

Figure 6.17: Frame details as analysed by Furumura and Shinohara [11].

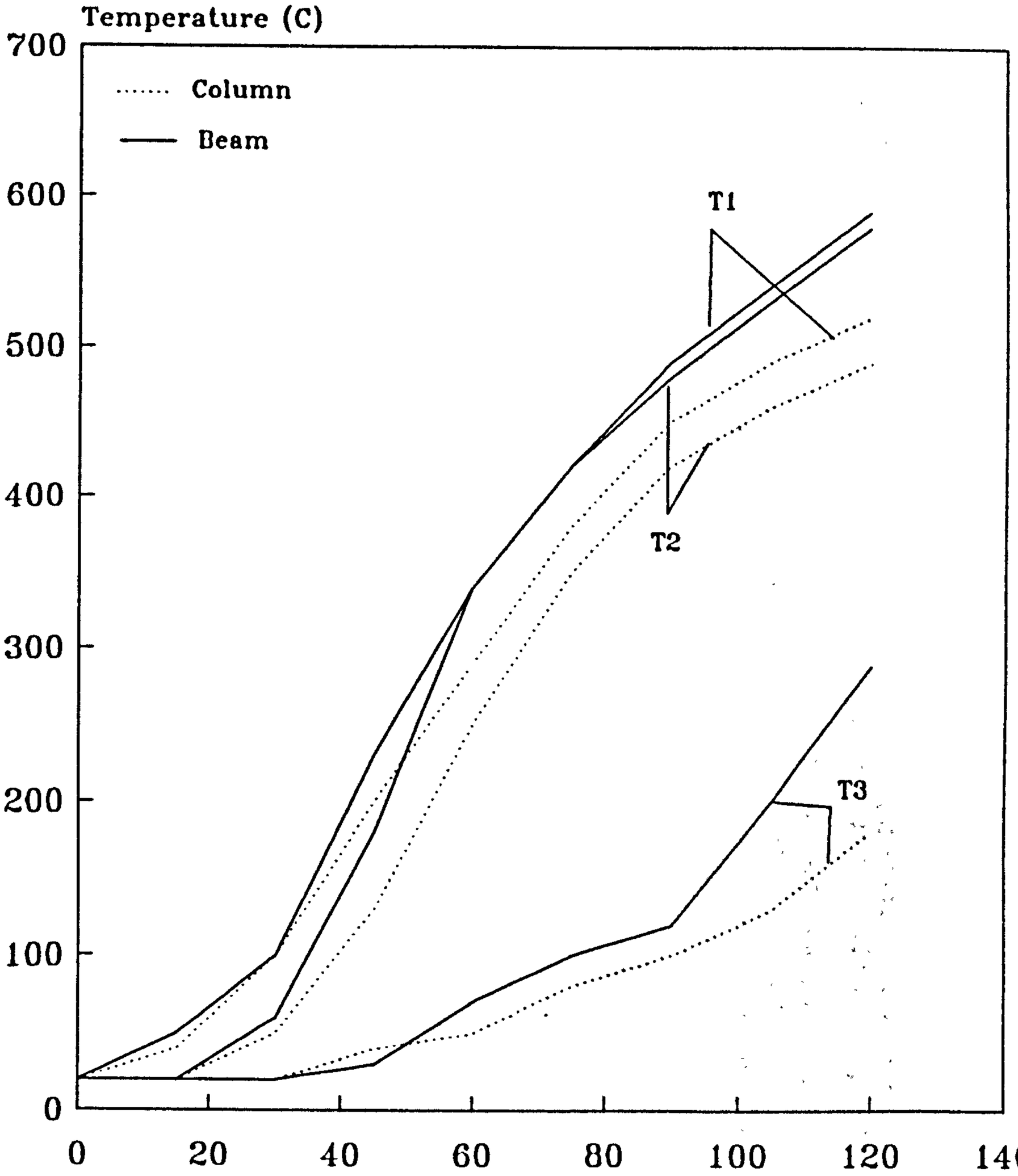

Figure 6.18: Temperature histories for frame members used by Furumura and Shinohara [11].

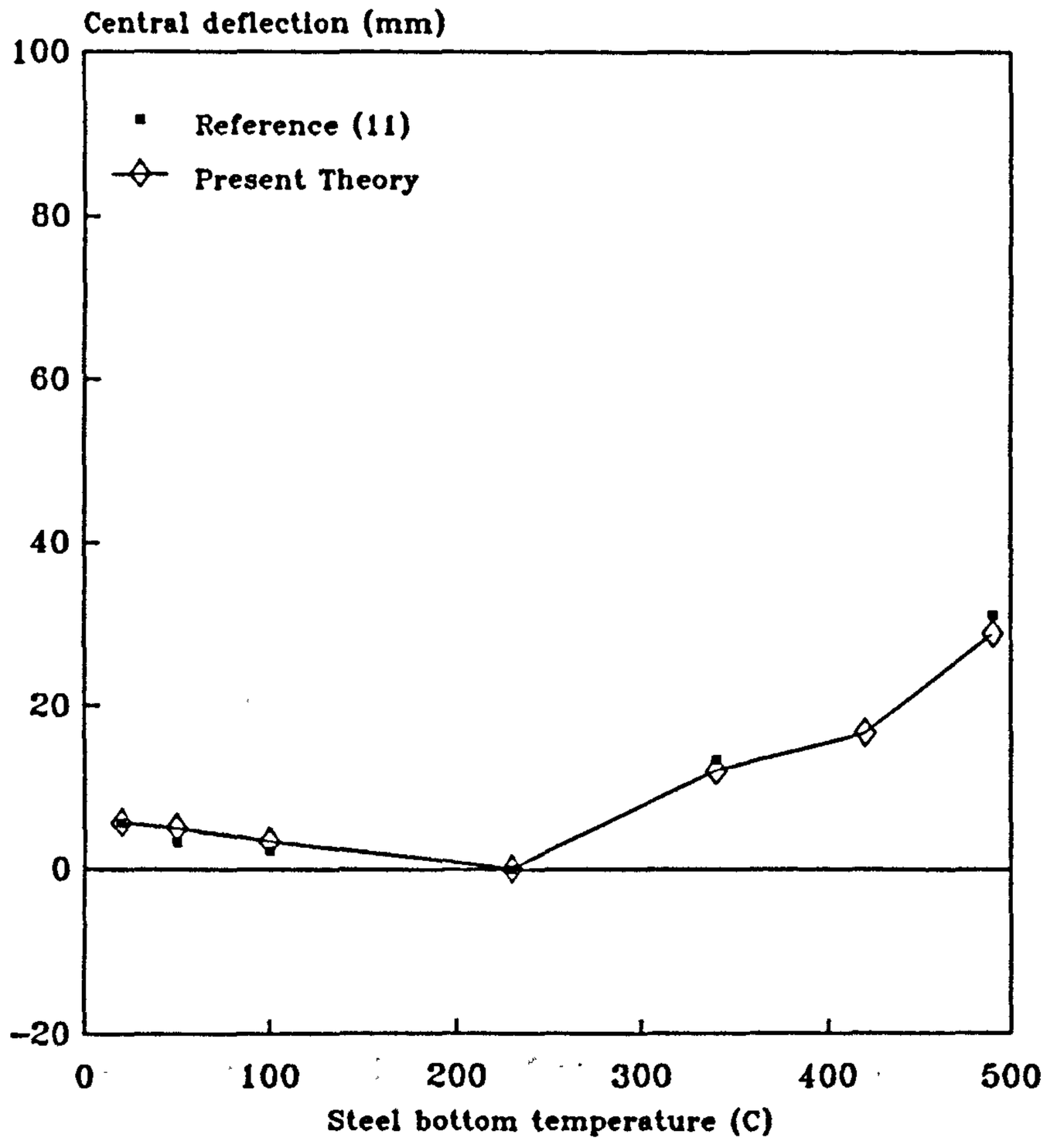

Figure 6.19: Comparison of central deflection of beam BC.

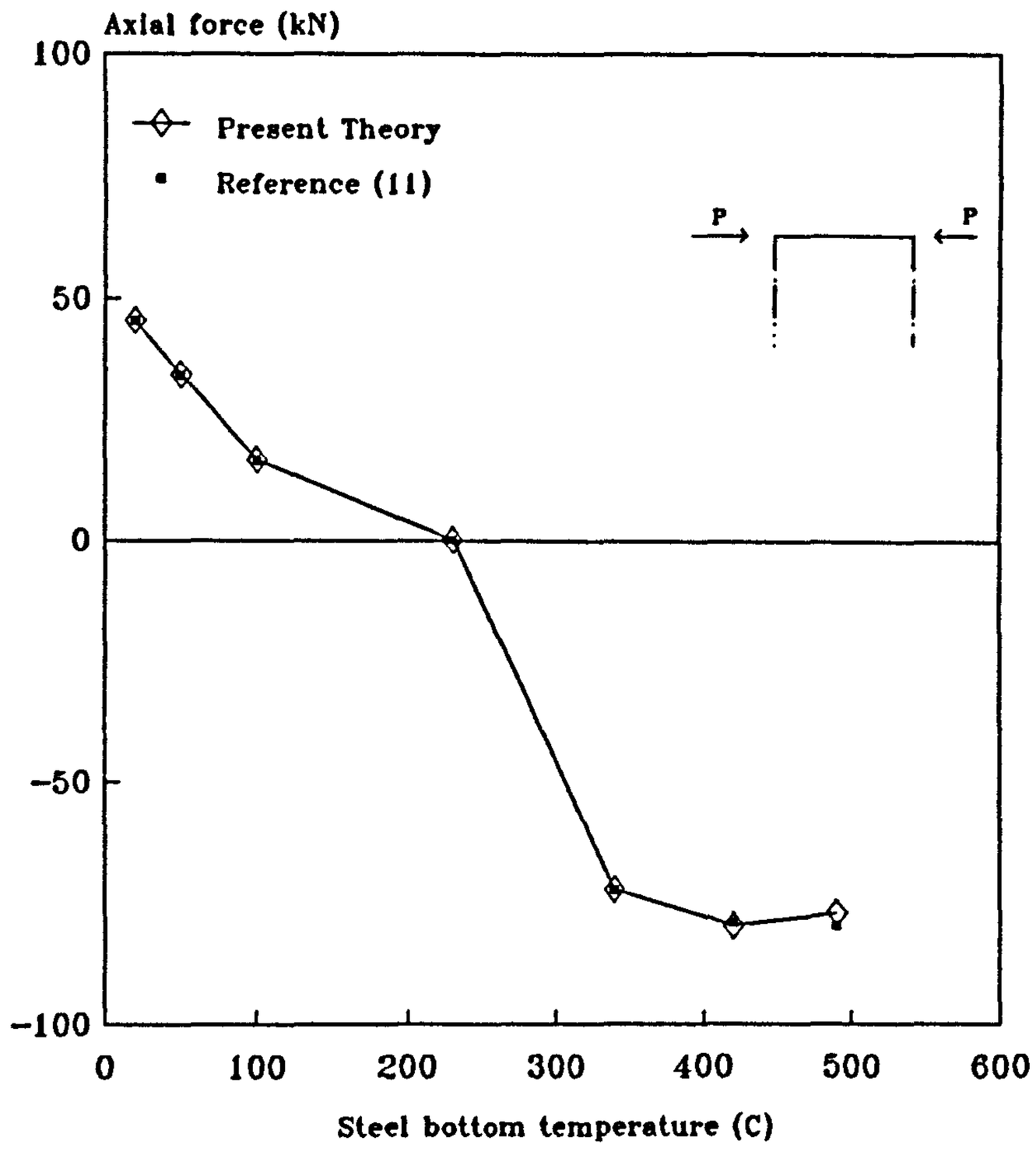

Figure 6.20: Comparison of axial force in beam BC.

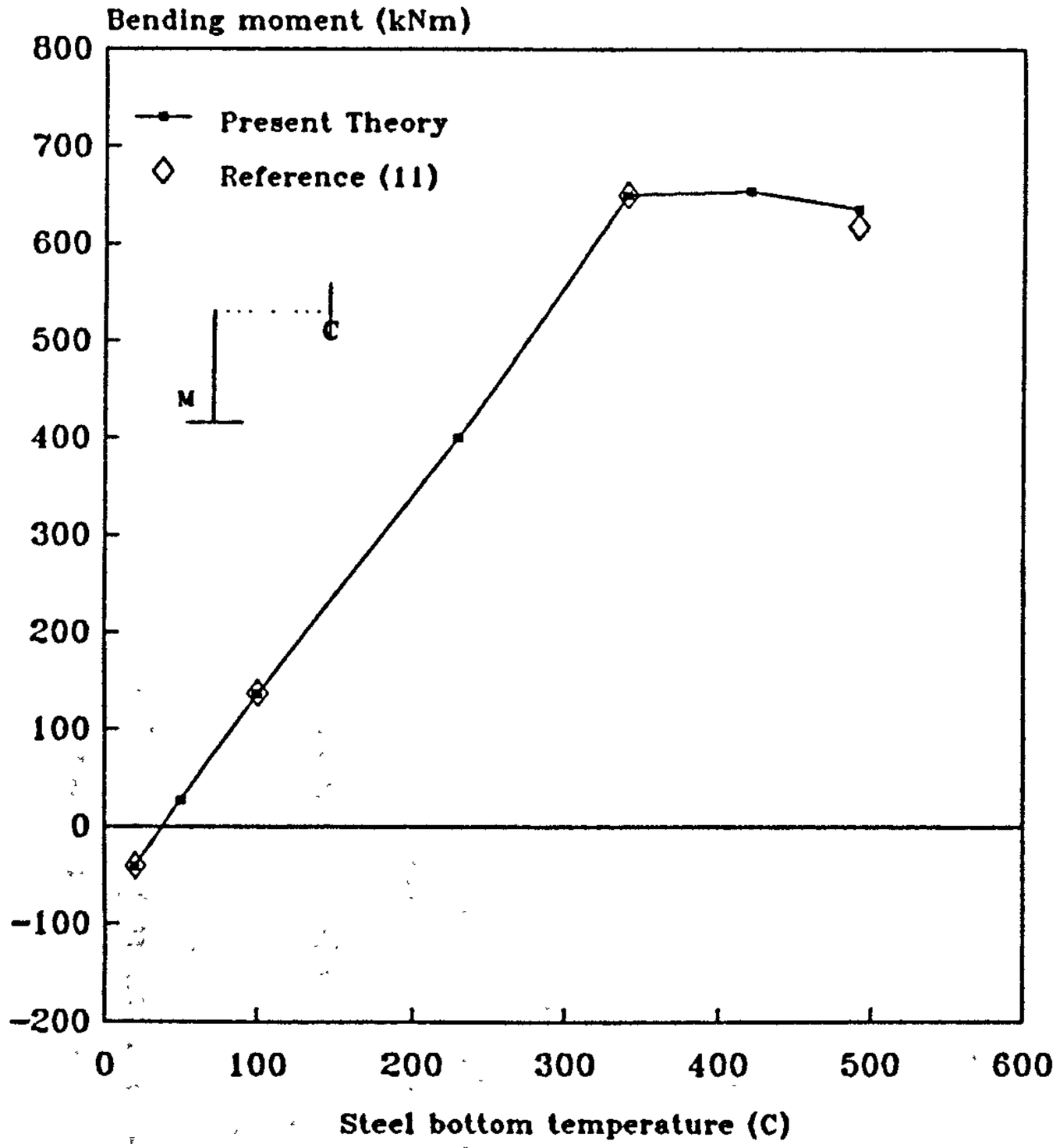

Figure 6.21: Comparison of bending moment at joint A.

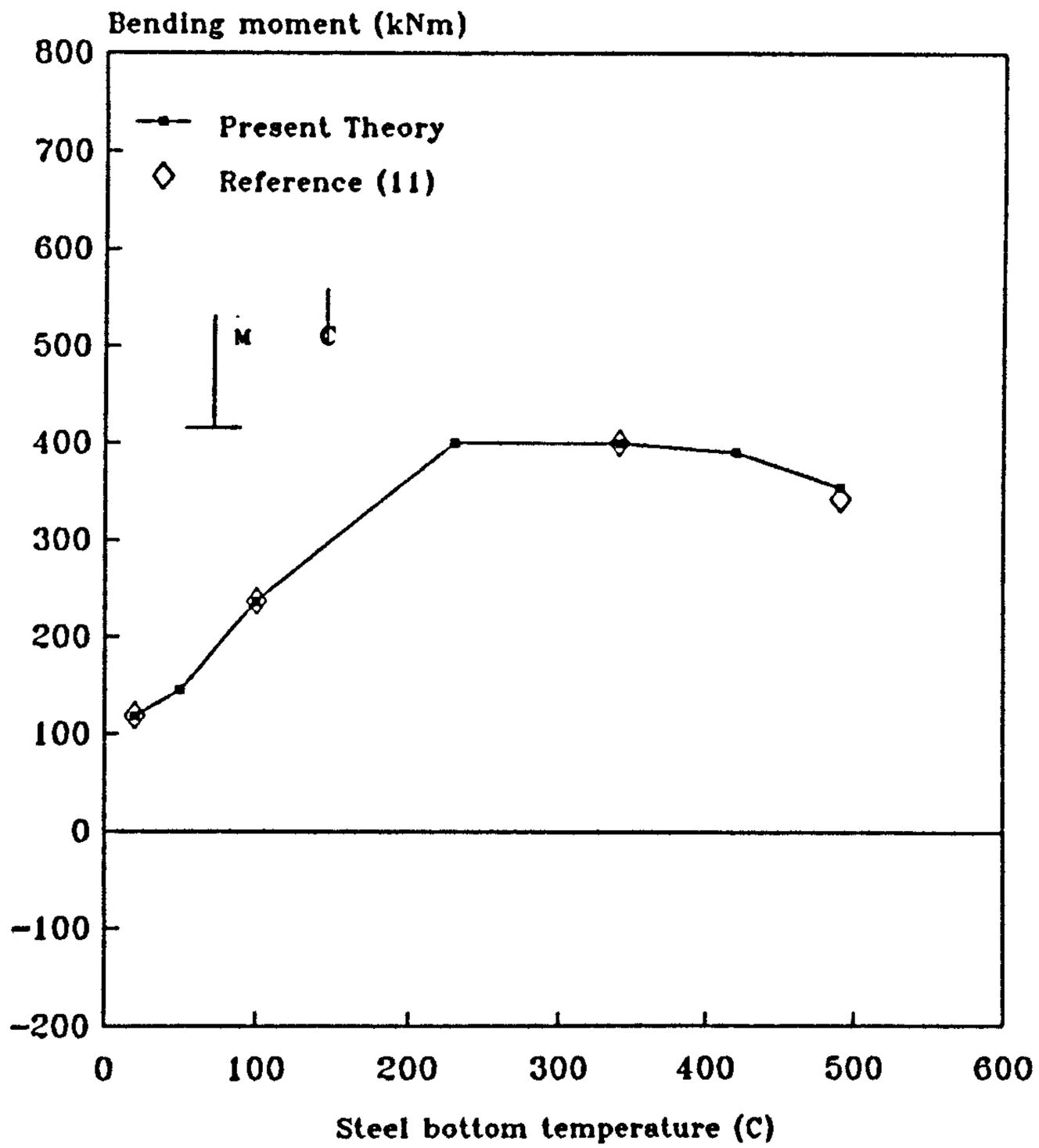

Figure 6.22: Comparison of bending moment at joint B.

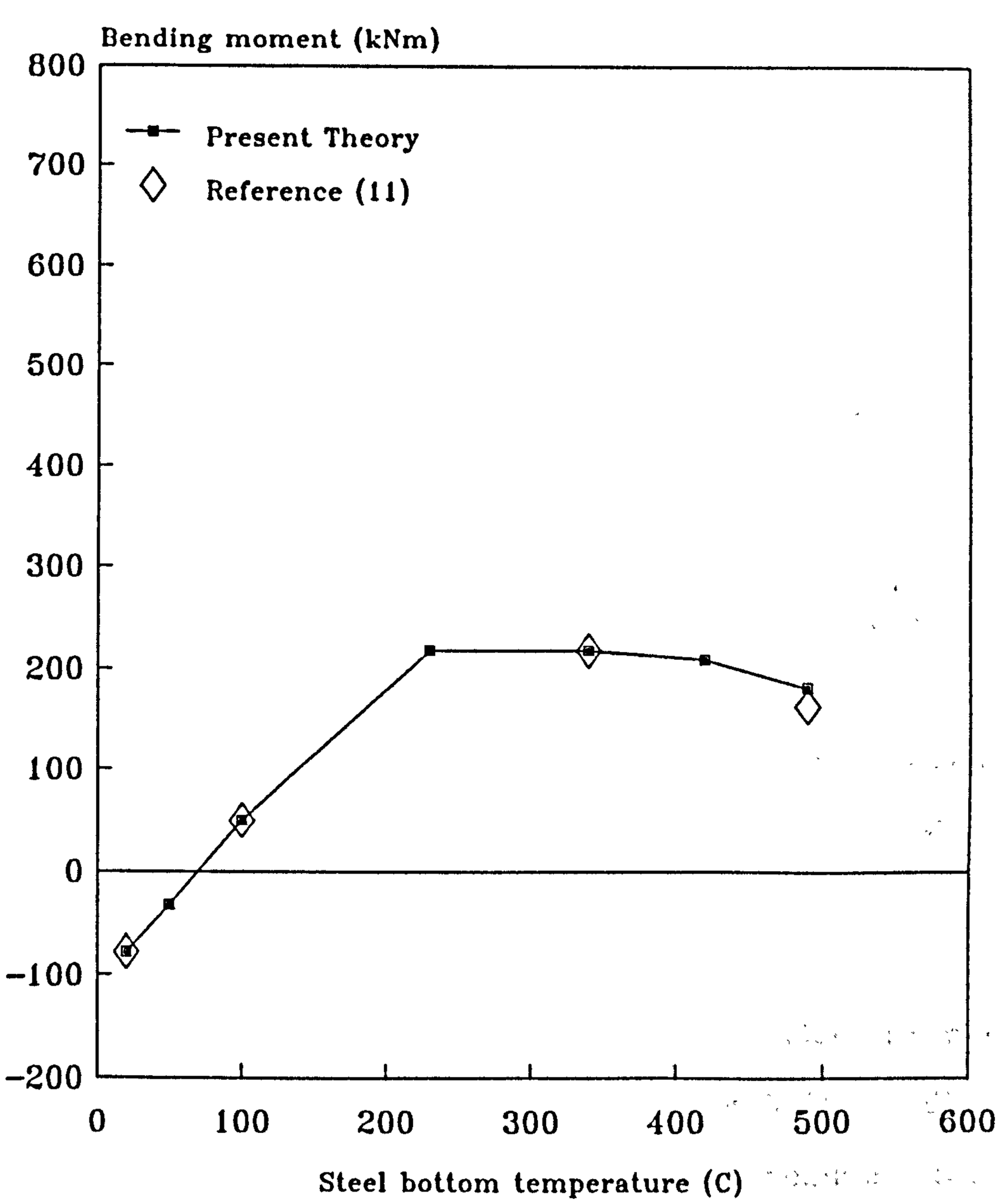

Figure 6.23: Comparison of bending moment at the mid-span of beam BC.

6.4.2 Comparison with experimental results.

A test on a simple portal frame in fire was carried out by Cooke and Latham [96]. It comprised a 4.55 m beam of 406x178x54 kg/m Universal Beam section and two 3.53 m columns of 203x203x52 kg/m Universal Column section. All steel was of grade 43A.

The complete assembly is shown in Figure 6.24. Each column, which extends above the beam, was pinned at its base. The web of each column was protected by autoclave aerated concrete blocks built-in between the flanges. The test beam remained unprotected but four 1200x1550x150 mm precast concrete slabs were placed on it to form part of the compartment roof. A maximum axial compressive load of 552 kN was applied to each test column by a hydraulic ram. The test beam was loaded to 39.6 kN at four positions along the span using two jacks and two spreaders.

The measured steel temperatures of the beam and column during the fire are shown in Figure 6.25. The idealised temperature profiles for beam and column are shown in Figures 6.26(a) and 6.26(b) respectively. The central deflection of the beam measured during the test is compared with the results obtained from the present theory in Figure 6.27. This shows good agreement up to 16 minutes. After this time the theory indicates that the beam reaches its failure condition (deflection = L/30) at 17.5 minutes.

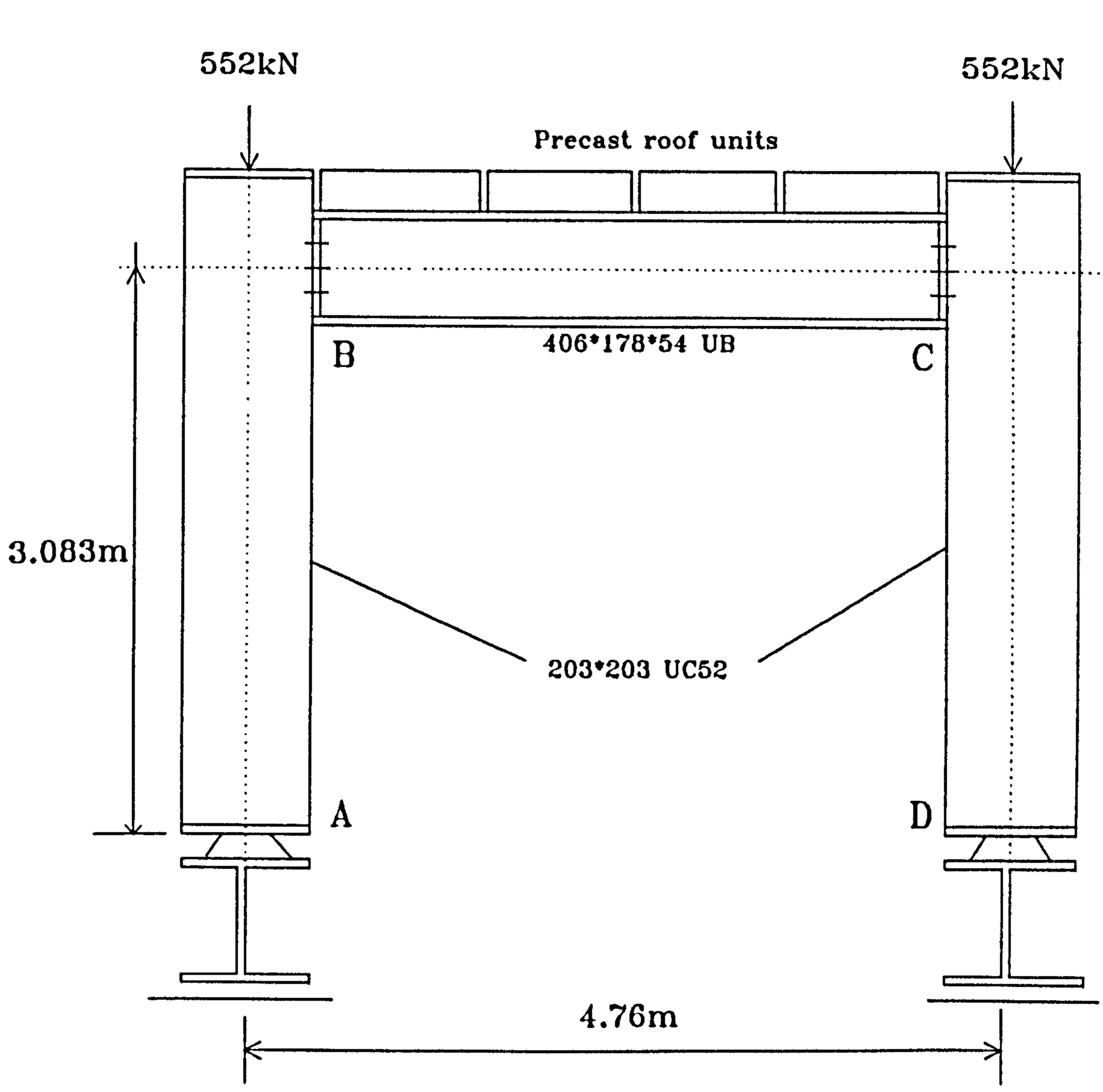

Figure 6.24: Details of test frame [96].

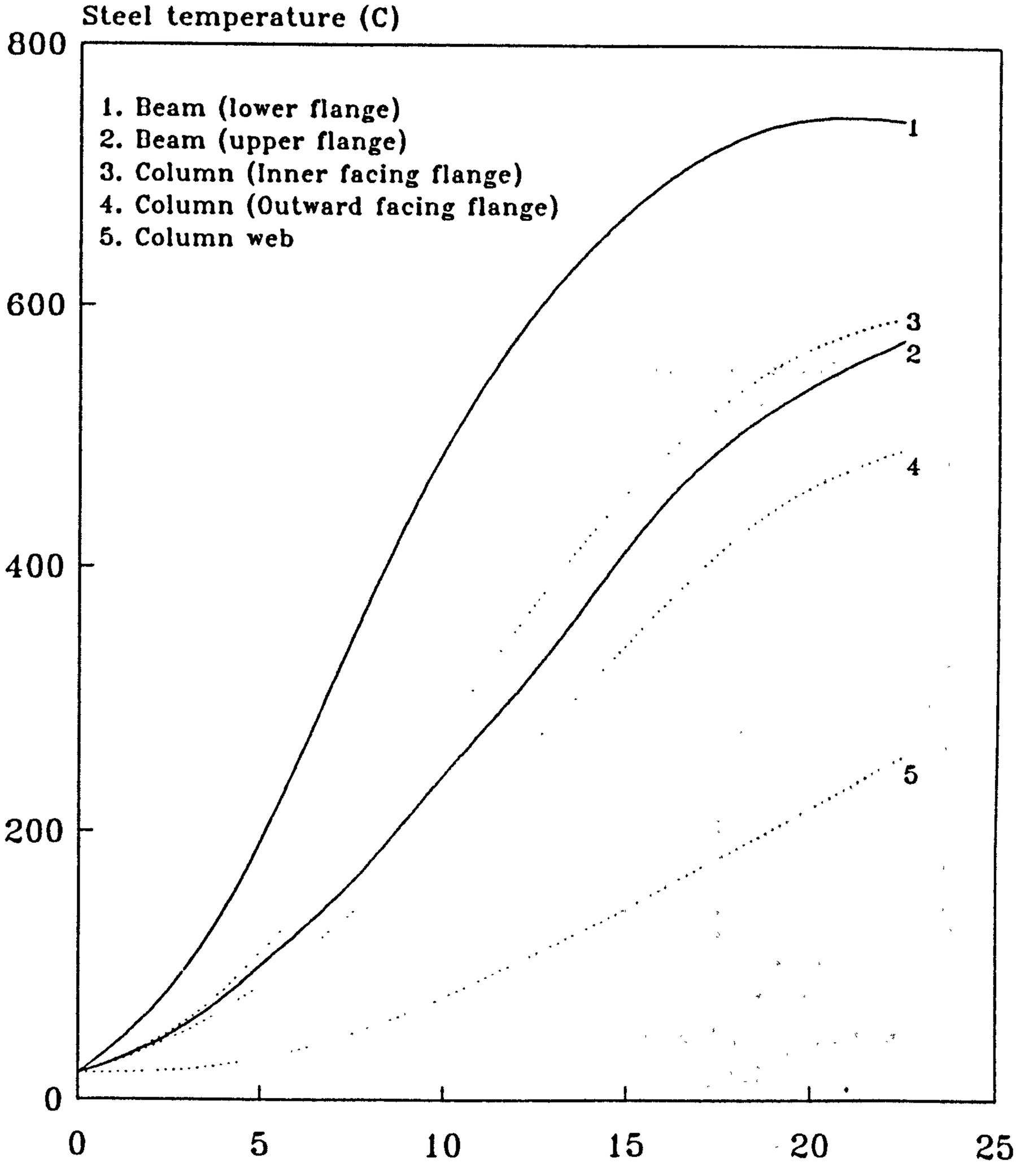

Figure 6.25: Steel temperature histories for the beam and column in the frame test [96].

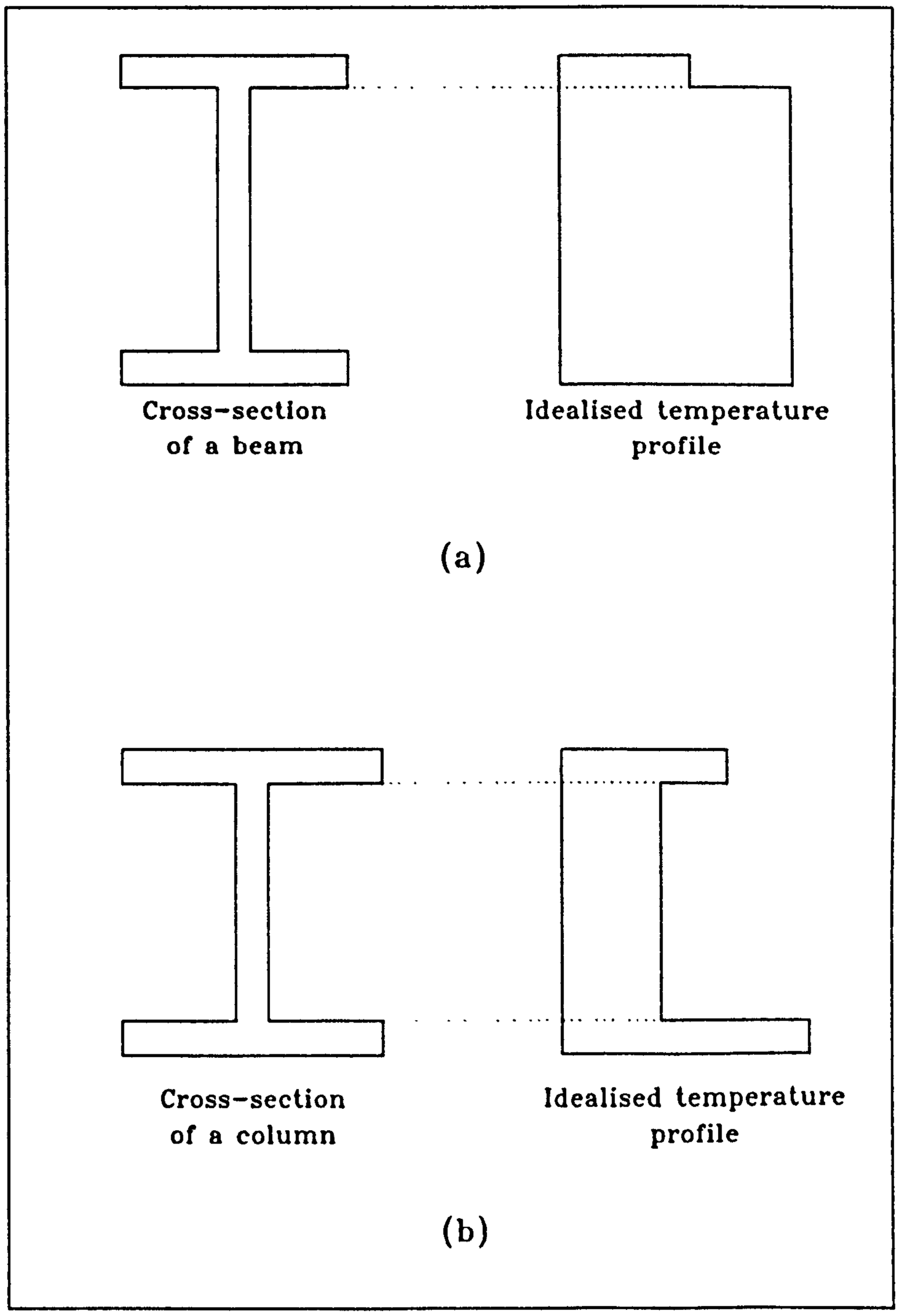

Figure 6.26: Idealised temperature profiles for the beam and column in the frame test.

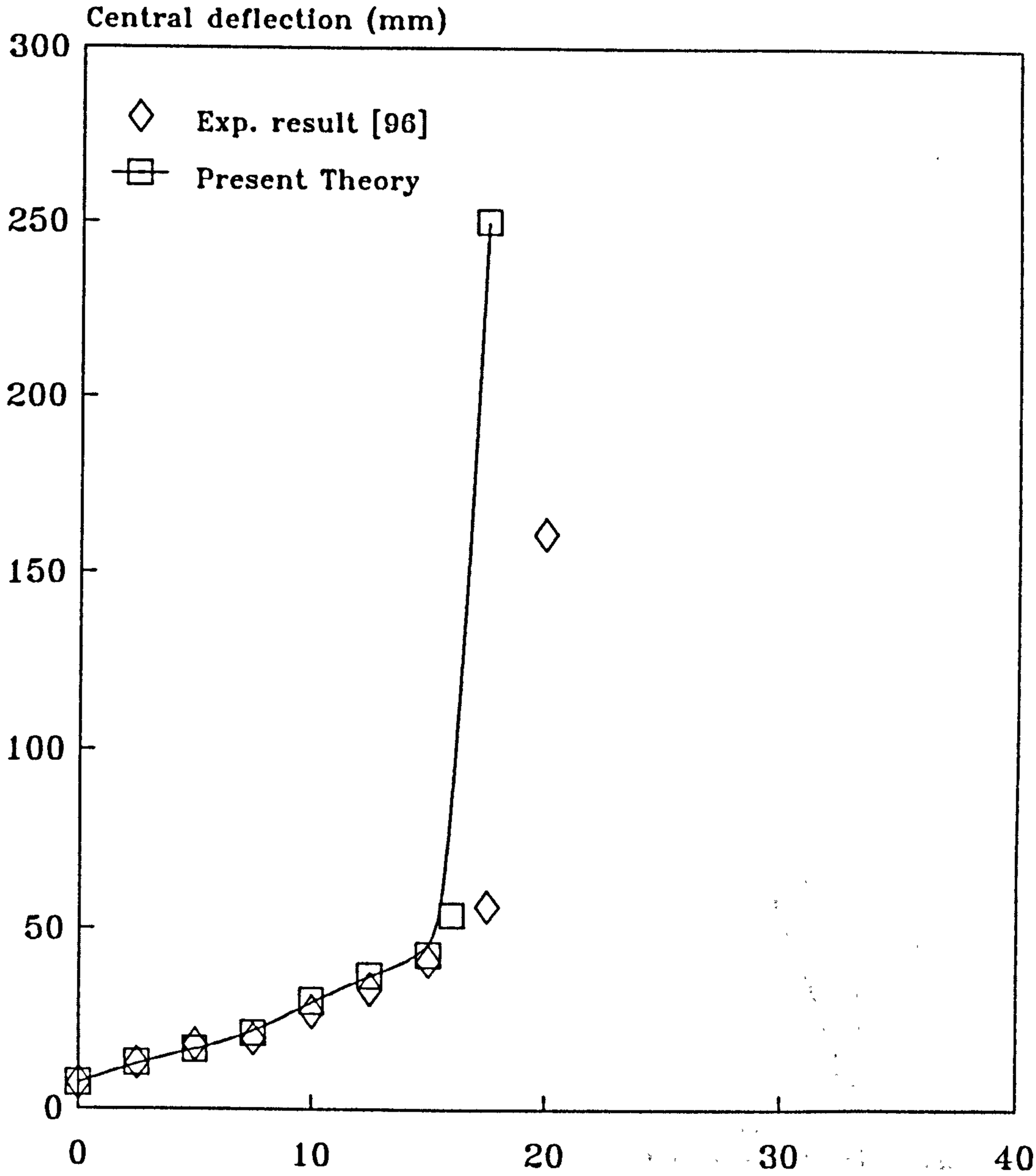

Figure 6.27: Comparison between predicted and experimental central deflections of beam BC.

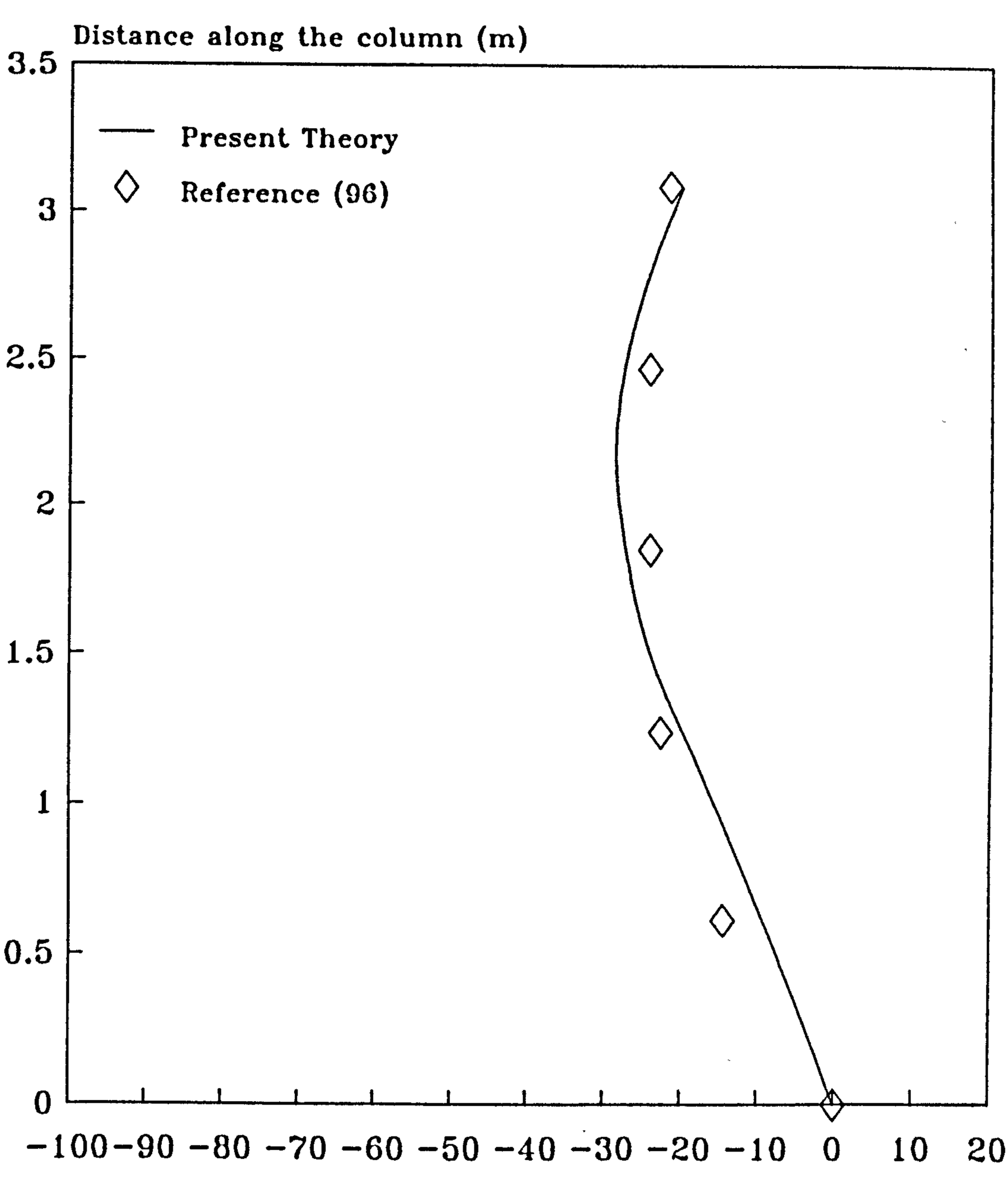

Figure 6.28: Comparison between predicted and experimental lateral deflection of column AB after 16 minutes of the test.

The bottom flange temperature of the beam at failure obtained from the present theory and the test are 725°C and 750°C respectively. A comparison has also been made for the lateral deflection profile of the column at 16 minutes. Figure 6.28 shows that these two results are in very good agreement.

The comparisons conducted in this chapter show the accuracy of the present analysis in predicting the behaviour of different types of steel structures. In the following chapter it will be used to study factors which may influence the behaviour of different types of steel structures in fire.

CHAPTER SEVEN

PARAMETRIC STUDIES

7.1 INTRODUCTION.

Although the use of fire protection materials for structural steel elements can provide required periods of fire resistance this can be very costly. Considerable savings can be made if the need for such fire protection can be reduced or eliminated. The main aim of this chapter is therefore to demonstrate the structural response of unprotected steel members and to highlight the principal parameters which influence the behaviour. The behaviour of statically determinate and indeterminate structures including simple portal frames, pin-ended and propped cantilever columns will be considered. Both non-uniform and uniform temperature profiles are included and the effect of temperature gradient along member lengths is studied. Where appropriate, the failure criterion is based on a limit state of deflection equal to (L/20). The temperature and time at which this criterion is reached are called the critical temperature and the critical time respectively.

In all cases the secant stiffness approach described in Chapters 3 and 5 is used for the analysis. The multi-

linear stress-strain relationship described in Chapter 2 is adopted unless otherwise stated. Various standard Universal Beam and Universal Column sections are used in this study. The temperature histories of the steel beams and columns are taken from test results [20] unless otherwise stated. The steel members are all designed according to BS 449: Part 2 which for the general case of combined bending and compression can be stated as:

$$(f_c/p_c) + (f_{bc}/p_{bc}) \leq 1 \quad .....(7.1)$$

where (f_c/p_c) = Ratio of the actual to permissible axial stress.

(f_{bc}/p_{bc}) = Ratio of the actual to permissible bending stress.

7.2 PIN-ENDED COLUMN SUBJECTED TO END MOMENTS AND UNIFORM TEMPERATURE PROFILE.

A typical beam/column connection is shown in Figure 7.1. In such cases the load from the beam is eccentric to the column and consequently generates a moment within the column. Because of this, a study will be carried out on the behaviour of a single pin-ended column subjected to end moments and axial force, including the p-delta effect. Since the present approach is based on a two-dimensional plane frame analysis out of plane behaviour, and in particular minor axis buckling, is excluded. The results

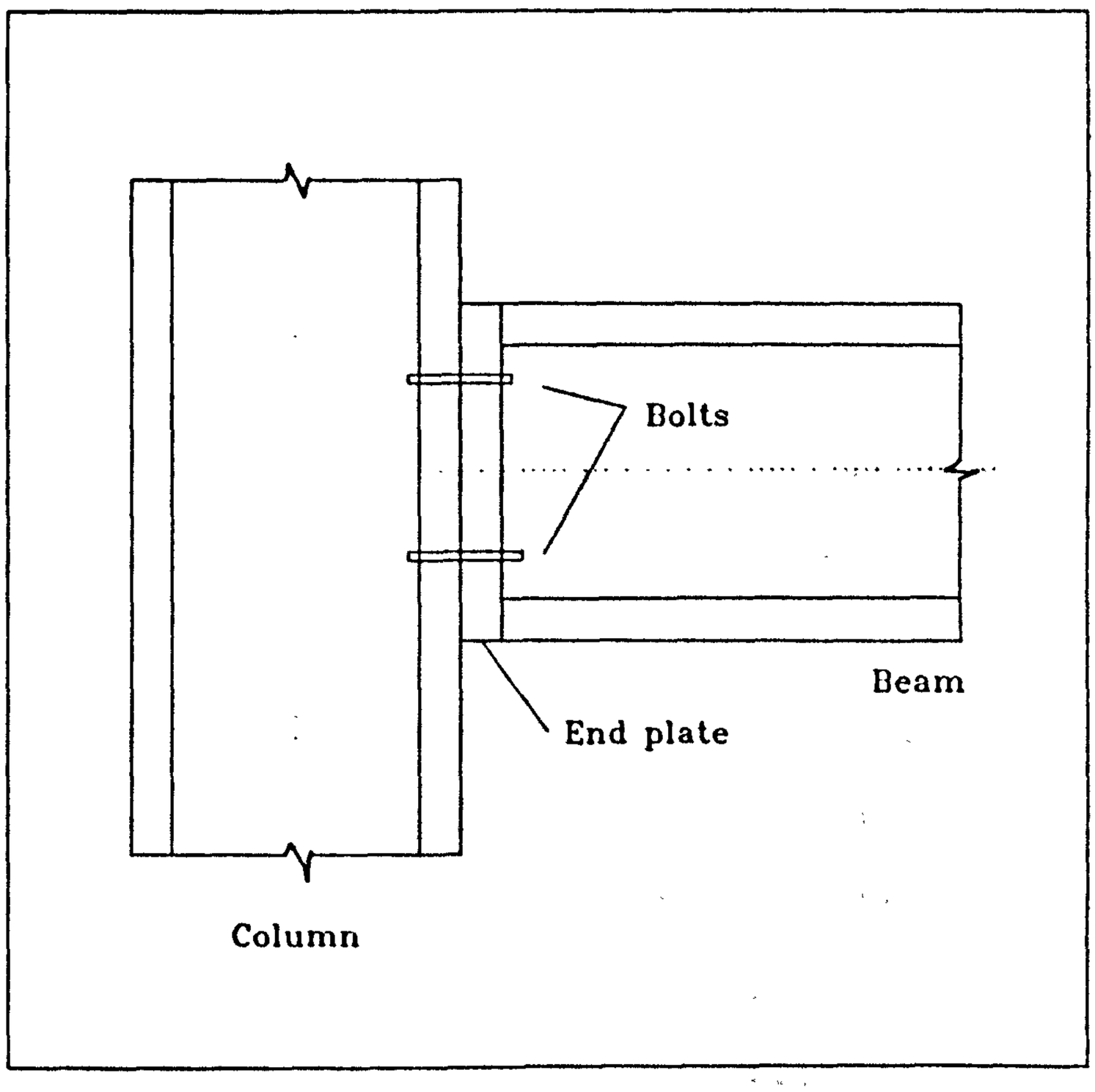

Figure 7.1: Typical beam/column connection

are therefore valid provided that such deformations are physically restrained. The slenderness of the structural member is considered as the (L/r_x) ratio in which L is the effective length of the member and r_x is the radius of gyration in the x (major axis) direction.

Various parameters will be studied including slenderness ratio, the relative magnitudes of bending moment and axial load, the size of the cross-section, the grade of steel, the influence of varying temperature along the member length, and the influence of end restraint.

The behaviour of pin-ended columns of different slenderness ratios (L/r_x) subject to constant loads will be considered first. A cross-section of UC 203x203x52 kg/m and an ambient temperature yield stress of 250 N/mm² are assumed for the analysis. Different slenderness ratios are considered by using different lengths. The amounts of end the moments and axial force applied to the column are assumed to be $0.1M_p$ and $0.1P_y$ respectively which consequently would result in different (f_c/p_c) and (f_{bc}/p_{bc}) ratios for different slenderness ratios.

Figure 7.2 shows the variation of central deflection with temperature for a range of slenderness ratios. This indicates that columns with higher slenderness ratios reach their failure condition faster than the stockier columns. For instance, the critical temperature for slenderness

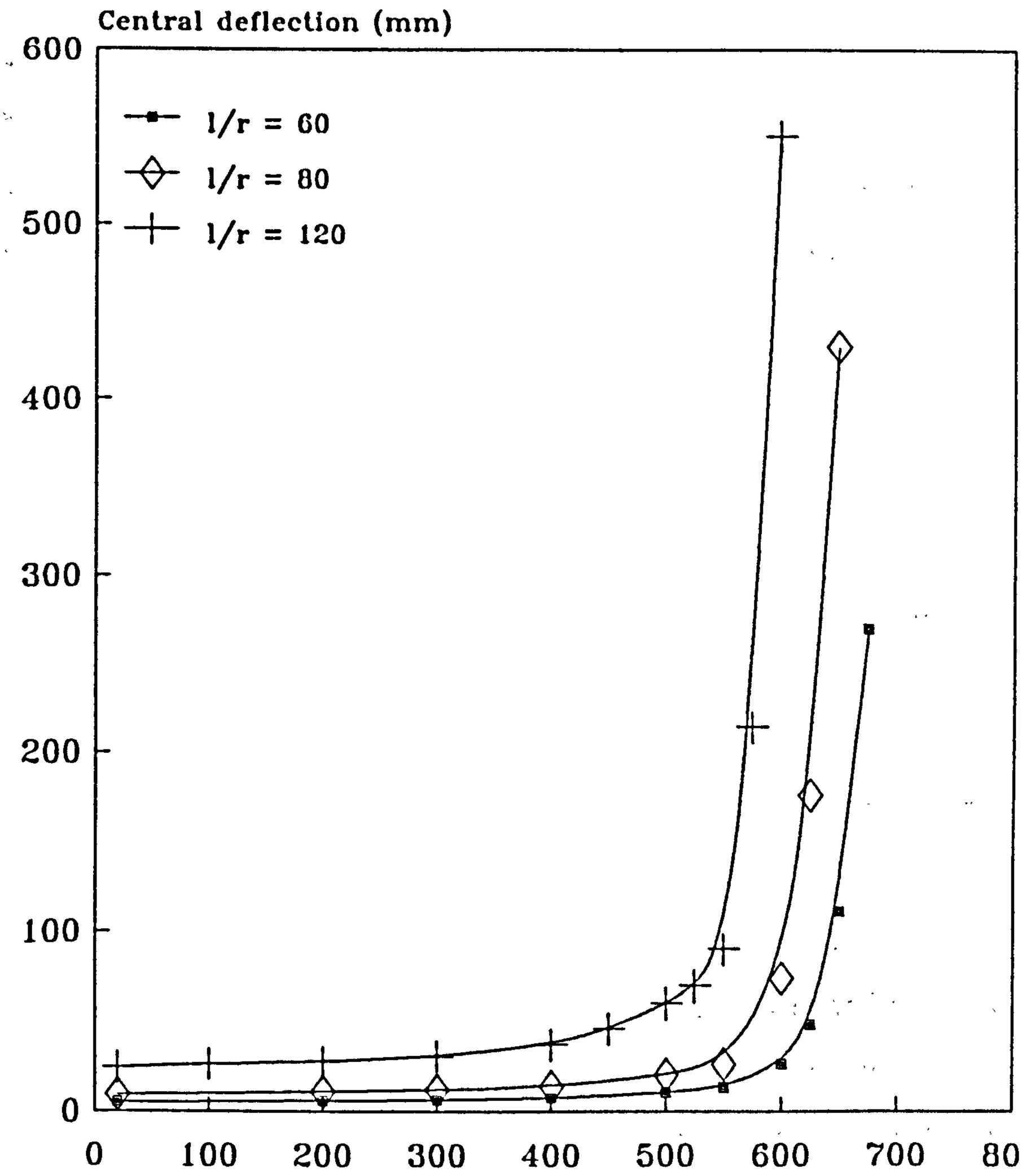

Figure 7.2: Change of deflection with temperature for pin-ended columns with different slenderness ratios subjected to a constant moment and axial load and a uniform temperature profile.

ratios of 120 and 60 are equal to 575°C and 675°C respectively. This may be because for stocky columns the secondary moment generated by an axial force is relatively small compared with more slender columns. Furthermore, since the failure criterion is related to the central deflection, slender columns, which are likely to deform significantly more than stocky columns even when subject to the same amount of bending moment and axial force, are likely to reach the failure condition much earlier. Of course in practice slender columns are likely to be subject to much lower loads than stocky columns.

7.2.1 Influence of slenderness ratio (L/r_x).

The influence of slenderness ratio on the critical temperature of columns subject to their maximum permissible axial load ($f_c/p_c = 1.0$), is considered next. Different magnitudes of end moments were applied ranging from $0.01M_p$ to $0.2M_p$.

Figure 7.3 shows a family of curves representing the steel critical temperature for the various end moments. This indicates a significant variation of steel critical temperature with slenderness ratio. For shorter columns with little end moment the critical temperature is about 550°C, which is almost the same as observed in the standard fire tests. For slenderness ratios in the range of 60 to 90 the steel critical temperatures are significantly lower

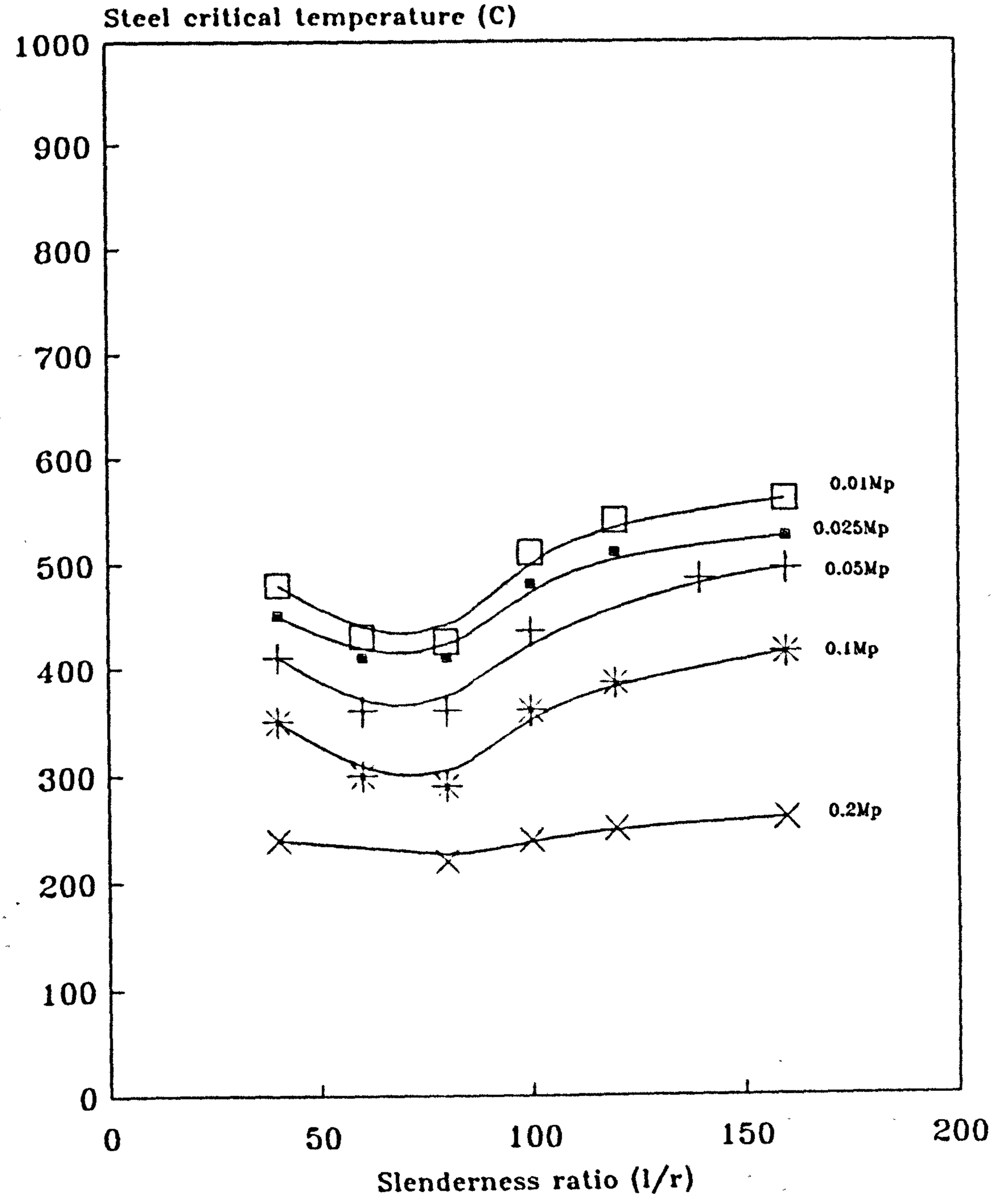

Figure 7.3: Influence of slenderness ratio on the critical steel temperature of pin-ended column for a uniform temperature profile.

than for either stockier or more slender columns. One possible explanation is that the permissible axial loads in this range are overestimated in BS 449. A bigger axial force will generate increased secondary bending moments along the member and consequently reduce the steel critical temperature. This observation is in keeping with the work of both Olawale [117] and Witteveen and Twilt [118], although in both cases the work was concerned with minor axis buckling. There are clearly significant implications for designers since slenderness ratios in the critical range are relatively common.

Figure 7.3 also demonstrates that the critical temperature reduces significantly when even a small amount of end moment is introduced. This highlights the significance of the p-delta effect on the structural performance of beam-column members in fire. This particular aspect will be discussed in more detail in the following section.

7.2.2 The influence of end moments.

The influence of the magnitude of end moments on the fire performance of columns is discussed in this section. The same section type is used as in Section 7.2.1.

In this analysis the slenderness ratio (L/r_x) of the column and the axial load ratio (f_c/p_c) are taken as 80 and 0.3 respectively while end moments are set at ratios f_{bc}/p_{bc} of

0.35 and 0.7. Figure 7.4 shows the variation of deflection with temperature for the two different moments. It can be seen that the steel critical temperature increases as the end moments reduce. For moment ratios of 0.7 and 0.35 the critical temperatures are about 450°C and 550°C respectively. This confirms the indications discussed in the context of Figure 7.3. Clearly design rules must account for this variation, although at present such rules are based largely on the behaviour of axially load columns only.

7.2.3 The influence of axial force.

Axial loads acting on a column normally result from the transmission of load from beams forming the frame structure, and the influence of the magnitude of this load on the critical temperature is considered in this section. The slenderness ratio (L/r_x) and moment ratio (f_{bc}/p_{bc}) are taken as 80 and 0.3 respectively. The section type used in the previous two sections is again used.

The variation of deflection with temperature for two different axial load ratios (f_c/p_c) of 0.7 and 0.35 is presented in Figure 7.5. This shows that the survival period of a steel column can be increased by reducing the axial load. The corresponding critical temperatures are equal to 450°C and 600°C respectively. This improvement at lower levels of axial load is clearly largely concerned with

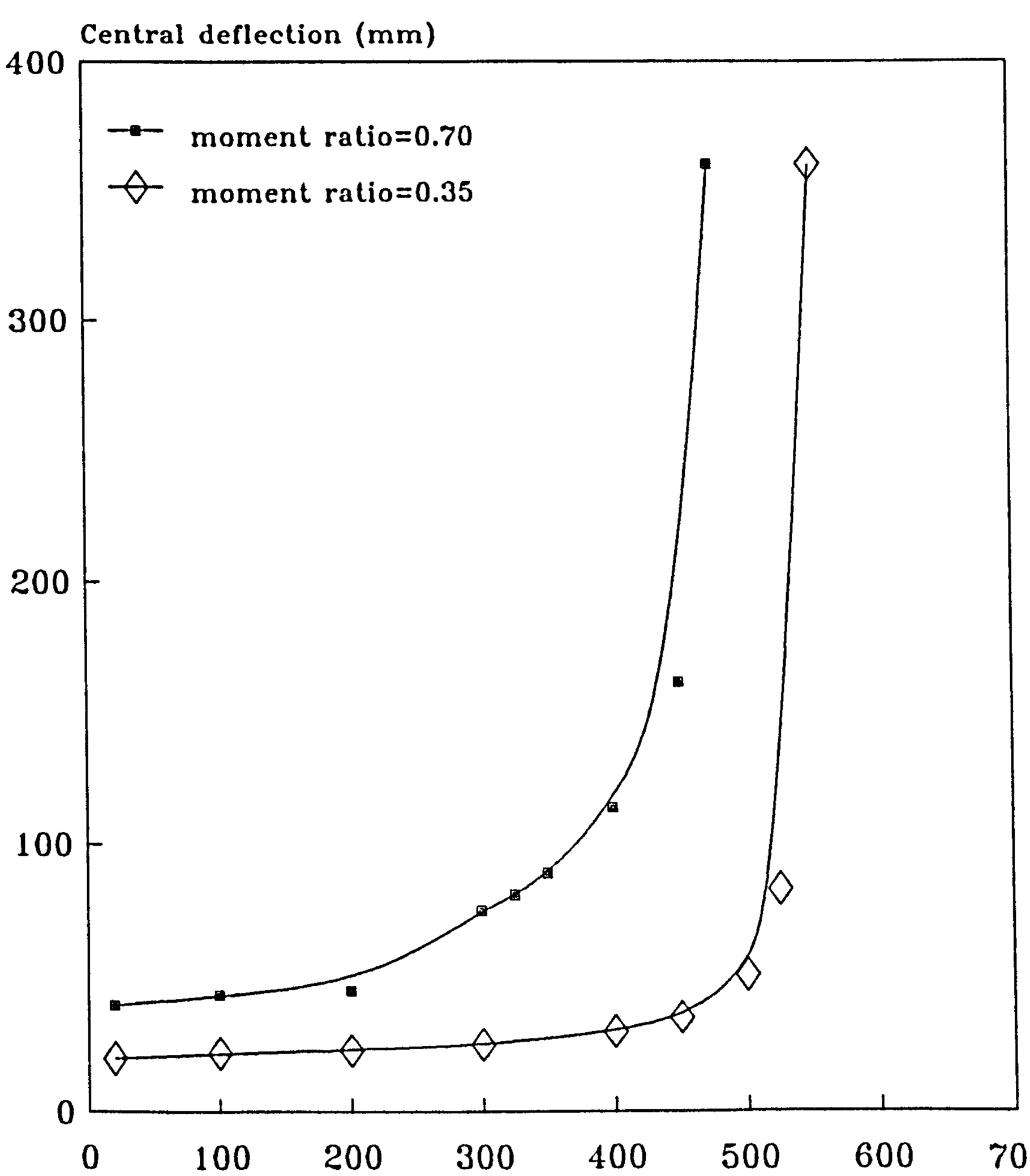

Figure 7.4: Change of deflection with temperature for a pin-ended column with a constant axial load and different bending stress levels (l/rx = 80) and a uniform temperature profile.

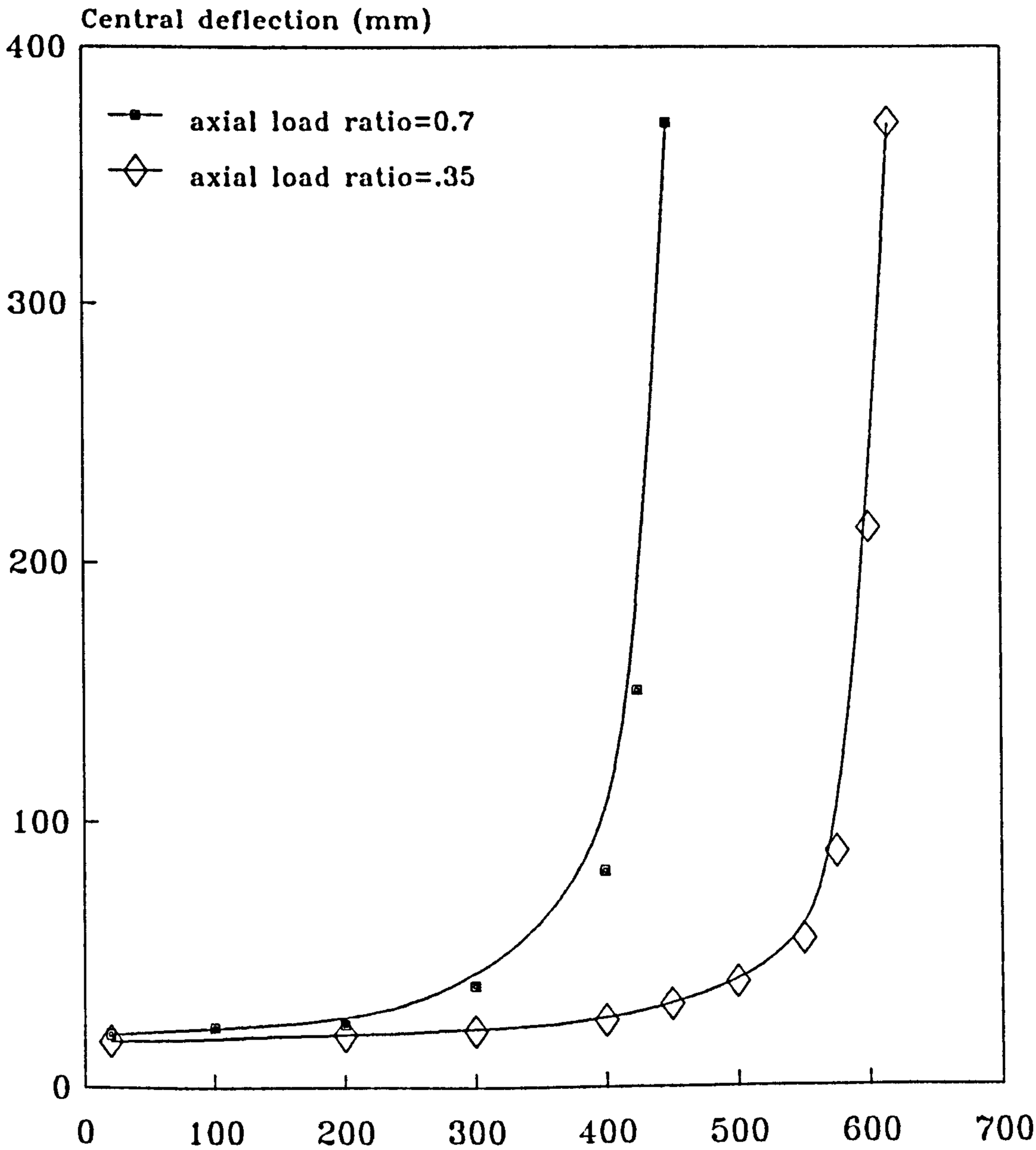

Figure 7.5: Change of deflection with temperature for a pin-ended column with a constant moment and different axial stress levels (l/rx=80) and a uniform temperature profile.

the additional reserve of strength but is also influenced by the smaller reduction in material stiffness in the presence of lower axial loads and also the reduced p-delta effect. For real construction the survival period of the steel column can therefore be increased by reducing the design load ratio (i.e, increasing the section size). However this must be justified economically and it may be that in order to achieve the necessary survival time in unprotected steelwork, excessively large section sizes would be required. This is the essence of the load ratio approach currently incorporated into BS 5950: Part 8 for axial loads only. A much more exhaustive study is required to include combinations of axial loads and end moments in the design rules.

7.2.4 Influence of size of cross-section.

The influence of the size of cross-section is considered in this section for the case of columns. Young's Modulus and yield stress at ambient temperature are assumed to be 205000 N/mm^2 and 250 N/mm^2 respectively. The slenderness ratio (L/r_x) is taken as 80 and the axial load (f_c/p_c) and moment (f_{bc}/p_{bc}) ratios are taken as 0.7 and 0.3 respectively.

Figure 7.6 shows the variation of deflection with temperature for three Universal Column sections 203x203x52, 254x254x167 and 305x305x283 kg/m. It can be seen that the steel critical temperatures are almost identical in each

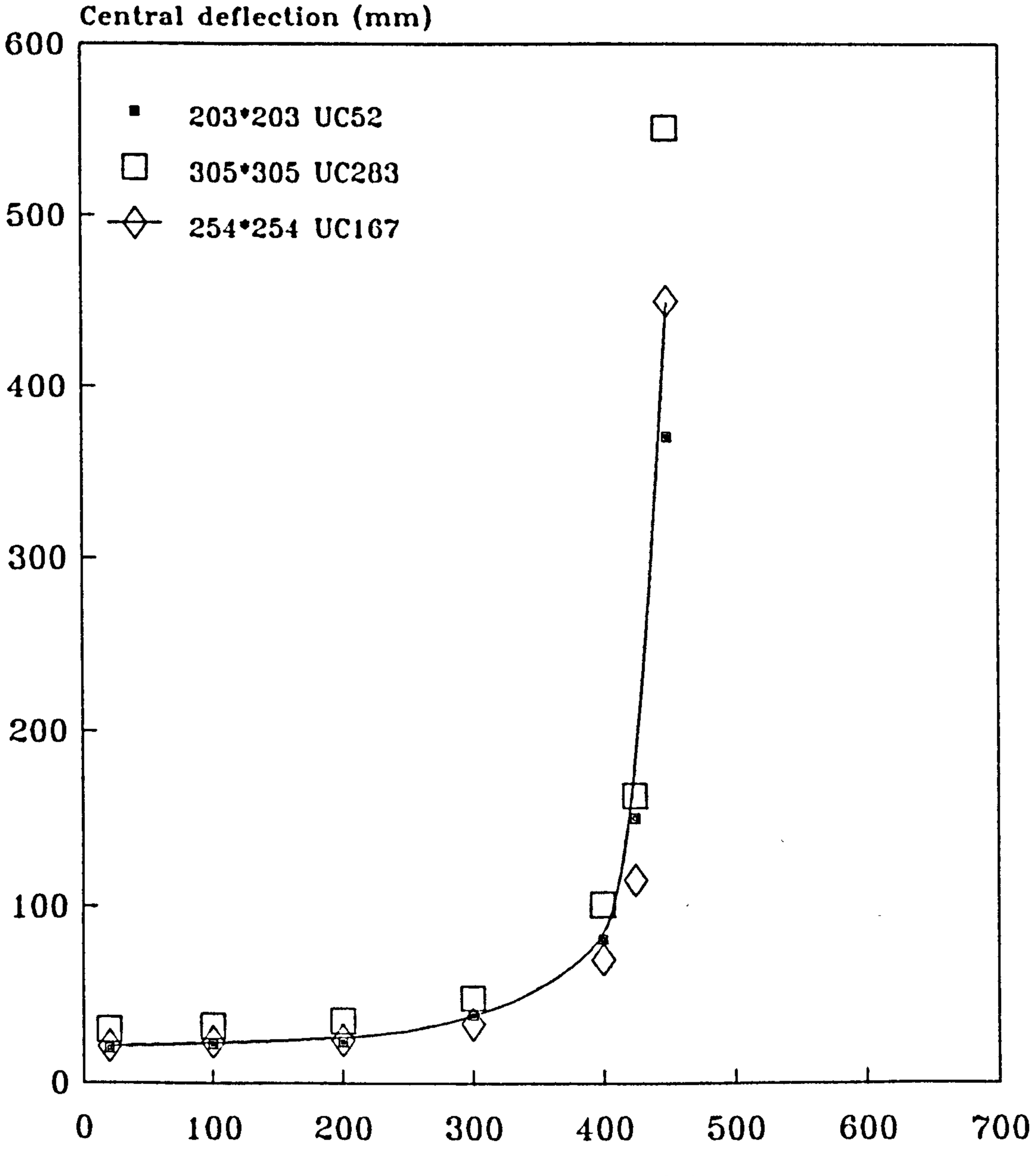

Figure 7.6: Influence of size of cross-section on the deflection of pin-ended columns for a uniform temperature profile and BS 449 design load (l/rx=80).

case. This implies that design rules can be applied generally for all column sections. It also suggests that small scale models can be used for experimental studies since the results can then be extrapolated to different sizes of cross-section provided that spot checks are made on full-scale sections. However, it must be remembered that more massive cross-sections heat up at a lower rate and hence, although the critical temperatures may be the same, the critical times will be quite different.

7.2.5 Influence of grade of steel.

In the United Kingdom the strength of structural steels is represented in terms of grades - 43, 50 and 55 for most structural steels. For grades 43, 50 and 55 the yield stress (prior to the publication of BS 5950: Part 1) were normally taken as 250 N/mm^2, 350 N/mm^2 and 425 N/mm^2 respectively. In this section the performance of columns in these grades are compared for a cross-section UC 203x203x52 kg/m and a slenderness ratio (L/r_x) of 80. The axial load (f_c/p_c) and moment (f_{bc}/p_{bc}) ratios are equal to 0.7 and 0.3 respectively.

Figure 7.7 shows the variation of deflection with temperature for the different grades of steel. It can be seen that the difference in the critical temperatures for grades 43 and 50 is only about 20°C. If the heating rate is assumed to be 15 °C/min the difference in the critical times

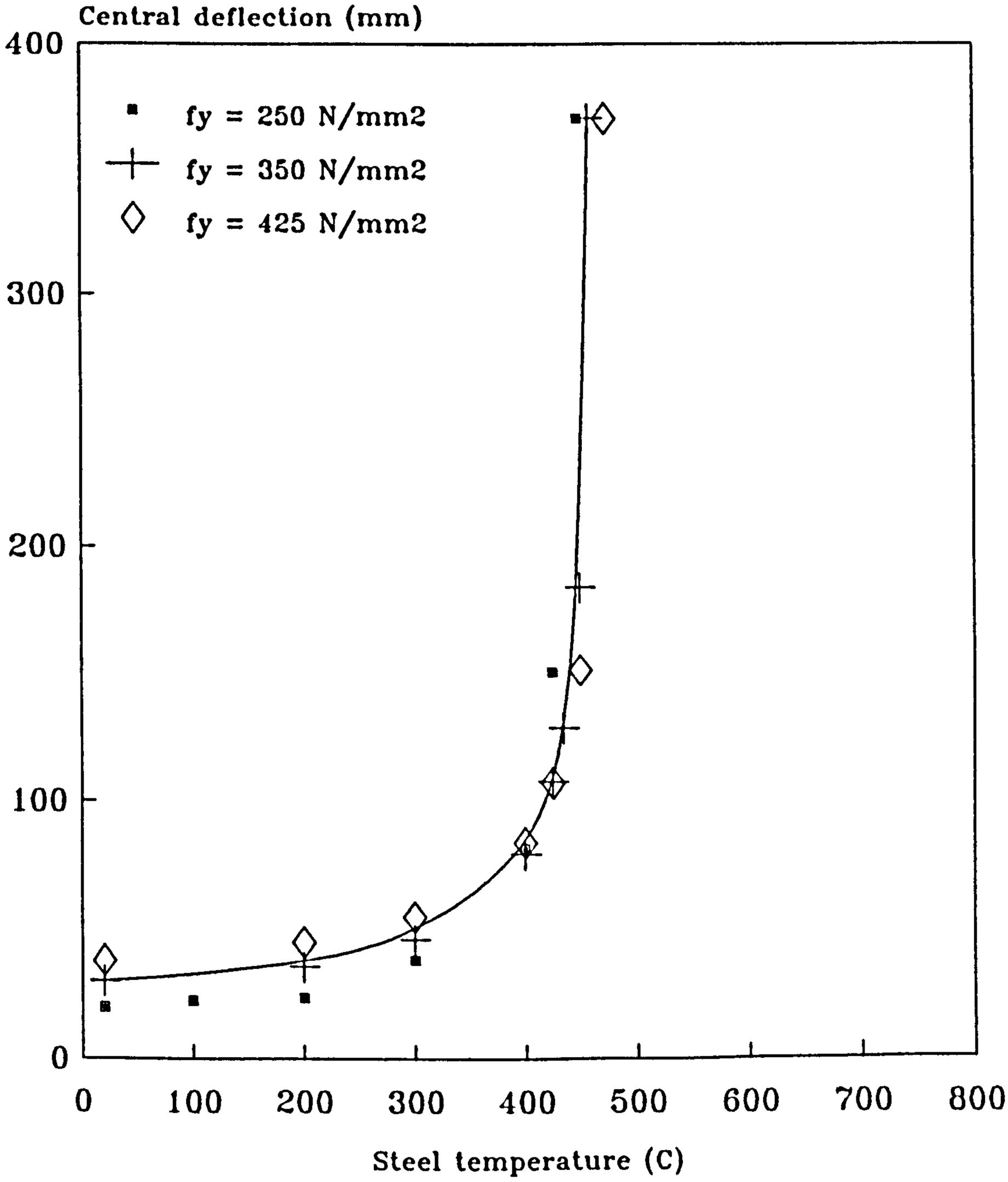

Figure 7.7: Influence of grade of steel on the deflection of a pin-ended columns for a uniform temperature profile and BS 449 design load (l/rx = 80).

is 1.5 minutes, which is not very significant. A similar improvement is observed for grade 55.

These differences are so small that in economic terms the steel grade should be selected on the basis of ambient temperature design considerations rather than introducing any aspects of fire performance. Of course, if a column section is designed on the basis of grade 43 steel and a higher grade is in fact used this constitutes a reduction in load ratio and survival time will increase as discussed in 7.2.3.

7.2.6 Influence of temperature profile along the span.

The influence of temperature profile along the member length is discussed in this section. This condition may occur when a column is heated at a certain location and the heat flows along the column length. A cross-section of UC 203x203x52 kg/m and slenderness ratio (L/r_x) of 80 are chosen for the analysis. The axial load (f_c/p_c) and moment (f_{bc}/p_{bc}) ratios are taken as 0.7 and 0.3 respectively and the idealised temperature profile is shown in Figure 7.8.

Figure 7.9 shows the variation of deflection with temperature for a uniform and a non-uniform temperature profile along the column. The steel critical temperatures for the former and latter cases are 450°C and 590°C respectively. This represents a very significant change.

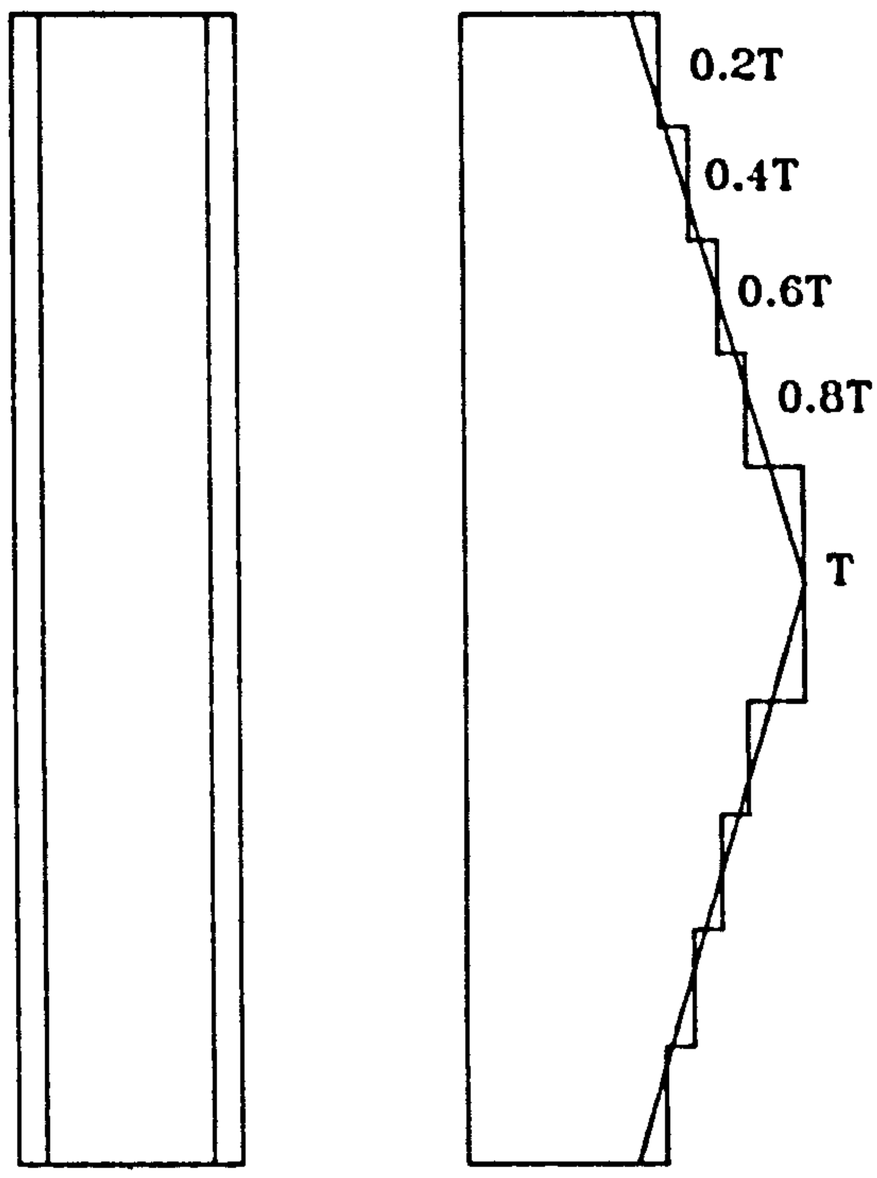

Column

Temperature profile
along the span

Figure 7.8: An idealisation of the steel temperature distribution along the length of a column in a fire compartment.

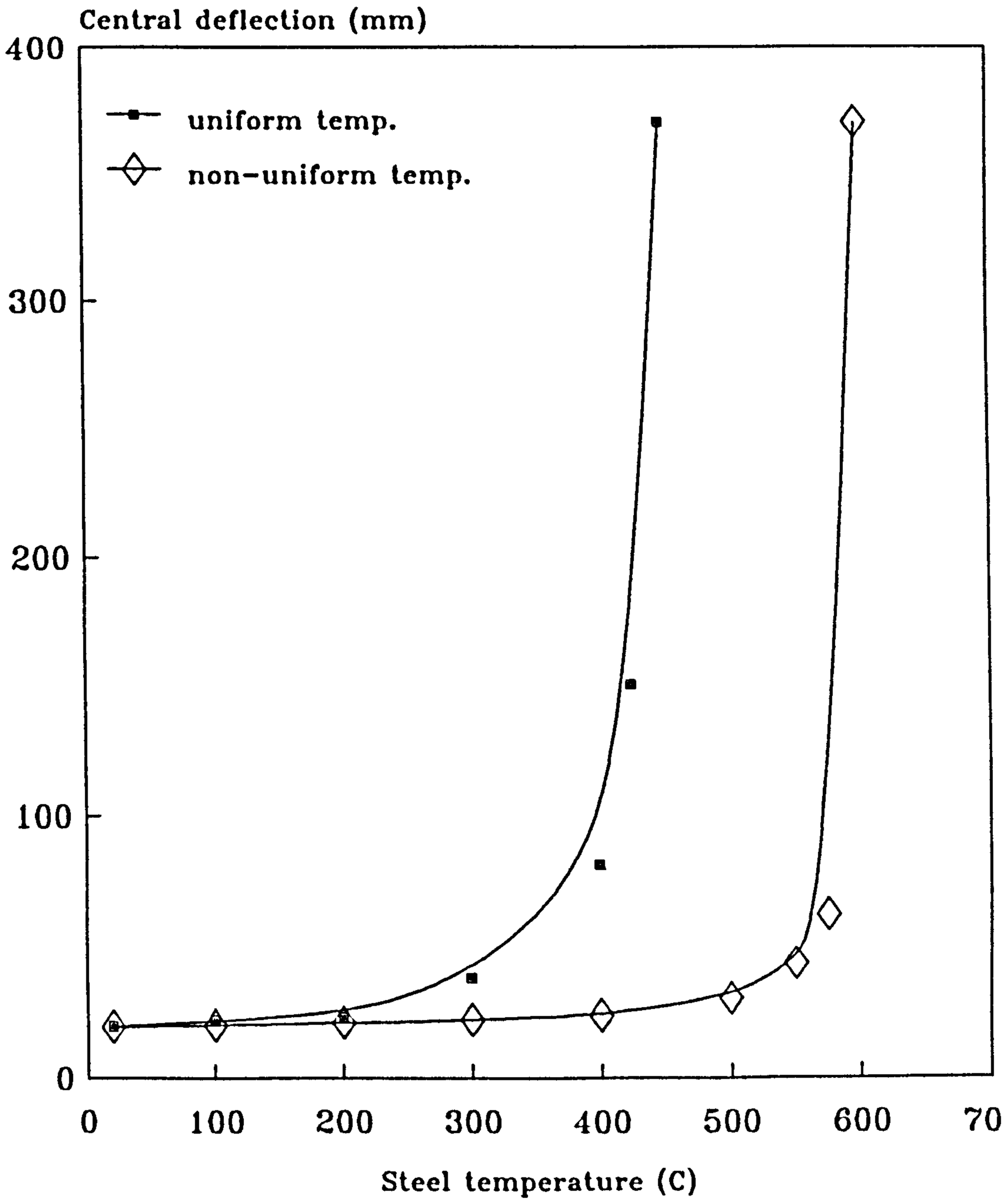

Figure 7.9: Influence of the non-uniform temperature distribution shown in Figure 7.8 on the deflection behaviour of a pin-ended column with uniform temperature profile within the section (l/rx = 80).

However the design implication of this must be limited since it is very difficult to predict, with any confidence, the precise distribution of temperature along a column length. In almost all cases it will therefore be necessary to base considerations of fire performance on a uniform temperature distribution along the column length.

7.2.7 Influence of end restraint.

Structural elements with increased end fixity have, in effect, extra strength and can consequently carry higher load. In addition such end fixity allows 'moment redistribution' to take place along the length of the member if localised yielding occurs. This is unlike the statically determinate case where the bending moment distribution is independent of whether the member is in an elastic or elasto-plastic condition. In this section the influence of end restraint is considered by comparing the behaviour of a propped cantilever and a pin-ended column of cross-section UC 203x203x52 kg/m. The length of the column, L, was taken to be 7.12m, corresponding to a slenderness ratio (L/r_x) of 80 for the pin-ended column. The axial load (f_c/p_c) and moment (f_{bc}/p_{bc}) ratios are taken as 0.7 and 0.3 respectively. In the case of propped cantilever column the length and the load ratios were unchanged, but the axial load capacity, p_c, was calculated for different effective length factors of 1.0, 0.85 and 0.7.

Figure 7.10 shows the variation of deflection with temperature for the two different types of column. Comparing the behaviour of the pin-ended column and the propped cantilever under the same load (M = 25.43kN, P = 483 kN) - that is based on an effective length factor of 1.0- the additional end restraint clearly results in a significant improvement in failure temperature, about 575°C compared with 425°C for the pin-ended condition. Of course in practice such restraint would be recognised in ambient temperature design and the axial load increased accordingly. For the end conditions considered, an effective length factor of 0.85 would be typically used in design resulting in a design load of P = 545 kN. Under this increased axial load, the failure temperature is clearly less than for the propped cantilever subject to a design load based on an effective length factor of 1.0 but is still 100°C higher than for the pin-ended case. Even when the load is increased to 599 kN which corresponds to the design load when the effective length factor is reduced to its theoretical value of 0.7, the propped cantilever maintains an improved failure temperature about 75°C above that for the pinned column. This suggests that the restraint provided at the ends of columns is of great significance in assessing the performance of column in fire, even more so than at ambient temperature, and that considerable benefit could be obtained by making use of the reserve of strength provided.

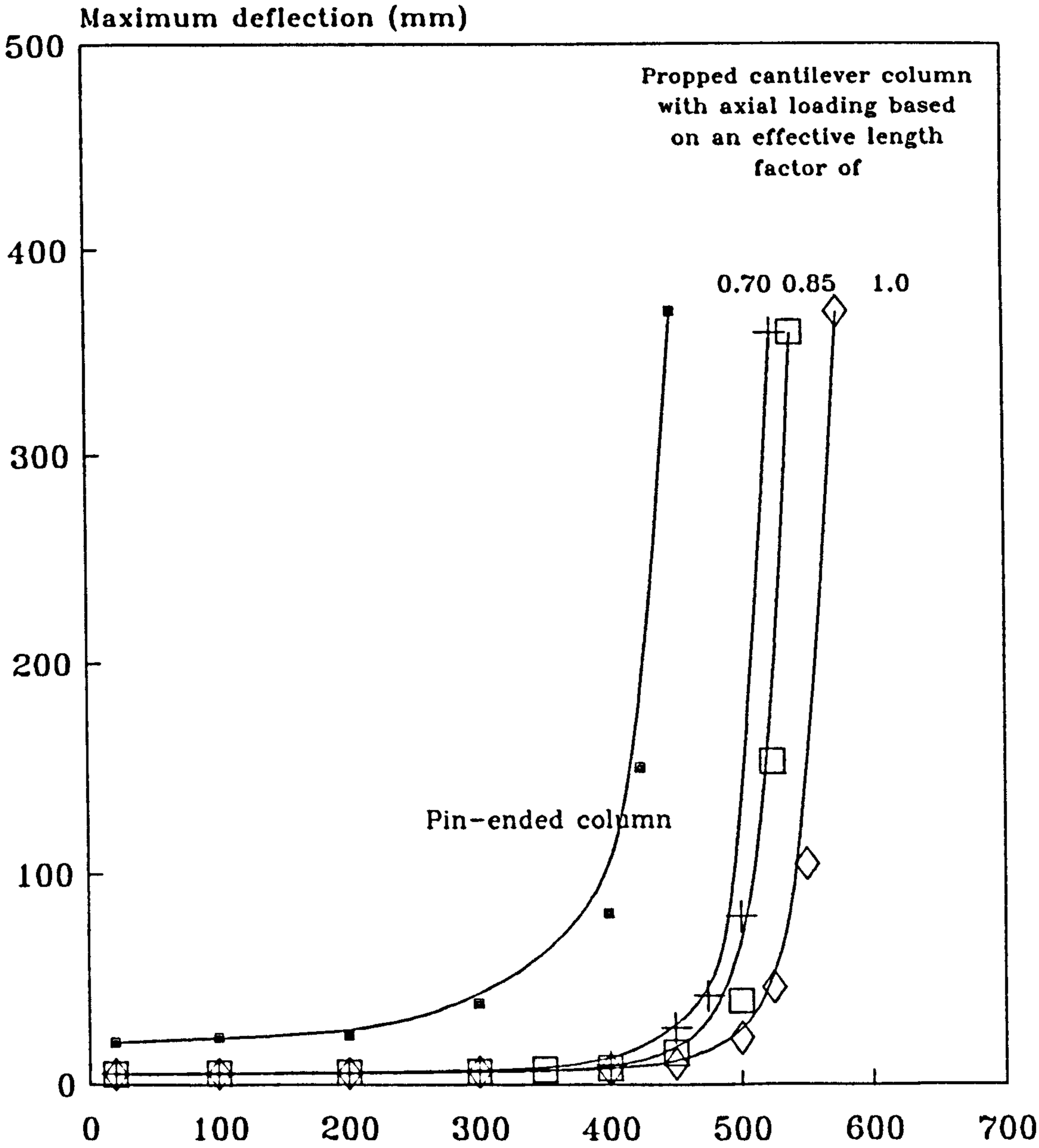

Figure 7.10: Comparison of the deflection behaviour of a pin-ended column and a propped cantilever with different axial loads based on different effective length factors for a uniform temperature profile.

7.3 PIN-ENDED COLUMN SUBJECTED TO END MOMENTS AND NON-UNIFORM TEMPERATURE PROFILE.

The behaviour of unprotected steel beams under fire conditions has been extensively discussed in reference [5]. This demonstrated that beams can survive for longer periods if the concrete floor slab is placed between the flanges of the cross-section (slim-floor construction). This is because the floor slab is providing shielding and acting as a heat sink, decreasing the steel temperature over much of its cross-section. Although the temperature profiles resulting from this lead to significant thermal bowing this has little influence on failure. However, in the case of columns thermal bowing is more critical since it may induce additional bending moments along the member due to the p-delta effect.

Typical types of partially protected steel columns include columns in walls and blocked-in-web columns as shown in Figure 7.11a. The behaviour of such partially protected pin-ended columns is discussed in this section. A cross-section of UC 203x203x52 kg/m with Young's Modulus of 205000 N/mm^2 and yield stress of 250 N/mm^2 at ambient temperature are chosen for the analysis. For the column-in-wall condition (Fig.7.11a-1) the steel temperature histories and the idealised temperature profile (as reported by Cooke [20]) within the cross-section given in Figure 7.11b are used. In the case of blocked-in-web columns (Fig.7.11a-2)

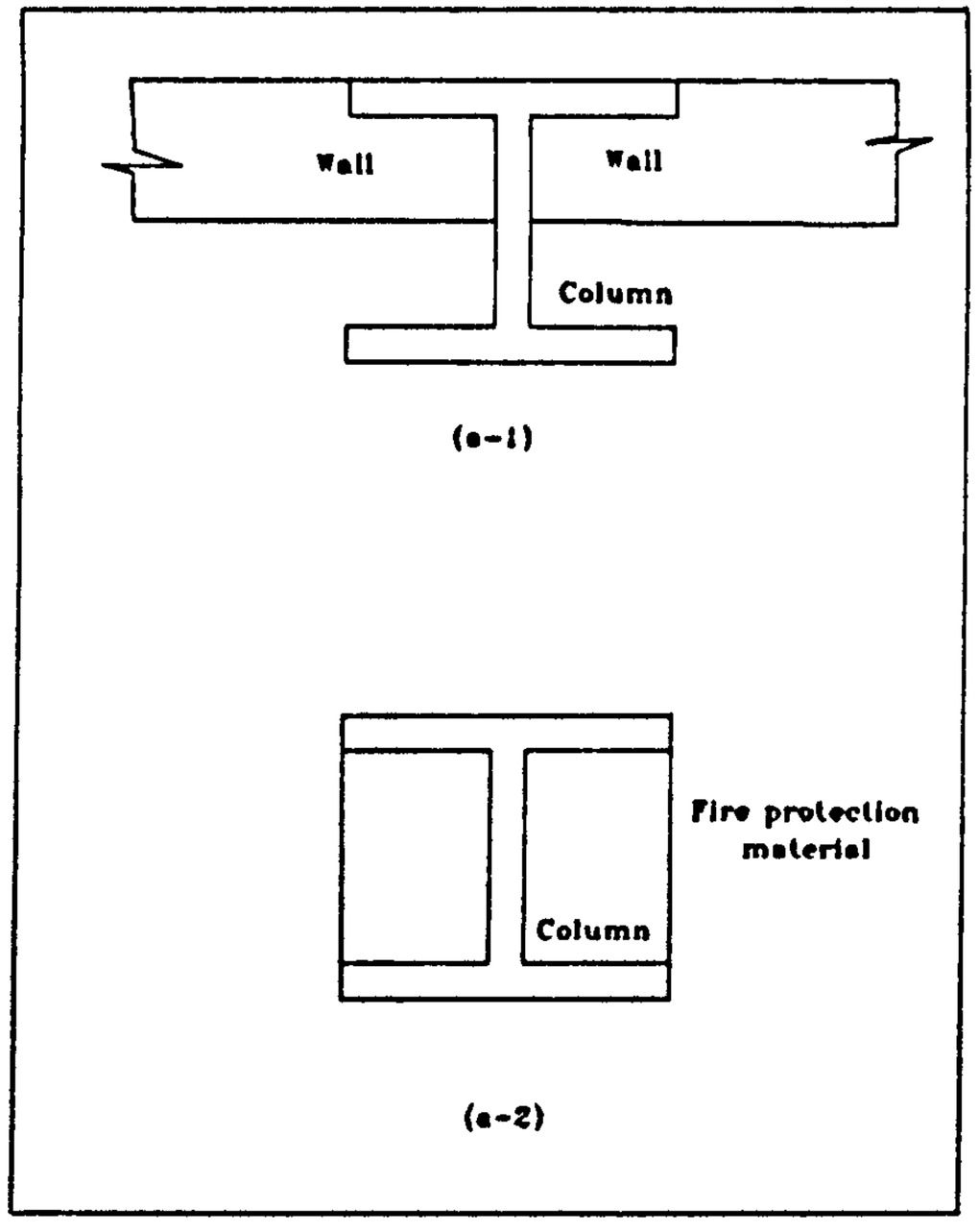

(a) Different types of partially protected steel column.

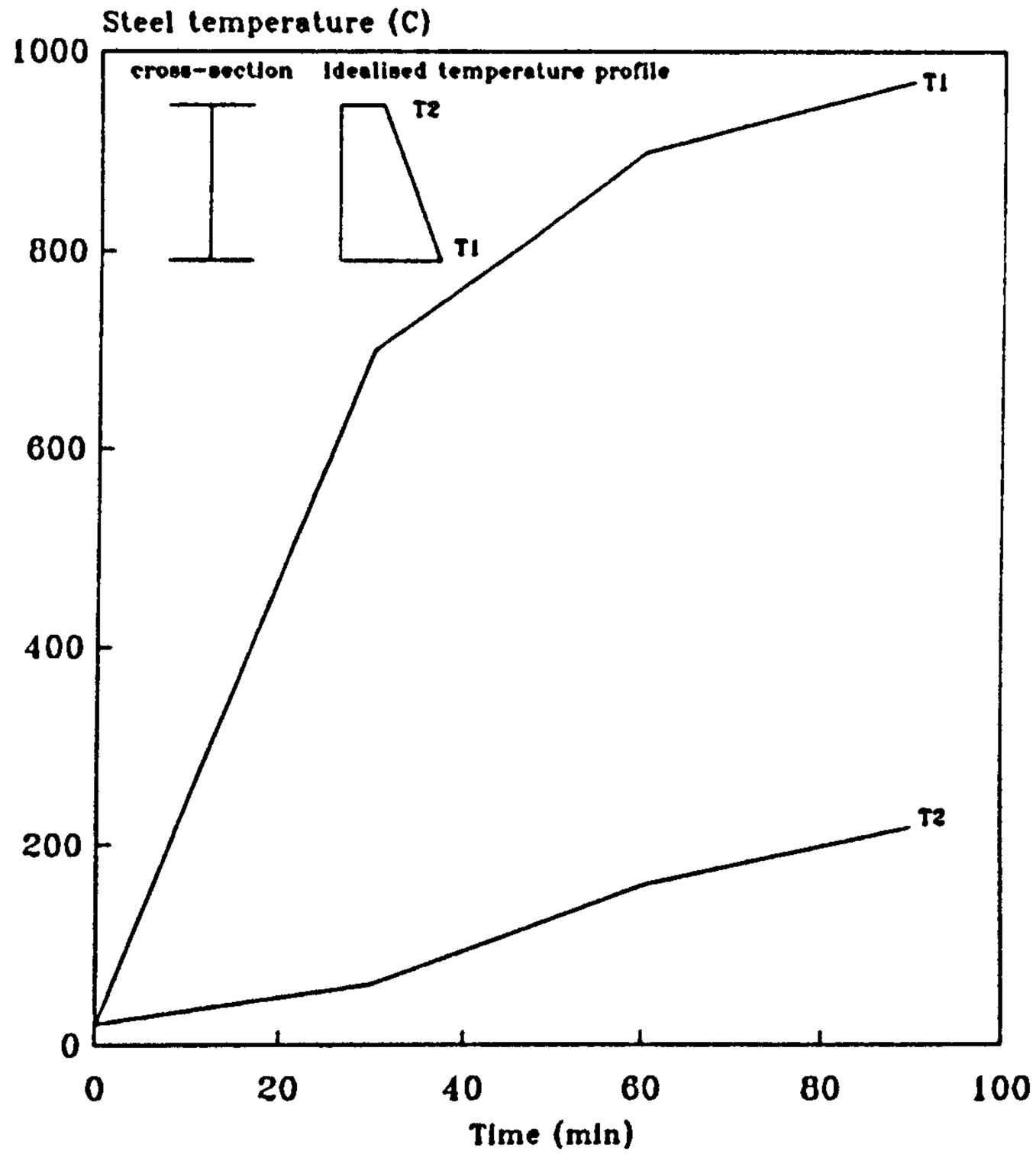

(b) Steel temperature history for column in wall.

Figure 7.11: Different types of partially protected steel columns and steel temperature history for column in wall as reported by Cooke [20].

the steel temperature histories and the idealised profile within the section are obtained from Figures 6.25 and 6.26b respectively. Various parameters are considered, including slenderness ratio (L/r_x), axial load and moment. It should be noted that in the study on the influence of end moments a positive sign indicates that the moment is applied in the same sense as thermal bowing while a negative sign indicates that it is in the opposite direction. In all cases the moment distribution along the length of the column is uniform.

7.3.1 The influence of different types of partially protected column.

The influence of the different types of partial protection is illustrated in Figure 7.12 for the UC 203x203x52 kg/m with a slenderness ratio (L/r_x) of 80. The steel temperature histories are as described in Section 7.3. The axial load (f_c/p_c) and moment (f_{bc}/p_{bc}) ratios are assumed to be 0.7 and 0.3 respectively.

Figure 7.12 shows for the column-in-wall construction, that even though the wall is acting as a heat sink and consequently reducing the steel temperature, it causes significant thermal bowing. This in turn creates additional bending moment due to the p-delta effect. As a result the critical temperature is only about 300°C, some 100°C lower than for a bare column, which is also shown in

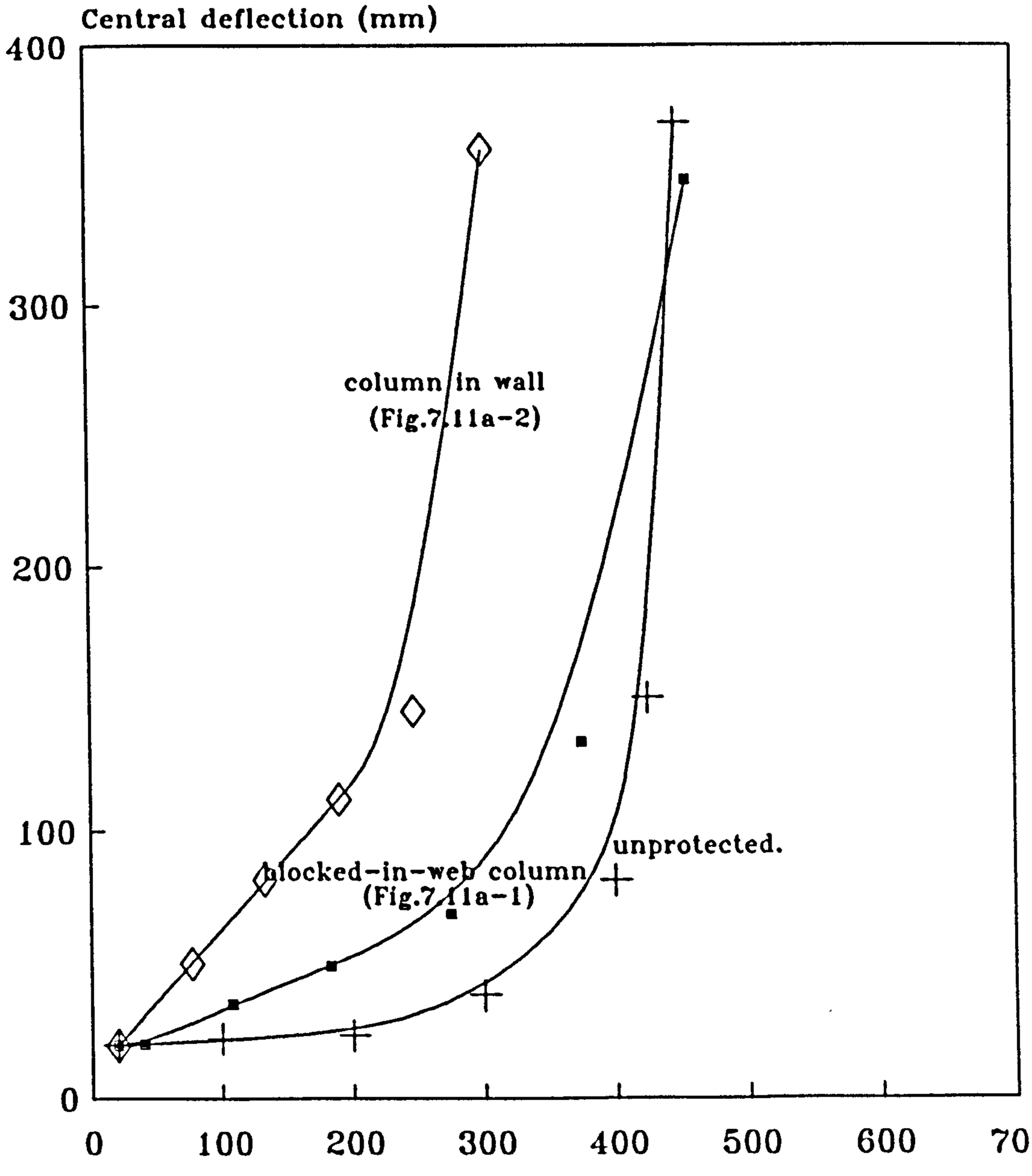

Figure 7.12: Comparison of the deflection history for columns with different degrees of protection.

Figure 7.12 for reference. The blocked-in-web column achieves a higher steel critical temperature of about 425°C. This is because thermal bowing is avoided while the steel temperature is reduced. Although this is a relatively small improvement compared with the unprotected column, experimental evidence indicates that the rate of temperature increase is reduced considerably by blocking in of the web. The improvement in critical time is therefore much more significant.

7.3.2 Influence of slenderness ratio.

The behaviour of partially protected (column-in-wall) pin-ended columns has been analysed for slenderness ratios (L/r_x) of 40, 60 and 80. The axial load (f_c/p_c) and moment (f_{bc}/p_{bc}) ratios are taken as 0.7 and 0.3 respectively.

Figures 7.13 and 7.14 show the deformation histories of unprotected and partially protected steel columns for slenderness ratios of 40 and 80. These show that the effect of the partial protection is to increase the steel critical temperature for a column with a slenderness ratio of 40 but to reduce it in the case of the more slender column. This happens because, even though the steel temperature within the cross-section is relatively low, the influence of thermal bowing is dominant. This not only causes lateral deformation in its own right but also leads to a considerable amount of extra moment due to the p-delta

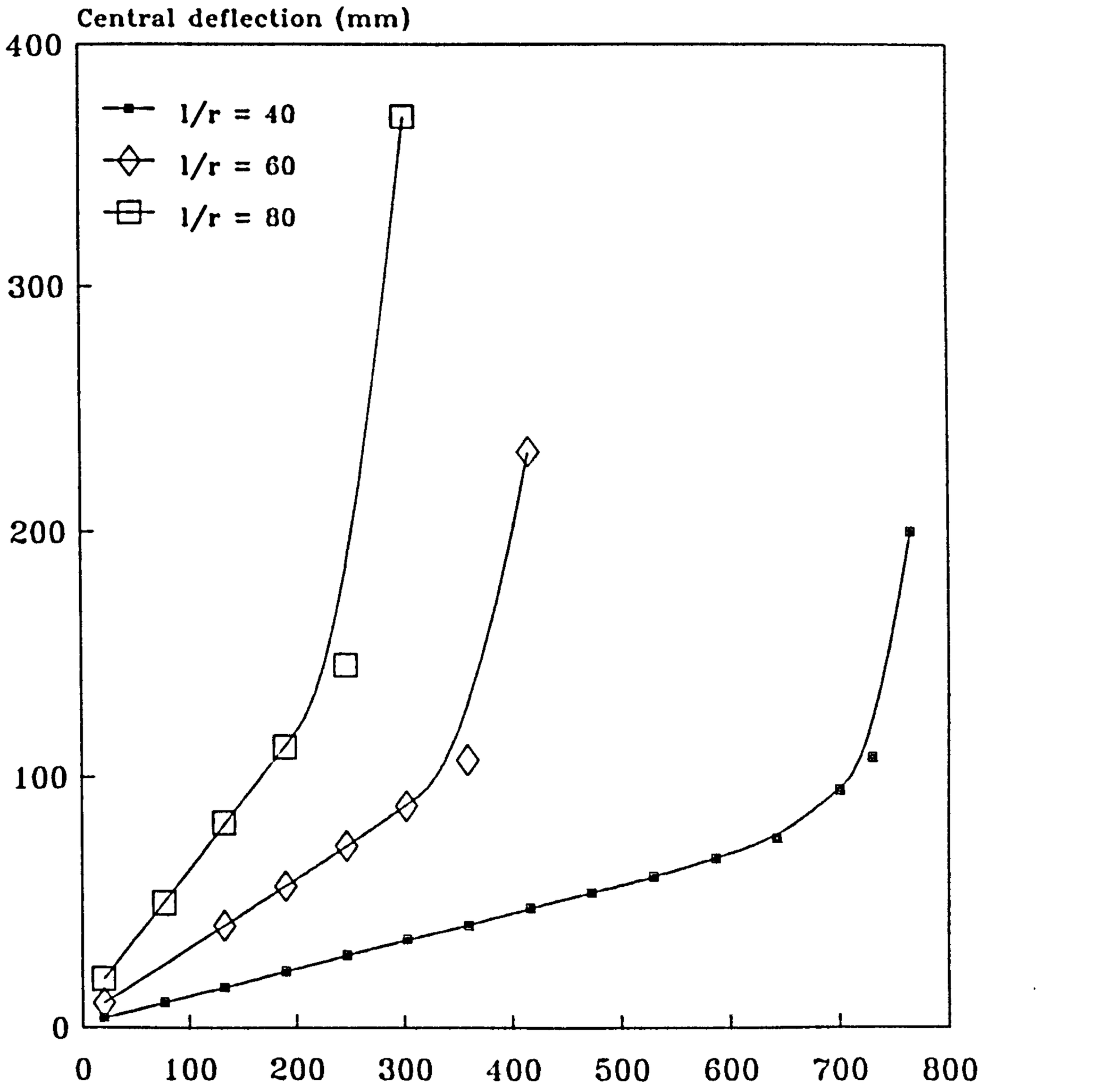

Figure 7.13: Change of deflection with temperature for columns-in-walls of different slenderness ratios at BS 449 design load.

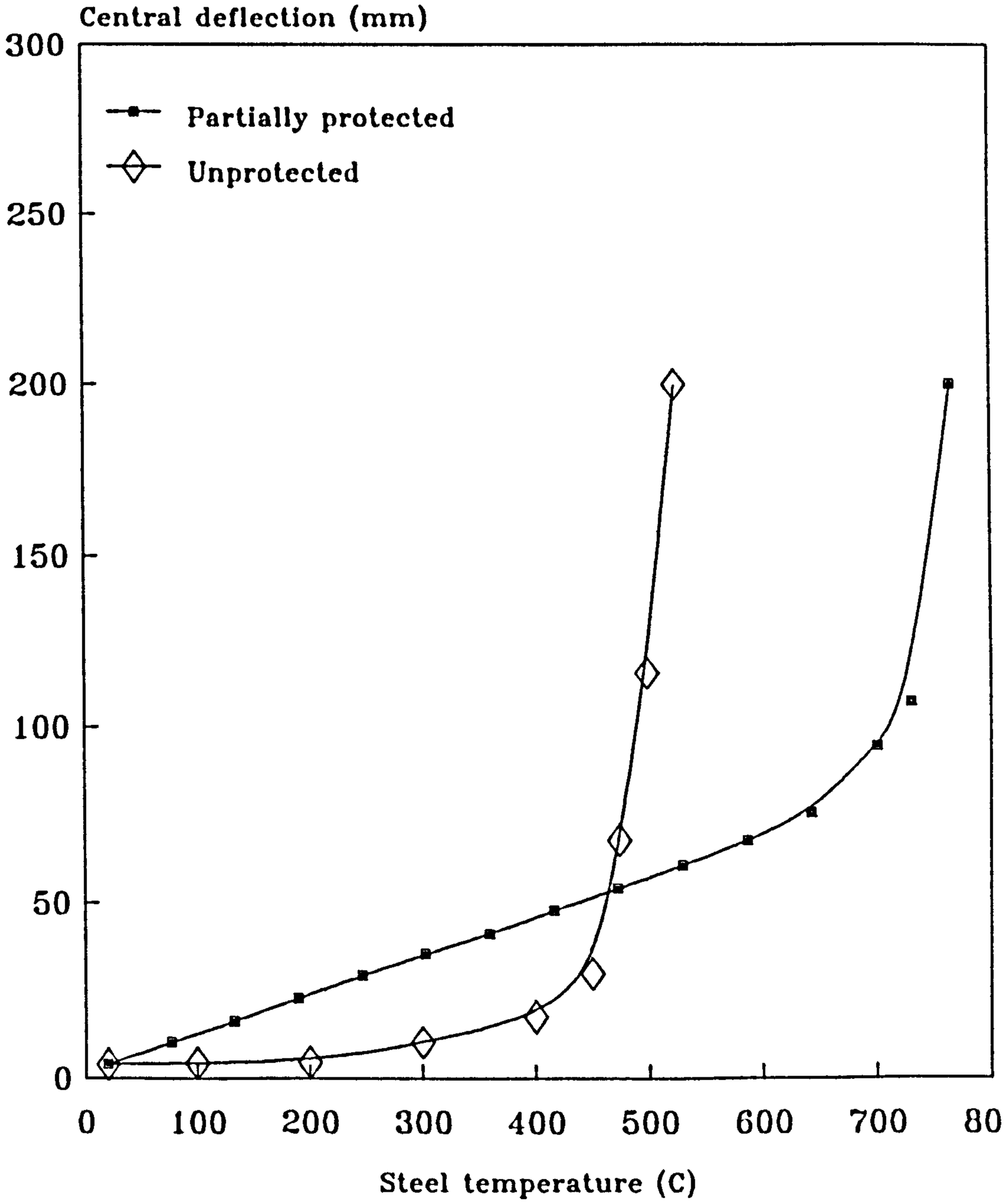

Figure 7.14: Comparison of the deflection behaviour of an unprotected column and a column in wall (l/rx = 40).

effect. Clearly a much more detailed investigation of this is required if designers are to be able to take advantage of such partial protection.

Figure 7.15 shows the variation of deflection of columns with temperature for the different slenderness ratios. The critical temperature for slenderness ratios of 40, 60 and 80 are equal to 750°C, 425°C and 310°C respectively.

7.3.3 Influence of end moments.

The influence of end moments on columns in walls is discussed in this section. A slenderness ratio (L/r_x) of 80 and an axial load ratio (f_c/p_c) of 0.7 are chosen for the analysis. Moment ratios of -0.3, 0.1 and 0.3 are used in this study. The negative sign indicates that the moments cause bending in the opposite direction from the thermal bowing.

Figure 7.16 shows the variation of deflection with temperature for a constant axial load but with different magnitudes of end moments. The figure shows that survival is enhanced with reduced end moments. For moment ratios of 0.3 and 0.1 the critical temperatures are 310°C and 425°C respectively. This suggests that significant improvements could be achieved in practice by minimising the degree of eccentricity of the column loads. The figure also shows that by applying the same end moments but in the opposite

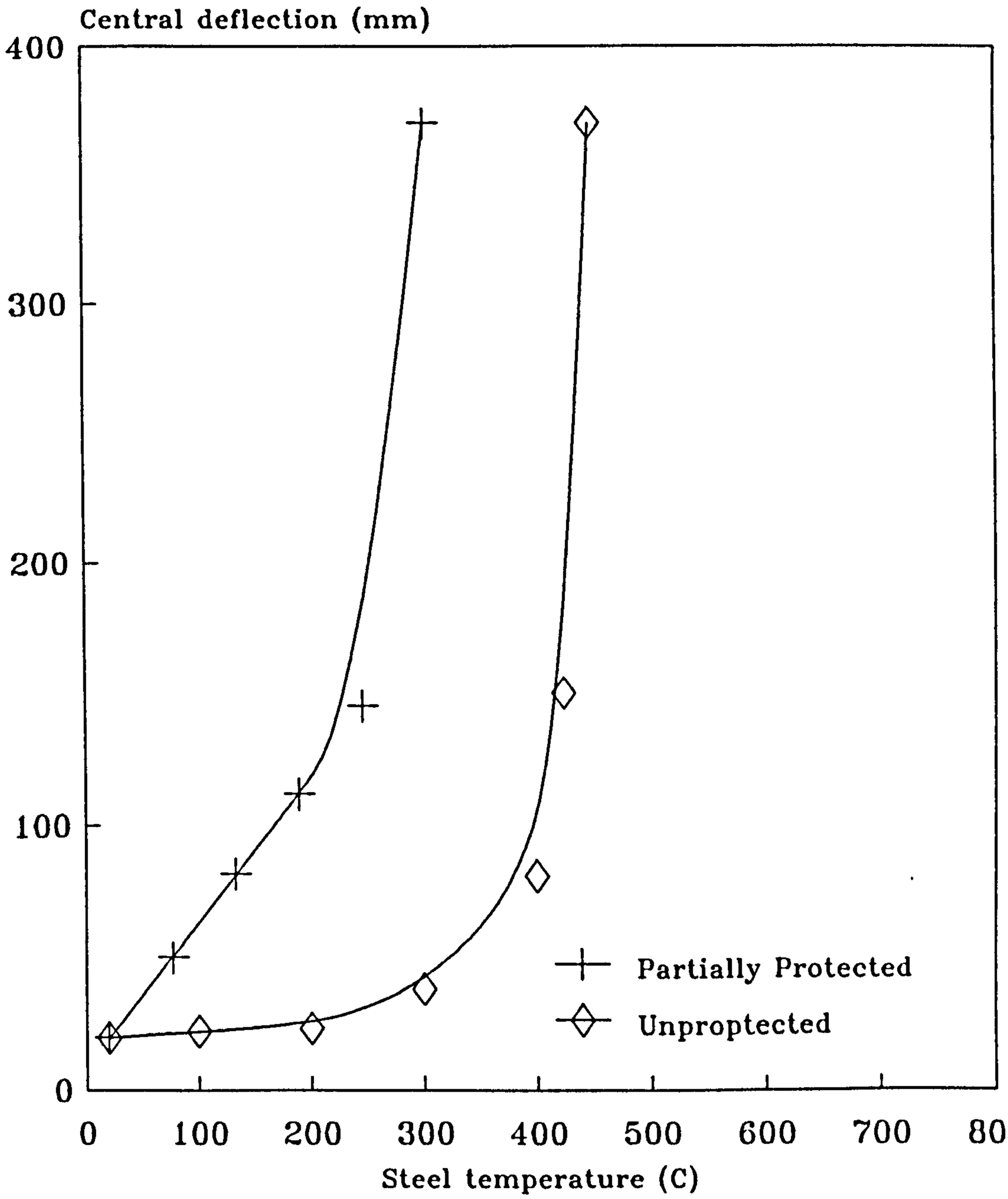

Figure 7.15: Comparison of the deflection behaviour of an unprotected column and a column in wall (l/rx = 80).

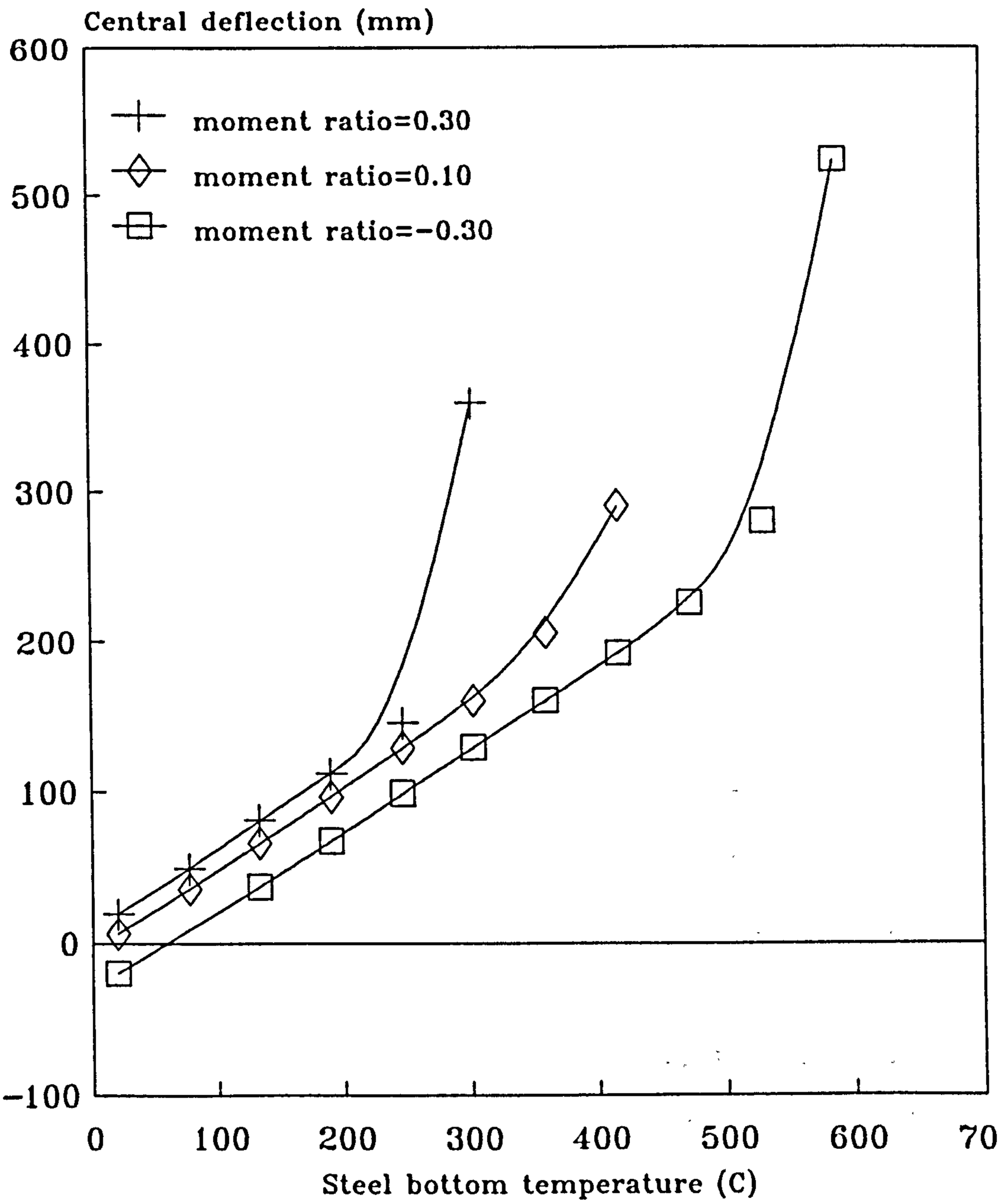

Figure 7.16: Change of deflection with temperature for a pin-ended column with a constant axial stress and different bending stress levels and a non-uniform temperature profile.

direction to the thermal bowing the steel critical temperature is increased up to 580°C. Further studies need to be carried, including the case with varying bending moment distribution along the column length, before these finding can be interpreted for practical design.

7.3.4 Influence of axial force.

The influence of axial force on partially protected steel columns (Fig.7.11a-1) is discussed in this section. A slenderness ratio (L/r_x) of 80, a moment ratio (f_{bc}/p_{bc}) of 0.3 and axial load ratios (f_c/p_c) of 0.7 and 0.35 are assumed.

Figure 7.17 shows the variation of deflection with temperature for constant end moment but at different magnitudes of axial load. This indicates that higher axial force results in a decrease in the steel critical temperature of the column from about 650°C to 310°C for axial load ratios (f_c/p_c) of 0.35 and 0.7 respectively. This is because of the effect of the design load ratio: the higher failure temperature corresponds to an equivalent load ratio ($f_c/p_c + f_{bc}/p_{bc}$) of 0.65 compared with 1.0 for the lower failure temperature. However, in practice this must be justified economically for design purposes if such oversizing of members is to be used.

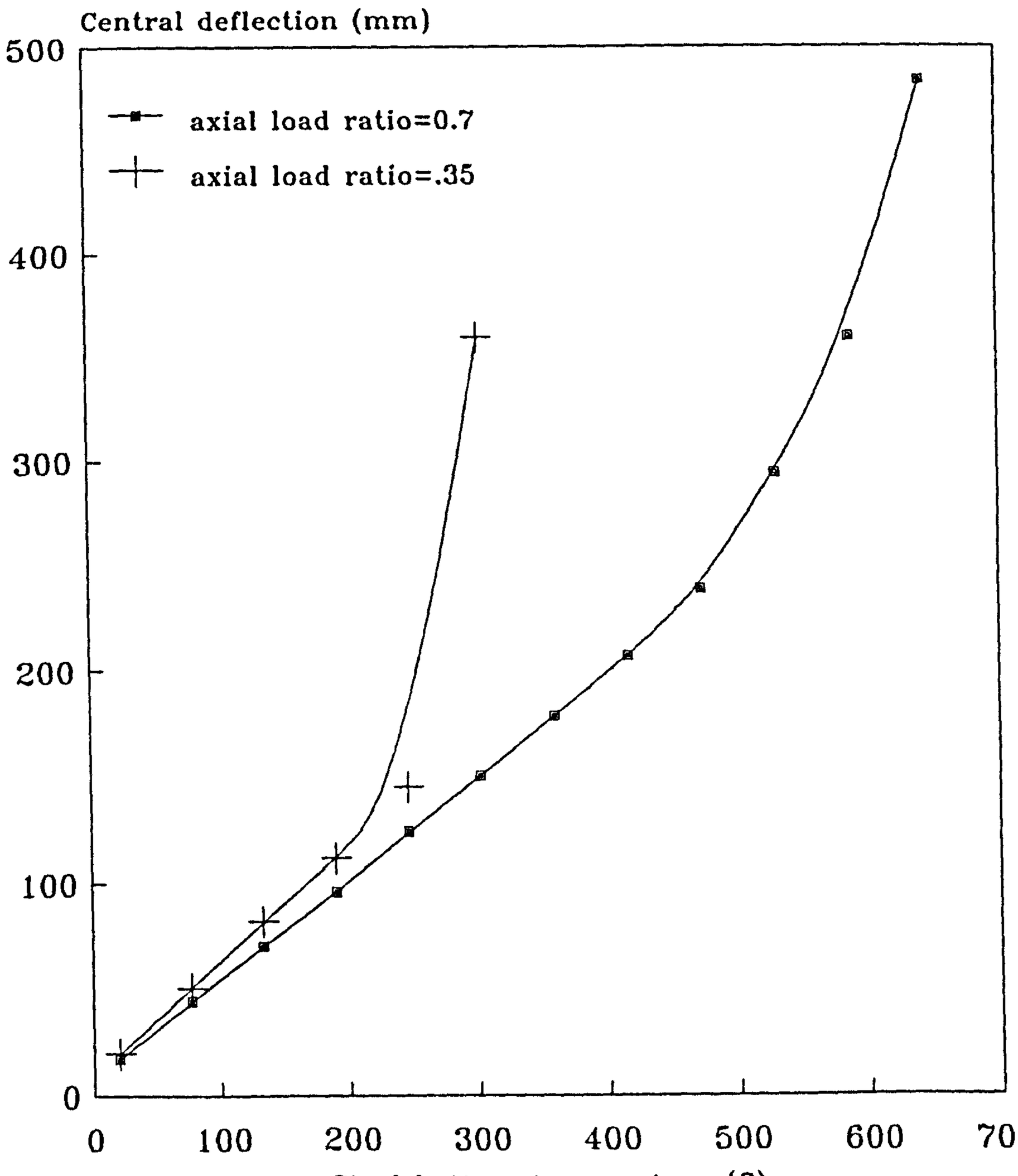

Figure 7.17: Change of deflection with temperature for a pin-ended column with a constant bending stress and different axial stress levels (l/rx = 80) and a non-uniform temperature profile.

7.4 SIMPLE PORTAL FRAME IN FIRE.

The influence of factors which might affect the behaviour of simple portal frames in fire is discussed in this section. Frame details are shown in Figure 7.18a, with a column height H and beam span L equal to 3m and 5m respectively. A uniformly distributed load is applied to the beam while each column is subjected to an axial superimposed load P. A column of UC 203x203x52 kg/m and beam of UB 406x178x54 kg/m are used for the analysis. Young's Modulus and yield stress at ambient temperature are assumed to be 205000 N/mm² and 250 N/mm² respectively. The steel temperature histories of the beam and columns are obtained from tests carried out on a similar frame [96]. Together with the idealised temperature profiles within the section these are shown in Figures 6.25 and 6.26.

The loads were calculated on the basis of design loads considering the members to be independent - that is the beam is assumed to be simply supported on the column.

7.4.1 Typical behaviour of beam and column in frames in fire.

The performance of the steel members forming part of the frame in fire can be assessed by conducting standard fire tests. However, these tests cannot easily account for the

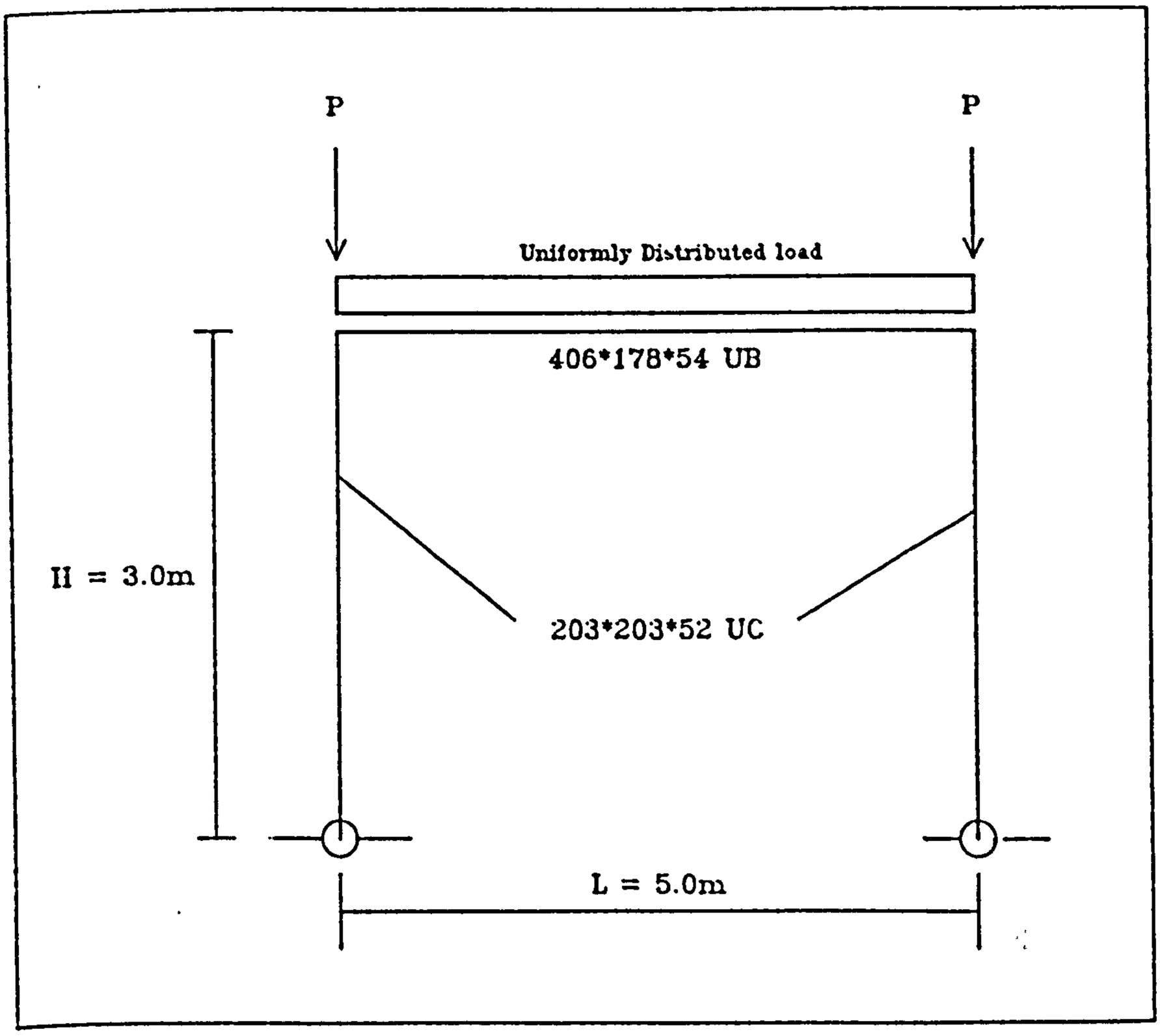

Figure 7.18a: Details of frame considered in all subsequent figures.

interaction of the beam and column, which has a significant effect on the structural behaviour. Analytical methods, however, offer an opportunity to investigate this interaction. For this reason the behaviour of beam within the frame is analysed and compared with the performance of an isolated beam. It should be noted that in both cases appropriate design loads are used.

Figures 7.18b and 7.18c show the deformation histories for the beam under these two assumptions. The figures show that the isolated beam reaches its critical temperature earlier than when considered as part of the frame structure. The difference in critical temperature and time are about 100°C and 2 minutes respectively. It can therefore be concluded that fire tests on a single member do not give a very good assessment of the structural performance for interconnected members although the results are conservative. More accurate results could be obtained from a full scale frame test but the cost of such tests is likely to be prohibitive. Analytical methods however provide an efficient means of studying this problem.

7.4.2 Effect of load level in beam.

The influence of design stress on the structural performance of beams forming part of a frame structure is discussed in this section. The column is assumed to be subjected to its maximum design load ($f_c/p_c + f_{bc}/p_{bc} = 1.0$) but the

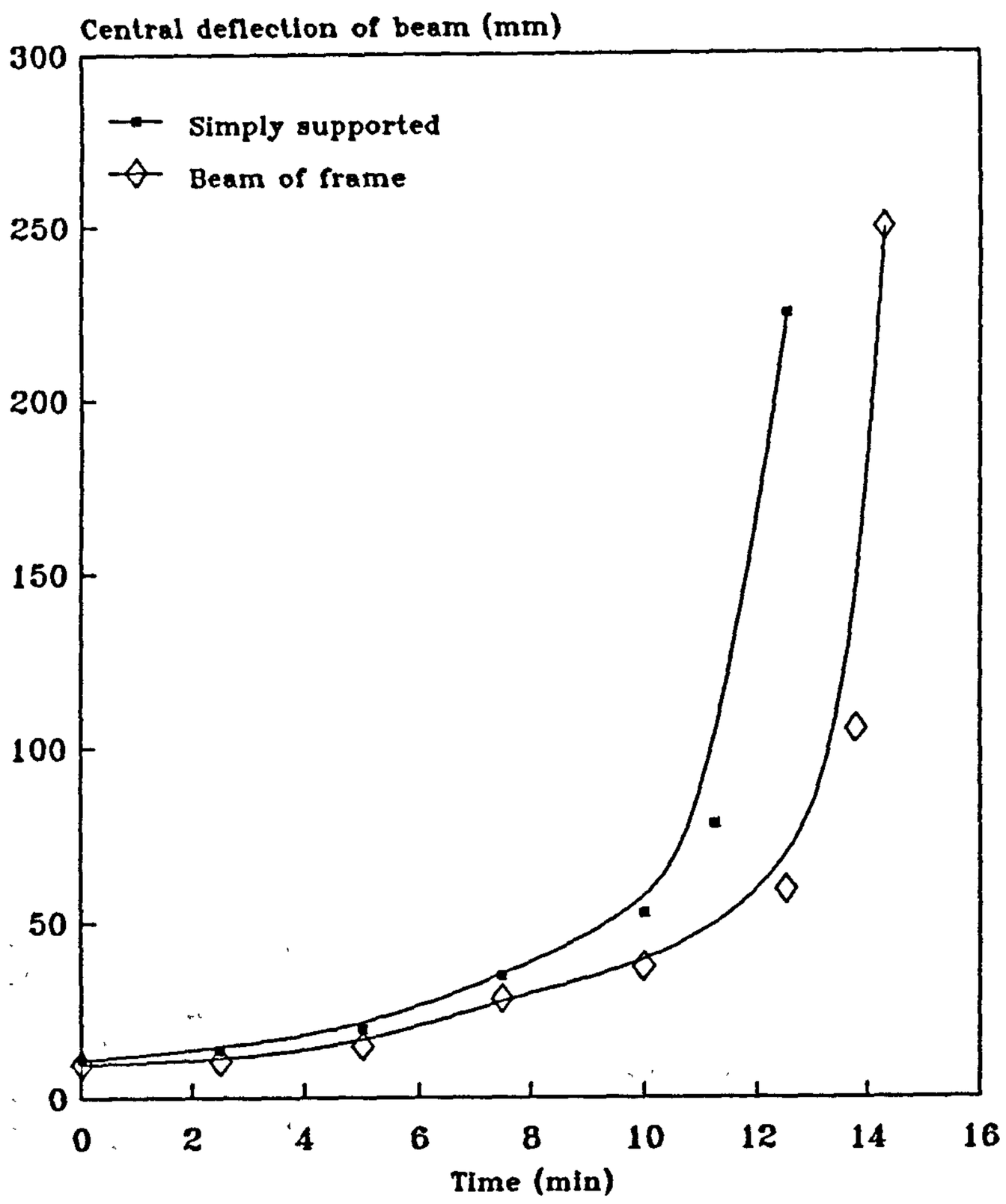

Figure 7.18b: Comparison of the central deflection–time relationship of the beam when considered as simply supported beam and part of the frame.

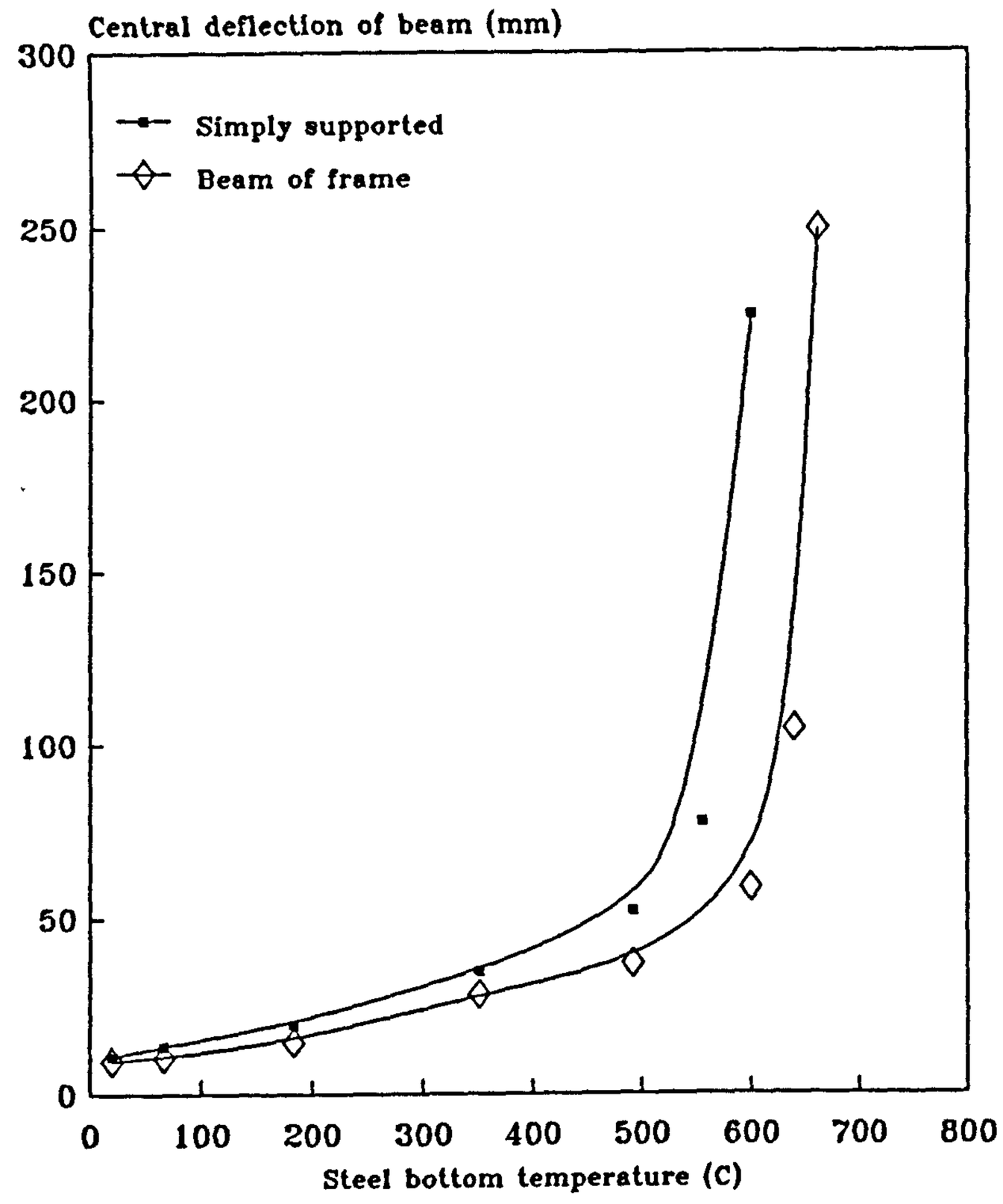

Figure 7.18c: Comparison of the central deflection–temperature relationship of the beam when considered as simply supported beam and as part of the frame.

lateral load acting on the beam is varied. Again the design load for the beam is based on the assumption that the beam is simply supported. Two values of loads are considered, corresponding to full design load and 50% of design load. The load on the column is in fact a combination of the beam reaction (wL/2) and axial load P acting at the centre of the cross-section. The beam reaction gives rise to a bending moment in the column, M_{ecc}. For the purpose of design this is assumed to be:

$$M_{ecc} = ewL/2 \quad \ldots\ldots\ldots (7.2)$$

where e = eccentricity = h/2

h = depth of column cross-section.

w = uniformly distributed load along the beam.

L = span of beam.

This value of bending moment can then be used to determine the moment ratio (f_{bc}/p_{bc}). The additional axial load applied to the column is then calculated such that $f_c/p_c + f_{bc}/p_{bc} = 1.0$.

Figures 7.19 and 7.20 show the influence of design stress within the beam on the deflected shapes of the beam and column in fire. Figure 7.19(a) shows that the critical bottom flange temperature of the beam is 640°C for a design stress equal to $0.66f_y$. This increases to 725°C for a design stress of $0.33f_y$. Again this indicates that the

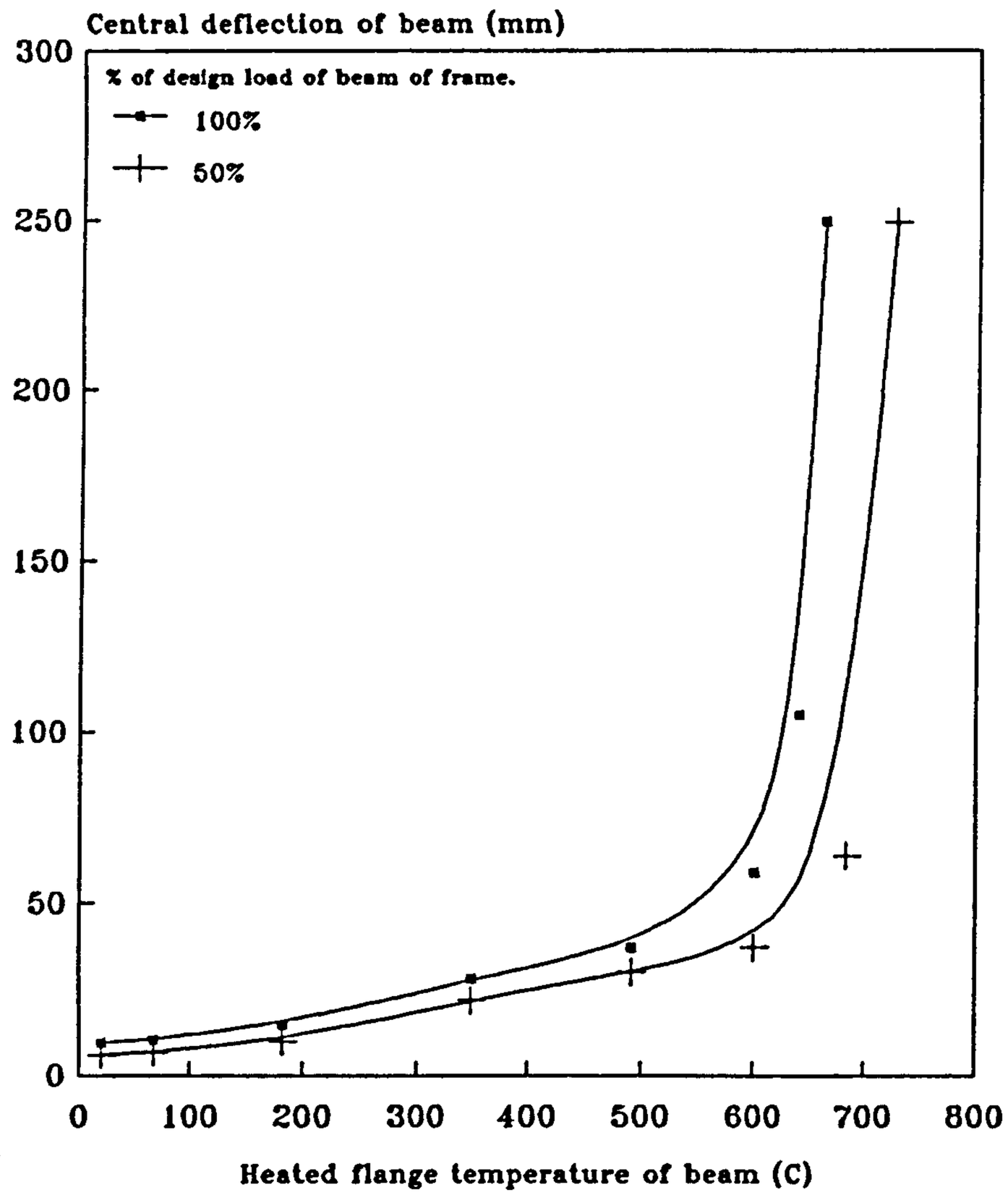

(a)

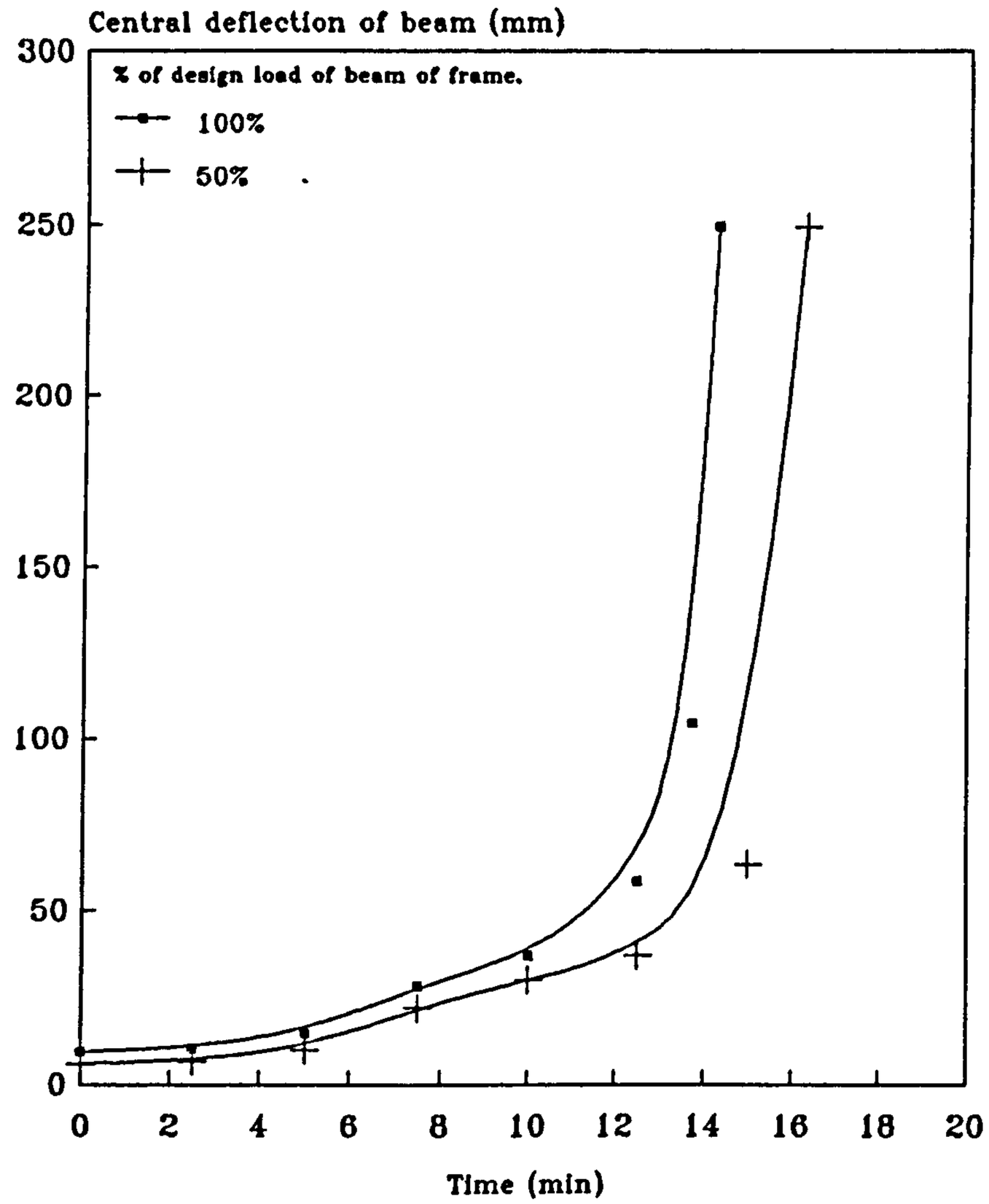

(b)

Figure 7.19: Effect of load level on the behaviour of the beam shown in Figure 7.18a.

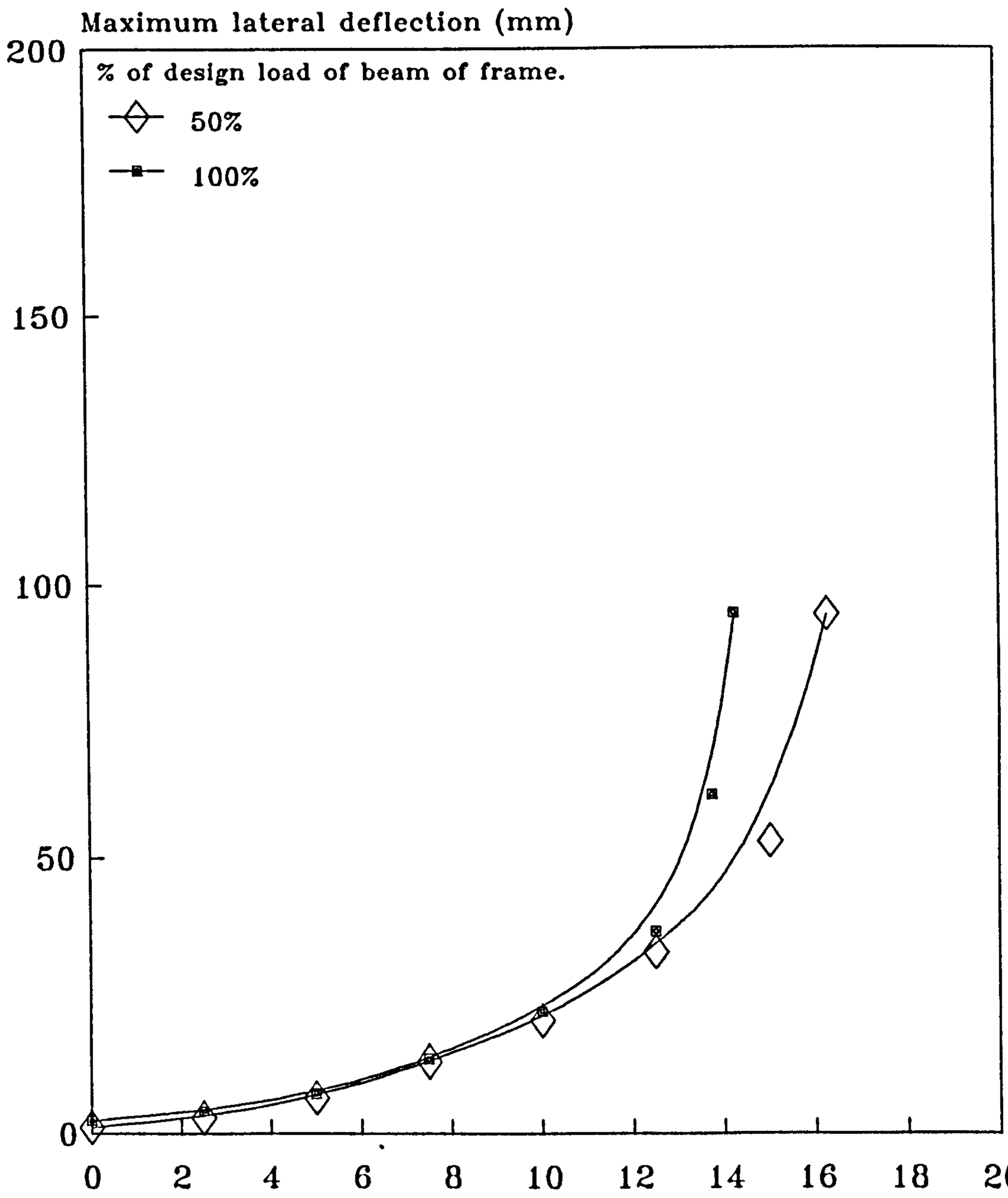

Figure 7.20: Variation of maximum lateral deformation of column with time for fully loaded and half loaded beam.

stocky (l/r_x = 40). Clearly a wider range of slenderness ratios for both columns and beams within frames should be included in a more thorough investigation.

Figures 7.21 and 7.22 show the deflected shape of the column and beam as part of a frame when both are subjected to their maximum design loads, at time intervals within the standard fire equal to 2.5, 5.0 and 7.5 minutes. The figures show the increase in deformation as the temperature increases.

7.4.3 Influence of axial load on column.

The influence of axial load on the structural performance of the frame in fire is discussed in this section. The beam is assumed to be subjected to its maximum design stress (f_{bc}/p_{bc} = 1.0) but the axial load acting on the column is varied.

Figures 7.23 and 7.24 show the lateral deflection of the beam and column with time and temperature respectively for design load ratios ($f_c/p_c + f_{bc}/p_{bc}$) for the column of 1.0 and 0.75. The figures show that when the design load ratio of the column is reduced from 1.0 to 0.75 the difference in the critical temperature and time are about 125°C and 3 minutes respectively. This again shows that the failure temperature can be increased by reducing the amount of axial load acting on the column even though the beam is still subjected to a maximum design stress.

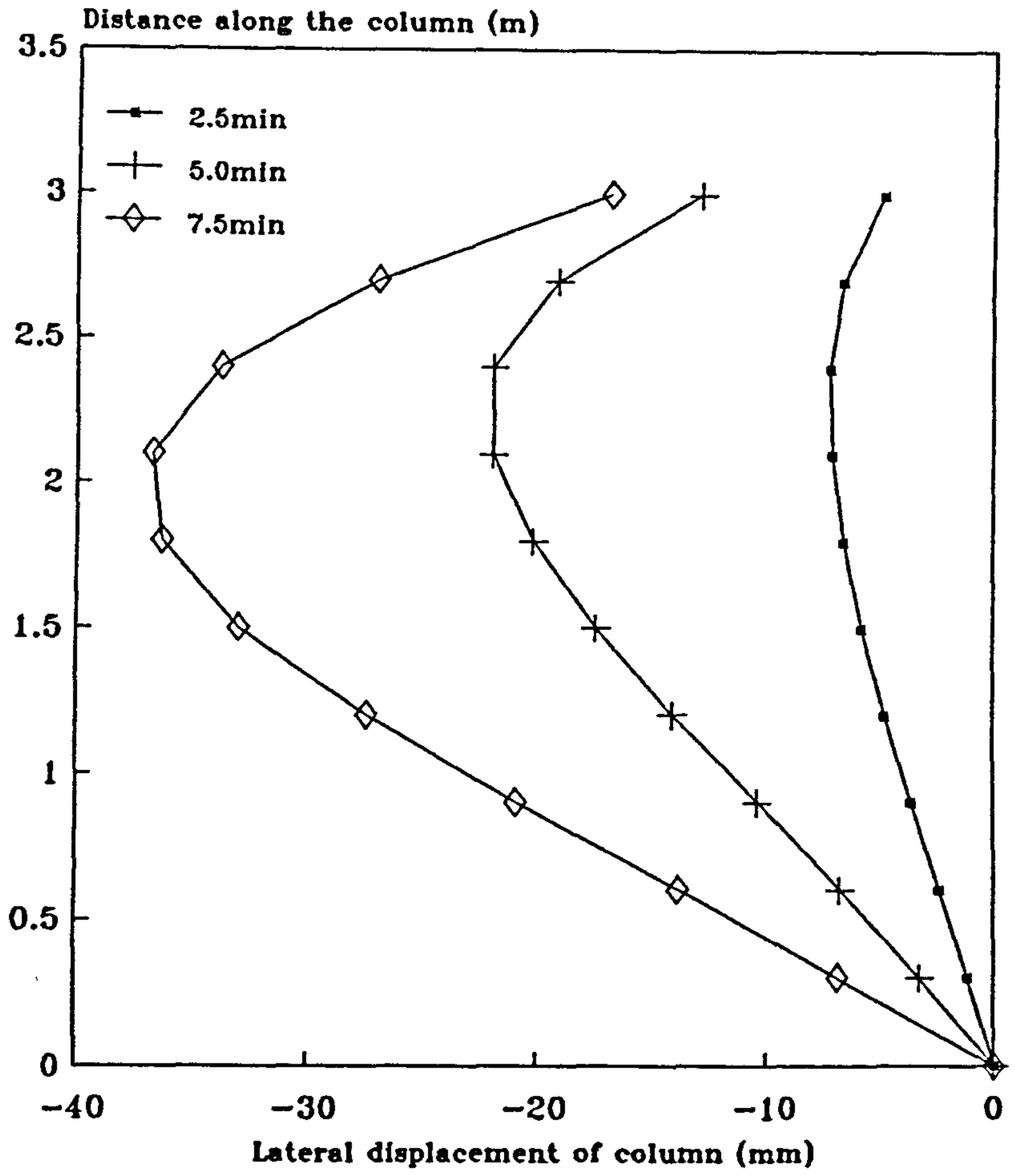

Figure 7.21: Lateral displacements of column at different times.

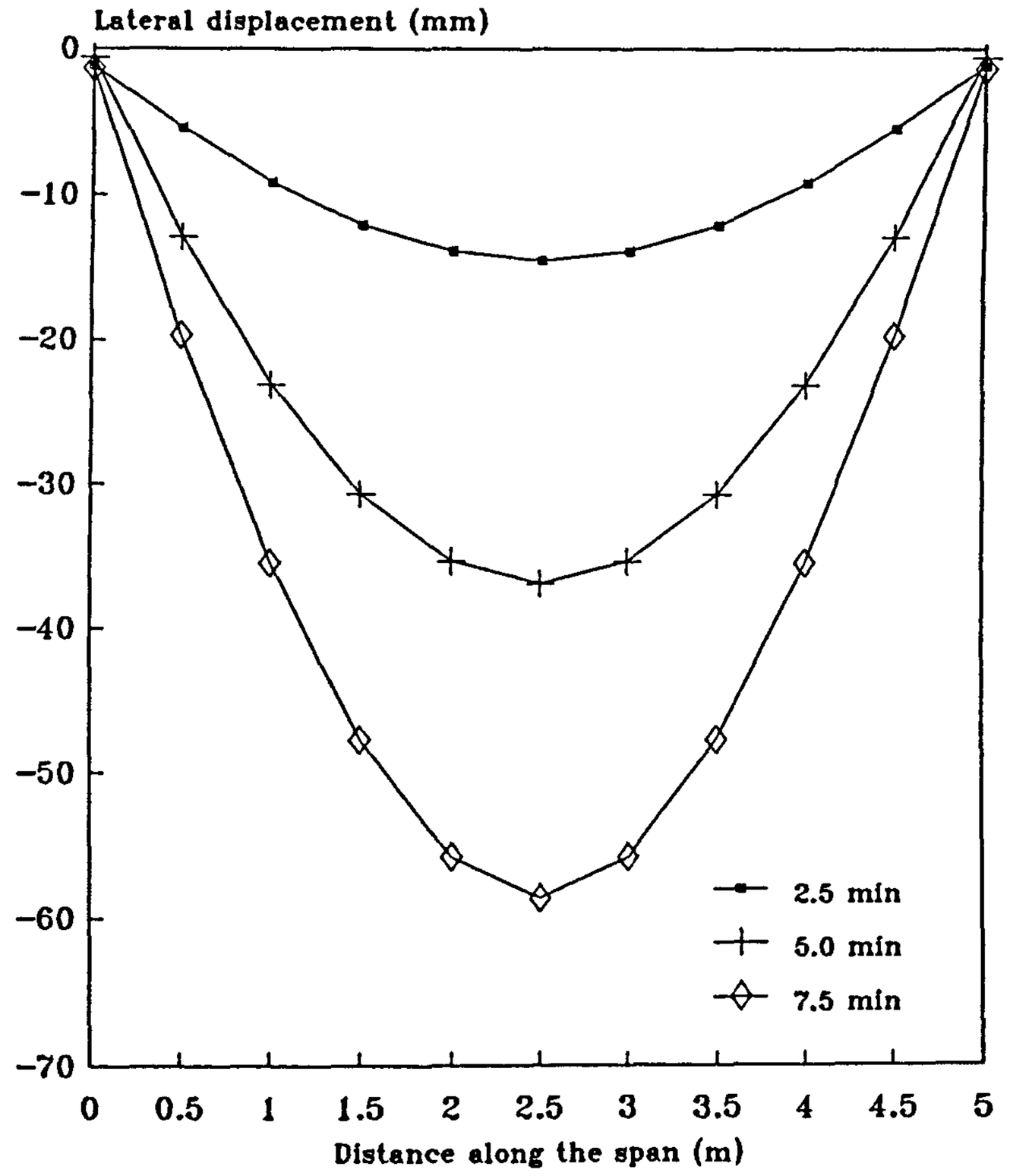

Figure 7.22: Lateral displacements of beam at different times.

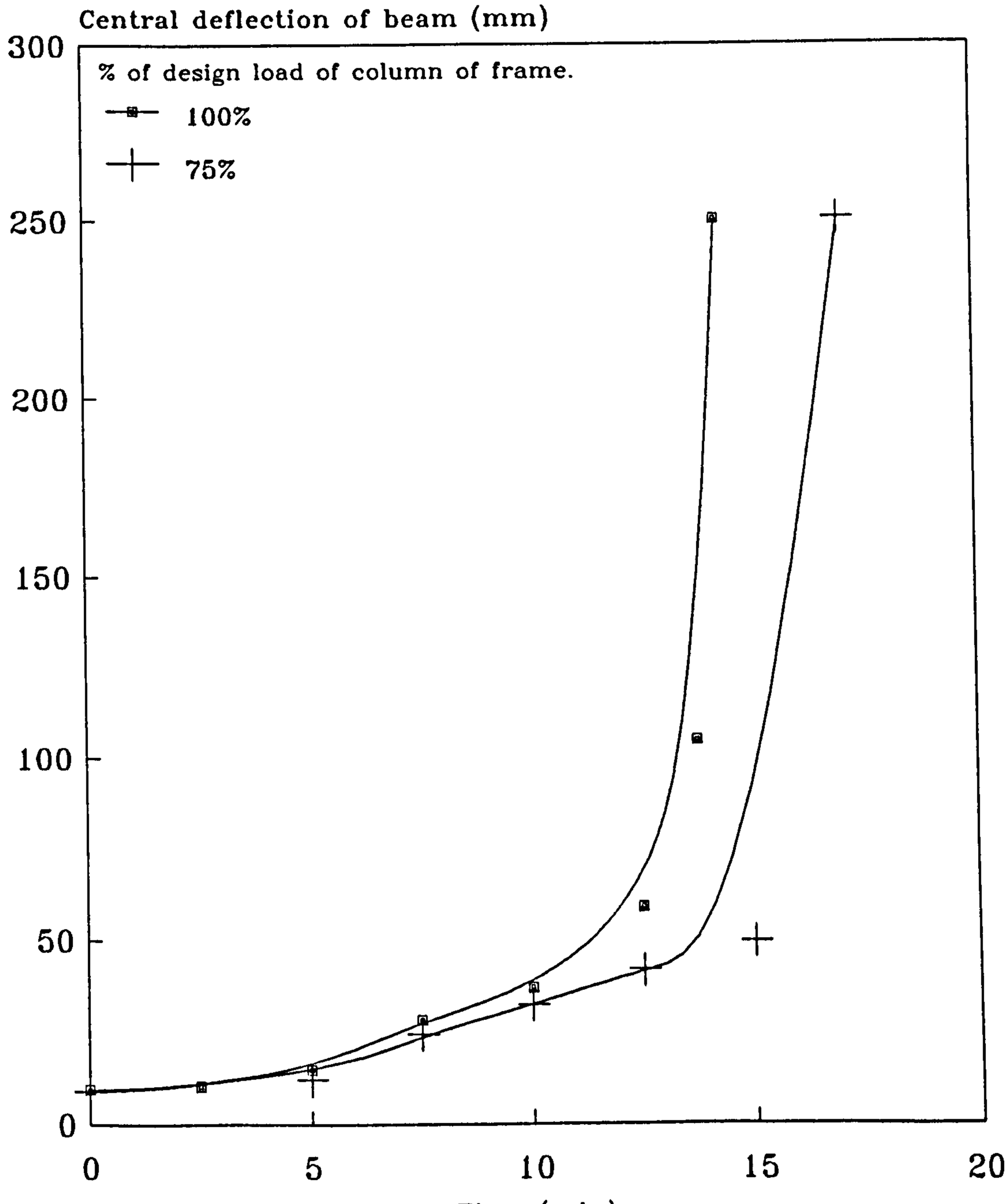

Figure 7.23: Variation of the central deflection of beam with time for different column loads.

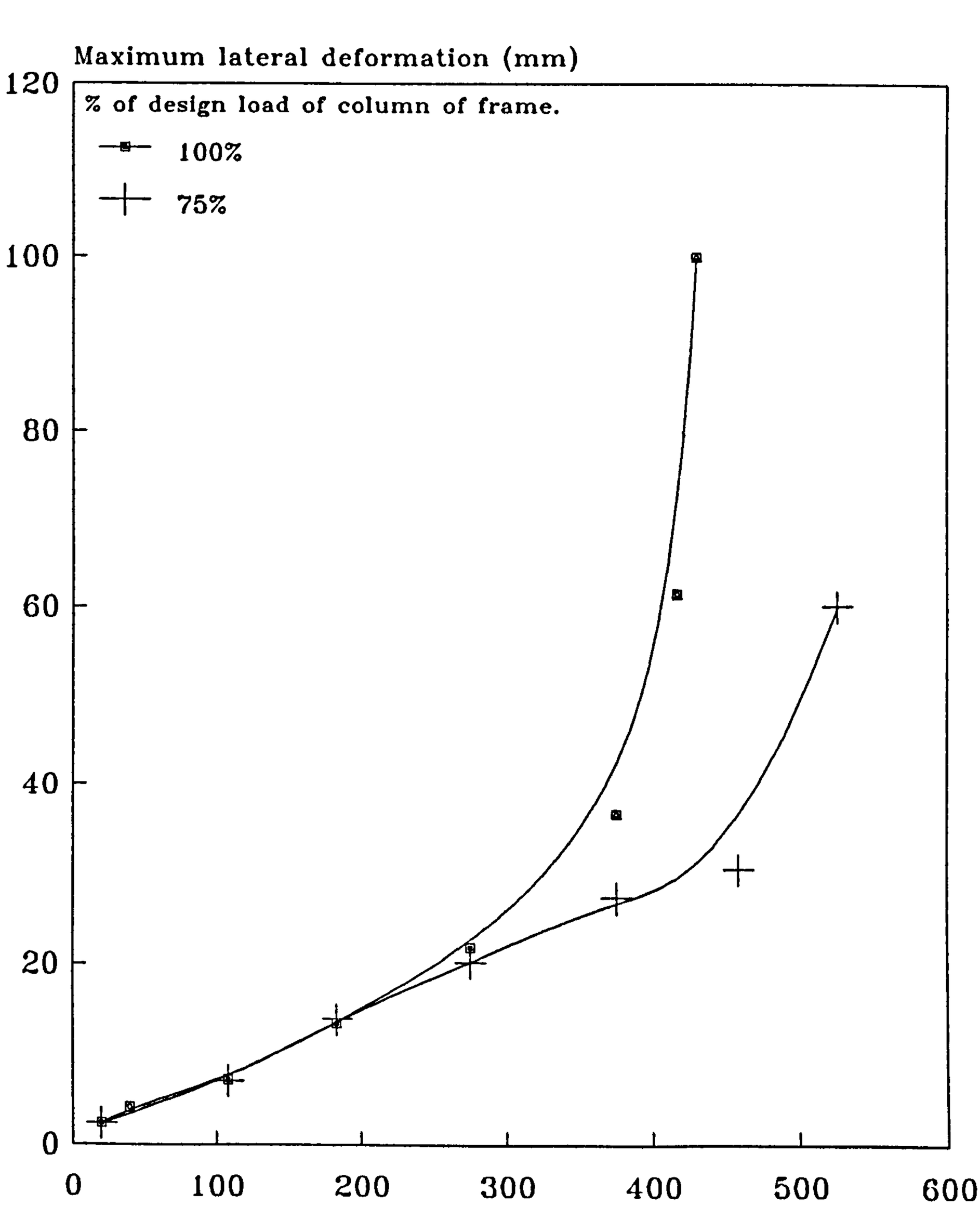

Figure 7.24: Variation of maximum lateral deformation of column with temperature for different column loads.

respectively. This again shows that the failure temperature can be increased by reducing the amount of axial load acting on the column even though the beam is still subjected to a maximum design stress.

7.5 CONCLUSIONS.

Several conclusions are indicated by this limited study. The investigation is no more than a preliminary study of various influences, and clearly more rigorous examination is needed if firm conclusions are to be drawn. Nevertheless the following points can be noted:

1. The variation of steel temperature along the span of a beam or column should be included in the frame analysis if this information is reliably available since the improvement in the critical temperature compared with the uniformly heated case is significant.

2.The steel critical temperature can be increased by reducing the design load, that is by reducing the axial load or end moment as a proportion of the member capacity by using a bigger cross-section. However this must be justified economically.

3. It has been noted that beam-columns subject to the same load ratio but due to different proportions of axial load and bending moment have the same critical temperature. This

should enable interaction curves relating the end moments, axial load and steel critical temperatures for any size of cross-section to be constructed. It also suggests that, fire tests on small scale models could be used to supplement full scale experimental data and analytical results.

4. For columns in walls the influence of the location of the wall has been shown to be very significant. Even though the wall acts as a heat sink, thermal bowing occurs. Because of this, for slender columns the p-delta effect becomes more important, consequently decreasing the steel critical temperature. However, the presence of the wall increases the critical temperature for stockier columns. This is because the p-delta effect is almost insignificant in such cases and it is the shielding effect of the wall which is most significant.

5. The survival period of steel columns can be increased by restraining their ends against rotation, transforming the member into a statically indeterminate structure.

6. Frame structures appear to have better fire resistance if their structural continuity is recognised, rather than by treating the structure as a series of isolated elements. Thus, it can be concluded that in standard fire tests, the failure temperatures of steel beams and columns will represent a conservative estimate of the critical temperatures for real structures.

CHAPTER EIGHT

CONCLUSIONS

8.1 CONCLUSIONS.

The main aim of the present research has been to develop a method for studying the deformation history of frame structures in fire, incorporating the influence of geometric and material non-linearities. These non-linearities include the inelastic nature of the stress-strain curves, the effect of curvature on longitudinal displacement, the influence of axial force in reducing the stiffness and the p-delta effect.

The method is based on the proven matrix stiffness formulation and has been implemented on a personal computer. The material non-linearities are represented using a secant stiffness approach rather than the tangent stiffness method in order to reduce computation time. The analysis is for two-dimensional structural behaviour only, covering the in-plane behaviour of frames. Where columns are considered, the deformation is with regard to major axis bending only.

The method is highly iterative with calculations based on

assumed curvatures and lateral displacements which are adjusted at each cycle of the analysis. The iteration process is considered complete when the condition of equilibrium is deemed to be satisfied - that is the difference between the internal and external axial force and bending moment are within a specified tolerance.

This general non-linear analysis has been applied to study the behaviour of steel structures in fire. The inclusion of temperature as a variable requires consideration of not only material softening but also thermal expansion and thermal bowing (under non-uniform temperature conditions). The treatment of beam-column elements raised the question of material unloading. Although this is generally ignored in ambient temperature analysis it was recognised as a potentially important consideration in the studies conducted at increasing temperature. In such cases the source of the phenomenon is rather complex, with axial loads changing due to restraint to expansion and material softening causing a spread of inelastic behaviour and a redistribution of bending stresses. For this reason a detailed study was conducted to investigate the influence of material unloading on the moment-axial force-curvature relationship. The behaviour at ambient temperature and in fire were considered for both rectangular and I sections. The study was conducted by examining a cross-section subjected to different combinations of axial force and bending moment including the effect of increasing temperature. The results

demonstrated quite wide variations in stress distributions depending on the heating or loading history. However the main aim was to examine the degree to which material unloading might influence the moment-axial force-curvature relationship. Here the results were quite remarkable in that, despite marked differences in stress profile, the moment-axial force-curvature relationship was hardly affected. The study therefore concluded that the influence of material unloading can safely be ignored for the structural analysis.

In the analysis the cross-section is divided depthwise into strips in each of which the strain, stress and temperature are assumed to be uniform. For the temperature distributions considered in this work a convergence test indicated that dividing the cross-section into 10 strips gave satisfactory accuracy. For an isolated member and accounting for both material and geometric non-linearities required a computation time of about 10 minutes for a single temperature level using a PC 286 personal computer with math co-processor. This time clearly increases for more extensive structures. For a simple rectangular portal frame the analytical time was between 30 and 45 minutes. However these times can be reduced if a more powerful computer is used.

Several comparisons were made with other experimental and theoretical studies both for isolated steel members and also

a complete frame. Six simply supported beams were analysed, one of which was fully restrained against longitudinal expansion. In the case of simple portal frames both pinned and fixed bases were analysed. Such comparisons were made with the work carried out by the British Steel Corporation [109], and by Furumura and Shinohara [11]. The comparisons showed very good agreement.

The analytical development and the investigation of the effect of material unloading was followed by a parametric study which was rather more limited than was desired due to time constraints. A wide range of parameters has been considered, but not exhaustively. The aim was not to provide specific design guidance or to make conclusive observations with regard to isolated parameters which might affect the performance of steel structures in fire. Instead the program has been used to demonstrate its capabilities and to give some indication of the relative importance of a broad range of variables. The influence of slenderness ratio for major axis buckling, axial force, bending moment, size of cross-section and grade of steel have been considered for isolated members subject both to uniform and non-uniform temperature distributions. It should be recalled that the present research deals only with in-plane behaviour, and deformation about the minor axis is prevented.

The results highlight some interesting aspects of the

behaviour of steel structures in fire. The slenderness ratio was shown to have a significant effect on failure temperatures, with very stocky and very slender columns performing better than columns with intermediate slenderness ratios which are arguably more typical of current construction of multistorey frames. This pattern was repeated for all combinations of axial load and bending moment considered.

No discernible difference was observed between the behaviour of beam-columns with identical load ratios and slenderness ratios but where different grades of steel or cross-section were used. Heavier sections may exhibit a slower rate of heating, but in terms of structural performance this suggests that a unified design approach independent of steel grade or size is satisfactory and that interaction curves relating slenderness ratio, axial load and end moments could be constructed. Of course substituting a larger section or a higher steel grade than is required for ambient temperature design conditions would reduce the load ratio and hence improve the failure temperature.

The effect of end restraint was also shown to improve the performance of individual members. This was demonstrated by comparing the behaviour of a pin-ended column with an equivalent propped cantilever. Of course in practice such restraint would be recognised in ambient temperature design and the axial load increased accordingly. However this

restraint still significantly increased the survival period even when an effective length factor of 0.7, based on the theoretical value, is used. The effective length factor of 0.85, which is typically used in design, resulted in a slightly higher critical temperature than one of 0.7.

The results generally indicated that the influence of the p-delta effect is very significant for beam-column behaviour. If this non-linearity is ignored, then gross errors can occur in the predicted performance of such elements. Clearly in analysing structures where bending and axial forces coexist it is essential that this feature is included. This is perhaps best illustrated by the case of a uniformly heated column subjected to its maximum permissible axial load. If even a small amount of end moment is applied the critical temperature dramatically reduces. In practice of course, columns are almost always exposed to some bending, whilst traditionally fire tests have been conducted under nominal conditions of axial load only. In association with this, thermal bowing is also very significant. This dramatically increases the moment due to the p-delta effect and consequently decreases the critical temperature. Where temperature variations exist throughout a cross-section, they must therefore be modelled in such a way that the thermal deformations are faithfully represented.

It was also noted that the performance of a beam forming

part of a frame is significantly better than when it is considered in isolation. However, this is a particularly difficult area since the end connections are likely to be semi-rigid. Analysis of complete frames, or at least sub-frames, is essential if the real restraint conditions are to be represented, and the connection characteristics, varying with temperature, must also be included. Not only does each analysis therefore become very time-consuming but also the range of parameters to consider expands significantly. The study presented here is an attempt to highlight which of those parameters should be the subject of a much more exhaustive study. The parameters which appear to have greater influence on failure temperature for individual beam-columns are slenderness ratio, temperature distribution through the cross-section and end restraint. In developing interaction curves, a comprehensive range of bending moments and axial loads should also be considered. For frames the influence of the relative sizes of beams and columns, the frame proportion (beam span to height of column) and location of walls or floor slabs which could result in different types of temperature distributions within the section are examples of parameters which need further investigation. The program developed during the work provides a powerful tool for performing an investigation of this nature.

8.2 RECOMMENDATIONS FOR FUTURE WORK.

Although the method developed as part of this research could be used to conduct a detailed study of steel frame behaviour in fire, some development of the analysis would be beneficial in extending its capabilities.

In the present formulation all members are assumed initially perfectly straight. Although this is a common assumption in analytical approaches it is not truly representative of real structural behaviour, and initial imperfections should ideally be included. In fact this could be achieved (for in-plane imperfections) quite easily since the main effect is the development of secondary moments which are already covered in principle.

In the present analysis the steel temperature must be defined as part of the input data. This is not a major limitation for isolated structural elements, for which there is a reasonable amount of data for different conditions and where the temperature distribution can be defined by specifying the temperature at just a few points. However, this may not be the case for frames, even if these are only simple rectangular portals. In such cases not only might the steel temperatures for the columns and beams be different but there may be significant variations through their cross-sections and along their lengths. In particular the temperature of the beam-column connection is

likely to remain cooler than the main elements, and since the degree of restraint at a joint has been shown to be an important parameter the temperature distribution should be determined quite precisely. It is therefore suggested that the thermal analysis should be integrated with the structural analysis, providing a detailed distribution of temperature without the need for excessive amounts of data input

In the present method the stress-strain relationships for steel at elevated temperature are based on stress-strain data derived from tests conducted on specimens of structural grades of steel manufactured in the UK. This representation is therefore strictly applicable to those grades of steel only. It is suggested that a more general form of stress-strain curve should be included in the present method to ensure that the method can be applied for any grade of steel from different countries. This can be done quite simply by introducing a general form of multi-linear stress-strain curve. Of course implementation of this would depend on the availability of test data for different steels, and this would be a useful supplement to the existing data.

Probably the most significant limitation of the present method is that it deals only with in-plane behaviour of the structure, implying that out-of-plane deformation is prevented. In practice this is often not the case, and it is suggested that the analysis should be extended to cater

for three-dimensional behaviour. This would enable the important phenomenon of buckling to be included. This would constitute a major piece of development work and would also have significant implications concerning the computational scale of the problem and the speed of solution.

In the present research the influence of material unloading on moment-axial force-curvature relationships has only been studied for uniform temperature conditions. In this case the material properties are represented by a single stress-strain curve which is a function of temperature. Although this simplifies the problem it is not typical of practical construction. It is therefore suggested that the study should be extended to include non-uniform temperature profiles within the section, in which case the stress-strain curve for each strip is in general different depending on the idealised temperature profile. In addition to the effects included in the present study, this non-uniformity of temperature will result in internal stresses within the section, further complicating the question of material unloading.

With regard to the indicative results obtained, some parameters clearly need more detailed investigation, and others appear to be suitable for more simplified treatment in the form of design guidance. For instance interaction curves could be established relating axial load, end moments

and temperature for different slenderness ratios.

The work presented in this thesis has been concerned with steelwork which has not been provided with additional fire protection, although the inherent shielding provided by slabs or walls has been shown to have a considerable effect on survival in fire. It is clearly desireable that designers should adopt a more rational, integrated way of designing economic steel-frames structures for ambient temperature strength and fire survival. This may include some reduction in load ratios and the elimination of retrospective fire protection in favour of inherently better shielded structural systems. If this more rational process is to come about, then it must surely be based on a better understanding of the behaviour of elements in fire, and this will be an important use for analytical tools such as that developed in the present work.

LIST OF REFERENCES

[1]. SMITH C.

"Fire Protection of Structural Steel in Multi-Storey Buildings".
Ref. No. BSC S 754 5M 7.83, British Steel Corporation.

[2]. SHIELDS T AND SILCOCK G.

"Buildings and Fire".
Longman Scientific and Technical, UK, 1987.

[3]. WITTEVEEN J.

"Some Aspects with Regard to the Behaviour of the Calculation of Steel Structures in Fire".
Symposium No.2 - Behaviour of Structural Steel in Fire, Held at Fire Research Station, Borehamwood Herts, 24/Jan./1967.

[4]. LATTER R.

"The Increasing Market For Steel in U.K Multi-Storey Buildings".
Paper Presented at IABSE-ECCS Symposium, Steel in Buildings, Luxembourg, 1985.

[5]. EL-RIMAWI J.

"The Behaviour of Flexural Members Under Fire Condition".
Ph.D. Thesis , University of Sheffield, England, April 1989.

[6]. LATHAM D.

"Developments in Multi-Storey Building - The Use of Unprotected Steelwork in Buildings".
National Structural Steel Conference, London, 11 and 12 Dec., 1984.

[7]. BABA S AND NAGURA H.

"Effect of Material Properties on the Deformation of Steel Frame in Fire".
Proc. of JSCE, Structural Eng/Earthquake Eng, Vol. 2, No.1, April 1985.

[8]. LAW M.

"A Basis for the Design of Fire Protection of Building Structures".
Structural Engineer, 61A, 1, pp 1-27, 1983.

[9]. MALHOTRA H.

"Fire Safety in Buildings".
Building Research Establishment Report, Department of the Environment, UK, Dec., 1986.

[10]. ADDLESON L.

"Materials for building, Volume 4 - Heat and Fire and Their Effect".
Newnes-Butterworth, 1976.

[11]. FURUMURA F AND SHINOHARA Y.

"Inelastic Behaviour of Protected Steel Beams and Frames in Fire".
Report of the Research Laboratory of Engineering Materials, Tokyo, No. 3, 1978.

[12]. HINKLEY P.

"Standard Time-Temperature Curve - Its Relevance".
Fire Surveyor, Vol. 13, No. 4, June, 1984.

[13]. BRITISH STANDARD BS476: PART 8:1972
"Test Methods and Criteria for the Fire Resistance of Elements of Building Construction". Now superseeded by BS 476: Part 20.

[14]. READ R AND MORRIS W.

"Aspects of Fire Precautions In Buildings".
Building Research Establishment, Department of the Environment, UK, 1983.

[15]. WITTEVEEN J.

"Trends in Design Method For Structural Fire Safety".
Acier-Stahl-Steel, 3/1984.

[16]. ROBERTSON J AND RYAN K.

"Proposed Criteria for Defining Load Failure of Beams, Floors and Roof Constructions During Fire Tests".
Journal of Research of National Bureau of Standard-C, Engineering and Instrumentation, Vol. 83C, No.2, Oct., 1959

[17]. LIE T AND STANZAK W.

"Structural Steel and Fire - More Realistic Analysis".
Engineering Journal/AISC, Second Quarter, 1976.

[18]. MAGNUSSON S, PETTERSON O AND THOR J.

"Fire Engineering Design of Steel Structures"
Swedish Institute of Steel Construction, Publication No.58, Stockholm, 1976.

[19]. BENNETTS I, PROE D AND THOMAS I.

"Simulation of the Fire Testing of Structural Elements by Calculation - Thermal Response".
Steel Construction, Vol. 19, No.3, 1985.

[20]. COOKE G.

"Development in Multi-Storey Buildings - Application of Steel Model Research".
National Structural Steel Conference 1984, The London Tura Hotel Kengsington, London, 11 and 12 Dec., 1984.

[21]. PURKISS J.

"Development in the Fire Safety Design of Structural Steelwork".
Journal of Construction Steel Research, Vol. 11, No. 3, 1988

[22]. BRESLER B, IDING R AND NIZAMUDDIN Z.

"FIRES-T3, A Computer Program for the Fires Response of Structures-Thermal".
Report No.UCB FRG 77-15, University of California, Berkeley, 1977.

[23]. KARDESTUNCER H.

"Elementary Matrix Analysis of Structures".
McGraw-Hill, Inc., USA, 1974.

[24]. ODEN J.

"Finite Element Applications in Non-linear Structural Analysis".
University of Alabama in Huntsville.

[25]. STRICKLIN J AND HAISLER W.

"Evaluation of Solution Procedures for Material and/or Geometrically Non-linear Structural Analysis".
AIAA Journal, Vol. II, No. 3, March 1973.

[26]. ALVAREZ R AND BIRNSTIEL C.

"Inelastic analysis of Multi-Storey Multibay Frames".
Journal of the Structural Division, ASCE, ST 11, Nov., 1969.

[27]. KAM T.

"Large Deflection Analysis of Inelastic Plane Frames".
Journal of Structural Engineering, ASCE, Vol. 114, No. 1, January, 1988.

[28]. EL-ZANATY M AND MURRAY D.

"Non-linear Finite Element Analysis of Steel Frames".
Journal of Structural Enginering, ASCE, Vol. 109, No. 2, Feb., 1973.

[29]. ZIENKIEWICZ O.

"The Finite Element Method in Engineering Science"
McGraw-Hill, USA, 1971.

[30]. CHEN W AND LUI E.

"Structural Stability - Theory and Implementation".
Elsevier Science Publishing Co., Inc., New York, 1987.

[31]. OSGOOD W.

"Stress-strain formulas".
Journal of the Aeronautical Sciences, Vol.13, No.1, Jan., 1964.

[32]. PHILLIPS A.

"Introduction to Plasticity".
Ronald Press Co., New York, 1956.

[33]. RAMBERG W AND OSGOOD W.

Descriptions of Stress-Strain Curves by Three Parameters",
NACA Technical note No. 902, 1943

[34]. TONG A.

"Elasto-Plastic Analysis by Numerical Procedures".
Journal of Engineering Mechanics Division, ASCE, Vol.86, No.EM6, Dec., 1960

[35]. WOLFORD D.

"Significance of the Secant and Tangent Moduli of Elasticity in Structural Design".
Journal of the Aeronautical Sciences, Vol.10, No.6, June, 1943.

[36]. CHAJES A.

"Inelastic Deflection of Beams".
Journal of the Structural Division, ASCE, ST6, June, 1968

[37]. SZULADZINSKI G.

"Moment-Curvature for Elasto-plastic Beams".
Journal of the Structural Division, Proceedings of ASCE, July 1975.

[38]. SZULADZINSKI G.

"Bending of Beams with Non-linear Material Characteristics".
Transaction of the ASME, Vol.102, Oct., 1980.

[39]. TIMOSHENKO S AND McCULLOUGH G.

"Element of Strength of Materials".
Third Edition, Van Nostrand, 1949.

[40]. HENDRY A.

" An Investigation of the Strength of Certain Welded Portal Frame In Relation to The Plastic Method of Design".
The Structural Engineer, Vol. 28, No. 12, Dec., 1950.

[41]. SHANLEY F.

"Inelastic Column Theory".
Journal of the Aeronautical Sciences, Vol.14, No.5, May, 1947.

[42]. HORNE M.

"The Elastic-Plastic Theory of Compression Members".
Journal of The Mechanics and Physics of Solids, 1956, Vol.4, pp 104-120, 1956.

[43]. DRISCOL G AND BEEDLE L.

"The Plastic Behaviour of Structural Members and Frames".
The Welding Journal, 36(6), Research Supplement, 1957.

[44]. TIMOSHENKO S.

"Strength of Material. Part 2: Advanced Theory and Problems".
Third Edition, Van Nostrand Reinhold, 1955.

[45]. TIMOSHENKO S AND GERE M.

"Theory of Elastic Stability".
Second Edition, McGraw-Hill Book Co., Inc., 1961.

[46]. LAY M AND GIMSING N.

"Experimental Studies of The Moment-Thrust-Curvature Relationship".
The Welding Journal, Welding Research Supplement, February, 1965.

[47]. Plastic Design in Steel : A Guide and Commentary / Joint Committee of the Welding Research Council and the American Society of Civil Engineers, Second Edition, ASCE, 1971.

[48]. GALAMBOS T AND KETTER R.

"Column under Combined Bending and Thrust".
Journal of Engineering Mechanic Division, ASCE, Vol. 85, No. EM2, April 1959.

[49]. GODDEN W.

"Numerical Analysis of Beam and Column Structure".
Prentice-Hall, London, 1965.

[50]. BAKER J.

"A Review of Recent Investigation into the Behaviour of Steel Frames in the Plastic Range".
Journal of the Institution of Civil Engineers, Vol. 3, Jan., 1949.

[51]. BLEICH F.

"Buckling Strength of Metal Structures".
McGraw-Hill Book Company, Inc., New York, 1952.

[52]. KETTER R, KAMINSKY E AND BEEDLE L.

"Plastic Deformation of Wide Flange Beam-Columns".
Transactions ASCE, 120, p1028, 1955.

[53]. CHEN W AND ATSUTSA T.

"Theory of Beam-Columns - Vol.1, In-Plane Behaviour and Design".
McGraw-Hill, USA, 1975.

[54]. EGAN M.

"Concept in Building Fire Safety".
A Wiley - Interscience Publication, New York, 1978.

[55]. BROCKENBROUGH R.

"Theoretical Stresses and Strains From Heat Curving".
Journal of The Structural Division, ASCE, ST7, July, 1970.

[56]. BIJLAARD F, TWILT L AND WITTEVEEN J.

"Theoretical and Experimental Analysis of Steel Structures at Elevated Temperatures".
IABSE, 10th Congress, Tokyo, Final Report, Zurich, 1977.

[57]. SKINNER D.

"Determination of High Temperature of Steel".
BHP Technical Bulletin, Vol. 16, No. 2, Nov., 1972.

[58]. JORGENSON J AND SORENSEN A.

"Mechanical Properties of Structural Steel at Elevated Temperatures".
Institute of Building Technology and Structural Engineering Report No. 8010, July, 1980.

[59]. SAITO H.

"Research of the Fire Resistance of Steel Beam". BRI Research Paper No. 31, Building Research Institute of Japan, 1968.

[60]. KRUPPA J.

"Collapse Temperature of Steel Structures".
Journal of The Structural Division, ASCE, ST 9, Sept., 1979.

[61]. CHENG W AND MARK C.

"Computer Analysis of Steel Frame in Fire".
Journal of The Structural Division, ASCE, ST 4, April, 1975.

[62]. COOKE G.

"Development in Multi-Storey Building - Practical Fire Engineering Design - Structural Application".
National Structural Steel Conference, London, 11 and 12 Dec., 1984.

[63]. SCHLEICH J.

"Fire Engineering Design of Steel Structures".
Steel Construction Today, Vol. 2, 1986.

[64]. KNIGHT D.

"Evaluation of the Behaviour of Steel in Fire".
BHP Tech. Bull. 15(2), Nov., 1971.

[65]. LANDAU H, WEINER J AND ZWICKY E.

"Thermal Stress in a Visco-elastic-plastic-plate With Temperature Dependent Yield Stress".
Journal of Applied Mechanic, 27, 1960.

[66]. BRESLER B AND IDING R.

"Effect of Fire Exposure on Steel Frame Buildings".
Final Report, WJE No. 78124' Janney, Elstner and Associates Inc., Sept., 1981.

[67]. BURGESS I, PLANK R AND EL-RIMAWI J.

"A Secant Stiffness Approach to the Fire Analysis of Steel Beams".
Journal of Constructional Steel Research, Vol. 11, 1988.

[68]. CHENG W.

"Theory and Application of the Behaviour of Steel Structures at Elevated Temperatures".
Computers and Structures, Vol. 16, No. 1-4, 1983.

[69]. DRAFT BRITISH STANDARD BS 5950.

"Code of Practice For The Fire Protection of Structural Steelwork, Part 8, 1985."

[70]. KIRBY B.

"Recent Development and Applications in Structural Fire Engineering Design - A review".
Fire Safety Journal, 11, 1986.

[71]. CONTRO R AND GIACOMINI S.

"A Method for Analysing Frame Structures Exposed to Fire".
Construzioni Metalliche, N2, 1981.

[72]. BECK V.

"The Prediction of Probability of Failure of Structural Elements Under Fire Conditions".
The Institution of Civil Engineers, Australia Civil Engineering Transactions, 1985.

[73]. European Convention for Constructional Steelwork. European Recommendation for the Fire Safety of Steel Structures, Elsevier, 1982.

[74]. BENNETTS I, THOMAS I AND PROE D.

"Thermal Response of Steel Members Under Fire Test Conditions".
Civil Engineering Transactions, I.E. Aust., Vol CE 26, No.2, May, pp 104-111, 1984.

[75]. MARCHANT E.

"A Complete Guide to Fire and Buildings".
Medical and Technical Publishing Co., London, 1972.

[76]. FIP/CIB REPORT.

"Methods of Assessment of Fire Resistance of Concrete Structural Members, Britain, 1978.

[77]. ANDERBERG Y.

"Mechanical Properties of Reinforcing Steel at Elevated Temperatures, Lund Institute of Technology, in Preparation.

[78]. PROE D, BENNETTS I AND THOMAS I.

"Simulation of the Fire Testing of Structural Elements by Calculation - Mechanical Response".
Steel Construction, Vol. 19, No. 4, 1986.

[79]. COOKE G.

"Fire Engineering of Separating Wall - Part 2".
Fire Surveyor, Vol. 16, No. 4, Aug., 1987.

[80]. LIE T.

"Temperature of Protected Steel in Fire".
Symposium No. 2 - Behaviour of Structural Steel in Fire, Fire Research Station, Boreham Wood Herts, Jan., 1967.

[81]. BARTHEMELY B.

"Heating Calculation of Structural Steel Members".
Journal of The Structural Division, ASCE, ST 9, Sept., 1979.

[82]. PROE B, BENNETTS I AND THOMAS I.

"Simulation of the Fire Testing of Structural Elements By Calculation - Overall Behaviour".
Steel Construction, Vol. 19, No. 4, 1986.

[83]. WICKSTROM U.

"TASEF-2 , A Computer Program for Temperature Analysis of Structures Exposed to Fire".
Report No. 79-2, Department of Structural Mechanics, Lund Institute of Technology, Sweden, 1979.

[84]. DOTREPPE J, FRANSSEN J AND SCHLEICH J.

"Numerical Simulation of Fire Resistance Tests on Steel and Composite Structural Elements or Frames".
Fire Safety Sci. - Proceeding of the First International Symposium, Oct., 1985.

[85]. BENNETTS I, THOMAS I AND PROE D.

"Thermal Response of Steel Members Under Fire Test Conditions".
Civil Eng. Transactions, I.E. Aust., Vol. CE 26, No. 2, May, 1984.

[86]. LIE T AND HARMATHY Z.

"A Numerical Procedure to Calculate the Temperature of Protected Steel Columns Exposed to Fire".
National Research Council of Canada, Division of Building Research, NRCC 12535, March, 1972.

[87]. LIE T AND HARMATHY T.

"Fire Endurance of Concrete Protected Steel Columns".
Journal of American Concrete Institute, No. 1, Proceeding Vol. 71, Jan., 1974.

[88]. STANZAK W AND LIE T.

"Fire Resistance of Unprotected Steel Columns".
Journal of The Structural Division, ASCE, Vol. 99, ST 5, May, 1973.

[89]. LIE T.

"Fire Resistance of Structural Steel".
Engineering Journal/American Institute of Steel Construction, Fourth Quarter, 1978.

[90]. LIE T.

"Optimum Fire Resistance of Structure".
Journal of the Structural Division, ASCE, Vol. 93, ST 1, Jan., 1972.

[91]. SAITO H.

"Behaviour of End Restrained Steel Members Under Fire".
Bull. of Fire Prevention of Society of Japan, Vol. 15, No. 1, June, 1966.

[92]. KNIGHT D.

"The Behaviour of Steel Structures in Fire".
BHP technical Bull., 16 (2), Nov., 1972.

[93]. CULVER C.

"Steel Column Buckling Under Thermal Gradients".
Journal of The Structural Division, ASCE, ST 8, Aug., 1972.

[94]. OSSENBRUGGEN P, AGGARWAL V AND CULVER C.

"Steel Column Failure Under Thermal Gradient".
Journal of The Structural Division, ASCE, ST 4, April, 1975.

[95]. CULVER C, AGGARWAL V AND OSSENBRUGGEN P.

"Buckling of Steel Columns at Elevated Temperature".
Journal of The Structural Division, ASCE, ST 4, April, 1973.

[96]. COOKE G AND LATHAM D.

"The Inherent Fire Resistance of a Loaded Steel Frame-work".
Steel Construction Today, Vol. 1, 1987.

[97]. THOR J, PETTERSON O AND MAGNUSSON S.

"A Rational Approach to Fire Engineering Design of Steel Buildings".
Steel Construction, Vol. 12, No.4, 1978.

[98]. LIE T AND STANZAK W.

"Fire Resistance of Protected Steel Columns".
Engineering Journal/AISC, Vol. 10, Third Quarter, 1973.

[99]. LIE T.

"Temperature Distribution in Fire - Exposed to Building Columns".
Journal of Heat Transfer, Vol. 99, Series C, No.1, pp 113-119, Feb., 1977.

[100]. FURUMURA F AND SHINOHARA Y.

"Inelastic Behaviour of Protected Steel Columns in Fire".
Report of the Research Lab. of Eng. Materials, No. 2, Tokyo, 1977.

[101]. MCLAUGHLIN E.

"Temperature Effects on Tall Steel Frame Buildings, Part 1- Response of Steel Columns to Temperature Exposure".
AISC, Engineering Journal, October, 1970.

[102]. JAIN P AND RAO M.

"Analysis of Steel Frames Under Fire Environment".
International Journal for Numerical Methods in Engineering, Vol. 19, 1983.

[103]. VANDAMME M AND JANSS J.

"Buckling of Axially Loaded Steel Columns In Fire Conditions".
IASBE Proceeding p-43/81, IASBE Periodica 3/1981.

[104]. KRUPPA J AND IDING R.

"Presentation of the European Recommendation for the Fire Safety of Steel Structures".
Acier - Stahl - Steel 3/1984.

[105]. PIERMAVINI O.

"Behaviour of Structural Steel in Fire".
Symposium No. 2 - Behaviour of Structural Steel in Fire, Fire Research Station, Boreham Wood Herts, Jan., 1967.

[106]. RASBACH D.

"Recent Development in Fire Safety Engineering".
Fire Surveyor, Vol. 13, No. 3, June, 1984.

[107]. HESELDEN A.

"Parameters Determining the Severity of Fire".
Symposium No.2 - Behaviour of Structural Steel in Fire, Fire Research Station, Jan., 1967.

[108]. BUTCHER E AND PARNELL A.

"Analysis of Fire Behaviour".
Fire Surveyor, Vol. 14, No. 3, June, 1985.

[109]. BRITISH STEEL CORPORATION.

"Compendium of UK Standard Fire Test Data on Unprotected Structural Steel".
Contract Report for Department of Environment, Ref. No. RS/RSC/S10328/187/B, March, 1987.

[110]. CHEN W AND ATSUTSA T.

"Theory of Beam-Columns - Vol. 2, Space Behaviour and Design".
McGraw-Hill, USA, 1977.

[111]. RASBACH D.

"Analytical Approach to Fire Safety".
Fire Surveyor, Vol. 9, No. 4, August, 1980.

[112]. COOKE G.

"Fire Engineering of Tall Fire Separating Walls".
Fire Surveyor, Vol. 16, No. 3, June, 1987.

[113]. DANIELS S.

"Inelastic Steel Structures".
The University of Tennessee Press, USA, 1966.

[114]. HARMATHY T.

"Deflection and Collapse of Steel Supported Beams and Floors During Fire Tests".
Division of Building Research DBR 203, August, 1960.

[115]. EBNER J AND UCCIFERRO J.

"A Theoretical and Numerical Comparison of Elastic Nonlinear Finite Element Methods"
Computers and Structures, Vol.2, pp.1043-1061, Pergamon Press 1972.

[116]. COATES R, COUTIE M AND KONG F.

"Structural Analysis".
Van Nostrand Reinhold (UK) Co. Ltd., 1972.

[117]. OLAWALE O.

"Collapse Behaviour of Steel Columns in Fire".
Ph.D. Thesis, The University of Sheffield, UK, April, 1988.

[118]. WITTEVEEN J AND TWILT L.

Int. Colloquium on Column Strength, Vol. 23, IABSE, Paris, 1972.